

TRANSIENTS IN ANTENNAS

A thesis presented for the degree of  
Doctor of Philosophy in Electrical Engineering  
in the University of Canterbury,  
Christchurch, New Zealand.

by

G.A. Burrell, B.E.(Hons.)

1971

The general antenna is not of great interest. Its generality is so great that any pile of tin with a transmission line exciting it may be called an antenna. It is evident on physical grounds that such a pile of tin does not make a good antenna, and it is worthwhile to search for some distinguishing characteristics that can be used to differentiate between an ordinary pile of tin and one that makes a good antenna. When the properties of a good antenna are considered, the only one that stands out is the general economy of metal. A good antenna does not have an ensemble of metallic ears, flaps, and springs that play no useful role in the business of radiating.

C.G. Montgomery

R.H. Dicke

## ABSTRACT

Measurement and computational procedures are developed for inferring the frequency responses (both driving point and far field) of an antenna or antenna system from measurements made in the time domain (using nanosecond time-domain-reflectometer techniques). A hybrid computer has been used to present simultaneous displays of the pulse response and the frequency response (in both magnitude and phase). The experimental technique is used to empirically design a new wideband antenna for the 3-30 MHz band from measurements made on scale models. A design principle for an antenna which is to faithfully and efficiently transmit a very wide bandwidth signal is also presented, and an experimental evaluation of a preliminary design is reported.

The frequency responses of individual parts of an antenna can be isolated and displayed simply with this experimental technique. To illustrate this, the input impedance and radiation from an effectively infinite monopole are presented. These results verify previous theories. Transmission and reflection coefficients describing the propagation of monochromatic current waves on thin bent wire antennas are inferred from parts of the reflected pulse response. Inspection of both the reflected pulses and the inferred frequency responses reveals the mechanism of current propagation on a bent wire antenna.

### ACKNOWLEDGEMENTS

I am greatly indebted to my supervisor Mr R.H.T. Bates for his encouragement and guidance over the duration of this project.

I also especially thank my wife Katharine for her patience and encouragement.

Mr E.J. Young of the New Zealand Post Office is thanked for his support in arranging the construction of the HF antennas developed in this thesis. I also thank the drawing office staff of the Post Office for their diligence in preparing most of the diagrams in this thesis.

The financial assistance of the New Zealand Post Office and the receipt of a CCC Electricity Department Scholarship are gratefully acknowledged.



## TABLE OF CONTENTS

	<u>Page</u>
Abstract	
Acknowledgements	
Table of contents	i
Glossary	vii
Preface	xi
 CHAPTER 1: Review of transient response of antennas	 1
 PART I. MEASUREMENT TECHNIQUES	
 CHAPTER 2: Inferring frequency responses from antenna measurements made in the time domain - the time-to-frequency transformation (TFT) technique	     11
2.1 Introduction	11
2.2 The pulse responses of an antenna system	14
2.3 The TFT technique	18
2.3.1 Measuring data from a sampling oscilloscope	21
2.3.2 Using a hybrid computer on-line	22
2.3.3 Errors in the calculated spectra	25
2.3.3.1 Errors inherent in calculating the spectrum of a signal from its time sampled values	25
2.3.3.1.1 Aliasing	25
2.3.3.1.2 Truncation	26
2.3.3.1.3 Timing shift	29
2.3.3.2 Noise-like errors	30
2.3.3.2.1 Amplifier noise	30
2.3.3.2.2 Timing jitter	33
2.3.3.2.3 Quantisation	34

2.3.3.2.4 Combined error from all noise-like sources	35
2.3.3.3 Error due to imperfections in connecting transmission lines	36
2.3.4 Measurement resolution	37
2.3.5 A practical evaluation of the error in an inferred reflection coefficient	38
2.3.6 3-point scanning using a hybrid computer	40
2.4 The far field transfer functions of an antenna	42
2.5 Inferring transmission and reflection coefficients for bends in wire antennas from a part of the reflected pulse response	44
CHAPTER 3: Measurement systems and experimental procedures	
3.1 Introduction	53
3.2 The driving point measurement range	53
3.2.1 Experimental procedure for measuring reflection coefficients	57
3.2.1.1 Measuring the test pulse	57
3.2.1.2 Measuring the pulse response	57
3.3 Apparatus for measuring the characteristics of bends in wire antennas	58
3.3.1 Experimental procedure for measuring bends	59
3.4 The far field measurement range	60
3.4.1 Calibrating the standard antenna	63
3.4.2 Experimental procedure for measuring far field transfer functions	65
3.4.2.1 Measuring the test pulse	65
3.4.2.2 Measuring the pulse response	65
3.4.3 Checking the measurement accuracy	67
3.5 Calibrating the sampling oscilloscope	69

CHAPTER 4: Generating high speed signals	78
4.1 Introduction	78
4.2 Avalanche mode switching	81
4.3 Construction of avalanche transistor pulse generators	83
4.3.1 Relaxation oscillators	83
4.3.2 A triggered pulse generator	86
4.4 Pulse forming	86
4.4.1 Differentiation	86
4.4.2 Stubs	86
 PART II. DRIVING POINT RESPONSES	
CHAPTER 5: Response of narrow band antennas	92
5.1 Introduction	92
5.2 Theoretical considerations	93
5.3 Experimental determination of the input impedance of an effectively infinite monopole	96
5.4 Discussion	96
5.4.1 The infinite antenna	96
5.4.2 Transient response of dipole	98
CHAPTER 6: Response of wideband antennas	107
6.1 Introduction	107
6.2 Theoretical considerations	109
6.2.1 Conical monopoles	109
6.2.2 Fan monopoles	113
6.3 Measured responses	115
6.3.1 Conical monopoles	115
6.3.2 Phase-corrected conical monopoles	115

6.3.3	Fan monopoles	116
6.3.4	Discussion of errors	119
6.4	Discussion	121
6.4.1	Conical monopoles	121
6.4.2	Fan monopoles	123
6.4.2.1	Reflected pulse responses	123
6.4.2.1.1	Sheet metal fans	123
6.4.2.1.2	Wire fans	124
6.4.2.2	Frequency responses	125
6.4.2.2.1	Sheet metal fans	125
6.4.2.2.2	Wire fans	127
6.5	A suggestion for further work	128
CHAPTER 7:	Some wideband wire antennas for HF	140
7.1	Introduction	140
7.2	The asymmetrical triangular fan	144
7.2.1	Scale model measurements	144
7.2.2	An HF asymmetrical triangular fan dipole	147
7.2.3	Comparison of measured input impedances of HF dipole and scale model monopole	149
7.3	The folded square fan	152
7.3.1	Scale model measurements	152
7.3.2	An HF folded square fan	152
7.4	Further developments	153

## PART III. FAR FIELD RESPONSES

CHAPTER 8: The faithful transmission of very wide band- width signals	169
8.1 Introduction	169
8.2 General theoretical considerations	169
8.3 A design principle for a faithful transmission system	173
8.4 Suitable types of antenna	174
CHAPTER 9: Measured Responses	178
9.1 Introduction	178
9.2 Radiation from base and tip of monopole	179
9.3 Conical monopoles	184
9.4 Phase-corrected conical monopoles	187
9.5 Fan monopoles	193
CHAPTER 10: Discussion of far field responses	202
10.1 Radiation from a monopole	202
10.2 Faithful transmission of wideband signals	206

## PART IV. PROPAGATION OF CURRENT ON BENT WIRE ANTENNAS

CHAPTER 11: Propagation of current on bent wire antennas	210
11.1 Introduction	210
11.2 The driving point pulse responses of bent wire antennas	214
11.2.1 Reflections from sharp bends	218
11.2.2 Reflections from gradual bends	220
11.2.3 Transmission along bent wires	222
11.3 Transmission and reflection coefficients for bent wire antennas	225

	<u>Page</u>
11.3.1 Computing the frequency responses	225
11.3.1.1 Transmission coefficients	225
11.3.1.2 Reflection coefficients	228
11.3.2 Computed responses	228
11.3.3 Discussion of errors	229
11.4 Discussion of the responses and suggestions for further work	233
APPENDIX 1: The organisation of a hybrid computer program for simultaneous display of time domain pulse responses and frequency responses of antennas	259
A1.1 The analogue computer	260
A1.2 The digital computer	261
APPENDIX 2: The organisation of an on-line hybrid computer program for 3-point scan sampling	266
A2.1 Timing the scan sequence	266
A2.2 The analogue computer	267
A2.3 The digital computer	267
A2.4 Paper tape format	268
A2.5 Card format for IBM 360/44 processing	268
A2.6 The effectiveness of 3-point scanning	269
A2.7 Subsequent improvements to the program	270
APPENDIX 3: Calculation of $T(f)$ and $R(f)$ for a 0.45 m long monopole at frequencies when it is a quarter-wavelength long and three quarter- wavelengths long	275
APPENDIX 4: Summary of sampling parameters for measure- ments reported in Parts I-III	278
REFERENCES	279

GLOSSARY

Symbols, abbreviations and definitions. Unless otherwise defined symbols have the meanings given below:

a	: radius of inner conductor of coaxial line; radius of antenna
ADC	: analogue to digital converter
b	: radius of outer conductor of coaxial line
c	: velocity of electromagnetic waves in free space $\approx 30 \text{ cm/ns}$
c.w.	: continuous wave
DAC	: digital to analogue converter
dB	: decibel
DFT	: discrete Fourier transform
dia.	: diameter
$E(f)$	: electric field intensity as function of frequency
eqn.	: equation
f	: frequency
FT	: Fourier transform
FFT	: fast Fourier transform
$g(t)$	: general function of time (signal)
$G(f)$	: FT of $g(t)$ ; gain of antenna as function of frequency
GHz	: gigahertz ( $10^9 \text{ Hz}$ )
$\underline{H}$	: magnetic field intensity vector
$H(f)$	: system transfer function of an antenna as function of frequency (section 2.3)
$h_e(f)$	: effective height of an antenna as function of frequency
HF	: high frequency

Hz	: hertz
j	: $j^2 = -1$
$\underline{K}$	: surface current density vector
k	: radian wave number = $2\pi/\lambda$
L	: length of antenna
m	: metres
MHz	: megahertz ( $10^6$ Hz)
ms	: millisecond ( $10^{-3}$ second)
mv	: millivolt ( $10^{-3}$ volt)
n	: refractive index
N	: number of samples
ns	: nanosecond ( $10^{-9}$ second)
narrow pulse:	pulse whose duration is short compared to the time it takes to propagate, at the velocity of light, along an antenna.
pf	: picofarad ( $10^{-12}$ farad)
ps	: picosecond ( $10^{-12}$ second)
pulse duration:	the duration of a pulse measured between the points at which its amplitude is -20 dB of its peak amplitude (section 4.1)
pulse risetime:	the time taken for a pulse to rise between 10% and 90% of its amplitude
r	: distance separating two antennas (chapters 1-10); radius of curvature of bend (chapter 11)
rad.	: radius
R(f)	: reception transfer function of an antenna as function of frequency (section 2.4)
RF	: radio frequency
RMS	: root mean square



- $s_{nm}(t)$ : time domain scattering parameter from port n  
 towards port m  
 $S_{nm}(f)$ : FT of  $s_{nm}(t)$   
 SWG : standard wire gauge  
 t : time  
 T : sampling interval  
 $T(f)$  : transmission transfer function of an antenna as  
 function of frequency (section 2.4)  
 TDR : time domain reflectometer  
 TEM : transverse electromagnetic  
 TFT : time to frequency transformation  
 TM : transverse magnetic  
 $u(t)$  : test pulse  
 $U(f)$  : FT of  $u(t)$   
 v : velocity factor (the ratio of the velocity of  
 propagation to c)  
 $v(t)$  : response of antenna or antenna system to  $u(t)$   
 $V(f)$  : FT of  $v(t)$   
 VHF : very high frequency  
 VSWR : voltage standing wave ratio  
 w : (1-w) is the fraction of the samples in a time  
 domain record to which a data window is applied  
 (section 2.3.3.1.2)  
 $Z_s$  : surge impedance (section 5.4.2)  
 $Z(f)$  : antenna input impedance as function of frequency  
 $\alpha$  : loss factor  
 $\beta(f)$  : transmission coefficient for bent wire antenna as  
 function of frequency (chapter 11)  
 $\Gamma(f)$  : current reflection coefficient for bend in wire  
 antenna as function of frequency ( chapter 11)

$\delta$	: quantising interval
$\epsilon$	: error; permittivity of free space
$\epsilon_r$	: relative permittivity
$\eta$	: characteristic impedance of free space ( $= 120\pi$ ohms)
$\theta$	: general angle
$\lambda$	: wavelength
$\mu$	: permeability of free space
$\mu v$	: microvolt ( $10^{-6}$ volt)
$v$	: amplitude jitter (section 2.3.3.2.1)
$\xi$	: confidence level (section 2.3.3.2)
$\rho(f)$	: voltage reflection coefficient at input of an antenna as function of frequency (section 2.3)
$\sigma^2$	: variance
$\tau$	: time delay
$\varphi$	: half flare angle (chapters 6 and 7)
$\phi$	: apex angle (chapter 7)
$\omega$	: radian frequency $= 2\pi f$
$*$	: convolution; complex conjugate

## PREFACE

During the last decade a number of papers have appeared (mainly in the IEEE Transactions on Antennas and Propagation) in which the time response of an antenna to transient input signals is obtained by a Fourier transformation of its frequency response. In many cases experiments were done to substantiate the calculations. These calculations can only be made for antennas for which the frequency response is known, and for effectively band limited input signals. On the other hand, with modern equipment, measurements of the transient response of VHF and microwave antennas can be made with less labour than conventional frequency domain measurements. The frequency response of an antenna is usually more useful in radio communications engineering than the transient response. This thesis is concerned with inferring the frequency response (in both magnitude and phase) of an antenna from a pair of measurements made in the time domain. The experimental procedure is called the time-to-frequency transformation (TFT) technique. Measurement and computational procedures are developed for obtaining the frequency responses (both input and far field) of an antenna or system of antennas by the TFT technique. The practical value of the TFT technique is shown by its use in the empirical design and development of a wideband antenna for the 3-30 MHz band from measurements made on scale models, and in the study of the propagation of current on bent wire antennas. A design principle for an antenna system which is to faithfully and efficiently transmit a very wide bandwidth signal is also

presented, and an experimental evaluation of a preliminary design is reported.

The increasing importance of the TFT technique is evident by the increasing attention being devoted to it in the literature. Recent issues of the IEEE journals contain papers which have been of considerable help to the author. These papers come from two places: the Sperry Rand Research Centre, Massachusetts, where the TFT technique has been applied to the measurement of coaxial transmission line components (including cables) and dielectric materials (Nicolson 1968, Nicolson and Ross 1970); and the IBM Watson Research Centre, New York, where the utility of the union of a sampling oscilloscope and a computer for making general network measurements has been realised, and software and hardware is being developed for a variety of measurement functions (Farber and Ho 1969, Stuckert 1969, Elliot 1970). As far as the author is aware, this thesis reports the first application of the TFT technique to antenna measurements.

Chapter 1 is introductory, and contains a review of previous work on the transient response of antennas. Only work relevant to this thesis is included, e.g. the radiation of transients into plasmas is excluded. New work is contained in the remainder of the thesis, which is divided into four parts. In the following discussion, the new work is indicated explicitly.

Part I includes chapters 2-4 and is concerned with the TFT technique and its application to antenna measurements. Because this measuring technique is essentially new it is discussed in considerable detail, and résumés of previous

work are included for completeness. Chapter 2 describes how to measure the driving point (reflected) and far field pulse responses of an antenna system and how to compute the reflection coefficient and system transfer function (as functions of frequency) from them. The far field transfer functions for an antenna on transmission and reception are introduced and how to infer them from a measurement using a standard antenna is described (the use of a standard antenna with TFT procedures is new). It is shown how a sampling oscilloscope (which is used for a receiver) can be connected to a small general purpose computer (which are now available at only a few times the cost of a sampling oscilloscope) so that the measurement and subsequent processing can be done automatically. A detailed discussion of the sources of error is included. Much of this follows Nicolson (1968) and Smith (1969) but some additions are made. The accuracy of the TFT technique is determined by comparison with a conventional slotted line measurement. The advantages of the TFT technique over conventional frequency domain methods for wideband antenna measurements are pointed out. In addition the frequency responses of different parts of an antenna can be isolated and displayed simply with the TFT technique. It is shown how transmission and reflection coefficients which describe the propagation and reflection of monochromatic current waves on bent wire antennas can be inferred from a measurement of only part of the reflected pulse response. This cannot be done simply with frequency domain methods.

Noise generated by the sampling oscilloscope electronics imposes a fundamental limit on the measurement accuracy. To

overcome this, Nicolson (1969) has devised a method of sampling called 3-point scanning which uses a small computer and a sampling oscilloscope in a control loop. This measurement method, for which Nicolson has a patent pending, is described in chapter 2. It was used for many of the measurements reported in this thesis. 3-point scanning represents a major advance for the TFT technique because, with careful experimental technique, the accuracy of precision frequency domain measurements can be equalled and possibly exceeded.

The design of the measurement apparatus which was used for all the measurements reported in this thesis is outlined in chapter 3. The calibration of the standard antenna for making far field measurements is described. The experimental procedures are given in detail.

Chapter 4 is concerned with generating high speed signals. When this project commenced there were no suitable pulse generators available in New Zealand. So, some had to be built. Some of the designs were so successful (200 pico-second risetimes were achieved) that construction details are included. The total cost of the circuit components is less than the cost of the coaxial output connector. The chapter also contains a brief review of methods of generating high speed signals.

The driving point responses of antennas are presented in Part II, which includes chapters 5-7. Chapter 5 is concerned with a representative example of a narrow band antenna (the dipole). The literature contains investigations of the transient responses of various narrow band antennas, but most have been concerned with the dipole. Consequently much of

chapter 5 is review and discussion. To illustrate how the TFT technique can be used to infer the frequency response of different parts of an antenna, the input impedance of an effectively infinite monopole is presented. This result, which has never been obtained directly from experiment before, verifies previous theories.

The characteristics of two wideband antennas, the conical monopole and the fan monopole are investigated in chapter 6. The driving point characteristics of the conical monopole are included because this antenna type is of interest in Part III. The remainder of chapter 6 is an investigation of some wire fan antennas. Fans constructed from a continuous sheet of metal are known to be good wideband antennas (Brown and Woodward, 1952) but there does not seem to be any information available on fans made of discrete wires. The investigation reported here identifies the differences in performance between metal fans and wire fans.

Chapter 7 continues from chapter 6 and explores the potential of wire fan dipoles as wideband antennas in the 3-30 MHz high frequency (HF) band. The New Zealand Post Office (NZPO) have a need for a simple (and hence robust) HF wideband antenna for radio telephone services to isolated parts of New Zealand and the Pacific Islands. During discussions with R.H.T. Bates (project supervisor) and E.J. Young (NZPO) the idea arose of using some sort of wire fan. In chapter 7, two HF antennas are developed empirically by inferring the input impedance of one-fiftieth size scale models with the TFT technique. Measurements made on full size antennas (61 metres long) show that the empirical designs

are satisfactory HF antennas. This demonstrates that the TTT technique for antenna measurements has practical value. Suggestions for improving the designs are included. An improved design (not reported in this thesis) is about to begin in-service assessments.

Part III (chapters 8-10) is concerned with the problem of characterising an efficient antenna system which will reproduce faithfully, at the output of the receiving antenna, a very wide bandwidth signal which has been applied to the input of the transmitting antenna. This cannot be done with existing antenna designs. A design principle based on a note by Bates (1967) for such an antenna is given in chapter 8, and suitable types of antenna are discussed.

The far field responses of conical monopoles are reported in chapter 9. It is shown that phase-correction (as suggested by the theoretical approach presented in chapter 8) of conical monopoles improves their system response. Included is an experimental verification of previous theoretical predictions of the frequency dependence of the radiation which occurs when a transient is radiated from the base of a thin cylindrical monopole.

Chapter 10 discusses the results presented in the previous two chapters, and is concerned with possible extensions of this work. Some errors in the literature are pointed out.

Part IV (chapter 11) contains an experimental study of the propagation of current on bent wire antennas. Accurate measurements of the driving point responses of bent wire antennas are presented. These measurements show that the



pulse reflected from a sharp bend is a compressed version of the incident pulse and that a pulse propagating around a gradual bend exhibits a continuous reflection from the whole length of the bend. Transmission and reflection coefficients (which were introduced earlier in chapter 2) describing the propagation and reflection of monochromatic waves on the bent wires are inferred from the measurements. Inspection of the shape of the pulse reflected from the tip of the bent wires and the inferred frequency responses reveals the mechanism of current propagation on the bent wire antennas. These results are new. The chapter concludes with suggestions for extending this work.

All the measurements reported in this thesis were performed automatically by the EAI-590 hybrid computer of the Electrical Engineering Department. The measurements were processed either by the EAI-590 computer or by the IBM 360/44 digital computer of the University of Canterbury Computer Centre. With the exception of the standard IBM scientific subroutine HARM, which was a fast-Fourier-transform algorithm, and a measurement program used in chapter 11, all computer programs used were written by the author in FORTRAN IV or EAI-640 ASSEMBLER language.

Papers published, accepted or submitted to date on topics from this thesis are:

- (i) R.H.T. Bates and G.A. Burrell: "Simultaneous display of frequency and pulse responses of antennas", paper presented at AICA-IFIP Conference on Hybrid Computation, Munich, August-September 1970, and to appear in the Proceedings.

- (ii) R.H.T. Bates and G.A. Burrell: "Towards faithful radio transmission of very wide bandwidth signals", paper to appear in IEEE Transactions on Antennas and Propagation.
- (iii) G.A. Burrell: "Experimental determination of the input impedance of an effectively infinite monopole", communication submitted to Proc. IREE (Australia).

## CHAPTER 1: REVIEW OF TRANSIENT RESPONSE OF ANTENNAS

During the last 15 years or so considerable interest has been shown in the transient radiation and driving point characteristics of antennas. In modern radar systems the trend is to use physically large antennas. At the same time the use of very short pulse modulated signals to improve range resolution has become important. Also, electronic scanning has made it possible to steer the beam of antenna arrays very rapidly. Ultimately it is the inability of the antenna system to respond to very rapid changes in the transmitted signals which limits the overall performance of the radar system. Similarly the bandwidth of the signal which can be faithfully transmitted by a radio communications system is ultimately limited by both the transient driving point and the transient radiation characteristics of the antenna system.

In the early 1960's fast pulse generators and fast oscilloscopes became available so that the transient responses of antennas which were a realistic physical size could be measured. This stimulated interest in transient responses because theoretical predictions could be substantiated by experiment. Papers appeared reporting the measurement of the transient radiation and driving point responses of various antenna types. The input signals used were usually baseband (i.e. dc) pulses or step functions which can readily be generated with semiconductor devices. The pulse duration, or the step risetime, was short compared with the propagation time of electromagnetic waves along the

antenna. Within the last few years interest has abated, and the only research team currently working on antenna transient responses, as far as the author is aware, is at the Sperry Rand Research Centre, Sudbury, Massachusetts under the leadership of Dr G.F. Ross.

It is customary in most antenna problems to assume an exciting voltage (or current) which varies sinusoidally with time<sup>1</sup>. Mathematical solutions are facilitated because time differentials and integrals are replaced by simple frequency dependences. This cannot be done if the input signal is an arbitrary time function, and consequently direct time domain solutions are extremely difficult. They have however been obtained for an infinite cylindrical antenna. Wu (1961b) derives a formula for the current distribution on a dipole antenna driven by a step function of voltage for times shortly after the switch on of the voltage. The same result is obtained in a different way by Morgan (1962). Latham and Lee (1970) obtain a formula for the fields of an infinite dipole excited by a step function of voltage. Similar results had earlier been reported by Brundell (1960a).

The characteristics of antennas can be described with equal validity in the time domain or the frequency domain. The two domains are related by a Fourier transform (FT). The time response of an antenna to any input signal can always (theoretically) be determined completely from the

---

<sup>1</sup>In practice the monochromatic characteristics are very important because most antenna applications require essentially monochromatic signals to be transmitted or received. Even when the signals are modulated the bandwidth of the signal is at most a few per cent. The characteristics of practical antennas change only slightly over these bandwidths.

frequency response. Consequently most theoretical transient responses have been obtained by taking the inverse FT of the frequency response.

A complete determination of the time response for any input signal requires knowledge of the frequency response up to the highest frequency for which the input signal has significant energy. Obtaining the monochromatic input and radiation characteristics of an antenna is essentially a problem of solving Maxwell's equations subject to the boundary conditions imposed by the antenna and the source. This can be surprisingly difficult. An idea of the enormous amount of effort which has been expended by many people over many decades on a mathematical analysis of the linear antenna can be had by thumbing through the pages of King (1956). Not all antennas have been solved theoretically, e.g. the formulas describing the input and radiation characteristics of helical antennas are empirical (Jasik 1961, chapter 7). Theoretical solutions, when available, are only for a restricted range of parameters, e.g. the theoretical values of the input impedance of electrically thin dipoles up to about 10 wavelengths long are given by Wu (1961a). However they are only for four values of the radius-to-wavelength ratio (spanning a 3:1 range). Thus they do not represent the input impedance of a fixed antenna over a wide frequency range. Lack of knowledge of the frequency response for high frequencies means that the time response can only be inferred for effectively band-limited input waves.

Schmitt (1960) infers the transient transmission and reception responses of a thin cylindrical dipole excited by

a step function of voltage. The responses were obtained for various source impedances. Some of his results were substantiated by a transmission experiment between two monopoles mounted above a ground plane. However, because Schmitt truncated his inverse FT prematurely his theoretical results are in error. This is discussed later in chapter 10. The transient transmission and reception responses of a thin cylindrical monopole excited by baseband pulses of various durations are presented by Schmitt et al. (1966). Their calculations are more accurate than those of Schmitt (1960) because their knowledge of the frequency response was more complete. Good agreement with experiment was obtained. They show that for monopoles which are very short compared to the wavelength of the highest significant frequency in the input signal, the shape of the radiated field is proportional to the second time derivative of the input signal. When the short monopole is receiving the shape of the received signal is proportional to the time derivative of the shape of the incident field. These differences between transmission and reception agree with Mayo et al. (1961), who were probably the first to point out that the impulse response of an antenna is different on transmission and reception. If a simple RC integrating circuit is used for a load, then the short receiving monopole is a faithful (but inefficient) receiver of transient signals. These results were also confirmed by experiment.

In a similar paper, Harrison and Williams (1965) infer the transmission and reception responses of wide angle conical antennas to baseband pulses of various durations.

They show that for very short cones the transient behaviour is the same as for the thin cylindrical antenna described in the previous paragraph. They also show that for a large cone the shape of the radiated field is a replica of the input pulse until such time as the input pulse is reflected from the cone rim. No experimental results are given.

The driving point transient response of a monopole has been investigated experimentally (using a narrow baseband pulse) by King and Schmitt (1962) and theoretically (inferred from the frequency response) by Williams (1963). Wu and King (1963) analyse theoretically the shape of the reflected current when step functions are incident upon the junction of a coaxial line and a straight wire antenna. Emphasis is given to incident signals having finite risetimes. Numerical results are presented which Schmitt (1963) substantiated experimentally<sup>2</sup>. Ross et al. (1966a, 1966b) infer the driving point impulse response of a 50 ohm matched conical monopole from theory by Papas and King (1949). They substantiate the result with a narrow pulse measurement. Measurements were also made on mismatched cones.

Palciauskas and Beam (1970) obtain the theoretical transient radiation fields of a thin cylindrical monopole excited by a baseband pulse for directions other than along the ground plane. Bolle and Jacobs (1962) show that the radiation pattern of long thin wire antennas for short pulse excitation is composed of two contributions from the ends of the antenna. They demonstrate how the familiar multilobed steady state pattern is a superposition of the two end

---

<sup>2</sup>These papers are discussed later in chapter 5.

patterns. Wait (1969) obtains an approximate expression for the transient radiation field of a dipole over a finitely conducting ground in which a finite, circular ground screen is embedded. The dipole current is a ramp function of time. The early time behaviour is shown to be that for a perfectly conducting ground and the late time behaviour approaches that expected for a homogeneous flat ground.

Harrison and King (1967) obtain the field radiated by an infinite monopole excited by a Gaussian voltage pulse by transforming the monochromatic far field derived by Papas (1949) into the time domain. The transient field was shown to be a fairly good replica of the input pulse, and they suggested its use as a known transient field for checking the distortion introduced by transient measuring equipment. The use of electric and magnetic probes for measuring transient fields, both in air and in dissipative media, had been previously discussed by Harrison (1964b). Prescribed electromagnetic pulses can also be generated by shock exciting (e.g. with a voltage step) a resistance loaded monopole (Merewether 1969, Taylor and Shumpert 1970). These repeatable and known fields can be used to investigate the effects of the transient electromagnetic fields generated by lightning flashes or nuclear explosions on both unprotected and shielded electronic equipment. The effectiveness of metallic shields against transient fields has been investigated by Harrison (1964a), Harrison et al. (1965) and Harrison and Papas (1965), and the effectiveness of the earth as a shield against transient fields has been investigated by King and Harrison (1968). The shape of the



driving point voltage required to produce a prescribed transient radiation field from a dipole has also been considered by Latham and Lee (1970).

The transient radiation field of a rectangular loop antenna excited by a voltage step is considered by Dion (1970). The loops are fed at the midpoint of one of their longest arms and are resistance loaded at the midpoint of the opposite arm to avoid ringing, and to simplify the analysis. The transient radiation field of the loop is obtained by integrating the contributions of each infinitesimal dipole around the loop. Reflections from the bends and the resistance load, and coupling between the branches of the loop, were neglected. It was also assumed that the current propagated around the loop undistorted and unattenuated. The transient radiation field of the infinitesimal dipole was inferred from the well known monochromatic formula. The received voltage was obtained in a similar way, and responses for transmission between two loops were obtained numerically and experimentally. Good agreement between theory and experiment was obtained for the early part of the response but significant differences occur for later times which means that the effects of the forementioned simplifications are not negligible. Consequently the method could not be used for an unloaded loop.

Katayama and Mushiake (1967) also start from the transient fields of the infinitesimal dipole in obtaining the transient radiation field of a two-element Yagi-Uda antenna excited by a step-modulated monochromatic wave. The antenna comprises a driven element and a reflector. They

obtained their antenna current from an RLC equivalent circuit, which means that their analysis is only valid for signals which have spectrums concentrated around the resonant frequency of the antenna. Consequently the early behaviour of the response (when the instantaneous bandwidth of the signal is highest) can be expected to be in error. Approximate numerical results are given and reasonable agreement with experiment was obtained. The results indicate that the buildup of the steady state radiation field of a two-element antenna takes about 12 cycles of the RF carrier.

The transient behaviour of aperture antennas has been analysed by Polk (1960), Mayo (1961) and Cheng and Tseng (1964). These authors seek analytical methods for determining the time required for the establishment (or re-establishment) of the main beam when sudden changes are made in the excitation. The analyses are based on the FT, although it does not appear explicitly in the result of Cheng and Tseng. The transient buildup of the radiation field of a travelling wave waveguide slot array is analysed by Borgiotti (1966). In all these papers the signals applied to the antenna are assumed to be band-limited and further, the antenna must be large in terms of the wavelengths at all the frequencies in the signal spectrum.

The driving point and far-field transient responses of horns and slotted waveguide antennas (including the coaxial line to waveguide transition) have been experimentally investigated by Ross et al. (1966b). The input signals used were a baseband pulse and a step modulated monochromatic wave. Heuristic arguments are presented to explain the

observed results.

A simple time domain method of obtaining the driving point transient response of a dipole is presented by Ross (1966c). The antenna is represented by a network of lossless, constant characteristic impedance transmission lines with lumped discontinuities at the ends and at the driving point to introduce radiation loss and dispersion. The model parameters are determined by a simple narrow pulse measurement, and the model can then be used to obtain the response to any input signal. The transmission line model is discussed later in chapter 5 where its limitations are pointed out. The transmission and reception responses of dipoles to step and impulse function excitation are also determined from transmission line models by Ross et al. (1966b) and Ross (1969a).

A time domain criterion for the design of elements for faithfully transmitting and receiving transients is suggested by Ross (1968) and several transient receiving elements have been designed and built on the basis of this criterion (Ross 1967a, Fenster and Ross 1968)<sup>3</sup>. All transient receiving elements so far reported are small compared with the wavelengths corresponding to the main range of frequencies for which they are designed. Thus, the elements are not efficient receivers of radio energy.

To sum up, it is apparent that three methods have been used to determine the transient characteristics of antennas. Direct analytical solutions in the time domain are extremely difficult. Inferring the transient response from the

---

<sup>3</sup>These elements are discussed in chapter 8.

frequency response is limited to antenna types for which the monochromatic driving point and far field characteristics are known. A further limitation is that the input signal must be effectively bandlimited because theoretical knowledge of the frequency response is never complete.

Presumably experiments can always be devised to determine the frequency response as completely as required, but continuous wave (c.w.) measurements are very tedious. It turns out that it is easier to measure the transient response and to infer the frequency response from it. Part I of this thesis is concerned with this measurement procedure. Simple time domain models, which are postulated to explain an observed response and are then used to obtain the response for other input signals, give results which are good enough for engineering applications. A simple narrow pulse measurement of the antenna (or a scale model of it) is all that is needed to determine the model parameters.

PART I

MEASUREMENT TECHNIQUES

CHAPTER 2: INFERRING FREQUENCY RESPONSES FROM ANTENNA  
MEASUREMENTS MADE IN THE TIME DOMAIN -  
THE TIME-TO-FREQUENCY TRANSFORMATION (TFT) TECHNIQUE

2.1 INTRODUCTION

Measuring the driving point and far field responses of VHF and microwave antenna systems to short pulse excitation is a natural development of the interest shown in the transient response of antennas during the last decade. There have been several examples of antenna ranges which use short pulse generators as transmitters and oscilloscopes as receivers (Schmitt 1960, King and Schmitt 1962, Ross et al. 1966a, Ross et al. 1966b, De Lorenzo 1967, Bates and Burrell 1970). Conventional real-time oscilloscopes were used as receivers during the early work of Schmitt (1960) and King and Schmitt (1962). The limited bandwidths of these receivers (300 MHz was reported by Schmitt) restricted the speed of the transmitted pulse to about 3 nanoseconds (ns). Large (14.6m by 7.3m) ground planes were used.

The availability of sampling oscilloscopes has revolutionised time domain measurements, and all recently published time-domain measurements have been made using sampling oscilloscopes as receivers. Currently available are 50 picosecond (ps) risetime (14 GHz bandwidth at -3 dB) oscilloscopes with sensitivities of several millivolts<sup>1</sup>. Pulses as short as a few tenths of a nanosecond can be generated with modern semiconductor devices (as shown later

---

<sup>1</sup>However such instruments when used at maximum sensitivity and speed give jittery displays.

in chapter 4). Distance resolution is reduced to a few centimetres allowing the reflections and radiation from individual parts of an antenna to be isolated (Bates, 1966). Consequently, smaller ground planes may be used. The driving point measurements reported in this thesis were performed on a 1.83m by 2.44m ground plane.

Time domain antenna measurements can be made more quickly and with less labour than conventional frequency domain measurements. The frequency response of an antenna system, which is often easier to interpret than the pulse response (because the human mind is conditioned to understanding a frequency response), is readily calculated from the pulse response. The potential simplicity and efficiency of calculating the steady state scattering matrix elements for a scattering body from measurements made in the time domain was recognised by De Lorenzo (1967), but he gives no indication of the likely errors or limitations of the method. Nicolson (1968) discusses the feasibility of the TTF technique, and demonstrates its capability by inferring the frequency response of broadband TEM mode microwave components from measurements of their response to a voltage step function. He also discusses the sources of error. A statistical assessment of many of the sources of error is given by Smith (1969). Some of his results are included in Nicolson's paper. Farber and Ho (1969) have presented a similar, but apparently independent paper to Nicolson's, but their error discussion is not as thorough.

Section 2.3 describes how to obtain the frequency response of antennas and antenna systems using the TTF

technique and section 2.3.2 describes how a hybrid computer has been used on-line to present simultaneous displays of the pulse response and the frequency response<sup>2</sup>. The treatment of errors given in section 2.3.3 mainly follows that of Nicolson's, but an important addition is made. The data window, which is a commonly used technique for reducing the ripples on a computed spectrum caused by sudden signal truncation, has been found essential when making antenna measurements and has not appeared in the literature pertaining to the TFT technique. Also included is a discussion of the error due to imperfections in feeder cables. The frequency resolution of the computed frequency response is discussed in section 2.3.4, and the utility of the TFT technique is demonstrated in section 2.3.5 where the reflection coefficient of an antenna obtained by the TFT technique is compared to a conventional continuous wave (c.w.) measurement.

Noise generated by the sampling oscilloscope electronics limits the accuracy with which low amplitude or fast risetime signals can be measured (see section 2.3.3). Elliot (1970) has devised a system which uses two sampling oscilloscopes in cascade, together with an auxiliary triggering circuit (which can be the triggering circuit in a conventional oscilloscope), to remove timing drift. The jitter (see section 2.3.3.2.2) is then removed by a low pass filter and an accurate low-speed replica of the high speed input signal is obtained. However, the system interprets amplitude drift as

---

<sup>2</sup>Any small general purpose computer with analogue-to-digital and digital-to-analogue converters could have been used. A hybrid computer was used because one was available.



timing drift so that the system is only useful for measuring high amplitude signals where amplitude drift is insignificant. Nicolson (1969) has developed a method (called 3-point scanning) for accurately measuring high speed, low amplitude signals. He uses a small computer and a sampling oscilloscope in a control loop. The implementation of this sampling method using a hybrid computer is described in section 2.3.6. Signals which are below the noise level when viewing the oscilloscope screen directly can be measured using this method: this is done later in chapter 11.

The far field transfer functions for an antenna on transmission and reception are introduced in section 2.4.

The frequency response of individual parts of an antenna can be inferred from parts of the pulse response. This is illustrated later in chapters 5 and 9. Section 2.5 describes how the TFT technique can be used to infer a transmission coefficient and a reflection coefficient to describe the propagation and reflection of current on a bent wire antenna from a measurement of only part of the driving point response. An experimental investigation of the propagation of current on bent wire antennas is reported later in chapter 11.

## 2.2 THE PULSE RESPONSES OF AN ANTENNA SYSTEM

Fig. 2.1 shows two antennas, one transmitting and the other receiving. The distance  $r$  is sufficient for the antenna to be in their respective far fields. A pulse generator, represented by its Thevenin equivalent circuit, produces a pulse  $u(t)$  (called a test pulse) which is short compared to the time it takes to travel, at the speed of light, the length  $L_1$  of transmission line to antenna 1.

Antenna 2 is connected by a length  $L_2$  of transmission line to a load impedance  $Z_L$ . For simplicity, the transmission lines are assumed to be lossless and non-dispersive. The origins of time for the test pulse, and the reflected and transmitted signals, are arranged so that the transmission delays introduced by the lengths  $L_1$  and  $L_2$  of transmission line, and the separation distance  $r$  of the two antennas, are removed. The excitation applied to antenna 1 is then  $u(t)$ . The driving point pulse response of antenna 1 is the signal reflected back towards the generator,  $v_1(t)$ . The transmission pulse response of the antenna system is the signal  $v_2(t)$  arriving at the load of antenna 2. Both these responses are easily measured using a sampling oscilloscope (see chapter 3). By representing the two antennas and their environment as a two-port network whose boundary passes through the antenna terminals, and describing this network by its scattering matrix, the system equations can be written (with an asterisk denoting convolution)

$$\begin{bmatrix} v_1(t) \\ v_2(t) \end{bmatrix} = \begin{bmatrix} s_{11}(t) & s_{12}(t) \\ s_{21}(t) & s_{22}(t) \end{bmatrix} * \begin{bmatrix} u(t) \\ 0 \end{bmatrix} \quad (2-1)$$

$s_{11}(t)$  is the impulse response of antenna 1 and  $s_{22}(t)$  is the impulse response of antenna 2.  $s_{21}(t)$  is the transmission impulse response of the antenna system, and from the symmetry of the scattering matrix (Montgomery et al. 1948, p.148)

$$s_{21}(t) = s_{12}(t). \quad (2-2)$$

If identical antennas are used then

$$s_{11}(t) = s_{22}(t). \quad (2-3)$$

An important advantage of making VHF and microwave measurements in the time domain is that the equipment may be designed so that unwanted reflections from the environment, and from mismatch in the feeder cables (e.g. Tee junctions or joins between cables of differing characteristic impedance) arrive separated in time from the response being measured. This is achieved by choosing sufficiently long feeder cables and by placing the antenna range sufficiently far from reflecting objects to introduce adequate time delays into the reflected signal paths. Thus it is possible to arrange that mismatches at cable junctions have negligible effect on the measurements without using large attenuators, which is a distinct advantage over conventional c.w. measurement methods. The effect of the loss in the necessarily long connecting cables can be removed from the measurement by recording  $u(t)$  in a special way which is described in chapter 3.

The time which is available for measuring the pulse response (either  $v_1(t)$  or  $v_2(t)$ ) before the arrival of unwanted reflections is termed the viewing window. It is convenient to define the measurement interval as the time interval within which the pulse response is to be measured. The measurement interval cannot be longer than the viewing window. No physical radiating system can have a strictly time limited impulse response. Consequently by limiting the measurement interval, truncation errors are introduced when the frequency response is computed: these are discussed later in section 2.3.3.1.2. The measurable duration of a pulse response is defined as the time for which it is above the mean noise level of the measuring equipment. Thus to measure

as much of the pulse response as possible the measurement interval should be equal to the measurable duration. If  $u(t)$  is short compared to the time it takes a current pulse to propagate along the antenna at the speed of light, then it is often possible to isolate reflections and radiation from individual parts of an antenna<sup>3</sup>. The viewing window then need only be long enough so that the desired part of the pulse response is received. Section 2.5 describes driving point measurements of bends in wire antennas in which the measurement interval includes only a part of  $v_1(t)$ .

Excluding all unwanted signals by using a viewing window means that the antenna system is in a simulated infinite and empty environment. Thus time domain antenna ranges can be accommodated in relatively confined spaces. Some of the measurements reported in this thesis could not have been performed simply in the frequency domain because there was no anechoic chamber nor suitable outdoor antenna range available.

It is impractical to make time domain measurements directly on high frequency (HF) antennas because very long delay lines would be required to give a viewing window of sufficient duration to enable the pulse response to be isolated. For example, on the basis of the measurements reported in Part II of this thesis, coaxial cable delay lines about 300 metres long would be required to be able to measure  $v_1(t)$  for an antenna designed to operate at 20 MHz. The advantage of making measurements in the time domain can be retained by making measurements on scale models. This is

---

<sup>3</sup>Such a pulse is termed a narrow pulse.

further discussed in chapter 7,

### 2.3 THE TFT TECHNIQUE

A graphical record of a short pulse measurement of an antenna represents a great deal of information stored in a small space. For this reason it is often difficult to interpret. It is desirable to transform the pulse response into a frequency response. This is especially true of responses from individual parts of an antenna.

The time history of an antennas responses  $v_1(t)$  and  $v_2(t)$  to a test pulse  $u(t)$  contain all the information required for calculating the antennas voltage reflection coefficient at the input of the antenna,  $\rho(f)$ , and the antenna system transfer function,  $H(f)$ , within the effective bandwidth of the test pulse.  $H(f)$  is the transfer function between transmitter and receiver, assuming that the propagation path is distortionless, and after removing the effect of antenna separation on phase and magnitude. Expressing eqn (2-1) in the frequency domain gives:

$$\begin{bmatrix} V_1(f) \\ V_2(f) \end{bmatrix} = \begin{bmatrix} S_{11}(f) & S_{12}(f) \\ S_{21}(f) & S_{22}(f) \end{bmatrix} \begin{bmatrix} U(f) \\ 0 \end{bmatrix} \quad (2-4)$$

Each variable in eqn(2-4) is the Fourier transform (FT) of the corresponding variable in eqn(2-1). Upper case letters are used for frequency responses (spectra) and lower case letters for signals, i.e.

$$G(f) = \int_{-\infty}^{\infty} g(t) e^{-j2\pi ft} dt; \quad (2-5a)$$

$$g(t) = \int_{-\infty}^{\infty} G(f) e^{j2\pi t f} df. \quad (2-5b)$$

The voltage reflection coefficient at the input of antenna 1 is given by

$$S_{11}(f) = V_1(f)/U(f), \quad (2-6)$$

and the antenna system transfer function by

$$S_{21}(f) = V_2(f)/U(f) \quad (2-7)$$

The effective bandwidth of  $u(t)$  is defined to be that band of frequencies, of width  $W$  centred on  $F$ , within which  $|U(f)|$  is well above the mean noise level. The limits of  $W$  were chosen to be the points where  $|U(f)|$  was -20 dB of its peak value. This limit was chosen because when  $|U(f)|$  was smaller than this the computations of the frequency response were observed to deteriorate. Consequently

$$\rho(f) = S_{11}(f), \quad F-(W/2) < |f| < F+(W/2); \quad (2-8)$$

$$H(f) = r S_{21}(f), \quad F-(W/2) < |f| < F+(W/2), \quad (2-9a)$$

where the distance  $r$  metres is included to remove the effect of antenna separation on the magnitude of  $H(f)$  (the effect of antenna separation on phase is removed by the appropriate choice of time origin for  $v(t)$ ). Knowledge of both  $\rho(f)$  and  $H(f)$  is required for a proper understanding of the operation of an antenna system.

The reflection coefficient of an antenna describes how well the antenna is matched to a transmission line of a certain characteristic impedance  $Z_0$ . The input impedance  $Z(f)$ ,

being a property of the antenna alone, is often more useful and may be simply calculated from the inferred reflection coefficient:

$$Z(f) = Z_o \left[ \frac{1+\rho(f)}{1-\rho(f)} \right] \quad (2-9b)$$

For accurate calculation of the frequency response,  $U(f)$ , which occurs in the denominator of eqns (2-6) and (2-7), must not contain any zeros or very small values of modulus, or any rapid phase changes. A baseband pulse was chosen as a test signal because of its well behaved spectrum (see chapter 4). The centre frequency  $F$  in eqns (2-8) and (2-9a) is then zero frequency.

The pulse responses were sampled (as described in the following two sections), and the frequency responses were calculated by a digital computer. When an IBM 360/44 computer was used, the FT's were computed by the fast Fourier transform (FFT) algorithm (Cooley and Tukey, 1965), which approximates eqn(2-5a) by the discrete finite series:

$$G_{SN}(f) = T \sum_{n=0}^{N-1} g(nT) e^{-jn2\pi fT}, \quad f = \frac{k}{NT}, \quad k = 0, \pm 1, \dots, \pm \frac{N}{2}. \quad (2-10)$$

$N$  is the number of samples taken,  $T$  is the sampling interval, and  $f_N = 1/2T$  is the Nyquist frequency. Descriptions of the FFT, and how to use it, are given by IEEE (1967), IEEE (1969) and Bergland (1969). The FFT algorithm greatly reduces computation time in comparison with straightforward numerical integration methods. However, the actual program which was available (the IBM scientific subroutine HARM) occupied significantly more storage than a simple numerical integration

program<sup>4</sup>. When an EAI-590 hybrid computer was used to compute the FT's (which is described later in section 2.3.2), a trapezoidal rule integration method was used because the FFT could not be fitted into the memory of the digital computer. Consequently a typical computation time for the measurements reported in this thesis was two minutes. The same results are obtained whichever method is used because the FFT is merely a speedy algorithm for trapezoidal rule integration (Cooley et al. 1967). Also, the trapezoidal rule is quite accurate when  $T$  is small because of the oscillating kernel in eqn(2-5a).

### 2.3.1 Measuring Data from a Sampling Oscilloscope

Modern sampling oscilloscopes are ideal instruments to connect to automatic measuring equipment, because they can be scanned at a real time rate which is convenient for the scanning equipment. Analogue recordings can be made with an X-Y pen recorder by scanning the time axis of the recorder and the time base of the sampling oscilloscope simultaneously. These analogue records may then be sampled manually for subsequent computer processing. This method was used during a preliminary evaluation of the TFT technique. However, when many samples are required from a large number of recordings the method is very tedious and consequently is error sensitive.

---

<sup>4</sup>FFT programs which replace the input data by its transform in the same vector require an involved procedure to sort the answers into the right positions in the vector. Consequently they are longer than the non-sorting programs which have the disadvantage of requiring two data vectors (see IEEE (1969)). A very concise sorting FFT programmed in USASI BASIC FORTRAN is now available from IBM Program Information Department, #360D-13.4.002. The listing is published by Mertz (1971).



In eqn(2-10) the frequency response is calculated at frequencies spaced by  $1/NT$ . Thus accurate timing of the sampling interval  $T$  is required to avoid errors in the frequency scale calibration.

Accurate samples of the pulse response are easily obtained by connecting the sampling oscilloscope to automatic data measuring equipment. Time synchronising is simple if the measuring equipment generates a staircase scanning voltage for the sampling oscilloscope time base. Accurate timing of the samples is obtained in this way provided the sampling oscilloscope horizontal time scale deflection factor (volts per cm of deflection) is known accurately. How to calibrate the sampling oscilloscope is described later in section 3.5.

### 2.3.2 Using a Hybrid Computer On-Line

A hybrid computer, which is a digital computer and an analogue computer interfaced with a data conversion and control unit, is ideal for automatically measuring and processing data from a time domain antenna range. All the measurements reported in this thesis were performed by an EAI-590 hybrid computing system. Some of the measurements were processed on-line by the same computer<sup>5</sup>. The frequency responses were displayed on a high-resolution storage CRT which has been specially interfaced to the digital computer, and the pulse responses were displayed on the sampling oscilloscope screen. Thus simultaneous displays of frequency

---

<sup>5</sup>The rest of the measurements were processed by an IBM 360/44 digital computer. This was because the output could be drawn by an IBM 1627 automatic graph plotter whereas the hybrid computer output had to be photographed from the CRT screen.

and pulse response were obtained. The two displays are complementary: the location of antenna discontinuities are given by the time display and their effect on the antenna performance is given by the frequency display.

Connecting a sampling oscilloscope to a small computer is reported by Nicolson (1968), who discusses the feasibility of making wideband measurements on microwave transmission line components using the TFT technique. He includes experimental results to demonstrate its capability. A hybrid computer is extremely versatile, and sophisticated supervisory routines could be included in the digital computer program which calculates the frequency response. The logic interface allowed a control box, which was remotely located at the antenna range, to be interfaced to the digital computer program. The digital computer was then programmed to have overall control of the measurement system, which could be operated either from the digital computer console or from the duplicated controls at the antenna range, Fig. 2.2 is a simplified block diagram of the TFT measurement system. Several digital computer programs were written and their basic organisation is given in Appendix 1.

The use of a general purpose computer as a control element for the measurement system has a number of advantages over a hardware controller. There is the flexibility that the stored program allows. Modification of the control functions and correction of errors are done by changing the program, not the wiring. Often this involves just changing a few instructions in memory, and can be done at the computer console in a matter of minutes. Magnetic discs or tapes can be used to store programs for different measurement

functions<sup>6</sup>.

The advantages of a hybrid computer controlled TFT measuring system for VHF and microwave antennas are:

- 1) wideband information is obtained from a single measurement;
- 2) cable and generator mismatch do not affect the measurement;
- 3) the effects of cable loss and dispersion are easily removed from the measurement;
- 4) a simulated infinite and empty environment allows measurements to be made in relatively confined spaces;
- 5) simultaneous displays of frequency response and time domain pulse response aid the understanding of an antenna system operation;
- 6) speed and ease of measurement enables many antenna configurations to be evaluated reasonably quickly;
- 7) flexibility of "software" control allows the system to be reorganised quickly (a matter of minutes) for different measurement functions;
- 8) the computer can be used for other engineering calculations when it is not being used for antenna measurements.

However, the arbitrarily fine resolution of the frequency domain measurement methods cannot be attained, although their high accuracy can be approached for measurements on wideband antennas by using a special sampling technique (Nicolson,

---

<sup>6</sup>IBM have recognised the potential of automatic measurement and processing using a computer and a sampling oscilloscope, and have developed hardware and software for such a measuring system (Stuckert, 1969).

1969). This is described later in section 2.3.6.

### 2.3.3 Errors in the Calculated Spectra

#### 2.3.3.1 Errors inherent in calculating the spectrum of a signal from its time sampled values

##### 2.3.3.1.1 Aliasing

It can be shown (Cooley et al., 1967) that eqn(2-10) is equivalent to

$$G_{SN}(f) = \sum_{\ell=-\infty}^{\infty} G(f+2\ell f_N), \quad f = \frac{k}{NT}, \quad k = 0, \pm 1, \dots, \pm \frac{N}{2}. \quad (2-11)$$

When  $N = \infty$ , eqn(2-11) describes a periodic function  $G_S(f)$  which is the superposition of the non-periodic function  $G(f)$  shifted by all multiples of the fundamental period  $2f_N$ .

$G_S(f)$  is said to be an aliased version of  $G(f)$ . For values of  $f$  within the range  $-f_N \leq f \leq f_N$ ,  $G_S(f)$  equals the required spectrum  $G(f)$  plus unwanted contributions from the aliases of  $G(f)$  at  $G(f \pm 2\ell f_N)$ ,  $\ell = 1, 2, \dots, \infty$ , since no practical signal is perfectly bandlimited.

The aliasing error is reduced by making  $f_N$  large, which is equivalent to making  $T$  small. This shifts the aliases further apart and reduces the unwanted contributions from them in the range  $-f_N \leq f \leq f_N$ . Decreasing  $T$  while keeping the measurement interval  $NT$  constant increases  $N$ , which requires more computer storage and more computation, and thus a compromise is necessary. The aliasing error may be further reduced by deliberately bandlimiting the signal. The spectra of the test pulses used to make the measurements reported in this thesis have maximums at  $f = 0$ , and their amplitudes decrease as the frequency increases. The signals were further bandlimited by the limited frequency response of the

sampling oscilloscope.  $T$  was chosen to make  $f_N$  five times the bandwidth of the sampling oscilloscope. The amplitudes of the computed spectra of the test pulses at  $f_N$  were then all less than 1% of their amplitudes at  $f = 0$ . Thus the aliasing error in the measurement bandwidth ( $0 \leq f \leq f_N/5$  if the full bandwidth of the sampling oscilloscope is used) is considerably less than 1%.

### 2.3.3.1.2 Truncation

If all of  $v(t)$  were received, it would be impossible to avoid accepting appreciable reflections from the environment<sup>7</sup>. So,  $v(t)$  must be gated which means that, having chosen some gating interval of duration  $NT$  beginning at  $t = 0$ , the receiver accepts only  $(v(t) \text{ gate}(t/NT))$ ; where  $\text{gate}(t/NT)$  is zero except for  $0 \leq t \leq NT$  where it is unity. The gating function  $\text{gate}(t/NT)$  is termed a rectangular data window. A suitable value of  $NT$  was chosen for each measurement which depended on the measurable duration of  $v(t)$ , with a maximum set by the arrival time of reflections from the environment. The loss of some of  $v(t)$  causes an error in the whole frequency response which is difficult to evaluate because it depends upon the portion of  $v(t)$  which has not been measured. Also, the FT of the received signal is the convolution of  $V(f)$  with the FT of  $\text{gate}(t/NT)$ , whose shape is  $\sin(\pi f NT)/\pi f$ . If the duration of  $v(t)$  is appreciably longer than the measurement interval, then the computed spectrum will exhibit ripples having a width of close to  $1/NT$ . This

---

<sup>7</sup>From now on  $v(t)$  is used to mean either the driving point pulse response  $v_1(t)$  or the far field pulse response  $v_2(t)$ . If  $v_1(t)$  or  $v_2(t)$  is meant in particular it will be obvious from the context.

effect has been called leakage (Bergland, 1969), and the response presented in Fig. 9.3(c) clearly exhibits such ripples showing that although the chosen value of  $NT$  permitted most of  $v(t)$  to be received, nevertheless the effects of truncation were sensible. However, the effects of truncation were never sufficient to mask the trends of the frequency responses of the measured antennas. It is also worth noting that it was not possible to identify the reciprocals of the widths of the ripples in the computed frequency responses with any major physical dimension of the antennas under test.

Leakage can be reduced by sampling  $v(t)$  with a data window which has lower sidelobes in the frequency domain than has  $\text{gate}(t/NT)$ . The data window which was used on the driving point and far field pulse responses in parts II and III of this thesis is the extended cosine bell window described by Bergland (1969):

$$d(t) = 1, \quad |t| \leq wNT,$$

$$d(t) = \frac{1}{2} \left[ 1 + \cos \frac{\pi(t-wNT)}{NT-wNT} \right], \quad wNT \leq |t| \leq NT,$$

$$d(t) = 0, \quad |t| > NT. \quad (2-12a)$$

where  $(1-w)$  is the fraction of the data to which the cosine half-bell is applied. Because  $v(t)$  is causal, eqn(2-12a) is only applied for  $t > 0$ , but is implied to exist in the interval  $-NT \leq t \leq 0$  even though no measurement is made in this interval. Errors due to the sharp edge of the truncation at  $t = 0$  have been found to be negligible.

The FT of eqn(2-12a) with  $w = 0$  is

$$D_0(f) = \frac{1}{2}D_1(f) + \frac{1}{4}\left[D_1\left(f + \frac{1}{2NT}\right) + D_1\left(f - \frac{1}{2NT}\right)\right] \quad (2-12b)$$

where  $D_1(f)$  is the FT of eqn(2-12a) with  $w = 1$  (i.e.  $d(t)$  is rectangular): (Blackman and Tukey 1958, p98). Thus eqn (2-12a) with  $w = 0$  can also be applied by convolving the values of the computed spectra at intervals of  $1/2NT$  with the weights  $\frac{1}{4}$ ,  $\frac{1}{2}$  and  $\frac{1}{4}$ . If gate  $(t/NT)$  cuts off any of  $v(t)$ , then a data window such as eqn(2-12a) cuts off more of it, and gives worse results. However, the data window eliminates the sharp edge of the truncation and reduces the ripple. Thus a compromise is necessary, and a suitable value for  $w$  is chosen for each measurement. Also, if the measurement interval is made much longer than the measurable duration so that even less of  $v(t)$  is cut off, then the computations of the frequency response will deteriorate because of the inclusion of extra noise.

An effect which is associated with leakage is called the picket fence effect (Bergland, 1969). Straightforward use of the FFT computes the frequency response only at discrete frequencies which are multiples of  $1/NT$ , and, because the record is truncated at  $NT$ , the required  $V(f)$  is not ideally sampled by a comb filter but by a set of spectral windows of shape  $\sin(\pi fNT)/\pi fNT$ . The picket fence effect becomes evident when the signal being analysed has strong frequency components which do not correspond to multiples of  $1/NT$ . Consider a signal which has a strong component at  $f_s$ , which is not a multiple of  $1/NT$ . This component is seen by all the adjacent spectral windows with weights corresponding to their level at  $f_s$ , which is always less than the level at multiples of  $1/NT$ .

Thus the component at  $f_s$  does not contribute properly to the computed spectrum. For example, the peak in the frequency response occurring at the resonant frequency of a narrow band antenna may not coincide with a multiple of  $1/NT$  (an example of this is given later in section 2.3.5).

A data window such as eqn(2-12a) reduces the problem by increasing the width of the main lobe and reducing the level of the side lobes of the spectral windows, but the problem is cured either by interpolating the computed complex Fourier coefficients or by using the easier, but equivalent, method of computing the frequency response at a finer spacing than  $1/NT$ . This is simple when using a straightforward numerical integration method, but the FFT resolution (not to be confused with measurement resolution, see section 2.3.4) can be increased by extending the time domain record with zeros. Most of the frequency responses presented in this thesis were computed at 10 MHz intervals.

Finally, it is worth pointing out that the paper by Farber and Ho (1969) contains an incorrect discussion of aliasing and truncation errors. Their comments on truncation errors actually refer to aliasing, and vice-versa.

#### 2.3.3.1.3 Timing Shift

If the time origin of  $v(t)$  is delayed by  $\tau$  with respect to the time origin of  $u(t)$ , then the computed frequency response will be multiplied by  $\exp(-j2\pi f\tau)$ , by the time shift theorem (Lathi 1965, section 6.15). This is a phase error which increases linearly with increasing frequency. The experimental procedures described in chapter 3 are designed to eliminate this.



### 2.3.3.2 Noise-like errors

#### 2.3.3.2.1 Amplifier noise

The disadvantage of using a single pulse for making measurements over a wide bandwidth is that the spectral intensity of the test pulse is low. The receiver gain must therefore be high and the noise thus introduced limits the measurement accuracy.

A sampling oscilloscope reconstructs a low speed real time replica of a high speed signal from successive samples taken from each repetition of the high speed signal. There are therefore two time scales, the equivalent time scale of the high speed input and the real time scale of the output. The ratio between them is determined by the rate at which the time base is scanned. The sampling oscilloscope amplifier and sampling gate contribute noise to the real time output and the effect that this has upon the computed equivalent frequency spectrum depends upon the real frequency spectrum of the noise and upon the ratio of the equivalent time and real time scales.

The sampling oscilloscope amplifier noise does not have a flat spectrum, and has high content at low frequencies ( $< 1$  Hz) due to slow random fluctuations in the zero level. The measurements shown in Fig. 2.3 were made at night from a Tektronix 1S1 sampling unit which was measuring a steady voltage at stationary equivalent time. There is an apparently random drift with a maximum excursion of  $\pm 2$  mv referred to the input over the 7.5 minute period. Smaller fluctuations of about 1 mv were observed in times as short as one second. Rapid fluctuations, which are made up of amplitude

jitter and additive noise, are shown expanded in the lower trace in Fig. 2.3. The noise and drift were of a constant level referred to the input regardless of the amplifier vertical scale. Steps of up to 1.5 mv referred to the input and with real risetimes of about 100 ms were also observed during the day, but these were found to be caused by sudden supply voltage variations and were eliminated by making measurements at night.

Assume that the sampled signal can be expressed in the form

$$g_m(nT) = (1+v_n) g(nT) \quad (2-12c)$$

where  $v_n$  is the amplitude jitter,  $g_m(nT)$  is the measured signal and  $g(nT)$  is the true signal. By assuming that  $v_n$  is a zero-mean normal random variable which is independent of the amplitude jitter in any other time sample, Smith (1969) has derived an expression for the bound on the spectrum error  $\epsilon_A$  caused by amplitude jitter:

$$\epsilon_A = \sigma_A \sqrt{\frac{T}{\pi} \int_{-\pi/T}^{\pi/T} |G(\omega)|^2 d\omega} \operatorname{erf}^{-1}[\sqrt{1-\xi_A}] \quad (2-13a)$$

where  $\sigma_A^2$  is the expected value of  $v_n^2$  (i.e. the variance of the amplitude jitter),  $\xi_A$  is an upper bound on the probability (a confidence level) that the error in the spectrum will exceed  $\epsilon_A$  (i.e. the fraction of the errors likely to exceed  $\epsilon_A$ ), and  $G(\omega)$  is the spectrum,  $\omega = 2\pi f$ . Eqn(2-13a) can be simplified to give

$$\epsilon_A \leq \sqrt{2} \sigma_A G_{\max} \operatorname{erf}^{-1}[\sqrt{1-\xi_A}] \quad (2-13b)$$

where  $G_{\max}$  is the maximum of  $|G(\omega)|$  for  $|\omega| \leq 2\pi f_N$ .

Although simpler than eqn(2-13a), eqn(2-13b) gives a higher bound than the more realistic eqn(2-13a). Both equations depend upon the true spectrum  $G(\omega)$  but good estimates can be made using the computed spectrum. A source of the jitter errors described by eqn(2-12c) is fluctuations in the sampling oscilloscope amplifier gain.

A bound on the error  $\epsilon_N$  due to the presence of zero-mean additive noise which is uncorrelated from sample to sample (i.e. white noise) has also been determined by Smith (1969):

$$\epsilon_N = T\sqrt{2N\sigma_N^2} \operatorname{erf}^{-1}[\sqrt{1-\xi_N}], \quad (2-14)$$

where  $\sigma_N^2$  is the variance of the white noise in the sampled values, and  $\xi_N$  is the confidence level of  $\epsilon_N$ .

The effect of amplitude drift in the computed spectrum may be minimised by rapidly scanning the time base of the sampling oscilloscope, thereby decreasing the ratio of equivalent time to real time, and causing the high-level low-frequency content in the real frequency spectrum to occupy only a small region (near zero frequency) of the required equivalent frequency spectrum.

Aliasing errors (section 2.3.3.1.1) have to be considered both in equivalent time and in real time, and a low pass filter should be connected between the output of the sampling oscilloscope and the recording equipment to limit the bandwidth of the signal in real time. Its risetime should be as long as possible without degrading the real time signal risetime. The smoothing control (sometimes

labelled resolution) provided on sampling oscilloscopes reduces the bandwidth of the amplifier and for measuring high amplitude signals where noise is less of a problem it is usually sufficient.

#### 2.3.3.2.2 Timing jitter

If the scanning voltage is held fixed corresponding to a stationary value of equivalent time then the measured voltage fluctuates as the sampling gate moves about its mean position. This is called timing jitter, and the error voltages generated depend upon the slope of the signal at that point.

The measurements shown in Fig. 2.4 were made at night from the output of a Tektronix 1S1 sampling unit which was measuring a 350 ps risetime slope at stationary equivalent time. They show the combined effect of amplitude noise and drift and timing jitter and drift. The drift period is seen to be much shorter than that in Fig. 2.3 which means that timing drift is more rapid than amplitude drift. Of the total drift excursion of  $\pm 2.5$  mv observed in the 7.5 minute period, probably  $\pm 1$  mv was due to timing drift. The jitter, shown expanded in the lower trace of Fig. 2.4, is of greater amplitude than that shown in Fig. 2.3, which shows the existence of timing jitter but no conclusions about its form can be drawn.

Assuming that the slope of the waveform is constant over the range of the timing jitter, and that the uncertainty in the time location of a sample can be described as a normal random variable which is statistically independent of the uncertainty at any other time, Smith (1969) has derived a

bound on the spectrum error  $\epsilon_T$  due to timing jitter:

$$\epsilon_T = \sigma_T \sqrt{\frac{T}{\pi} \int_{-\pi/T}^{\pi/T} \omega^2 |G(\omega)|^2 d\omega} \operatorname{erf}^{-1}[\sqrt{1-\xi_T}], \quad (2-15)$$

where  $\sigma_T^2$  is the variance of the timing jitter and  $\xi_T$  is an upper bound on the probability that the spectrum error will exceed  $\epsilon_T$ . The  $\omega^2$  weighting in eqn(2-15) means that the errors are caused mainly by the high frequencies, which are contained in the fast risetime portions of the sampled signal. Eqn(2-15) can be simplified to:

$$\epsilon_T \leq \sqrt{\frac{2}{3}} \sigma_T \frac{\pi}{T} G_{\max} \operatorname{erf}^{-1}[\sqrt{1-\xi_T}], \quad (2-16)$$

but the same reservations on its use apply as in eqn(2-13b).

The methods used to minimise amplitude noise and drift also apply to timing jitter and drift.

### 2.3.3.2.3 Quantisation

When the time samples are converted to digital form the range of amplitude values is divided into a finite set of equal increments, and all of the amplitude values which fall within the same interval are assigned the same value. This causes an error, called quantisation error, which can be no larger than half the size of the intervals used. If the quantisation interval  $\delta$  is very much smaller than the signal being measured the errors in the samples can be assumed to be independent since we expect the signal to pass through many quantisation intervals between samples. It is also reasonable to assume that the quantisation error can have any value within the interval with equal probability, again because  $\delta$  is very much smaller than the signal being measured. Making

these assumptions Smith (1969) has derived a bound on the spectrum error  $\epsilon_Q$  due to quantisation:

$$\epsilon_Q = T\delta \sqrt{\frac{N}{6}} \operatorname{erf}^{-1}[\sqrt{1-\xi_Q}] \quad (2-17)$$

where  $\xi_Q$  is the upper bound on the probability that the spectrum error will exceed  $\epsilon_Q$ . Generally  $\delta$  is chosen to make the quantisation error very much smaller than the other sources of error.

The accuracy of analogue-to-digital (A/D) converters is usually expressed as a number of bits, e.g. a 10 bit converter has  $2^{10}$  or 1024 increments, and thus slightly better than 0.1% accuracy. The digital voltmeter in the hybrid computer which was used as an A/D converter worked to 16 bit accuracy, and the quantisation errors were considered to be negligible. The example given later in section 6.3.4 confirms this.

Another source of quantisation error is the error in the scanning voltage caused by quantisation of the digitally generated scanning data. However, since the D/A converter also worked to 16 bit accuracy this source of error was also considered to be negligible.

#### 2.3.3.2.4 Combined error from all noise-like sources

The errors from all noise-like sources add in an RMS fashion, provided they are statistically independent (which is likely). Thus the combined error bound  $\epsilon_c$  is given by

$$\epsilon_c = \sqrt{\epsilon_A^2 + \epsilon_N^2 + \epsilon_T^2 + \epsilon_Q^2} \quad (2-18)$$

### 2.3.3.3 Error due to imperfections in connecting transmission lines

No coaxial connector is reflectionless, nor is the characteristic impedance of coaxial air-line or flexible cable exactly equal to its nominal impedance. Also, coaxial cable exhibits variations in its characteristic impedance along its length because of irregularities in the braid. Consequently small reflections occur from connections between different sections of air line and different sections of cable, and from braid irregularities in cables (typically  $\rho \approx 0.0125$  for GR-874 air line, i.e. the reflected signal is -38 dB of the input signal, and  $\rho \approx 0.03$  or -30.5 dB for GR-874-A2 coaxial cable with GR-874 connectors). Long coaxial air-lines require dielectric support beads spaced about 30 cm apart to preserve the conductors' concentricity. Although these beads can be designed for minimum reflection (typically  $\rho = 0.01$ : e.g. see Moreno 1948, p85), they are never reflectionless. Consequently the measured signal is contaminated by a multitude of small reflections which are reflections of all the signals in the transmission lines from these imperfections, e.g. the received signal is  $v(t) + y(t)$ , where  $y(t)$  are the reflections from the line. The computed spectrum is then  $V(f) + Y(f)$ .

It is necessary to choose transmission line of sufficiently high quality so that the reflections are below the noise level of the measuring equipment.  $Y(f)$  is then negligible in comparison with  $V(f)$ . Flexible coaxial cable (type GR-874-A2) was found to be satisfactory for most of the measurements reported in this thesis. However, when

precise measurements are made using 3-point scanning (an accurate measurement method described later in section 2.3.6) even the reflections from air-line junctions can be revealed. Often it is possible to devise some method of measuring the reflections so that they can be subtracted (in the computer) from the desired signals. An example of this procedure is given later in section 11.2.

#### 2.3.4 Measurement Resolution

The frequency resolution of the measurement is defined as  $1/NT$  (Bracewell 1965, p131) which is half the width of the main lobe of the spectrum of  $\text{gate}(t/NT)$ . The extra information necessary to reveal fluctuations in the frequency response which occur within a frequency interval finer than  $1/NT$  cannot be measured because the measurable duration of  $v(t)$  is noise limited. Conversely, if the signals being measured are reasonably noise free (as most of the driving point responses shown in Part II of this thesis are), and if the signals are measured until they have become so small that they are immersed in the noise, then no significant fluctuations in the frequency response occur in frequency intervals finer than  $1/NT$ .

In this thesis the frequency responses are computed at intervals finer than  $1/NT$ . This is equivalent to interpolating the values of the frequency response which correspond to multiples of  $1/NT$ , and cannot reveal fluctuations in the frequency response in intervals finer than  $1/NT$ . It does not correspond to an increase in the measurement resolution. Interpolation is necessary to eliminate the picket fence effect (section 2.3.3.1.2), and it provides a smooth curve



suitable for graphical presentation.

Frequency resolution is reduced with a data window such as eqn(2-12a) is used (e.g. when  $w = 0$  the resolution is  $2/NT$ , because the width of the main lobe of the spectrum of  $d(t)$  is twice that of a rectangular window of duration  $2NT$ ; Blackman & Tukey 1958, p14). This must be considered when choosing a value for  $w$ .

### 2.3.5 A Practical Evaluation of the Error in an Inferred Reflection Coefficient

To be able to make realistic estimates of the error in the computed  $U(f)$  and  $V(f)$ , measurements of the variance of the error voltage due to each cause must be made.  $\sigma_N^2$  can be estimated with an RMS millivoltmeter when the oscilloscope is measuring zero voltage, and  $\epsilon_Q$  can be determined easily. However,  $\sigma_A^2$  and  $\sigma_T^2$  cannot be determined simply and the effects of amplitude drift and timing drift cannot be estimated because they are highly correlated from sample to sample. The effects of truncation also cannot be estimated.

What is really wanted is the error in the computed frequency response. If the errors in  $U(f)$  and  $V(f)$  are normally distributed and have the same variance, then it follows from eqns (2-6) and (2-8) that the probability density of the errors in the frequency response follows a Cauchy distribution (Meyer 1965, p187). An estimate of the error could be made by evaluating the area under this distribution but it is doubtful if it would be realistic. Also, the variance of the error in both  $U(f)$  and  $V(f)$  is unlikely to be the same. Error analyses as involved as this are seldom carried out in practice, and some simpler method

is usually sought. The approach used here is to evaluate the combined effect of all the errors by comparing an inferred reflection coefficient with a direct c.w. measurement.

Fig. 2.5 shows the modulus of the reflection coefficient of a 30 cm long, 4 mm diameter monopole determined by both a conventional slotted line measurement (Silver 1949, chapter 15) and the TFT technique (following the experimental procedure described later in chapter 3). The agreement is seen to be within 5% except when the reflection coefficient is close to unity. It is worth remembering however that the accuracy of slotted line measurements falls off as the reflection coefficient increases because of line losses and detector calibration errors.

The inferred reflection coefficient was computed at 10 MHz intervals from a measurement interval of 14.6 ns, which means that the measurement resolution  $1/NT$  is 69 MHz. Notice that the resonant frequency of the monopole is 235 MHz (see Fig. 2.5), which does not correspond to a multiple of  $1/NT$ . Thus if the frequency response had only been computed at intervals of  $1/NT$  then the shape of the resonance would have been lost.

Fig. 2.6 shows the reflected pulse response of the monopole. For times greater than  $t_0 = 14.6$  ns the response is below the noise level, so that the measurable duration is  $0 < t < t_0$ . The effects of truncation have been investigated by comparing the reflection coefficient  $\rho_0(f)$ , computed using this measurement interval, with the reflection coefficients  $\rho_m(f)$  computed using the measurement intervals

$0 < t < t_m$  for  $m = 1, 2, 3$ . The times  $t_1$ ,  $t_2$  and  $t_3$  are shown on Fig. 2.6. Fig. 2.7 shows the percentage differences between  $\rho_m(f)$  and  $\rho_0(f)$ . What is actually plotted is

$$D_m(f) = 100[\rho_m(f) - \rho_0(f)] / \rho_0(f) \quad (2-19)$$

The difference is seen to be less than 5% for  $m = 1$  so it can be assumed that the error involved in taking  $0 < t < t_0$  for the measurement interval is appreciably less than 5%. The ripples observed are due to leakage. Notice that the magnitudes of both  $D_2(f)$  and  $D_3(f)$  are greater than 20% near the monopole resonances. This shows that even though that portion of the time response between  $t_2$  and  $t_0$  is small nevertheless it has an appreciable effect on the frequency response, affecting in particular the measurement resolution.

### 2.3.6 3-Point Scanning Using a Hybrid Computer

Very low frequency drift and jitter are the primary limitations on the accuracy of sampling low-level, high-speed signals. To overcome this Nicolson (1969) has devised a method of sampling he calls 3-point scanning which uses an on-line computer to continuously monitor the amplitude and timing drift of the oscilloscope and correct the sampled values. This permits slow scanning of the sampling oscilloscope so that a very low frequency cutoff filter may be used to reduce the jitter and high frequency noise. Averaging several scans further reduces this noise, and the method considerably improves the signal-to-noise ratio of the sampled signal.

Determining the value of each sample involves the measurement of a sequence of three values. With Fig. 2.8 as

an illustration, the time  $t_1$  identifies a point on the waveform of zero slope,  $t_2$  identifies a point of known slope, and  $t_3$  is the time at which the value of the waveform is required. The value  $V_1$  is measured and its change from the  $V_1$  measured in the previous sequence is the amplitude drift which has occurred since the last scan sequence.  $V_2$  is then measured and corrected for amplitude drift. Using the corrected  $V_2$  from the previous scan sequence and the known reference slope, the time shift of the sampling gate which has occurred since the last scan sequence is calculated. This timing shift is then applied as a correction to the scanning voltage representing  $t_3$ , and  $V_3$  is measured, is corrected for amplitude drift, and stored. The scan sequence is repeated with  $t_3$  incrementing across the measurement interval.

Amplitude and timing drift must be negligible during the scan sequence. This requires a fast scan. To allow heavy filtering of jitter and noise a slow scan is required (to allow the filter to settle). Thus a compromise is necessary, and suitable timing can be chosen by inspecting noise measurements such as those shown in Fig. 2.3 and 2.4.

The known reference slope (which is assumed to be linear over the range of timing drift) can be arranged by delaying a portion of the measurement pulse and superimposing it on the waveform outside the viewing window. A second pulse generator, synchronised to the test pulse, cannot be used because timing errors caused by the fluctuations in relative timing of the two pulse generators will be introduced. Part of the waveform being measured can be used as a reference

slope. The reference slope can be measured quite accurately from the oscilloscope screen by arranging the oscilloscope scales so that the slope fills the whole screen. Alternatively the computer can be programmed to measure the slope automatically.

The 3-point scanning method is simple to implement on a hybrid computer, and a program organisation is given in Appendix 2. An experiment which demonstrates the effectiveness of 3-point scanning is also reported.

#### 2.4 THE FAR FIELD TRANSFER FUNCTIONS OF AN ANTENNA

The system transfer function  $H(f)$  describes the overall performance of an antenna system but gives little insight into the radiating and receiving properties of the individual antennas which comprise the system. It is convenient to introduce both the transmission transfer function  $T(f)$ , which is defined as the electric field intensity in the far field, after removing the effect of antenna separation on phase and magnitude, when the antenna is excited by unit voltage; and the reception transfer function  $R(f)$ , which is defined as the received voltage when a linearly polarised plane wave, having unit electric field intensity, is incident upon the antenna. If  $E_1(f)$  is the electric field intensity at a distance  $r$  from a transmitting antenna and if  $E_2(f)$  is the electric field intensity incident upon a receiving antenna then

$$E_1(f) = T(f) U(f) \frac{e^{-jkr}}{r} ; \quad (2-20)$$

$$V(f) = R(f) E_2(f) \quad (2-21)$$

where  $k = 2\pi/\lambda$  is the radian wave number. Notice that  $T(f)$

is dimensionless and  $R(f)$  has the dimensions of length. Notice also that from eqns (2-9a), (2-20) and (2-21)

$$H(f) = T(f) R(f), \quad (2-22)$$

which also has the dimensions of length.

The transmission and reception transfer functions are related by

$$T(f) = \frac{\eta}{Z_0 c} R(f), \quad (2-23)$$

where  $\eta$  is the characteristic impedance of free space (Mayo et al., 1961)<sup>8</sup>.  $T(f)$  and  $R(f)$  could be computed from signals radiated between two identical antennas from eqns (2-9a), (2-22) and (2-23). But, consider a radiating system containing two antennas, one for transmitting and one for receiving. One antenna is a standard with known transmission and reception properties, and the other is the "antenna under test". From a measurement of the signal radiated between these two antennas,  $T(f)$ ,  $R(f)$  and  $H(f)$  can be straightforwardly derived for the antenna under test. The advantage of using a standard antenna is that only one test antenna need be made. The design and calibration of the far field measurement system which was used for the measurements reported in Part III of this thesis is detailed in section 3.4.

The impulse responses of the antenna on transmission and reception are given by the inverse FT of  $T(f)$  and  $R(f)$  respectively. It follows from eqn(2-23) and from simple FT

---

<sup>8</sup>The difference between  $T(f)$  and  $R(f)$  does not contravene reciprocity; see chapter 8.

theory (Lathi 1965, p143) that the reception impulse response is proportional to an integration of the transmission impulse response. Since an arbitrary driving function can be expressed as a continuous sum of impulse functions (Lathi 1965, p395) it follows that the reception response to an arbitrary incident field is proportional to the integration of the transmission response to the same arbitrary driving voltage. This seems a surprising result at first sight, because it implies that if an impulse function is radiated then the received signal is a step function, which is unbounded. However, no practical antenna can efficiently radiate a signal which has an average value. Inefficient reception of step functions, and hence transmission of impulses, can theoretically be achieved with an infinitesimal electric dipole with an infinite source impedance (Harrison, 1964b).

## 2.5 INFERRING TRANSMISSION AND REFLECTION COEFFICIENTS FOR BENDS IN WIRE ANTENNAS FROM A PART OF THE REFLECTED PULSE RESPONSE

It is shown later in chapter 11 that the shape of the reflection of a narrow pulse from the tip of a wire antenna changes when the wire is bent, and that this is mainly due to radiation from the base of the antenna being received by the bent section and attenuation of the current as it propagates around the bend. Reflections from the bend are also observed. In this section it is shown how the TFT technique can be used to obtain a transmission coefficient  $\beta(f)$  which describes the coupling and attenuation of the current as it propagates

along the wire and a current reflection coefficient  $\rho(f)$  which describes the reflection of current from the bend. The meaning of these functions is discussed later in section 11.3.

Consider the simple network model of a bent wire antenna mounted above a ground plane shown in Fig. 2.9. The base region, the bend and the tip of the antenna are represented as lumped two port networks A, B and C which are described by their time domain scattering matrices  $s_A(t)$ ,  $s_B(t)$  and  $s_C(t)$  respectively. The networks are joined by lossless and non-dispersive transmission lines which represent the straight sections of the wire<sup>9</sup>. The excitation applied to the bent wire is a narrow test pulse  $u(t)$ , and it is assumed that the straight sections are long enough for the primary reflections of the test pulse from the bend and from the tip to be separated in time from all secondary reflections. Also, it is assumed that the primary reflections are themselves not so dispersed that they overlap each other or the secondary reflections.

Let  $v_B(t)$  be the part of the pulse response which is the primary reflection from the bend and  $v_C(t)$  be the part of the pulse response which is the primary reflection from the tip.

---

<sup>9</sup> Straight wires of constant cross section are dispersive and current propagating along the wire is attenuated due to radiation loss (unless the wire is infinitely thin). However thin wires are only dispersive near their driving points (see chapter 5) and energy loss due to radiation from thin wires occurs mainly as current is incident upon the driving point and the tip (see chapters 9 and 10). Thus lumping these effects into the networks A and C is a good approximation for thin wires. It is shown later in chapter 11 that  $\beta(f)$  depends upon the geometry of the whole wire and is not a property of the bend alone as suggested by the simple model presented here. For the purposes of this section the simple model is sufficient.



It is convenient if all parts have their time origins shifted to remove the delay of propagation along the wire.  $v_B(t)$  and  $v_C(t)$  are related to the test pulse by (with an  $*$  denoting convolution)

$$v_B(t) = u(t) * s_{A_{12}}(t) * s_{B_{11}}(t) * s_{A_{21}}(t); \quad (2-24)$$

$$v_C(t) = u(t) * s_{A_{12}}(t) * s_{B_{12}}(t) * s_{C_{11}}(t) * s_{B_{21}}(t) * s_{A_{21}}(t). \quad (2-25)$$

Let  $v_s(t)$  be the part of the pulse response which is the reflection from the tip when the wire is straight, i.e. the network B is removed. The received part  $v_s(t)$  is related to the test pulse by

$$v_s(t) = u(t) * s_{A_{12}}(t) * s_{C_{11}}(t) * s_{A_{21}}(t). \quad (2-26)$$

Using eqn(2-2), and taking the Fourier transforms of the scattering matrix coefficients in eqns (2-24), (2-25) and (2-26) we obtain

$$[S_{B_{12}}(f)]^2 = \frac{V_C(f)}{V_S(f)}; \quad (2-27)$$

$$S_{B_{11}}(f) = \frac{V_B(f)}{V_S(f)} S_{C_{11}}(f). \quad (2-28)$$

The effective bandwidth of  $v_s(t)$  is defined to be that band of frequencies, of width  $W$  centred on  $F$ , within which  $|V_S(f)|$  is well above the mean noise level. It is seen later in chapter 11 that  $W$  depends upon the physical dimensions of the base region. Thus

$$\beta(f) = S_{B_{12}}(f), \quad F-(W/2) < |f| < F+(W/2); \quad (2-29)$$

and with the assumption that  $S_{C_{11}}(f) = 1$  within the measurement bandwidth,

$$\Gamma(f) = -S_{B_{11}}(f), \quad F-(W/2) < |f| < F+(W/2), \quad (2-30)$$

The minus sign denotes the change in direction of the reflected current.

The reflection scattering coefficient of the tip  $s_{C_{11}}(t)$  has been obtained by Ross (1969a) from a narrow pulse measurement. He finds that it is essentially real and equal to about 0.97 within the effective bandwidth of the test pulse he used. Neither the diameter of the wire nor details of the test pulse were given, but his experimental results suggest that the pulse duration was less than 500 ps, which means that its effective bandwidth extends to several GHz. Thus for computations of  $\Gamma(f)$  up to several GHz the assumption that  $S_{C_{11}}(f) = 1$  only introduces about 3% error.

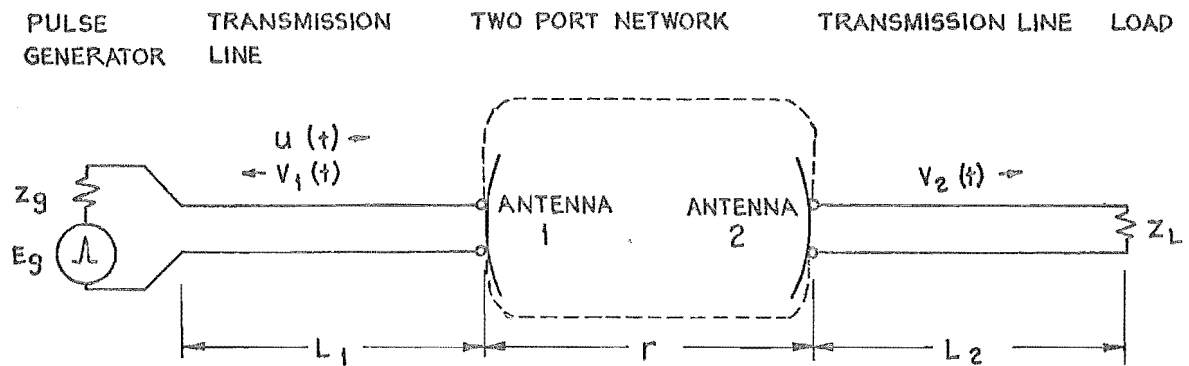


FIGURE 2.1 : TRANSMITTING AND RECEIVING ANTENNAS

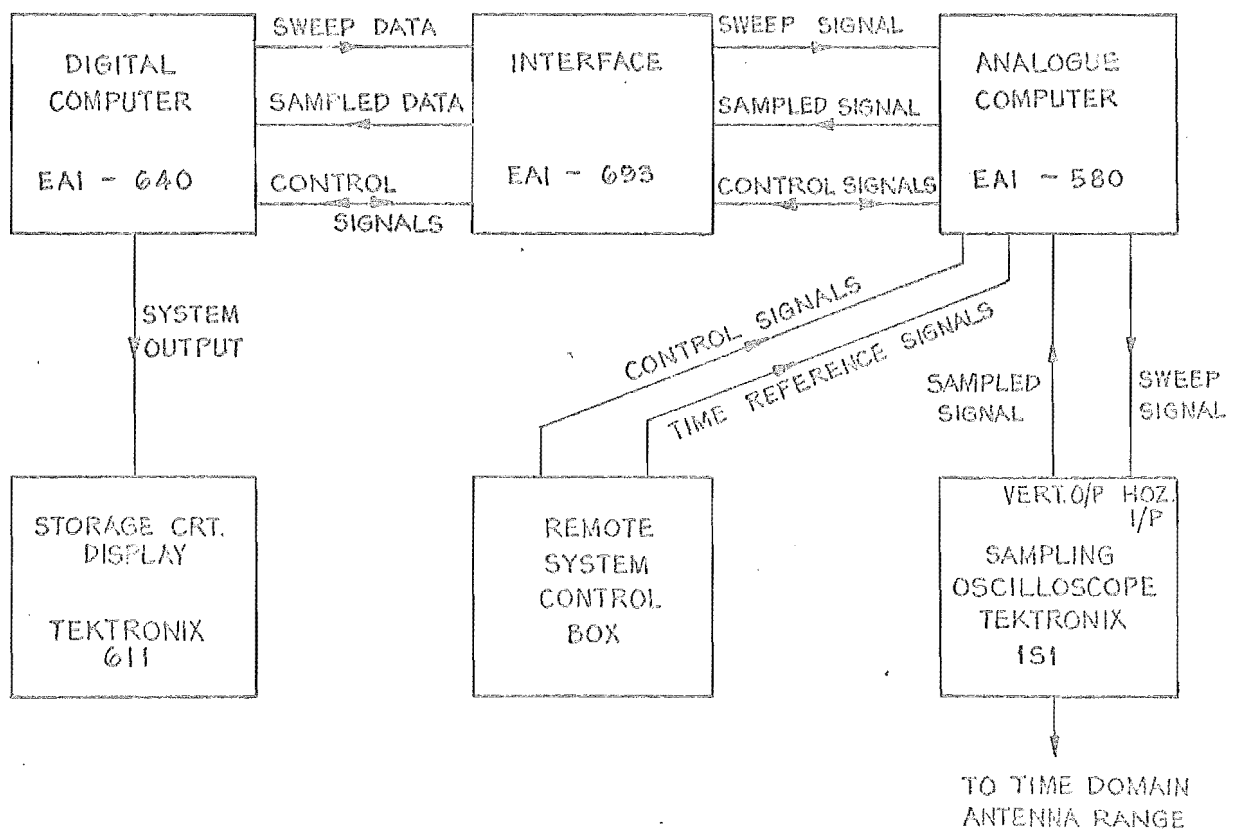


FIGURE 2.2 : SIMPLIFIED SYSTEM BLOCK DIAGRAM FOR DISPLAY OF ANTENNA RESPONSE IN FREQUENCY DOMAIN .

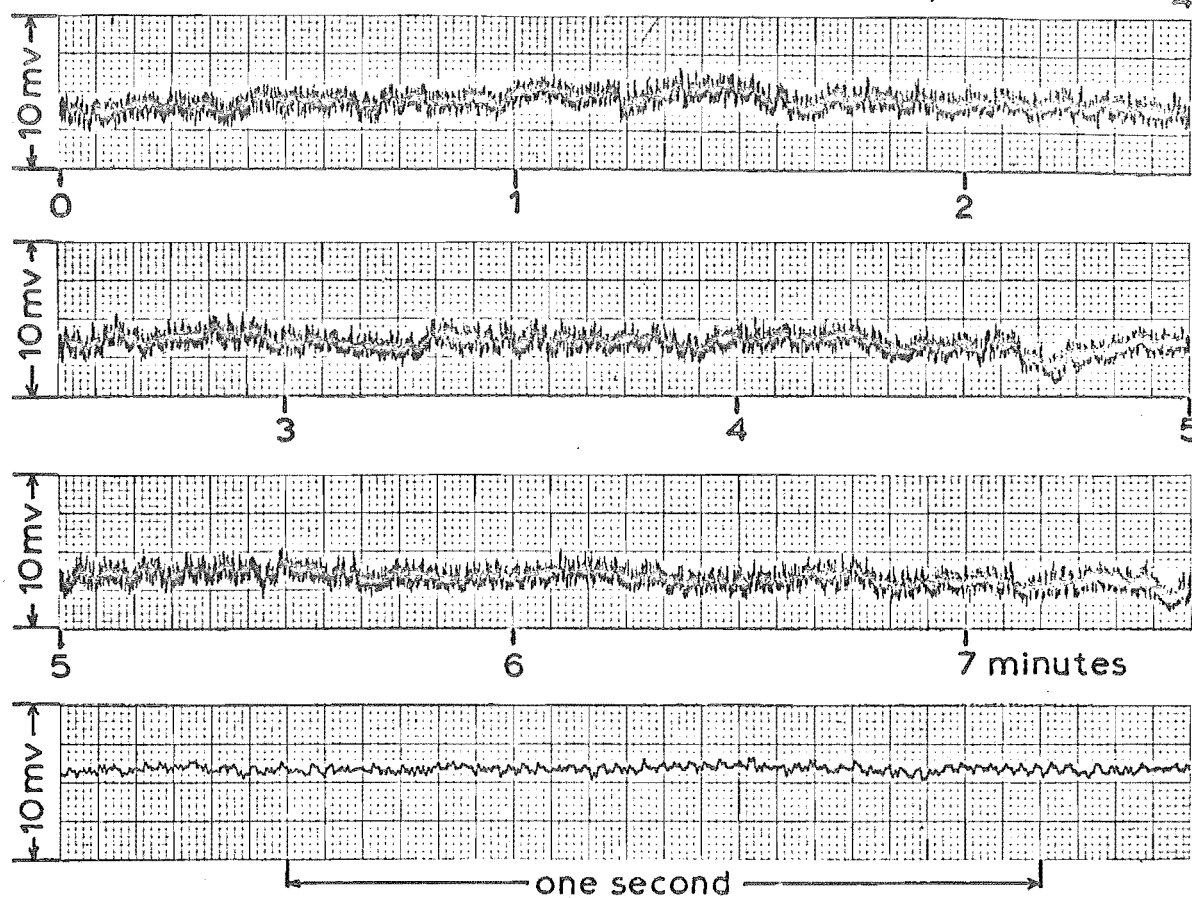


Figure 2.3: AMPLITUDE NOISE OF TEKTRONIX 1S1 SAMPLING UNIT MEASURED AT NIGHT

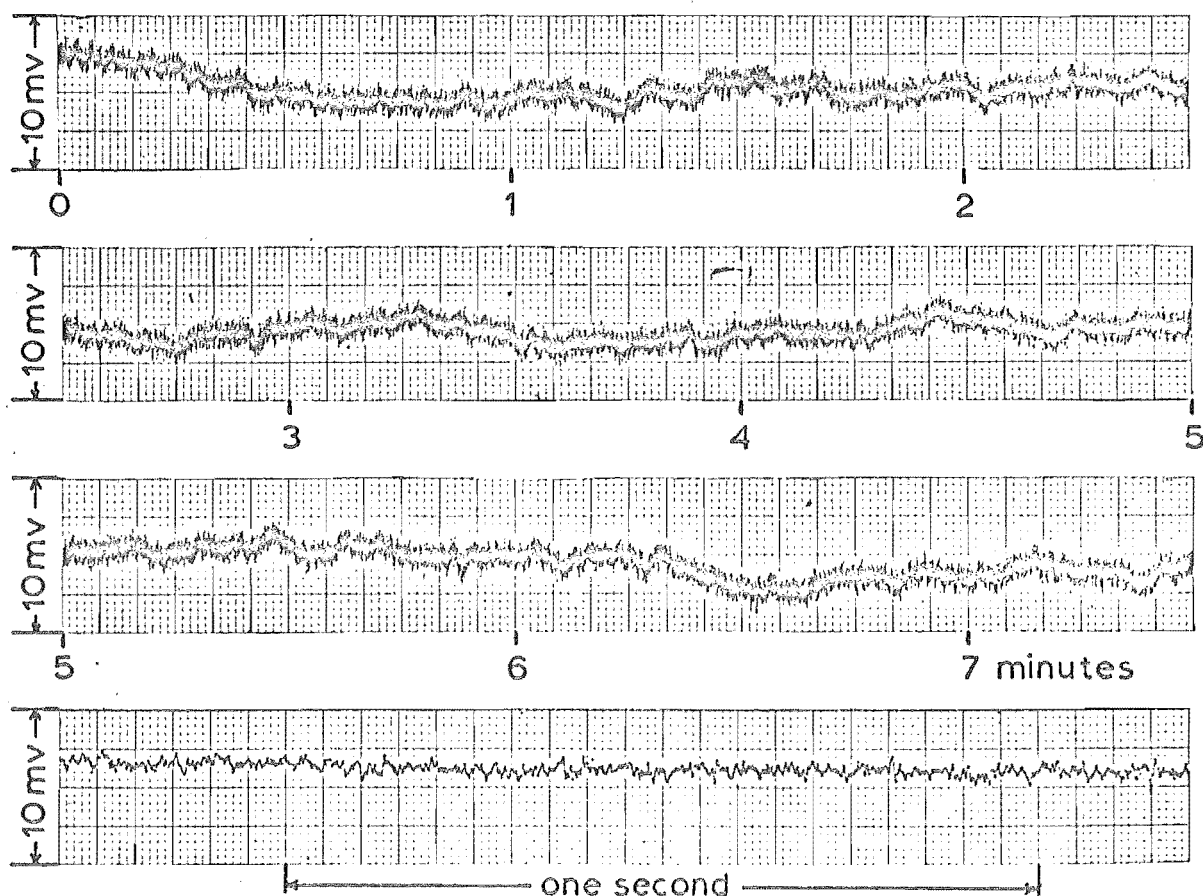


Figure 2.4: COMBINED EFFECT OF AMPLITUDE NOISE AND TIMING NOISE OF TEKTRONIX 1S1 SAMPLING UNIT MEASURED AT NIGHT

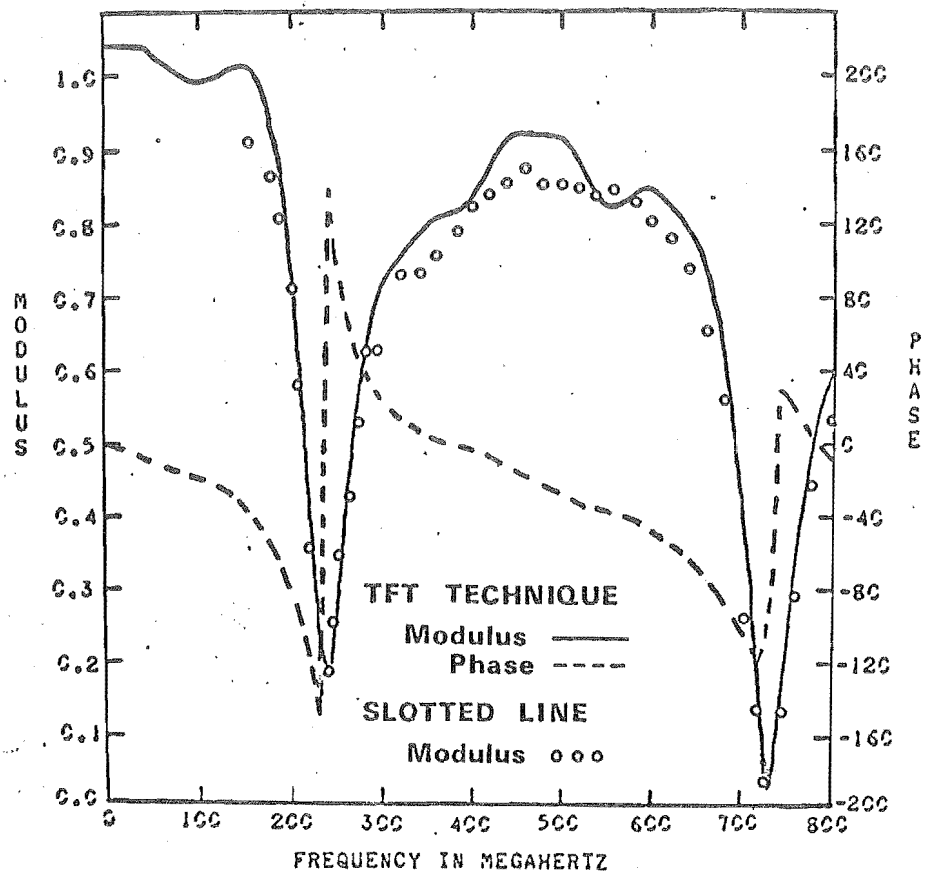


Figure 2.5: COMPARISON OF REFLECTION COEFFICIENTS OF 30cm LONG, 4mm DIA. MONOPOLE MEASURED IN TWO WAYS.

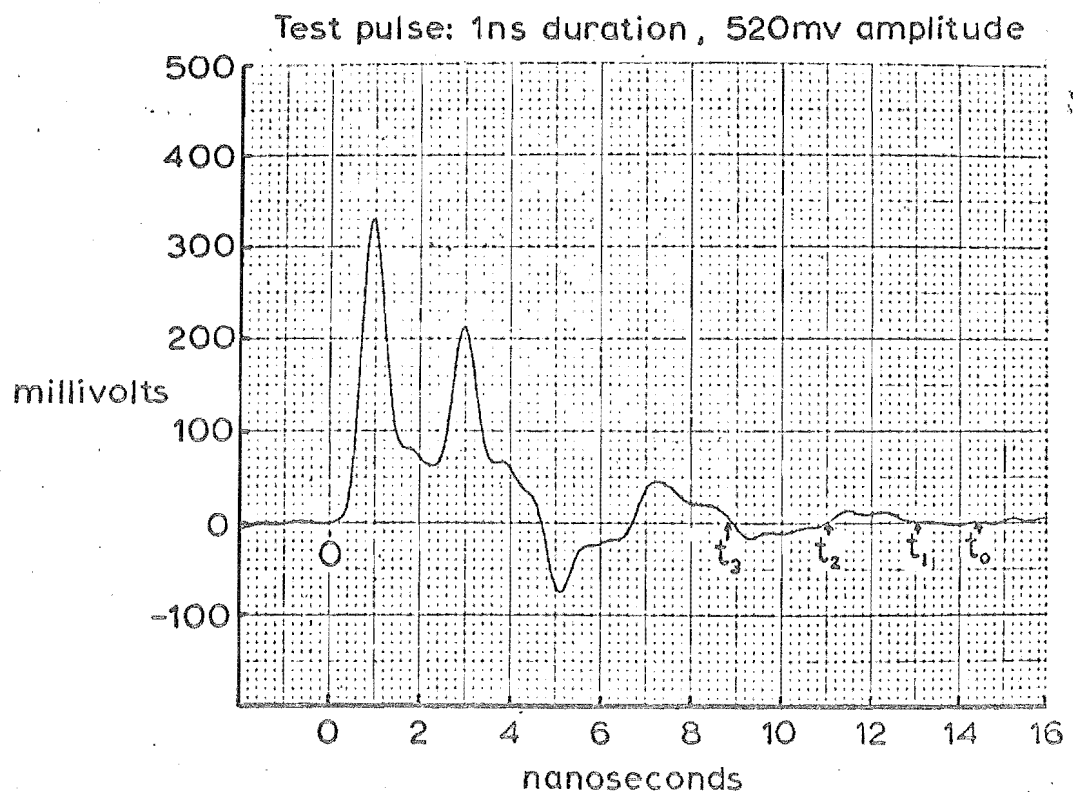


Figure 2.6: REFLECTED TIME DOMAIN RESPONSE OF MONOPOLE

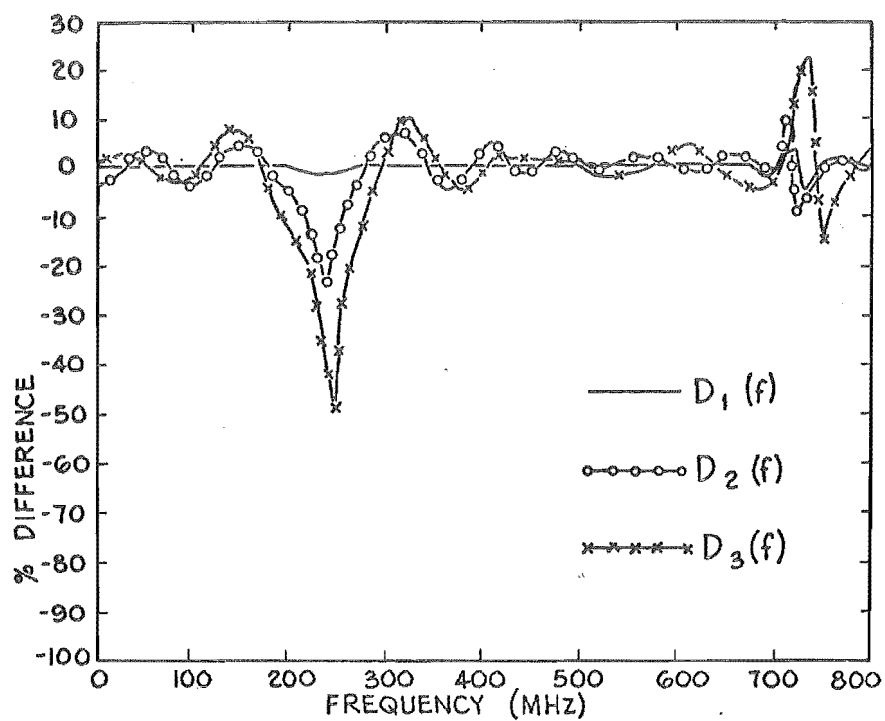


FIGURE 2.7 : DISTORTION DUE TO TRUNCATING REFLECTED TIME DOMAIN PULSE RESPONSE OF MONOPOLE

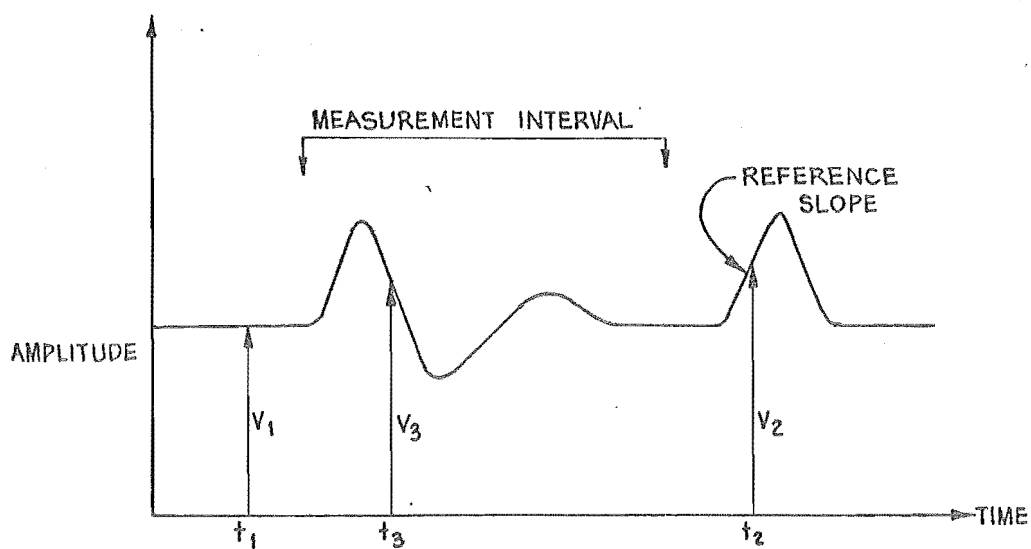


FIGURE 2.8 : ILLUSTRATION OF 3 POINT SCANNING

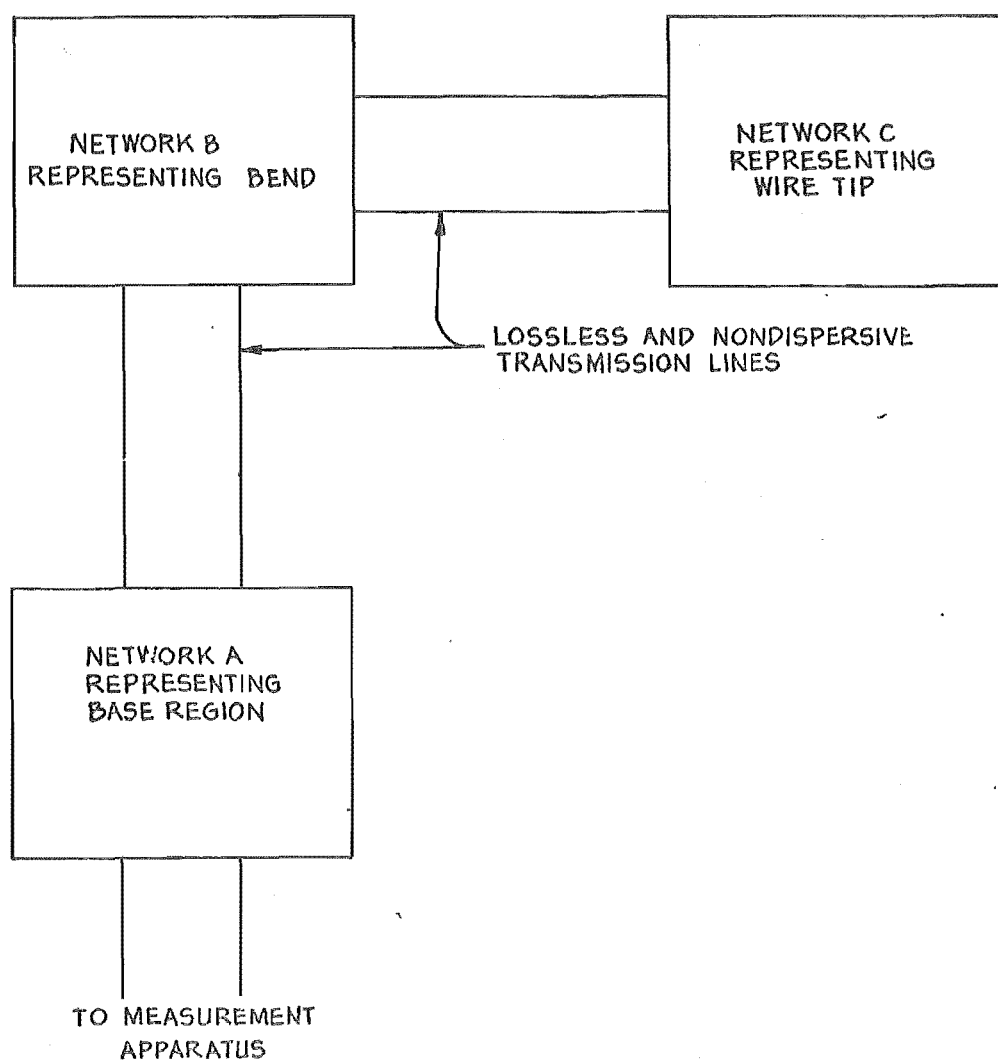


FIGURE 2.9 SIMPLE NETWORK MODEL OF A BENT WIRE ANTENNA

## CHAPTER 3: MEASUREMENT SYSTEMS AND EXPERIMENTAL PROCEDURES

### 3.1 INTRODUCTION

This chapter outlines the design of the driving point and far field measuring systems which were used for all the measurements reported in this thesis. The design procedures essentially follow those of Ross et al. (1966a, 1966b).

The calibration of the standard antenna for measuring the far field transfer functions, and the method of substantiating the far field measurements are described in detail. A hybrid computer was used on-line for measuring the signals. For some of the measurements it was also used to process the measured data. The experimental procedure is given in sufficient detail to enable the experiments to be duplicated. The pulse generators which were used are described later in chapter 4.

It is experimentally convenient for the antennas to be mounted on a ground plane: the measurement apparatus is then shielded from the radiation space, as shown in Fig. 3.1. Ground planes should be made square or rectangular to reduce the effects of reflections from the edges (Kraus 1950, section 15-7). Rectangular ground planes were used for all the measurements reported in this thesis. All cables and components used in the experiments had a characteristic impedance of 50 ohms.

### 3.2 THE DRIVING POINT MEASUREMENT RANGE

The ground plane should be several wavelengths along a side at the lowest measurement frequency if errors caused by



its finite size are to be insignificant (Kraus 1950, section 15-7). Limitations on funds and accommodation space set the size of the ground plane at 1.83 m by 2.44 m (6 ft by 8 ft). It was constructed from two 10 S.W.G. aluminium alloy sheets which were securely fishplate jointed together with counter-sunk head screws spaced 4 cm apart. The antennas were mounted on short sections of 50 ohm air-dielectric coaxial line which ended flush with the surface of the ground plane. These are shown in Fig. 3.2. Two of these mounting sections were spaced 0.61 m apart on the major axis of the ground plane. This meant that the ground plane could also be used for some radiation measurements<sup>1</sup>.

Although the ground plane was limited in size, a careful examination of the reflected pulse response of a 1.5 m long monopole showed that no observable reflections arrived with a time delay corresponding to the return time of propagation of the pulse to the edges of the plane (6 ns). Also, no observable reflections were caused by the join in the plane. Since the noise level of the measuring equipment (including the multitude of ripples which are reflections from the cable connectors and from irregularities along the whole length of the flexible coaxial cables, see section 2.3.3.3) was 34 dB less than the amplitude of the pulse which was reflected from the tip of the monopole when these observations were being made, it was concluded that the ground plane was large enough for making meaningful measurements on antennas whose pulse responses were longer than the return time of propagation of the pulse to the edge of the

---

<sup>1</sup>It was used for a radiation experiment reported later in section 9.4.

plane. The driving point pulse responses of many of the antennas measured lasted more than 20 ns.

The measurement apparatus is shown in Fig. 3.3. The lengths of coaxial cable A and B are set by the required viewing window W. The length C of cable connecting the sampling oscilloscope to the Tee does not affect the viewing window because of the perfect termination at the sampling oscilloscope input, but it should be kept short to minimise loss and dispersion of the signals. The lengths A and B are calculated by considering the arrival times of the first secondary reflections. The pulse upon arriving at the Tee is partially transmitted and partially reflected: the reflection is itself reflected from the pulse generator and arrives back at the Tee as a secondary reflection. Thus

$$\frac{2A}{vc} \gg \frac{2B}{vc} + W \quad (3-1)$$

where v is the velocity factor of the cable and c is the velocity of electromagnetic waves in free space. The reflected pulse response of the antenna arriving at the Tee is also partially reflected and travels the return path to the antenna before arriving back at the Tee as a secondary reflection. Thus

$$\frac{2B}{vc} \gg W \quad (3-2)$$

The required duration of the viewing window is set by the bandwidth of the antennas to be measured (narrow band antennas, which have frequency sensitive frequency responses, have longer driving point pulse responses than have wideband antennas). Assuming that a thin monopole is the most frequency sensitive antenna to be measured, experimental

observations indicate that  $W$  (in ns) should equal the antenna length in centimetres<sup>2</sup>. A viewing window of 30 ns was sufficient for the planned experiments, and, assuming a value for  $v$  of 0.67, eqns (3-1) and (3-2) give an  $A$  of 6.2 m and a  $B$  of 3.1 m. The ground plane was kept further than 4.5 m from reflecting objects in the laboratory so that unwanted reflections would not arrive within the viewing window.

If the 3-point scanning method (section 2.3.6) is used to measure the signals then a reference slope which is independent of the reflected signal can be arranged by using a 4-port cross connector instead of a Tee, and connecting an open ended length of GR-874-A2 coaxial cable to the other port. The length of this cable is chosen so that the reflection of the test pulse from the end arrives immediately before the end of the viewing window. It cannot be timed to arrive before the viewing window because secondary reflections in the shorter length of cable would arrive within the viewing window. A GR-874-TPDL power divider and a Tee may be used in the absence of a cross connector.

The oscilloscope is triggered by the first arrival of the test pulse, and the time position control on a Tektronix 1S1 sampling unit has enough range to display the pulse response with the cable lengths calculated above. External triggering would be necessary if longer cables had been used.

---

<sup>2</sup>If only a part of the pulse response is of interest (e.g. see sections 2.5 and 3.3) then  $W$  can be made shorter.

### 3.2.1 Experimental Procedure for Measuring Reflection Coefficients

#### 3.2.1.1 Measuring the test pulse

The lengths A, B and C of coaxial cable have significant loss and dispersion within the measurement bandwidth and it is necessary to remove these effects from the measurement<sup>3</sup>. Let the transmission loss and dispersion of the cable be represented by  $\alpha(f)$  per unit length. When measuring the driving point response of the antenna, what is actually being received at the input of the sampling oscilloscope is

$$v(t) = F^{-1} \{ U_1(f) \rho(f) A B^2 C \alpha^4(f) \} \quad (3-3)$$

where  $F^{-1}$  denotes the inverse FT, and  $U_1(f)$  is the spectrum of the pulse which is generated at the pulse generator. If the test pulse suffers the same loss before being recorded then the loss terms cancel when  $\rho(f)$  is calculated. The loss is arranged by short circuiting the antenna mount at the surface of the ground plane to make  $\rho(f) = -1$  in eqn(3-3) and recording the reflected pulse as  $-u(t)$ . The measurement interval is then identified (see Appendix 1) and the test pulse is measured. The device used to short circuit the antenna mount is shown in Fig. 3.2.

#### 3.2.1.2 Measuring the pulse response

The short circuit is replaced by the antenna under test and the measurement interval for  $v(t)$  is identified (see Appendix 1).  $v(t)$  is then measured and  $\rho(f)$  is calculated and displayed. Allowance is made for the  $180^\circ$  phase shift

---

<sup>3</sup>GR-874-A2 coaxial cable has a loss of 2.6 dB/30.5 m at 100 MHz and 10.5 dB/30.5 m at 1 GHz.

introduced because of the way  $u(t)$  is measured. Timing shift errors (section 2.3.3.1.3) are eliminated if the time origins of  $u(t)$  and  $v(t)$  are the same. Thus the reference voltage which identifies the time origin (see Appendix 1) must not be altered between measurements.

### 3.3 APPARATUS FOR MEASURING THE CHARACTERISTICS OF BENDS IN WIRE ANTENNAS

A Tektronix 1S2 Time Domain Reflectometer (TDR) and sampling unit was used for measuring the properties of bends in wire antennas. This instrument contains a 50 ps tunnel diode step generator whose output can easily be formed into a very fast pulse (see section 4.4.2). The pulse is about 300 ps long when displayed on the 1S2 sampling oscilloscope (which has a risetime of 90 ps) and is ideal for making measurements on bends in wire antennas because the desired parts of the pulse response (see section 2.5) are easily separated even when moderately short antennas are used (the spatial length of a 300 ps pulse is 9 cm).

The measurement apparatus is shown in Fig. 3.4. The 25 ohm short circuited stub forms the step into a pulse. GR-874 50 ohm coaxial air line is used for all connections to minimise transmission loss and dispersion on the signals. The length of the bent wire antennas was chosen to be about 1 metre, since this was about 10 times the spatial length of the test pulse and allowed satisfactory separation of the desired parts of the pulse response. The viewing window needs only to be long enough so that the part of the pulse response which is the first reflection from the tip of the

antenna is received; 12 ns is sufficient. The output impedance of the tunnel diode step generator is 50 ohms so that the reflection from the stub towards the generator is completely absorbed. However, a small but significant reflection was observed from the sampling head of the oscilloscope (which was a signal feedthrough channel). This was shifted outside the viewing window by calculating the line lengths A and B in exactly the same way as those for the driving point measurement range (section 3.2), giving 1.82 m for A and 3.64 m for B. The 1 m long antennas were near resonance at the local TV frequency ( $\approx 66$  MHz) and quite severe interference was experienced. This was minimised by separating the short circuited stub and the sampling head by a wavelength at the TV centre frequency (a line stretcher was adjusted for minimum interference). The length B was increased to about 4.5 m. Measurements were usually made after TV close-down to avoid interference, but minimising the interference in the way described here enabled the equipment to be set up during the day.

The bend in the wire must be positioned so that multiple reflections of the pulse travelling on the wire do not overlap the segments of the pulse response which are of interest. Fig. 3.5 shows the required positions of the bend.

### 3.3.1 Experimental Procedure for Measuring Bends

The amplitude of the test pulse is low (120 mv) and the 3-point scanning method (section 2.3.6) was used to measure the pulse responses. The leading edge of the pulse which is reflected from the base of the wire is essentially straight

near its midpoint, and this was used as a known reference slope. The slope was measured from the oscilloscope screen in the way described in section 2.3.6.

The pulse response of the straight wire is displayed, the measurement interval is identified as the pulse response truncated after the first reflection from the tip, and this part of the pulse response is measured. The straight wire is then replaced by the bent wire, which is made exactly the same length as the straight wire to eliminate timing shift errors, and the same part of its pulse response is measured. No equipment adjustments are made between measurements. The procedures used to compute the bend transfer functions are described later in chapter 11.

### 3.4 THE FAR FIELD MEASUREMENT RANGE

The size of the ground plane required for making far field measurements is set by the characteristics of the test pulse. The antennas must be constructed large enough to radiate efficiently within the effective bandwidth of the test pulse, and the separation  $r$  which is required between the transmitting and receiving antennas is then set by the Fraunhofer condition (Montgomery 1947, p900):

$$r = \frac{(D_1 + D_2)^2}{\lambda} \quad (3-4)$$

where  $D_1$  and  $D_2$  are the maximum dimensions of the apertures of the two antennas and  $\lambda$  is the wavelength of the highest significant frequency in the test pulse spectrum. When the antennas are mounted above a ground plane,  $D_1$  and  $D_2$  are the total heights of the antennas and their images. The

measured far field intensity will not be more than 2.5% lower than the true far field intensity if the criterion of eqn(3-4) is observed (Montgomery 1947, p902). The test pulse must then have sufficient amplitude so that measurable signals are received, especially when one of the antennas is a small standard antenna with known  $T(f)$  and  $R(f)$ . The test pulse which was used for making the far field measurements had an amplitude of 50 volts and an effective bandwidth of about 800 MHz. The distance  $r$  was set at 5.5 m. Eqn(3-4) was then satisfied provided the sum of the heights of the antennas was less than 0.72 m, and the frequency was no greater than 800 MHz. This restricts the height to 0.36 m when identical transmitting and receiving antennas are used, but antennas of this size can radiate efficiently down to about 200 MHz. Signal levels ranging between 5 and 30 mv were received when using the standard antenna described in section 3.4.1, and it is demonstrated in section 3.4.3 that this is sufficient to make meaningful measurements. The measured field is made up of the induction field and the radiation field. As the frequency decreases the induction field becomes a greater proportion of the measured field (Silver 1949, section 3.13). The lower frequency limit is set by the requirement that the magnitude of the induction field should be less than 10% of the magnitude of the radiation field: this is true when  $r = 5.5$  m if the frequency is greater than 100 MHz.

The ground plane measured 10 m by 4 m, and was made from wire mesh, with a 1.25 cm mesh, because it was inexpensive. Each sheet of the mesh was dip galvanised which



ensured uniform electrical properties, and the joins between the sheets (which were  $\approx 1$  m wide) were carefully soldered to preserve this uniformity. The mesh was laid on tables and tensioned so that the deviations from a true plane were less than  $\pm 5$  cm or about  $\pm \lambda/8$  at 800 MHz. This was the largest tension which could be applied easily. The antennas were mounted, using the sections shown in Fig. 3.2, at the centre of 60 cm square brass plates which were smoothly and securely clamped at their edges to the mesh. Careful examination of the pulse response of a 1.5 m long monopole showed that no observable reflections were caused by these joins. Also, no reflections were observed from the joins in the wire mesh. The antenna mounting sections were made the same electrical length as a standard GR-874 fixed attenuator. The transmitted pulse could then be measured with the same time origin as the received signals by connecting the feed cables together through two attenuators.

The measurement apparatus is shown in Fig. 3.6. The viewing window is set by the arrival time of reflections from the environment and secondary reflections due to the length  $A$  of coaxial cable. The antenna range was about 6 m from the steelwork of the laboratory building, which earlier tests had shown to cause significant reflections. This set the maximum viewing window at about 40 ns. Secondary reflections caused by the test pulse travelling in the length  $A$  of coaxial cable radiate at  $t = 2A/v_c$  later than the primary signal, and a length  $A$  of 4.1 m is required to give the 40 ns viewing window. The length actually used was 4.5 m, and although the length of cable connecting the sampling oscilloscope to the receiving antenna does not affect the viewing

window, it was physically convenient to use another 4.5 m length.

The sampling oscilloscope was triggered by a signal from the pulse generator (see Fig. 4.7) which was delayed by 8 m of general purpose coaxial cable (loss was unimportant). The test pulse  $u(t)$ , shown in Fig. 3.7 together with its spectrum  $U(f)$ , was measured after travelling the 9 m of coaxial line. The effective bandwidth is about 600 MHz. Consequently the far field responses presented later in chapter 9 are only continued out to 600 MHz.

### 3.4.1 Calibrating the Standard Antenna

A short monopole (operating below its fundamental resonance over the measurement bandwidth) was chosen as a standard antenna because its input impedance can be computed easily (Jasik 1961, eqn 3-1). The standard monopole had a length of 7.6 cm and a diameter of 0.32 cm. Fig. 3.8 shows the equivalent circuits used for calculating the transmission and reception transfer functions  $T_S(f)$  and  $R_S(f)$  respectively, of the standard monopole. The source impedance is set at 50 ohms because this was the characteristic impedance of the coaxial lines feeding the antennas. The radiated electric field intensity measured at the surface of the ground plane a distance  $r$  metres from a short monopole is (Jasik 1961, section 2.1)

$$E_1(f) = \frac{j \eta I_0(f) h_e(f) e^{-jkr}}{\lambda r} \quad (3-5)$$

where  $I_0(f)$  and  $h_e(f)$  are defined in Fig. 3.8,  $\eta = 120\pi$  ohms is the characteristic impedance of free space, and the time dependence  $e^{j\omega t}$  is understood. From the equivalent circuit

for transmission

$$I_o(f) = \frac{V_g(f)}{50 + Z(f)} \quad (3-6)$$

and

$$V_g(f) = 2U(f) \quad (3-7)$$

since  $U(f)$  is measured when the antenna terminals are terminated in 50 ohms. Substituting eqns (3-6) and (3-7) into eqn(3-5), and using  $\lambda = c/f$

$$E_1(f) = \frac{j 240\pi f h_e(f) U(f) e^{-jkr}}{c[50 + Z(f)]r}, \quad (3-8)$$

and, by comparison with eqn(2-20)

$$T_S(f) = \frac{j 240\pi f h_e(f)}{c[50 + Z(f)]}. \quad (3-9)$$

When the monopole is receiving

$$V_L(f) = 50 I_L(f) = \frac{50 h_e(f) E_2(f)}{50 + Z(f)}, \quad (3-10)$$

and, by comparison with eqn(2-21)

$$R_S(f) = \frac{50 h_e(f)}{50 + Z(f)}. \quad (3-11)$$

$Z(f)$  was taken from Jasik (1961, eqn 3-1) and  $h_e(f)$  from Jordan (1950, p336).  $Z(f)$  was also verified at spot frequencies using a "width of minimum" slotted line measurement method (Montgomery 1947, section 8.8), and the correspondence between the computed and measured values of the resistance and reactance of the monopole are shown in Fig. 3.9. A deterioration of the slotted line measurements at the lower frequencies is noticed, and this is probably due to reflections from objects in the room and to the finite

size of the ground plane. The  $T_S(f)$  and  $R_S(f)$  calculated from eqns (3-9) and (3-11) are shown in Fig. 3.10.

Straightforward manipulation of eqns (2-20) and (2-21) gives

$$T(f) = \frac{r V(f)}{R_S(f) U(f)} ; \quad (3-12)$$

$$R(f) = \frac{r V(f)}{T_S(f) U(f)} , \quad (3-13)$$

where the phase factor  $e^{-jkr}$  is removed because the time origin for  $v(t)$  is shifted to remove the propagation delay. Eqns (3-12) and (3-13) were incorporated in a modified version of the on-line hybrid computer program of Appendix 1 which has values of  $T_S(f)$  and  $R_S(f)$  stored in the digital computer memory at frequency intervals of 10 MHz.

### 3.4.2 Experimental Procedure for Measuring Far Field Transfer Functions

#### 3.4.2.1 Measuring the test pulse

The test pulse  $u(t)$  is recorded after travelling the 9 m of coaxial cables to remove the effects of their dispersion and loss from the measurements. The cables are disconnected from the antenna mounts and connected together through two GR-874 20 dB fixed attenuators to reduce the pulse amplitude to a level acceptable to the input of the sampling oscilloscope. The measurable duration of  $u(t)$  is identified (see Appendix 1) and  $u(t)$  is measured.

#### 3.4.2.2 Measuring the pulse response

The cables are connected to the antenna mounts, the antennas under test are mounted, and the measurable duration of the received signal  $v(t)$  is identified (see Appendix 1).

To eliminate timing shift errors (section 2.3.3.1.3) the reference voltage which identifies the time origin of  $u(t)$  is not altered. The received signal is measured and the transfer function is calculated and displayed. When one of the antennas is the standard monopole the program for computing  $T(f)$  and  $R(f)$  (from eqns 3-12 and 3-13) is used. When two identical antennas are measured the program for computing  $H(f)$  (from eqn 2-9a) is used. Allowance is made for the 40 dB loss introduced when measuring  $u(t)$ . Allowance is also made for the propagation delay of the signals travelling the distance  $r = 5.5$  m between the two antennas.

It was found when making measurements that it was more convenient to use different time and amplitude scales when measuring  $u(t)$  and  $v(t)$ . These equipment adjustments mean that the common time origin is lost. The beginning of both signals was always well defined and with care could be identified within about  $\pm 100$  ps for  $v(t)$ , which was always displayed with a more compressed time scale than  $u(t)$  and was consequently more difficult to identify accurately. An error in the relative time origins of  $u(t)$  and  $v(t)$  causes an error in the phase characteristic which increases linearly with increasing frequency (section 2.3.3.1.3). The error at 600 MHz caused by a 100 ps shift is about  $23^\circ$ . Since the primary purpose of the measurements was to make observations of flatness of modulus and linearity of phase (see chapter 8), the actual average slope of the phase/frequency characteristic is immaterial. So it was decided to accept the linear phase error.

It was experimentally convenient for the standard antenna always to receive. So,  $R(f)$  for the test antenna was calculated using reciprocity.

### 3.4.3 Checking the Measurement Accuracy

The experimental system was checked by making measurements on a monopole with a height of 0.45 m and a diameter of 0.32 cm. The results are shown in Fig. 3.11. Observe the peaks at 150 MHz and 450 MHz. These correspond to the resonances which occur when the length of the monopole is one quarter-wavelength and three quarter-wavelengths. The accuracy of the experimental procedure was estimated by comparing the amplitudes of these two peaks with the theoretical values which are calculated in Appendix 3. Table 3.1 shows the comparison, which is within 5% except for  $|R(f)|$  at 450 MHz. This suggests that the computation of  $T_S(f)$  is inaccurate (it has not been found possible to make any improvement however).

Frequency (MHz)	T(f)		R(f)	
	Measured	Theory	Measured	Theory
150	$1.4/100^\circ$	$1.41/90^\circ$	$0.16/10^\circ$	$0.168/0^\circ$
450	$1.15/-70^\circ$	$1.165/-90^\circ$	$0.053/-150^\circ$	$0.0464/180^\circ$

Table 3.1: Comparison of measured and theoretical  $T(f)$  and  $R(f)$  for a 0.45 m long, 0.32 cm diameter monopole.

There is an appreciable phase error at the second resonant frequency, 450 MHz. This is due to the (unimportant) linear phase error already discussed in section 3.4.2.2. Notice

that the accuracy deteriorates as the frequency increases: this is due to the test pulse energy falling off as the frequency increases.

Fig. 3.12 shows  $H(f)$  computed (using eqn 2-9a) from the signal transmitted between two identical monopoles together with values of  $H(f)$  calculated using eqn(2-22) from the results shown in Fig. 3.11. These results also support the overall accuracy estimate of 5%. The computations of  $H(f)$  are seen to deteriorate above about 550 MHz because the test pulse has little energy above 550 MHz (see Fig. 3.7).

These test measurements demonstrate that  $T(f)$  and  $R(f)$  can be obtained over about a 6:1 bandwidth with this measuring system. The accuracy might be improved by using a capacitive "top-hat" on the standard monopole to increase  $h_e(f)$ , thus increasing the received signal amplitude, but the measurement bandwidth is still limited by the very small values of  $T_S(f)$  and  $R_S(f)$  at low frequencies.

Increased measurement bandwidth could be obtained by using a matched monopole type (MTT) of antenna (Fenster and Ross, 1968) as a standard. The reflection of the input signal from the tip of the monopole is suppressed by a "top-hat" having a resistance of 377 ohms/square, which makes the monopole appear infinitely long over a very wide frequency range (2.5 decades is claimed)<sup>4</sup>.  $Z(f)$  in eqns (3-9) and (3-11) is then approximately equal to the input impedance of an infinite monopole, which is given in Fig. 5.3. Thus the frequency sensitivity of  $T_S(f)$  and  $R_S(f)$  is reduced allowing measurements to be made over a wider bandwidth. The lower

---

<sup>4</sup>377 =  $120\pi$  ohms is the characteristic impedance of free space.

frequency limit is set by the size of the resistive "top-hat".  $Z(f)$  and  $h_e(f)$  could be determined by measurement, but the problem remains of manufacturing the "top-hat", which is a sub-micron thickness metallic film deposited on a glass substrate (this is not within our technological capacity in New Zealand). The idea of providing the matched termination at the base (Ross, 1967a) by matching the surge impedance at the base with a tapered line transformer is of no use at these frequencies because the taper would have to be several wavelengths long at the lowest measurement frequency for an acceptable match (Moreno 1948, chapter 3). This is impractical at 100 MHz. Also, the match is only approximate, as shown later in section 5.4.2.

### 3.5 CALIBRATING THE SAMPLING OSCILLOSCOPE

The external horizontal deflection factor for the Tektronix 1S1 sampling unit is quoted by the manufacturer as 1 volt/cm  $\pm 4\%$ . The calibration accuracy of the frequency scales depends upon accurate sample timing (see section 2.3.1). Consequently it is necessary to accurately determine the deflection factor for the particular sampling unit being used. The scale factor is then included in the analogue computer patching (see Appendix 1).

The deflection factor is determined by using the driving point measurement apparatus with a known delay line replacing the antenna and antenna mount. GR-874 50 ohm air line was



used as a standard<sup>5</sup>. The sampling oscilloscope is externally scanned with a manually variable voltage, and the voltage required to position the sampling gate to the peak of the pulse reflected from the open end of the cable is measured both with and without the delay line connected. The deflection factor (in volts/cm) is then calculated from a knowledge of the particular time scale being used and the return propagation time of the delay line. The peak of the pulse can be identified accurately by monitoring the vertical output of the oscilloscope with a voltmeter.

While the deflection factor is not necessarily the same for each time scale, the variations were found to be less than 1% for the commonly used time scales on the particular sampling units used. Consequently a mean value was taken.

---

<sup>5</sup>The propagation delays for GR-874 50 ohm coaxial air line are specified as:

30 cm line, delay = 1.0036 ns  $\pm$  0.0018 ns;

20 cm line, delay = 0.6698 ns  $\pm$  0.0018 ns;

10 cm line, delay = 0.3362 ns  $\pm$  0.0018 ns.

The required delay is obtained by connecting the appropriate pieces in series.

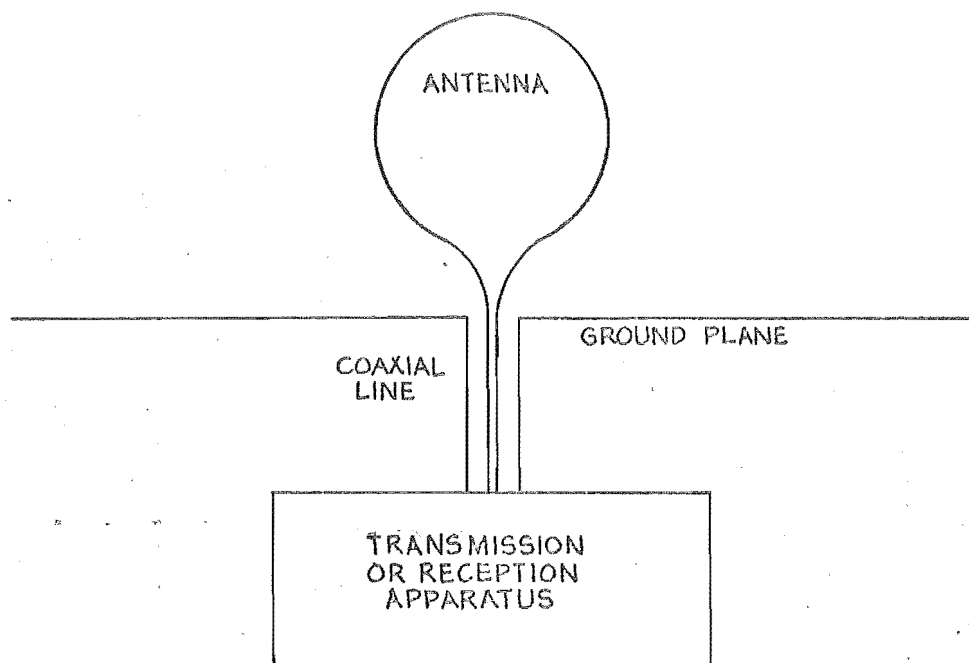


FIGURE 3-1: RELATIVE ARRANGEMENT OF ANTENNA, GROUND PLANE AND MEASUREMENT APPARATUS.

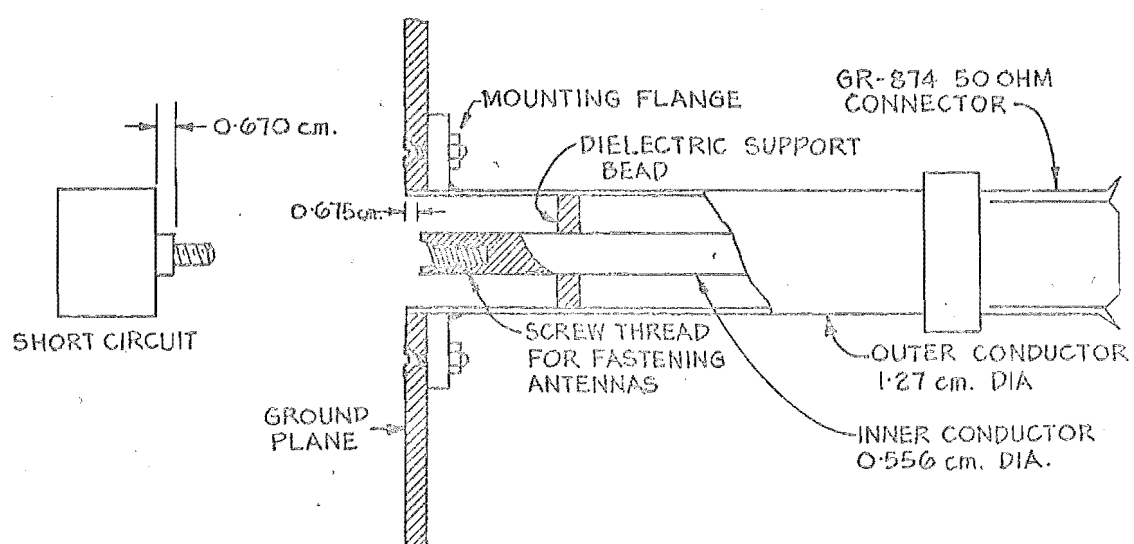


FIGURE 3-2: ANTENNA MOUNTING SECTION WITH SHORT CIRCUIT.

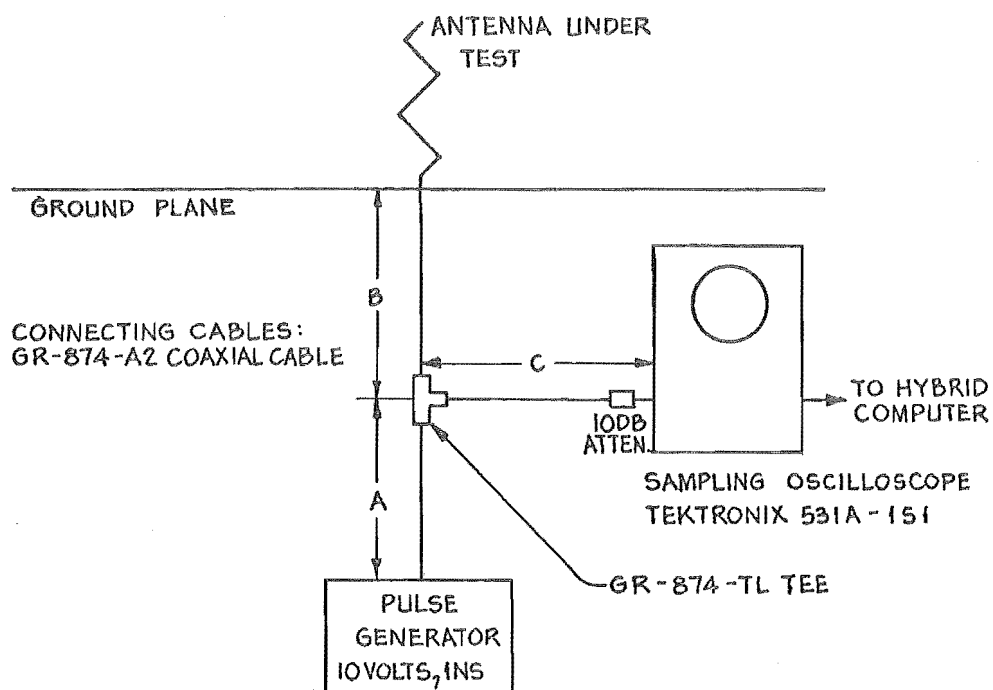


FIGURE 3-3 : DRIVING POINT MEASUREMENT APPARATUS

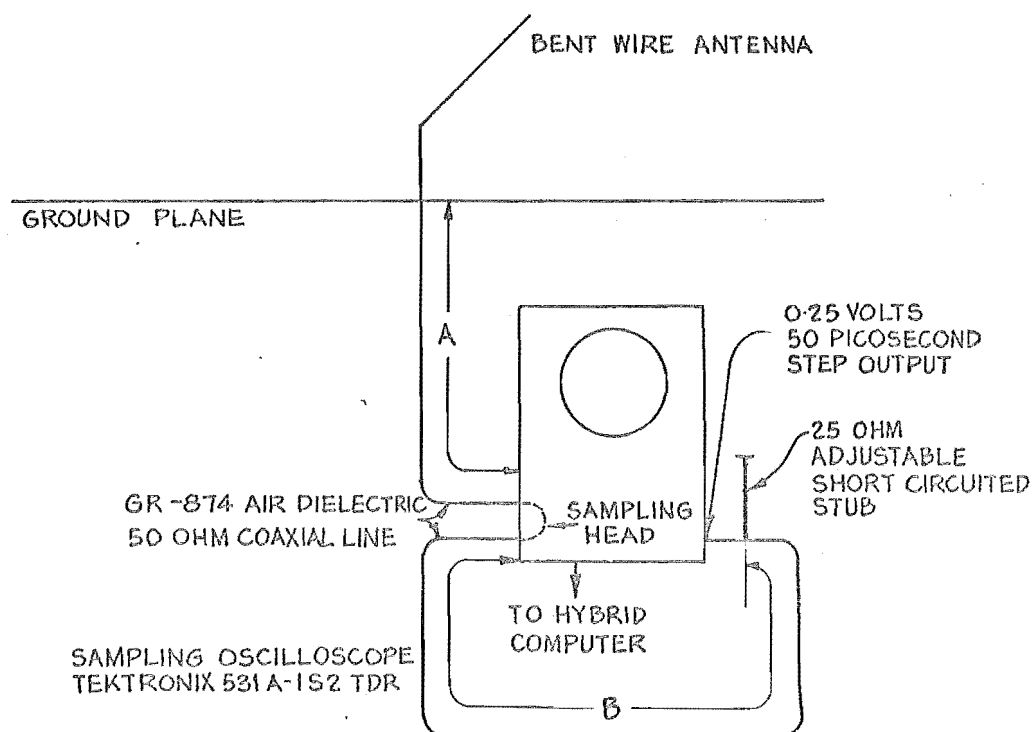


FIGURE 3-4 : APPARATUS FOR MEASURING REFLECTIONS OF NARROW PULSES FROM BENT WIRE ANTENNAS

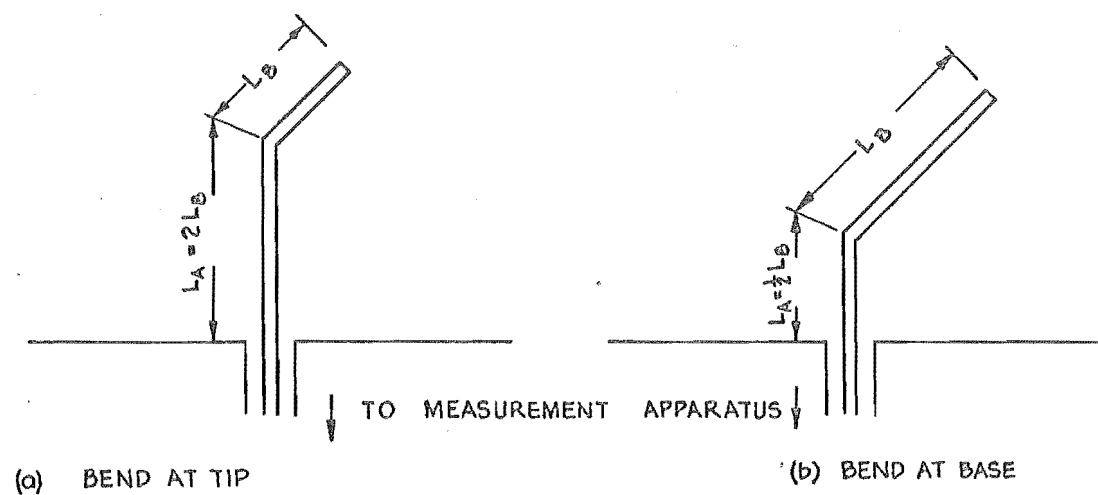


FIGURE 3.5 : POSITIONS OF BEND IN WIRE ANTENNA

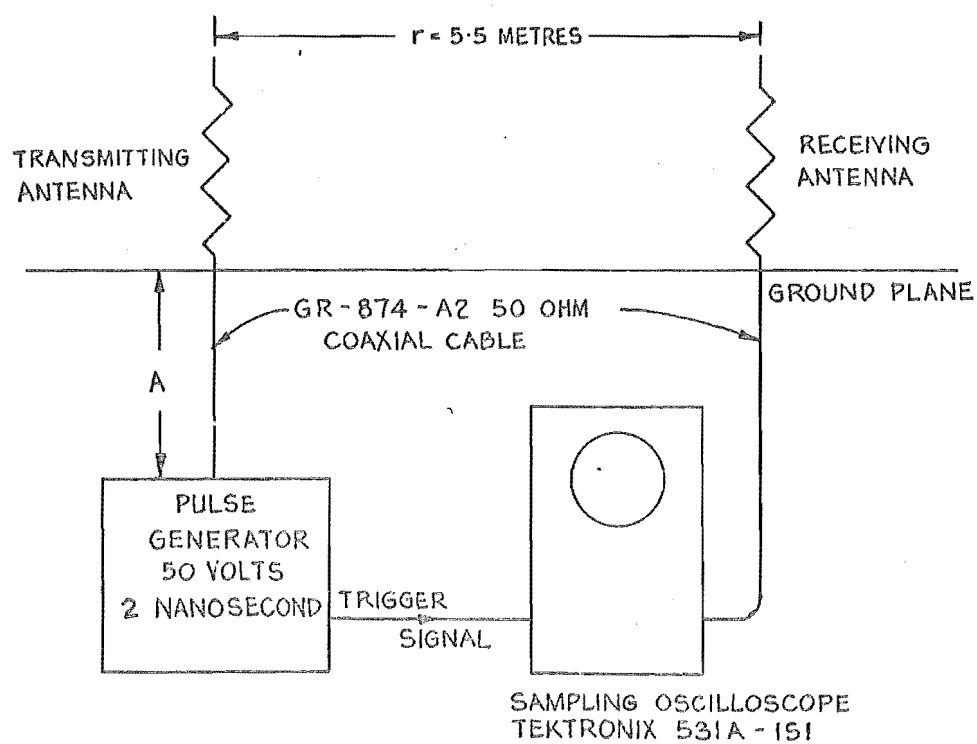


FIGURE 3.6 : FAR FIELD MEASUREMENT APPARATUS

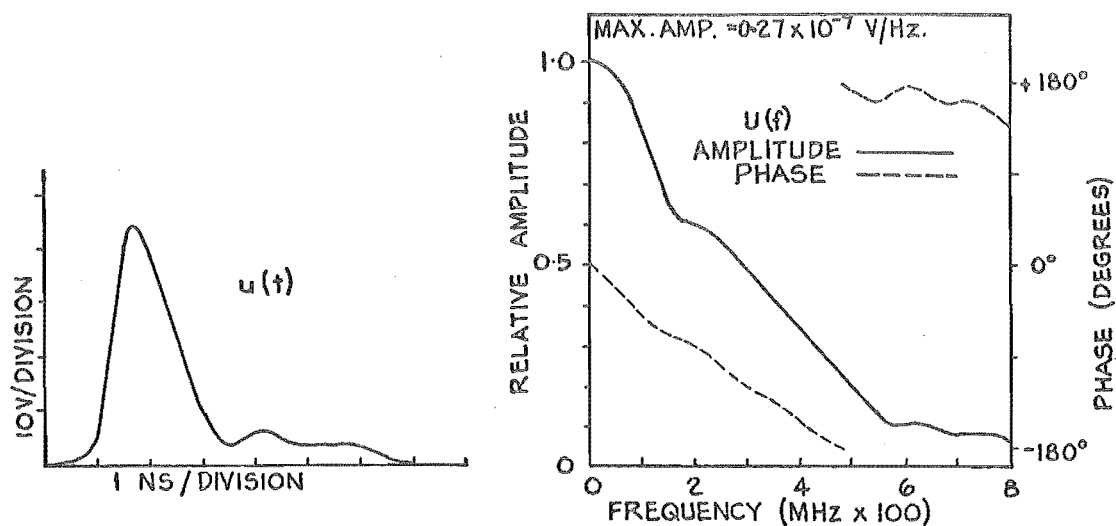
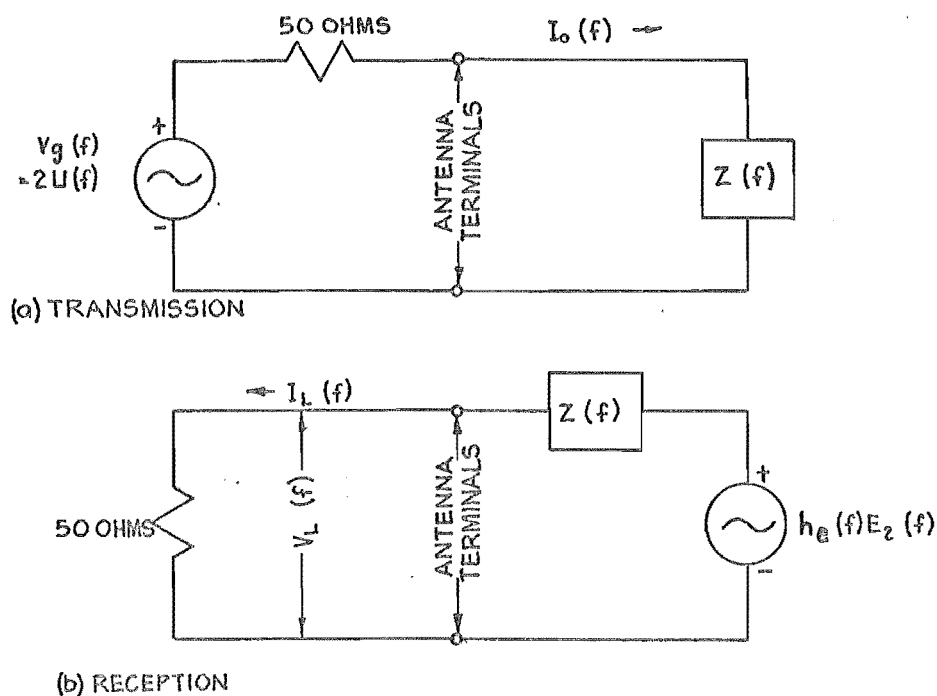


FIGURE 3-7: FARFIELD MEASUREMENT TEST PULSE  $u(t)$  AND SPECTRUM  $U(f)$  MEASURED AFTER TRAVELLING 9 METRES OF COAXIAL CABLE



- $Z(f)$  = DRIVING POINT IMPEDANCE OF MONOPOLE.  
 $I_0(f)$  = CURRENT IMPRESSED ON MONOPOLE AT DRIVING POINT.  
 $V_g(f)$  = THEVENIN GENERATOR VOLTAGE.  
 $I_L(f)$  = CURRENT FLOWING IN LOAD.  
 $V_L(f)$  = VOLTAGE MEASURED ACROSS LOAD.  
 $h_0(f)$  = EFFECTIVE HEIGHT OF MONOPOLE.  
 $E_2(f)$  = ELECTRIC FIELD INTENSITY INCIDENT UPON MONOPOLE.

FIGURE 3-8: TRANSMISSION AND RECEPTION EQUIVALENT CIRCUITS IN FREQUENCY DOMAIN FOR STANDARD MONOPOLE ANTENNA.

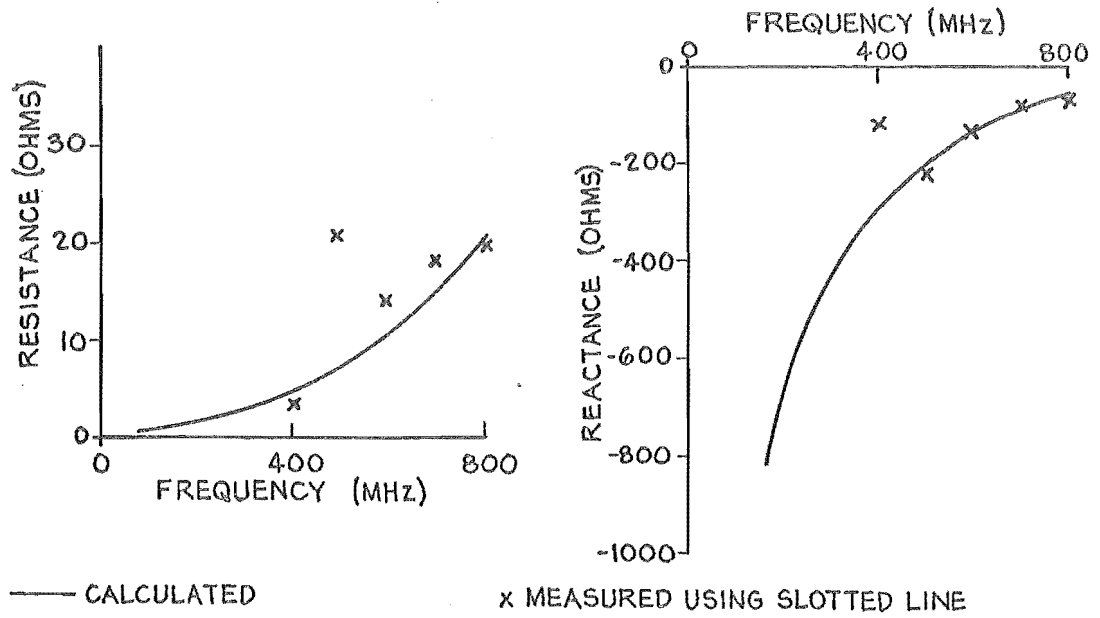


FIGURE 3.9: RESISTANCE AND REACTANCE OF STANDARD MONOPOLE

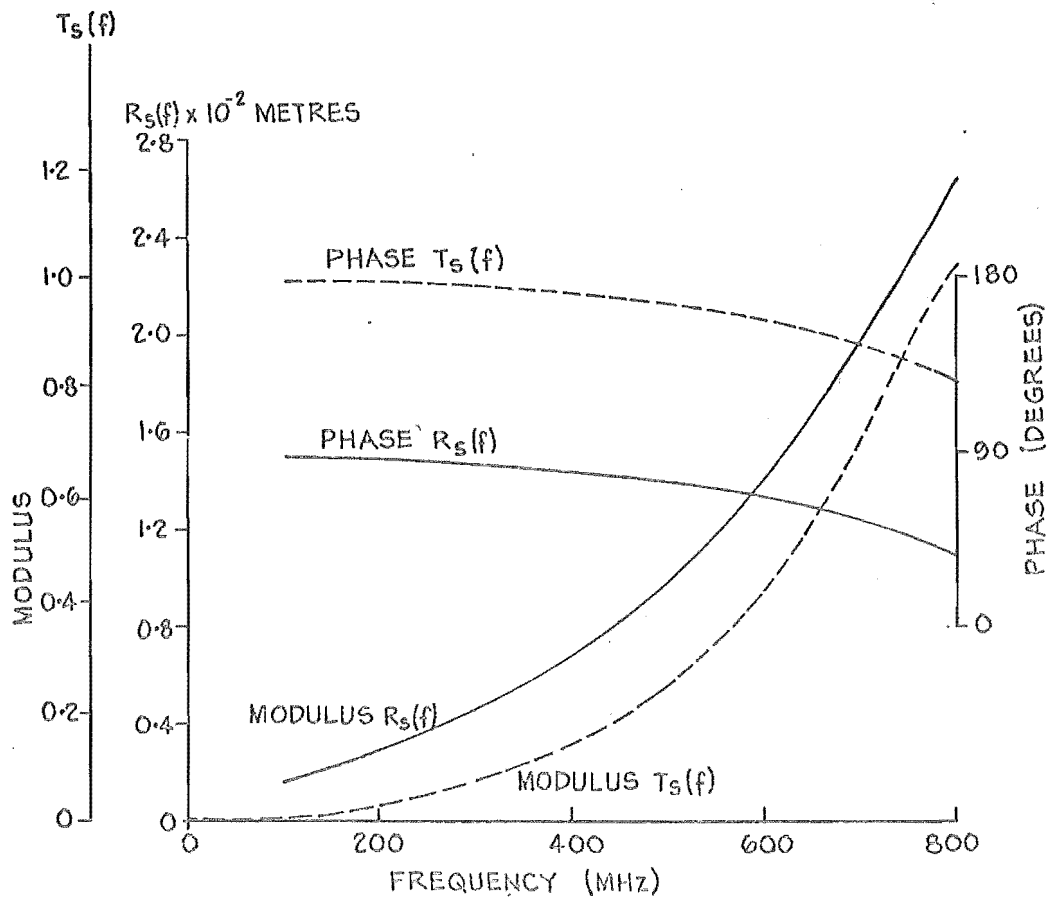
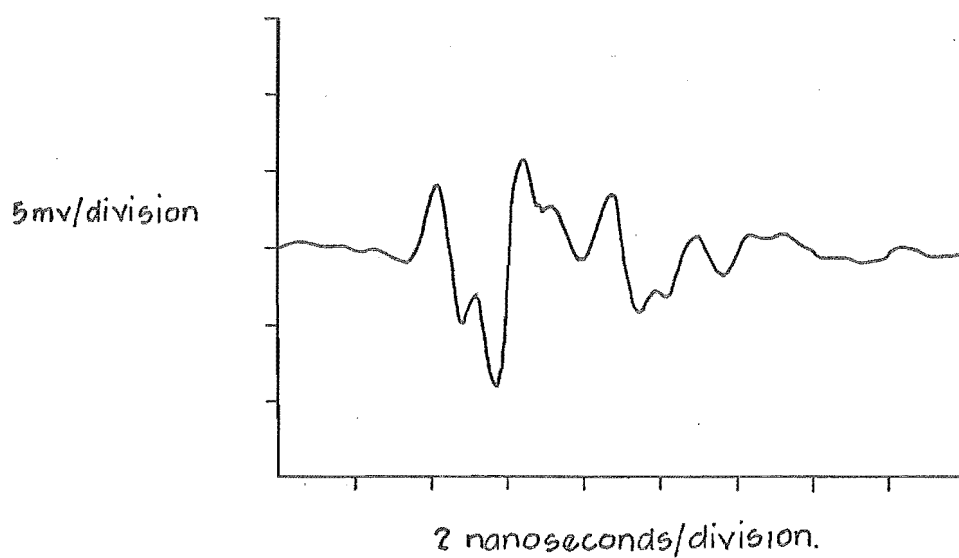
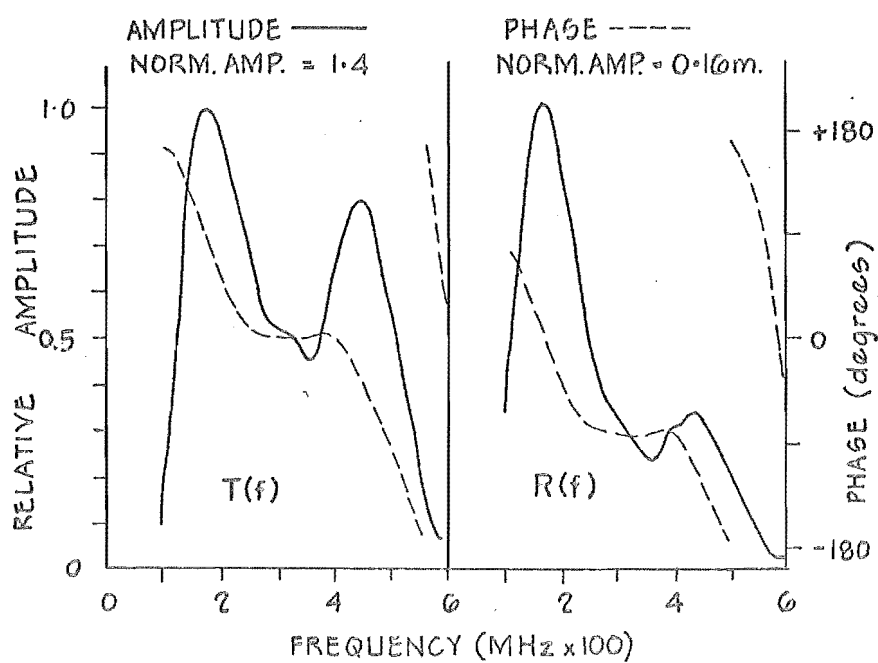
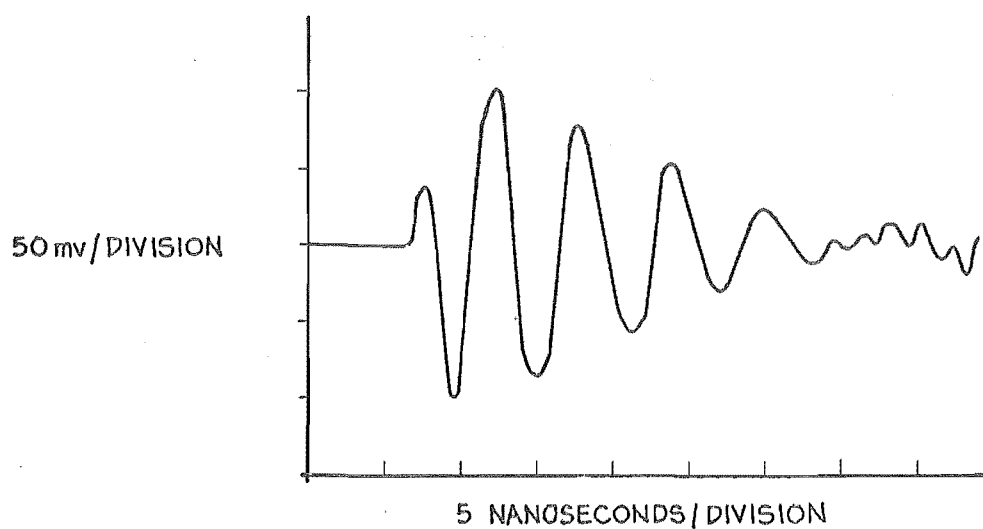


FIGURE 3.10: TRANSMISSION AND RECEPTION TRANSFER FUNCTIONS FOR STANDARD MONOPOLE ANTENNA

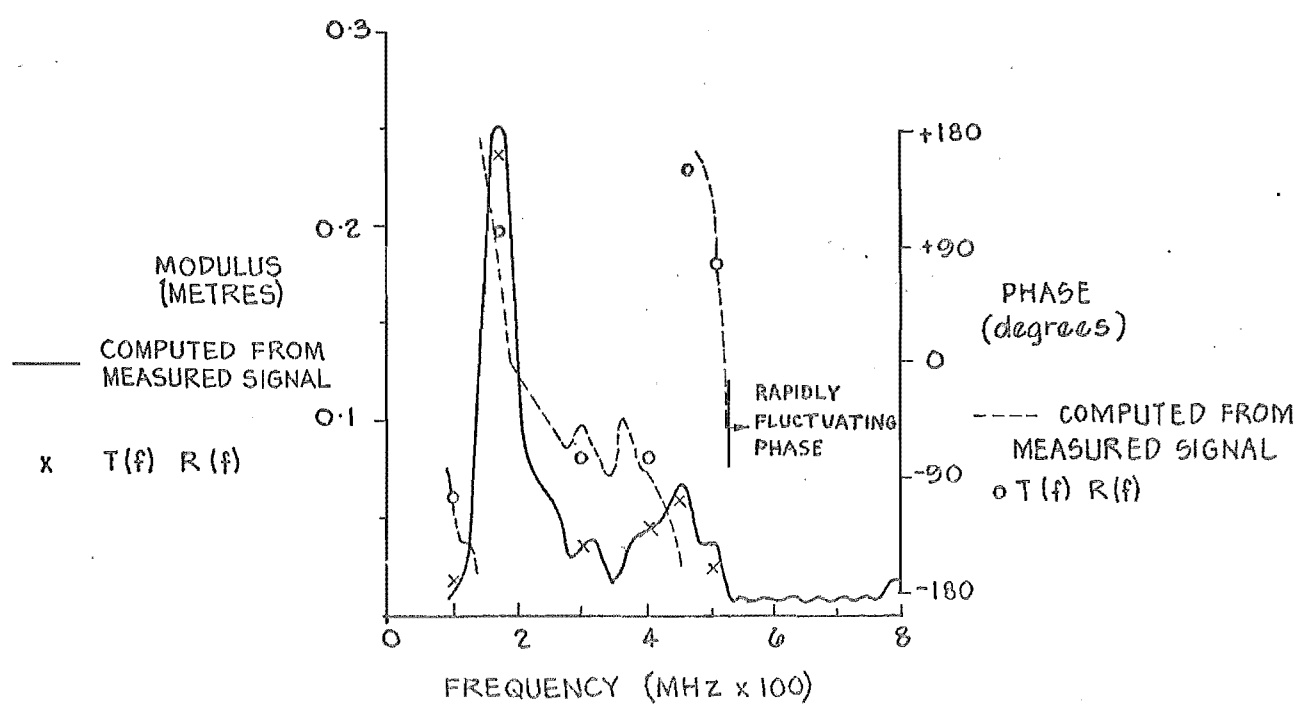


(a) RECEIVED SIGNAL.

(b) COMPUTED TRANSMISSION AND RECEPTION  
TRANSFER FUNCTIONSFIGURE 3.11. FAR FIELD RESPONSES OF 0.45m LONG  
0.32 cm. DIAMETER MONOPOLE.



(a) RECEIVED SIGNAL



(b) SYSTEM TRANSFER FUNCTION COMPUTED IN TWO WAYS

FIGURE 3.12: SYSTEM RESPONSES FOR TWO 0.45 METRES LONG, 0.32 cm. DIA. MONOPOLES.



## CHAPTER 4: GENERATING HIGH SPEED SIGNALS

### 4.1 INTRODUCTION

When this project commenced the fastest pulse generator in the Electrical Engineering department, University of Canterbury, had a risetime of 10 ns. Baseband pulses with durations as short as 1-2 nanoseconds (ns) were necessary if the experimental apparatus was to be a realistic size<sup>1</sup>. Consequently an experimental program for developing pulse generators was embarked upon.

There are four commonly used methods of generating fast risetime signals: (1) mercury switches, (2) tunnel diodes, (3) step recovery diodes and (4) avalanche transistors. Table 4.1 summarises the characteristics of each method. Mercury switches (which are reed switches with mercury wetted contacts to eliminate the effects of contact bounce) were used by Schmitt (1960), King and Schmitt (1962), Schmitt (1963) and Schmitt et al. (1966). However, the repetition frequency is too low for a flicker free, high resolution sampling oscilloscope display.

A tunnel diode (Pierce 1967, p40) has two stable operating points and switching between them can occur in as short a time as 10 picoseconds (ps). A step generator using a tunnel diode can have a leading edge risetime as fast as 25 ps (the speed of the diode is reduced when it is packaged

---

<sup>1</sup>In this thesis the duration of the pulse is defined to be its width between the points where its amplitude is -20 dB of its peak amplitude. This gives a better idea of whether reflections of the pulse from discontinuities on antennas can be separated in time than does the commonly used definition of pulse duration, which is the width between the half-power (0.707 voltage) points.

in a cavity, Elliot 1969), and can be triggered and reset at GHz rates. However, the step amplitude is only about one quarter-volt. Many sampling oscilloscopes have fast tunnel diode step generators built into them, and these instruments are called Time Domain Reflectometers (TDR's). A Tektronix 1S2 TDR was used for the measurements reported in chapter 11.

Method	Mercury switch	Tunnel diode	Step recovery diode	Avalanche transistor
Output waveform	step* or pulse	step*	step*	step* or pulse
Output voltage	up to 300	0.25	up to 30	up to 50
Repetition frequency	<100Hz	>1GHz	>100MHz	>1MHz
Triggering required	Yes	Yes	Yes	Not necessary
Risetime (picoseconds)	≈100	≈25	≈100	200
Cost	\$1	>\$10	\$20->\$100	<\$1

\*A pulse with a duration longer than the viewing window can be regarded as a step

Table 4.1: Summary of characteristics of common methods of generating high speed signals.

When a forward biased step recovery diode (Giorgis, 1963) (also called a snap diode or a charge storage diode) is

rapidly reverse biased, current continues to flow through the junction until all the stored charge has been swept out. Conduction then ceases abruptly. The turn-off (or recovery) time is (typically) about 100 ps. This characteristic can be used to generate fast steps or pulses from slower input signals (Giorgis 1963, Hu 1963). Step recovery diodes are expensive. The Hewlett Packard 5082-0182 (recovery time 200 ps) costs \$NZ18.75 and the 5082-0183 (recovery time 150 ps) costs \$NZ45.00 (in New Zealand). Devices with higher power ratings cost \$100 or more. Step recovery diodes are used to generate the very narrow pulses required to operate the sampling gates in sampling oscilloscopes.

Junction transistors exhibit a negative resistance region, called the avalanche region, in their common-emitter output characteristics at high collector voltages (Beale et al., 1957). Very high switching speeds, with moderately high output voltages (see Table 4.1) can be obtained by operating a transistor in the avalanche region. Excellent results can be obtained from silicon planar transistors which are marketed as high-speed switches (Magnuson, 1963). Because of the low cost (<\$1) of suitable transistors, and because the characteristics of the output pulses were suitable for the planned measurements, development was confined to avalanche transistor pulse generators. The operation of a transistor in the avalanche mode is briefly described in section 4.2. Many fast pulse generators were constructed, and a selection of these are described in detail in section 4.3.

The output waveforms of some fast-risetime signal generators are step functions (see Table 4.1). The tunnel diode generators built into TDR's are arranged to generate step functions. Narrow pulses were required for the planned experiments, and section 4.4 describes two methods of forming step functions into narrow pulses.

#### 4.2 AVALANCHE MODE SWITCHING

The physics of common-emitter avalanche breakdown in transistors is complicated, and a simplified explanation, which is sufficient to understand the operation of a simple pulse generator, is given here. A complete explanation of avalanche breakdown is given by Thornton et al. (1966, chapter 1).

There are two possible modes of operation, (a) punch through mode and (b) non-punch through mode, which depend upon the characteristics of the transistor used. Discussions of both modes, together with practical circuits, are given by Beale et al. (1957) and Seeds (1960). Avalanche circuit design is also published by Motorola (1963, chapter 9).

Relaxation oscillators which generate narrow pulses (about 1 ns) with repetition rates up to several MHz can be constructed from transistors which operate in either mode (a) or mode (b). Triggered pulse generators can also be constructed from transistors which operate in either mode provided collector triggering is used (Seeds, 1960). Base triggering is only suitable for transistors which operate in mode (b). Silicon planar transistors are manufactured by a diffusion process: hence they usually operate in mode (b)

(Thornton et al. 1966, chapter 1; Magnuson 1963).

Fig. 4.1 shows the common-emitter collector characteristic for a transistor plotted to high voltage and Fig. 4.2 is a schematic of an avalanche relaxation oscillator which operates in mode (b) (this means that the punch through voltage, which is the collector voltage at which the base width becomes zero, is greater than the avalanche voltage, so that breakdown occurs at the avalanche voltage). The base-emitter junction is reverse biased by  $-V_b$  and the reverse base current which flows is  $-I_b$ . On applying a voltage  $+V_{cc}$  to the circuit the collector capacitor  $C_c$  charges through  $R_c$  towards  $V_{cc}$  and an increasing collector-base leakage current flows which assists  $-I_b$  and raises the potential of the base. When the avalanche voltage is reached the collector-base current increases rapidly, the rise in base potential brings the emitter into conduction and a pulse of current flows through the emitter as  $C_c$  suddenly discharges to  $V_{min}$ .  $V_{min}$  is lower than  $V_s$  (see Fig. 4.1) because the collector voltage continues to fall as charge which is stored in the base of the transistor at peak current diffuses out:  $V_{min}$  may be as low as zero. The time taken for the stored charge to completely diffuse out of the base is often several times the pulse risetime, and gives the pulse a "tail". A voltage pulse is obtained by sampling the discharge current with a small value resistor in series with either the capacitor or the emitter, depending on the pulse polarity required. A pulse amplitude of tens of volts into 50 ohms with a risetime of 500 ps is typical of a single transistor. The fastest switching times are obtained when

the avalanche voltage is close to the punch through voltage (Magnuson, 1963) and some transistors give risetimes as fast as 200 ps. The output voltage may be increased to many hundreds of volts by connecting transistors in series (O'Dell, 1969). However, the pulse risetime is increased. The pulse duration may be increased beyond a few nanoseconds by using a charge line instead of a collector capacitor (Magnuson, 1963).

#### 4.3 CONSTRUCTION OF AVALANCHE TRANSISTOR PULSE GENERATORS

##### 4.3.1 Relaxation Oscillators

Many silicon planar transistors were tested in the avalanche mode, and the Fairchild 2N3643 and 2N3646 were found to give particularly good results. Several relaxation oscillators were experimentally developed from the circuit shown in Fig. 4.2, and it was found that the base resistor  $R_b$  could be connected to ground. Thus only a single power supply is required.

Fig. 4.3 shows a pulse generator which uses the 2N3643. The effective bandwidth of the pulse is about 700 MHz, and the tail on the pulse which is caused by stored charge (see section 4.2) is clearly visible. The output impedance when the transistor is on is very low. No attempt was made to make the output impedance exactly 50 ohms when the transistor is off ( so that no secondary reflections are caused by signals being reflected from the pulse generator; see section 3.2) because the transistor capacitance varies with the amplitude of any signal appearing at the output connector. The 55 ohm resistor is made of four 220 ohm carbon

composition resistors connected in parallel to reduce inductance. Carbon film resistors were avoided because they have a spiral track and are inductive. The value of the 20 pf collector capacitor (which is four 5 pf capacitors connected in parallel) was selected experimentally for optimum pulse shape and duration. The value of the base resistor is not critical and reliable oscillation with a selection of transistors in the circuit was obtained with a value of 6.8K ohms. In stubborn cases its value can be decreased. The pulse amplitude depends upon the particular transistor used, but most were found to give about 20 volts. The transistor which gave the pulse shown in Fig. 4.3 had an uncommonly high avalanche voltage. The pulse repetition frequency was about 400 KHz.

Long duration, fast risetime pulses can be generated by using the circuit shown in Fig. 4.4, which is a modification of one published by Magnuson (1963). The capacitor  $C_1$  is adjusted to obtain the fastest risetime without overshoot and  $C_2$  is adjusted to obtain the flattest pulse top. The output pulse shown in Fig. 4.4 was obtained with a charge line length of about 2.75 m. Lower repetition frequencies must be used when generating long pulses to prevent excess power dissipation in the transistor: the pulse repetition frequency for the generator shown in Fig. 4.4 was 25 KHz.

Greater switching speed is obtainable from the 2N3646, and Fig. 4.5 shows a pulse generator with an effective bandwidth greater than 1 GHz. The output pulse shown in Fig. 4.5 was measured on a Tektronix 1S1 sampling unit (risetime  $\approx 350$  ps) so it is likely that this pulse is even faster than

pictured<sup>2</sup>. No optimum value could be found for the collector capacitor C, so it was made adjustable thus allowing the pulse amplitude and duration to be altered (see Fig. 4.5). The emitter resistor was decreased to 25 ohms to fully exploit the transistors speed. The pulse repetition frequency depends upon C, and is about 3 MHz when  $C = 2$  pf. Ten transistors were tried in this circuit (with  $C = 2$  pf), and pulse amplitudes ranging from 12.5 to 20 volts were obtained. The mean was 15 volts. This pulse generator was used for most of the driving point measurements reported in this thesis.

Both the pulse generators shown in Figs 4.3 and 4.5 were constructed inside a metal cavity at the end of a section of air dielectric coaxial line, and photographs of the mechanical layout are shown in Fig. 4.6. The small size of the generators is apparent from the GR-874 coaxial connectors.

Fig. 4.7 shows the high amplitude pulse generator which was used for making the far field measurements. The high amplitude was obtained at the expense of risetime by using a high value emitter resistor. The collector capacitor then discharges into the coaxial cable (the 470 ohm resistor is necessary to start the discharge). Two 27 K ohm resistors attenuate the output pulse to provide a trigger signal for the sampling oscilloscope (the capacitance across a single resistor prevents sufficient attenuation).

---

<sup>2</sup>When the Tektronix 1S2 sampling unit became available, the risetime of this pulse generator was found to be faster than 200 ps.



### 4.3.2 A Triggered Pulse Generator

The circuit of a pulse generator which can be triggered is given in Fig. 4.8. Reliable triggering is effected by a positive trigger pulse with a 5 ns risetime and an amplitude of 2-20 volts.

## 4.4 PULSE FORMING

### 4.4.1 Differentiation

A step function can be formed into a pulse by differentiating it. A simple differentiator is shown in Fig. 4.9 together with its implementation in coaxial line. As an example the pulse shown in Fig. 4.10 is formed by differentiating the leading edge of the pulse shown in Fig. 4.4.

### 4.4.2 Stubs

A step may also be formed into a pulse by placing a short-circuited stub in parallel with the line (Ross 1965, 1967b, 1969b). The characteristic impedance of the stub is half that of the line. The step response of the resulting network, which is depicted in Fig. 4.11, is a pulse whose duration equals twice the propagation time of the step down the stub. Fig. 4.12 shows a pulse formed from the 50 ps risetime step output of a Tektronix 1S2 TDR. This pulse was used for the bent wire measurements reported in chapter 11.

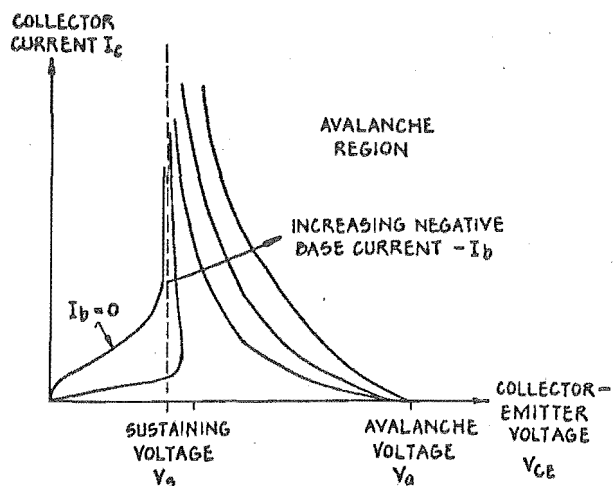


FIGURE 4.1. TRANSISTOR COMMON-EMITTER COLLECTOR CHARACTERISTICS.

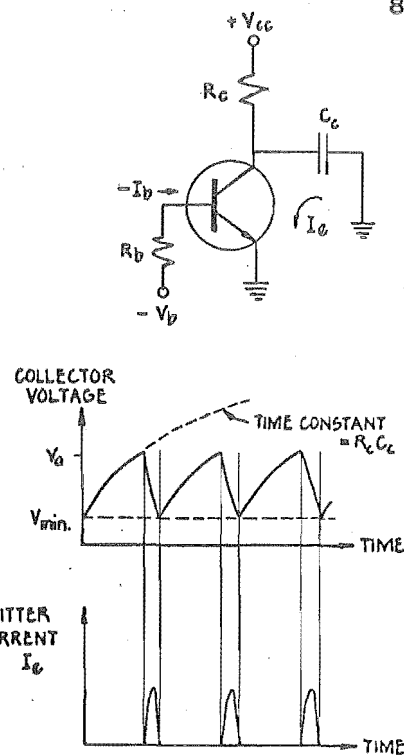
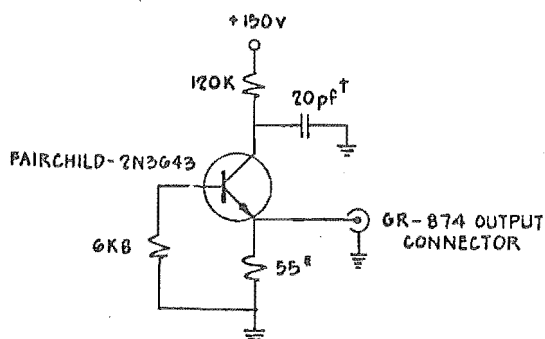
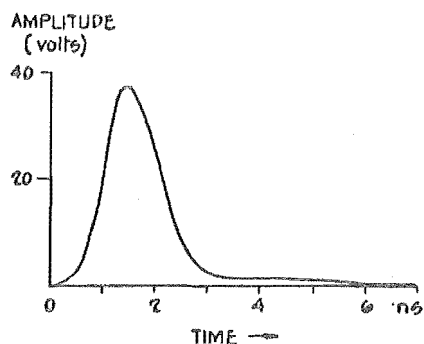


FIGURE 4.2. AN AVALANCHE TRANSISTOR RELAXATION OSCILLATOR

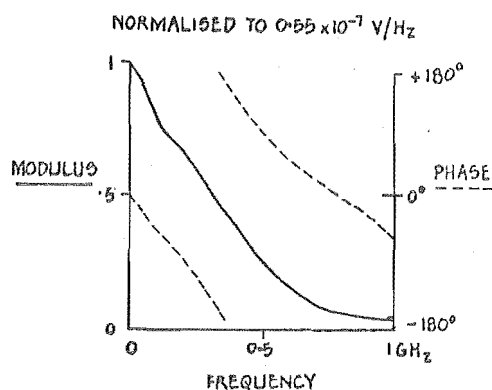


\* FOUR 220  $\Omega$  CARBON COMPOSITION RESISTORS IN PARALLEL  
 † FOUR 5pF CERAMIC CAPACITORS IN PARALLEL.

(a) CIRCUIT



(b) OUTPUT PULSE



(c) PULSE SPECTRUM

FIGURE 4.3. A PULSE GENERATOR USING THE 2N3643.

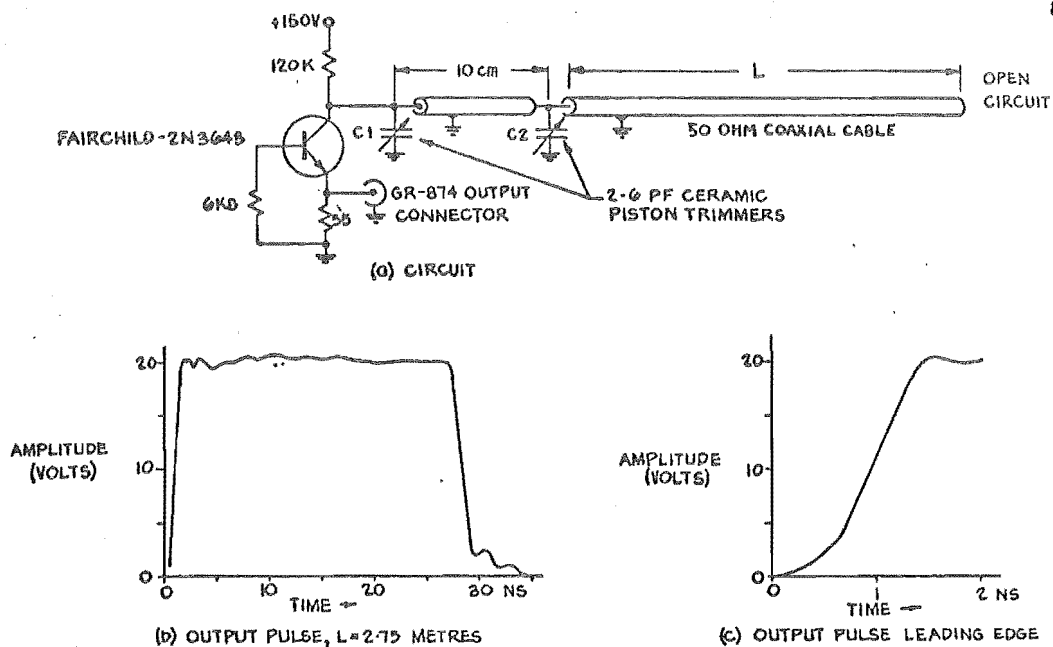


FIGURE 4-4: A CHARGE LINE PULSE GENERATOR USING THE 2N3643

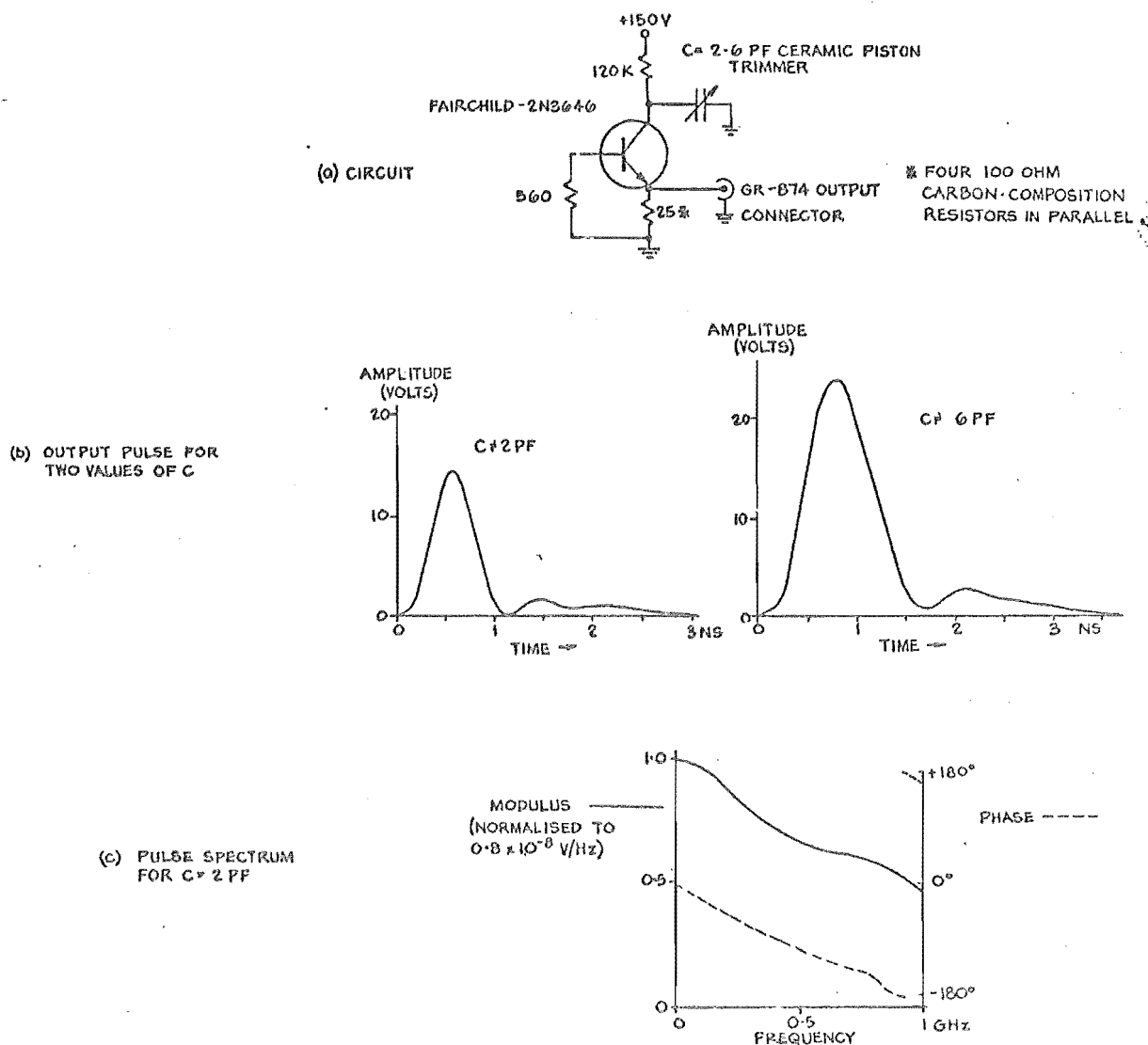
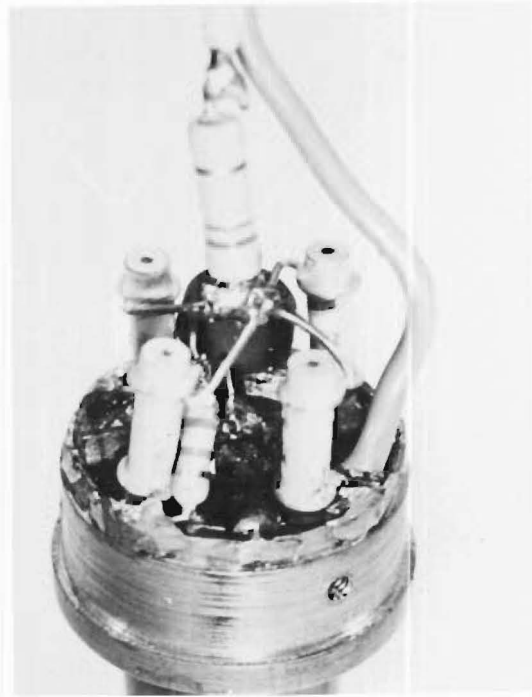


FIGURE 4-5: A PULSE GENERATOR USING THE 2N3646



2N3643 PULSE GENERATOR Internal construction



2N3643 PULSE GENERATOR  
Assembled



2N3646 PULSE GENERATOR  
Internal construction

Figure 4.6: CONSTRUCTION OF PULSE GENERATORS

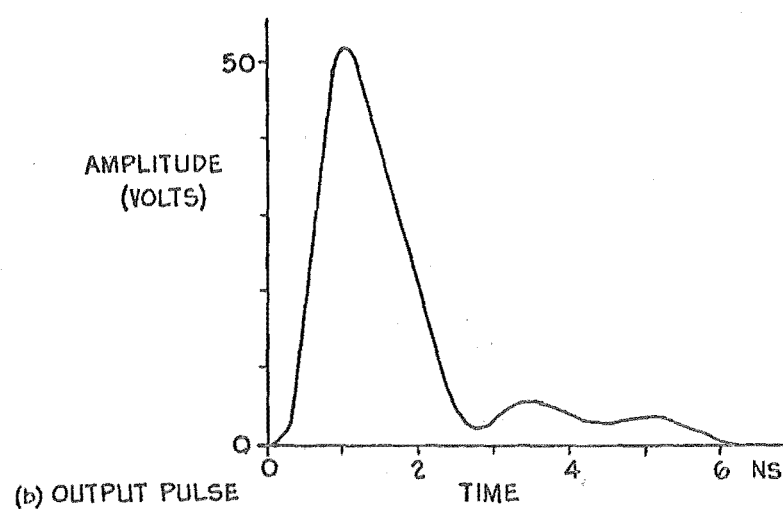
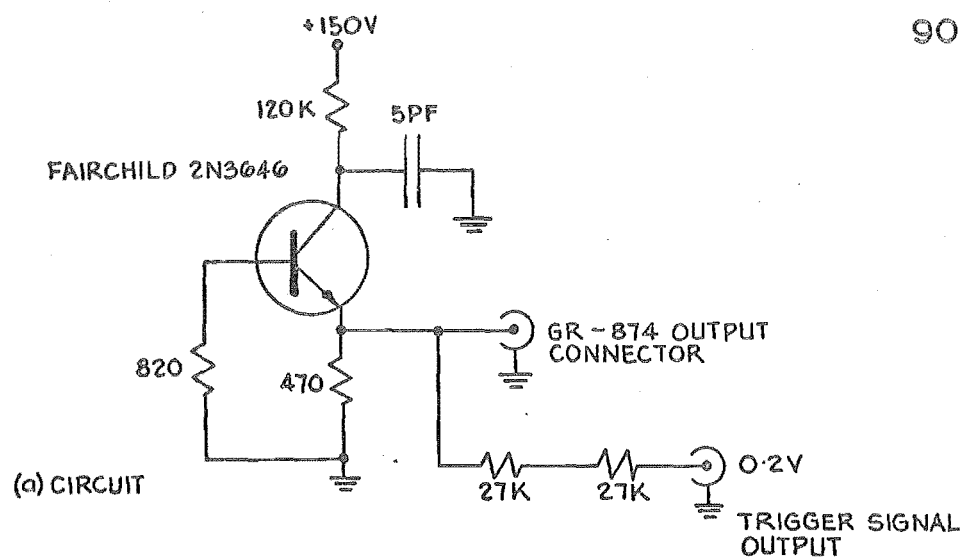


FIGURE 4.7: A HIGH AMPLITUDE PULSE GENERATOR WITH TRIGGER SIGNAL OUT PUT

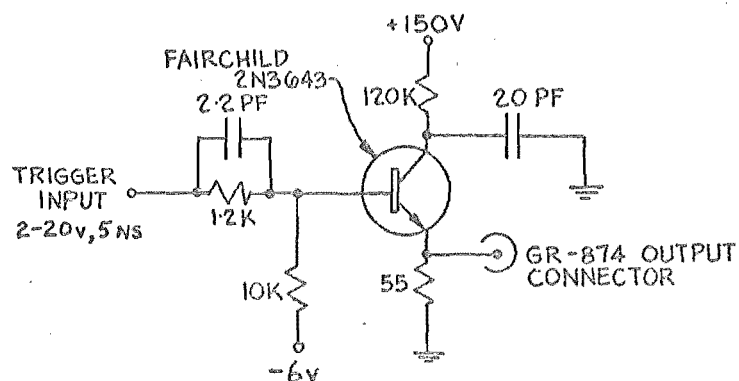


FIGURE 4.8: A TRIGGERED PULSE GENERATOR

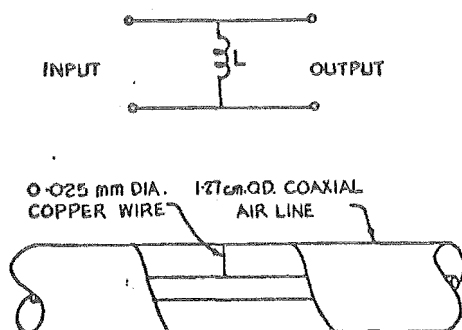


FIGURE 4-9: A SIMPLE DIFFERENTIATOR

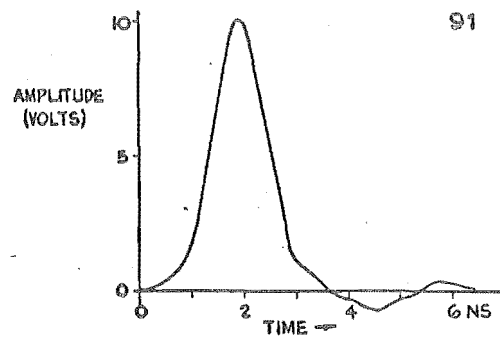


FIGURE 4-10: A PULSE FORMED BY DIFFERENTIATING A STEP.

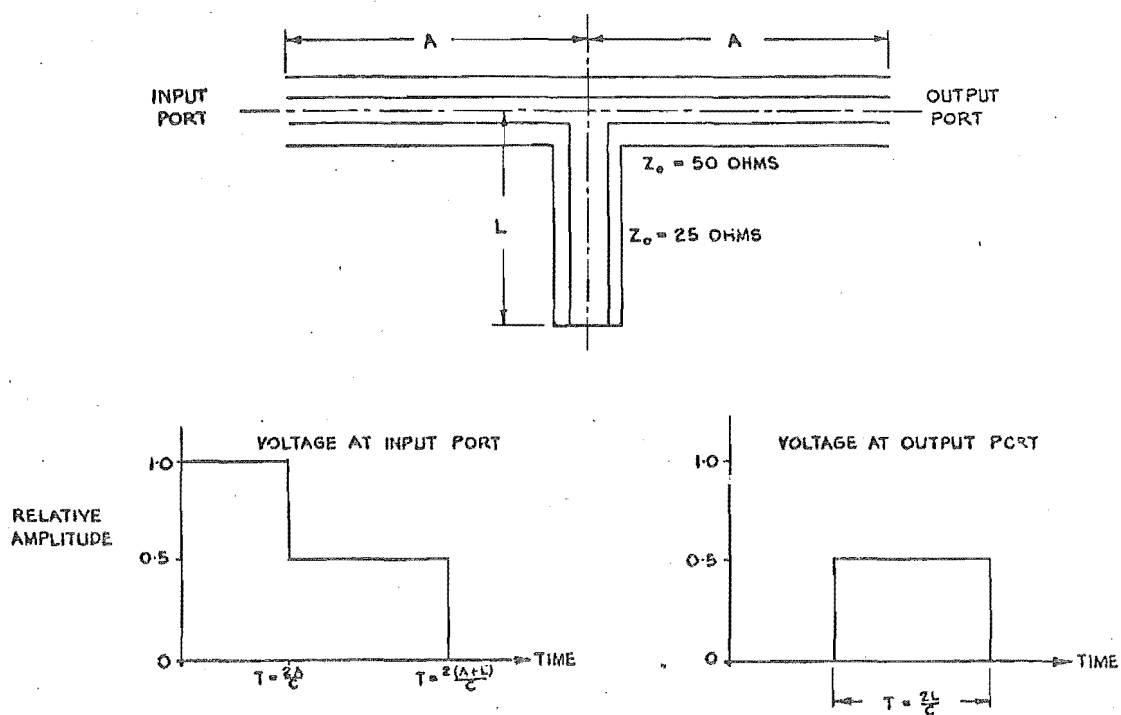


FIGURE 4-11: PULSE FORMING WITH A SHORT CIRCUITED STUB (REPRODUCED FROM ROSS, 1965)

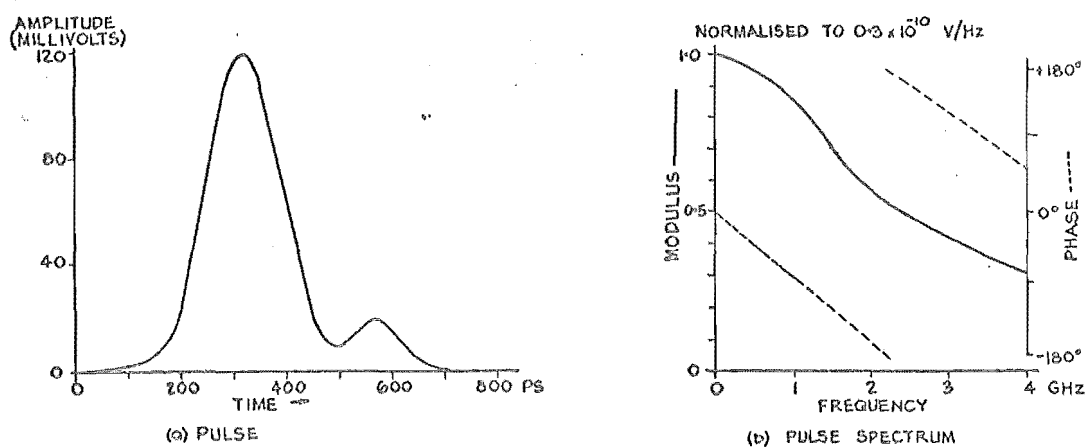


FIGURE 4-12: A SHORT PULSE FORMED FROM A 250 mV TUNNEL DIODE STEP GENERATOR BY A SHORT CIRCUITED STUB

PART II

DRIVING POINT RESPONSES

## CHAPTER 5: RESPONSE OF NARROW BAND ANTENNAS

### 5.1 INTRODUCTION

In this chapter the transient driving point characteristics of a thin dipole are examined. The dipole is the simplest example of a narrow band antenna<sup>1</sup>.

The transient driving point characteristics can be obtained from the input impedance. There are numerous papers concerning the input impedance of the dipole. An excellent history of the problem is given by Hurd (1969, part A), who catalogues over 400 references. Probably the most famous contribution to thin cylindrical antenna theory is the integral equation of Hallen (1938) (also in Hallen 1962, section 35.1). Hallen succeeded in simplifying the integrals and presented extensive numerical results for the input resistance and reactance for various thicknesses of dipole (Hallen, 1948). These results can also be found in Jordan and Balmain (1968, pp566-567). Extensive experimental measurements had earlier been presented in a similar form by Brown and Woodward (1945). Other theoretical solutions are described by King (1956). The monochromatic characteristics are related to the transient characteristics in section 5.2.

Wu (1961a) derives an expression for the input admittance of a long, thin dipole antenna. King and Schmitt (1962) extend his work and derive an expression for the input

---

<sup>1</sup>In this thesis a narrow band antenna is defined as one which is only matched to its feedline over a 5% bandwidth. A VSWR of 2 constitutes a match.



impedance of a monopole as its length becomes infinite<sup>2</sup>. Otto (1969) presents numerical results from accurate theory (Otto, 1967). Andersen (1968; 1971, section 2.2.2) has inferred the input admittance of an infinite monopole indirectly from continuous wave (c.w.) measurements. In section 5.3 the input impedance, as a function of frequency, is computed for an (effectively) infinite monopole from a short pulse measurement of the driving point response of a long monopole. The result verifies the previous theories, and is discussed in section 5.4.1.

The transient response of the dipole has been investigated theoretically and experimentally by a number of authors (see chapter 1). Section 5.4.2 contains a detailed discussion of this previous research.

## 5.2 THEORETICAL CONSIDERATIONS

Pocklington (1897) demonstrates that the current on thin perfectly conducting wires is propagated approximately with the velocity of light, and that between any two points of monochromatic excitation the current distribution is approximately sinusoidal. Thus the current distribution on a monochromatically excited dipole is approximately sinusoidal (the open ends act like sources). This is now known to hold fairly well for very thin wires, and is a commonly used engineering approximation for calculating the radiation characteristics of the dipole (which are relatively insensitive to the current distribution). Actually the amplitude of the current wave propagating along the wire decreases slowly

---

<sup>2</sup>In this thesis the terms dipole and monopole are used interchangeably. The input impedance of a monopole, which is assumed to be driven over an infinite ground (or image) plane, is half that of a dipole whose half-length is equal to the length of the monopole.

with distance because it is damped by radiation losses (the effect being greater for electrically thick wires than for thin wires) and its phase velocity is slightly slower than the velocity of light, which it approaches asymptotically as the distance from the driving point increases (Andersen, 1968)<sup>3</sup>. The phase velocity of the current at a given point on an antenna is frequency sensitive. This is because both the antenna diameter, and the distance from the driving point in terms of wavelengths, change with frequency. As the frequency increases the electrical thickness of the antenna increases, which tends to slow the wave. However, the electrical distance from the driving point increases, which tends to speed up the wave. The net effect is that the phase velocity at a given point increases with increasing frequency (Andersen, 1968). Thus the dipole acts like a non-uniform transmission line (recall the theory which treats the dipole as a transmission line with an evenly distributed loss to account for radiation: Jordan and Balmain 1968, section 11.14). A current pulse propagating along the dipole exhibits slight dispersion and a slight continuous reflection from the whole length of the dipole.

The driving point response of a monopole  $v(t)$ , to an incident signal  $u(t)$  can be obtained from the input impedance  $Z(f)$ :

$$v(t) = \int_{-\infty}^{\infty} \rho(f) U(f) e^{j2\pi ft} df \quad (5-1)$$

---

<sup>3</sup> e.g. the phase velocity is within 0.05% of the velocity of light 3.33 wavelengths from the feedpoint of a 1/300 wavelength diameter wire. This corresponds to 1 metre from the driving point of a 1 mm diameter wire at 1 GHz.

where

$$\rho(f) = \frac{Z(f) - Z_0}{Z(f) + Z_0} \quad (5-1a)$$

$U(f)$  is the spectrum of  $u(t)$  and  $\rho(f)$  is the voltage reflection coefficient when the monopole terminates a transmission line of characteristic impedance  $Z_0$ .

Williams (1963) uses eqn(5-1) to numerically calculate  $v(t)$  for a 3 m long, 3.32 mm dia. monopole for two incident signals, one of which is a narrow Gaussian pulse:

$$u(t) = \exp\left[-\frac{t^2}{2t_1^2}\right], \quad t_1 = 1.5 \text{ ns} \quad (5-2)$$

When  $Z_0 = 50$  ohms Williams shows that  $v(t)$  consists of a series of pulses, which correspond in time to the instants at which  $u(t)$  is reflected from the base as it travels up and down the monopole at (approximately) the speed of light, alternately being reflected from the base and the tip. Some dispersion is perceptible on the third, fourth and fifth pulses pictured by Williams (only five pulses are shown), as predicted above. No continuous reflection is perceptible. Williams also shows that when  $Z_0 = 300$  ohms the reflection from the base is very small, and  $v(t)$  consists of only one main reflection, which is the reflection of the incident pulse from the tip. When observed in the transmission line the amplitude of the tip reflection is only 0.6 times the amplitude of the incident pulse. The monopole appears, from the driving point, to be a length of lossy and slightly dispersive transmission line which has a characteristic impedance of about 300 ohms.

### 5.3 EXPERIMENTAL DETERMINATION OF THE INPUT IMPEDANCE OF AN EFFECTIVELY INFINITE MONOPOLE

If a monopole is infinitely long then  $v(t)$  consists of a single reflection of the test pulse from the base. Consequently by only accepting the first reflection of a narrow pulse from a long monopole (i.e. that from the base),  $p(f)$  and hence  $Z(f)$  of an effectively infinite monopole can be computed.

Fig. 5.1 shows the test pulse and the pulse reflected from the base of a 1.5 m long monopole of diameter  $2a = 0.556$  cm (which was the same as the inner diameter of the coaxial line which fed it). Fig. 5.2 shows the computed  $p(f)$  for the monopole terminating a 50 ohm line.  $Z(f)$  (plotted as resistance and reactance) is shown in Fig. 5.3 together with the theoretical results of King and Schmitt (1962) (translated for  $2a = 0.556$  cm) and Otto (1969). Otto's numerical results were interpolated to obtain values for a coaxial line with an outside to inside radius ratio  $b/a = 2.3$  (i.e.  $Z_0 = 50$  ohms). Values inferred indirectly from c.w. measurements by Andersen (1963) are also included.

### 5.4 DISCUSSION

#### 5.4.1 The Infinite Antenna

In Fig. 5.3 a close agreement is obtained above 200 MHz between the experimental results and King and Schmitt's (1962) and Otto's (1967, 1969) theories. The results inferred from c.w. measurements by Andersen (1968; 1971, section 2.2.2) are also in close agreement with the pulse experiment. The accuracy of the experimental results deteriorates below 200 MHz because the signals were truncated

at 9.5 ns. This means that the reflection of the pulse from the monopole lasts longer than 9.5 ns, in agreement with the theoretical considerations presented in section 5.2.

Wu (1962) (also in Collin and Zucker 1969a, chapter 10) shows that the apparent input admittance of an infinite, thin dipole antenna driven from a thin coaxial line can be separated into two parts. One is dependent on the dimensions of the antenna and independent of the dimensions of the transmission line; this is the intrinsic admittance of the antenna. The other is independent of the antenna dimensions but is dependent on the dimensions of the transmission line; this is equivalent to a frequency independent base capacitance. The expression used by King and Schmitt is independent of the transmission line dimensions, but their experimental observations show that the effect of the base capacitance is too small to be detected for the range of frequencies in their test pulse spectrum ( $< 300$  MHz). Although the measurement reported in section 5.3 was more accurate than King and Schmitt's early measurement, the results show that the effect of the base capacitance is too small to be detected at the frequencies for which the results are computed.

Otto (1967) uses a frill of magnetic current to model the excitation of the antenna: this corresponds to TEM excitation from a coaxial line. He presents an argument which shows that for small  $b/a$  and  $ka$  the effect on the input impedance of the TM modes in the aperture is small. The results presented here confirm this.

The input impedance of an infinite antenna could also be obtained by measuring a travelling wave antenna. This is a

finite antenna in which reflections from the ends are avoided by some means. Lumped resistive loading is used by Altshuler (1961), lumped reactive loading by Nyquist and Chen (1968) and distributed resistance and multiple impedance loading by Taylor (1968). However, in practice a small standing wave ratio exists on the antenna. To infer the infinite antenna impedance, Andersen (1968) requires two c.w. measurements. Precise c.w. measurements are very tedious. The experiment reported here is simple to perform, and gives the input impedance for a range of  $ka$  of about 4:1 from a pair of measurements. Thus from only a few measurements results spanning a wide range of  $ka$  and  $b/a$  are obtained.

#### 5.4.2 Transient Response of Dipole

Measurements of  $v(t)$  for a monopole fed from a 50 ohm coaxial line for narrow pulse excitation are reported by King and Schmitt (1962) and Ross (1966c), and their measurements agree with the  $v(t)$  computed by Williams (1963)<sup>4</sup>. Ross used superior equipment, and his measurements clearly show the dispersion which is noticeable on the third, fourth and fifth pulses of the  $v(t)$  computed by Williams.

King and Schmitt (1962) used a 3 ns long pulse with a 1 ns risetime, and their monopole was 0.476 cm dia. and 2.75 m long. Details of the driving point geometry are not given but it appears that the monopole was connected to the inner conductor (0.295 cm diameter) of a length of 50 ohm coaxial cable which terminated flush with the surface of the ground

---

<sup>4</sup>The measured pulse response of a monopole terminating a 50 ohm line is shown in Fig. 2.6.

plane. By dividing the peak amplitude of the pulse reflected from the base of the monopole by the peak amplitude of the pulse reflected from the unterminated line (i.e. with the monopole removed), they obtained a pulse reflection coefficient of 0.72. This corresponds to a surge impedance  $Z_s$  of 307 ohms<sup>5</sup>. To explain this pulse reflection coefficient,  $Z(f)$  was calculated for an infinitely long monopole by extending a theory by Wu (1961a). From  $Z(f)$ ,  $\rho(f)$  was calculated for the monopole terminating the 50 ohm line. They then assumed that the pulse was band-limited at  $f_c$  and calculated an average reflection coefficient  $\bar{\rho}$  in two ways:

$$1) \quad \bar{\rho} = \frac{\overline{Z(f)} - Z_0}{\overline{Z(f)} + Z_0} \quad (5-3)$$

where  $\overline{Z(f)}$  is an average impedance given by

$$\overline{Z(f)} = \frac{1}{f_c} \int_0^{f_c} Z(f) df \quad (5-4)$$

$$2) \quad \bar{\rho} = \frac{1}{2f_c} \int_{-f_c}^{f_c} \frac{Z(f) - Z_0}{Z(f) + Z_0} df. \quad (5-5)$$

With the assumption that  $U(f) = 1$  for  $-f_c < f < f_c$ , the numbers given by eqns (5-3) to (5-5) agreed with the measured pulse reflection coefficients of several monopoles of different diameters.

Wu and King (1963) have studied analytically the reflections from the base of straight wire antennas driven

---

<sup>5</sup>The surge impedance is the apparent impedance terminating the transmission line as seen by the pulse. Its value depends only on the properties of the antenna near its base.

by coaxial lines<sup>6</sup>. They present numerical results for incident current pulses having exponential rises and decays. They show that the shape of the reflected pulse is nearly the same as the incident pulse if  $Z_0$  is 50 ohms or less, and if the risetime of the incident pulse is much longer than a characteristic time  $t_0$  defined as

$$t_0 = \frac{aa'}{cb} \quad (5-6)$$

where  $a'$  and  $b$  are the inner and outer radii respectively of the coaxial line and  $a$  is the antenna radius. Unless  $a$  is large,  $t_0$  is much smaller than the risetimes of the fastest pulse generators currently available (e.g.  $t_0$  for the monopole measured in section 5.3 is 4 ps). For one set of numerical results they used data corresponding to the experiment reported by King and Schmitt (1962), and the pulse reflection coefficient agreed with that from the experiment. For the same antenna, but for a faster risetime pulse (69 ps), and for  $Z_0$  ranging from 105 ohms to 285 ohms they found that the reflected current pulse was initially positive, but reduced to zero and became negative later in time<sup>7</sup>. This is because the sharper pulse contains higher frequency components in its spectrum, and  $Z(f)$  for an infinite monopole decreases with increasing frequency (see Fig. 5.3). Thus for some value of  $Z_0$  the current reflection is positive for the high frequencies and negative for the low frequencies. The initial behaviour of the reflected current pulse is primarily

---

<sup>6</sup>This paper has been combined with King and Schmitt (1962) and appears as chapter 11 of King and Harrison (1969).

<sup>7</sup>The observed voltage reflection is related to the current reflection by  $-1$ .



determined by the characteristics of the junction at high frequencies; hence it begins with a positive peak. Later in time, when the low frequency end of the signal becomes dominant, the reflected current pulse becomes negative. The results of this approximate theory were substantiated experimentally by Schmitt (1963) who observed the reflections of an incident step function of voltage, which had an approximately exponential rise, from monopoles of various radii driven from a 50 ohm and a 120 ohm line. The same behaviour is also seen in the responses computed by Williams (1963), who demonstrates theoretically that when  $Z_0$  is large ( $>600$  ohms) the negative peak dominates the voltage reflected from the base. Wu and King conclude that a pulse reflection coefficient can only be defined when there is little distortion of the incident pulse, i.e. when  $Z_0$  is small and the risetime of the incident pulse is long compared to  $t_0$ .

Williams (1963) criticises the concept of a pulse reflection coefficient. He points out that eqn(5-5) only gives the value of the reflected signal at  $t = 0$  (which may not be the peak) when the incident signal is

$$u(t) = \frac{\sin 2\pi f_c t}{2\pi f_c t} \quad (5-7)$$

(the Fourier transform of eqn 5-7 is  $U(f) = 1/2f_c$  for  $-f_c < f < f_c$ ,  $U(f) = 0$  otherwise, so that substituting this into eqn 5-1 and setting  $t = 0$  gives eqn 5-5, since  $u(t) = 1$  for  $t = 0$ ), and that King and Schmitt have only shown that the numbers given by eqns (5-3) and (5-5) fortuitously have about the same value as the measured pulse reflection coefficient under certain conditions (which is for one shape

of incident signal that is assumed to be bandlimited, and for  $Z_0 = 50$  ohms). A pulse reflection coefficient which relates the peak amplitudes of the reflected signal and the incident signal tells nothing of the shape of the reflected signal. The peak values of the signals may not even occur at the same instant in time. Williams concludes that the best general relation between the reflected signal and the incident signal is stated in principle by eqn(5-1). The reflected signal may be calculated from it for specific incident signals.

A pulse reflection coefficient as defined by King and Schmitt is not meaningful unless the risetime and duration of the pulse are specified<sup>8</sup>. For a monopole Wu and King (1963) have shown that its value depends on these two parameters (or, more specifically, on the spectrum of the incident pulse). This is demonstrated in Table 5.1 which compares King's and Schmitt's measurement to three other monopole reflection measurements using different incident pulses. The second measurement is from the experiment reported in section 5.3, and the last two were made using the bend measuring apparatus described in section 3.3. The pulse duration was altered by adjusting the stub. Notice also that the peak amplitude of the reflected pulse in Fig. 5.1 occurs 100 ps after the arrival of the incident pulse. Nevertheless the concept of the pulse reflection coefficient and the surge impedance is sometimes useful. This is seen later in section 6.4.2.1.2.

---

<sup>8</sup>The conical antenna is an exception (see section 6.2.1). Its surge impedance is equal to its characteristic impedance which is frequency independent.

Pulse risetime	Pulse duration	Pulse reflection coefficient	Surge impedance (ohms)
1 ns	3 ns	0.72	307*
0.4 ns	1 ns	$0.648 \pm 0.005$	234
0.1 ns	1 ns	$0.66 \pm 0.02$	244
0.1 ns	0.5 ns	$0.54 \pm 0.02$	168

\*Due to King and Schmitt

Table 5.1: Pulse reflection coefficients and surge impedances for 0.556 cm dia. monopole for different incident pulse shapes.

Ross (1966c) presents a simple flow graph model of the dipole to explain its observed narrow pulse response. An open circuited length of uniform, lossless, TEM mode transmission line of characteristic impedance  $Z$  represents the dipole. The base region is represented by a non-causal, dispersive filter having a Gaussian shaped impulse response to introduce dispersion, and a loss factor to account for the loss due to radiation. The impedance  $Z$  and the loss factor of the Gaussian filter were determined from a simple narrow pulse measurement. The standard deviation of the Gaussian filter was determined by calculating approximately the impulse response of an infinitely long monopole from its input impedance (obtained from King and Schmitt, 1962). However, it could also have been determined from the pulse measurement (as was shown in section 5.3). The time domain response of the dipole to any incident signal can be determined graphically from the flow graph model. This is simplest when the incident signal is also a Gaussian. Pulses

generated by semiconductor pulse generators are rough approximations to a Gaussian.

This model is only valid for feedlines of low characteristic impedance, for when  $Z_0$  is large the filter no longer has a Gaussian shaped impulse response (Williams, 1963).

One comment about the experimental technique used by both King and Schmitt and Ross is in order. They both measured the pulse reflected from the unterminated end of the coaxial line as their reference pulse. Because of the end effect (Jordan and Balmain 1968, p394) this technique can introduce errors, particularly if the frequency response is being computed. Consequently it is more satisfactory to measure the pulse reflected from a short circuit and to allow for the inversion in the calculations, as has been done throughout this thesis.

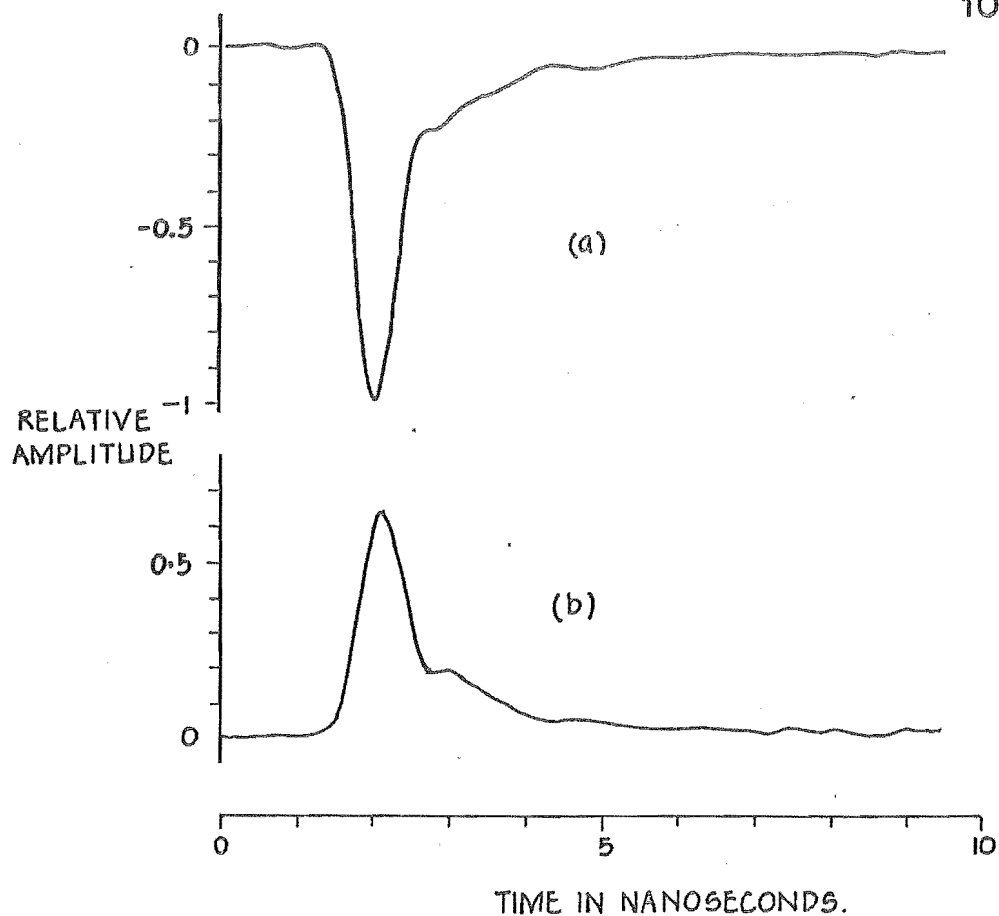


FIGURE 5.1: (a) INCIDENT PULSE (shown inverted) AND (b) PULSE REFLECTED FROM BASE OF 0.550 cm. DIAMETER MONOPOLE

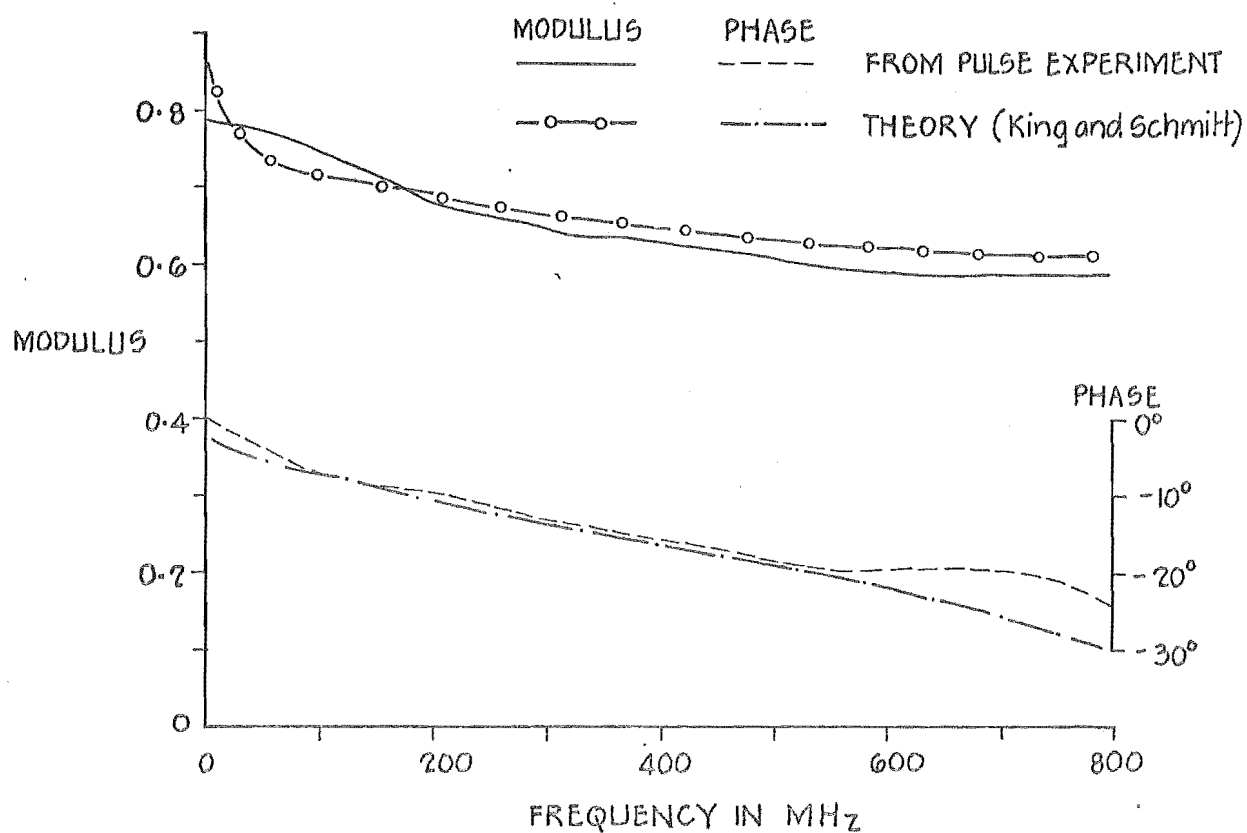


FIGURE 5.2: REFLECTION COEFFICIENT OF EFFECTIVELY INFINITE 0.550 cm. DIAMETER MONOPOLE TERMINATING A 50 OHM. LINE.

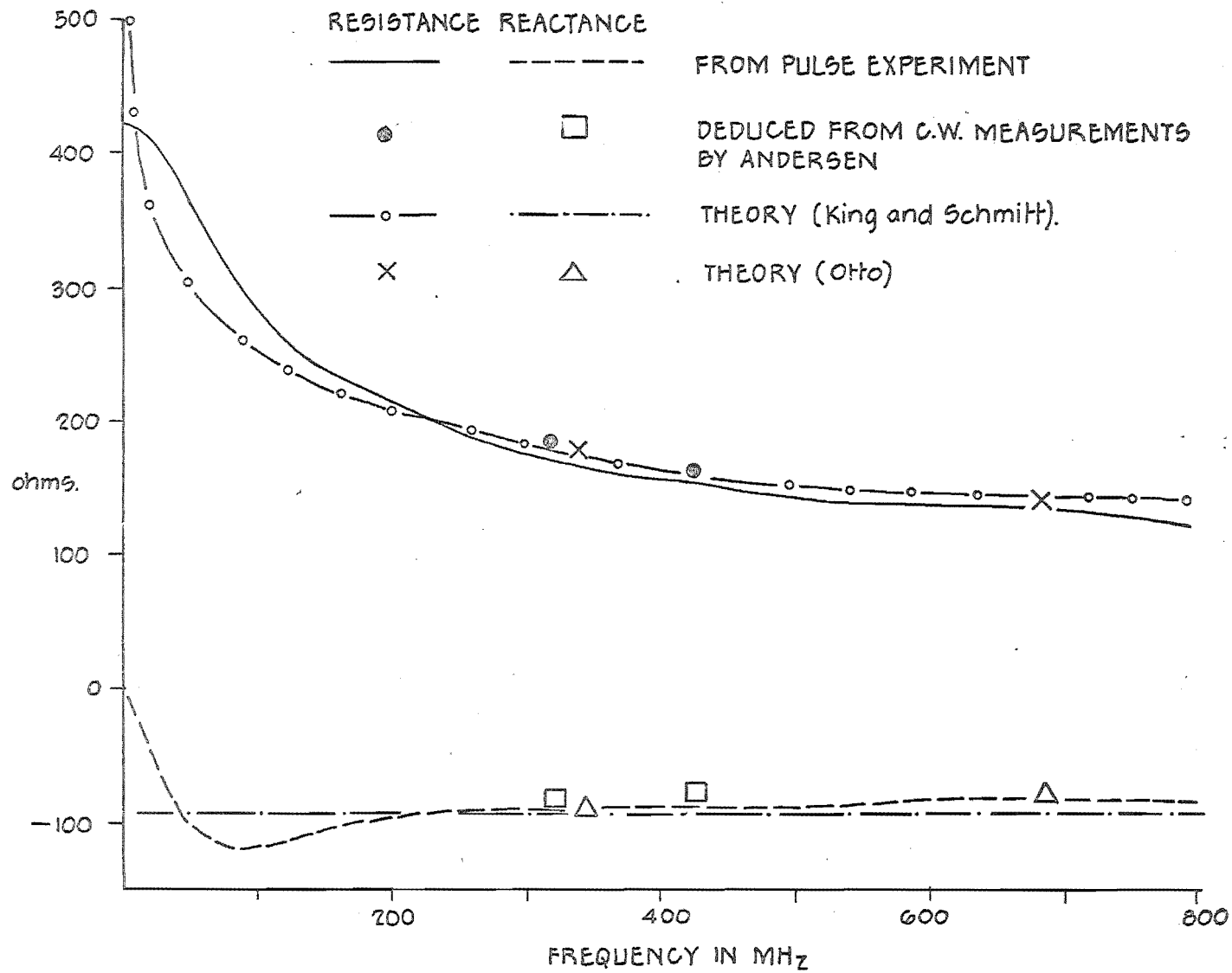


FIGURE 5.3. INPUT RESISTANCE AND REACTANCE OF EFFECTIVELY INFINITE MONOPOLE

## CHAPTER 6: RESPONSE OF WIDEBAND ANTENNAS

### 6.1 INTRODUCTION

Since World War II various wideband antennas have been developed: many can operate over bandwidths of several octaves. Some types have bandwidths which are limited only by practical construction. These are the frequency independent antennas proposed by Rumsey (1957) and experimentally developed by Dyson (1959a, 1959b), and the logarithmic periodic antennas<sup>1</sup> proposed by Du Hamel and Isbell (1957). Equiangular spiral antennas have been constructed to operate over bandwidths of 40:1 (Dyson, 1962). Reviews of recent developments in broadband antennas are given by Dyson (1962) and Jordan et al. (1964).

It is shown later in chapter 8 that log-periodic antennas and frequency independent antennas are unsuitable for use in a system that is required to faithfully transmit signals which have bandwidths of an octave (2:1) or more. It is also suggested that a phase-corrected conical monopole (or biconical dipole) is suitable. The conical monopole was one of the first antennas to operate over a bandwidth of several octaves. The discone antenna (Jasik 1961, section 3.8) is still commonly used. Conical monopoles which are made from continuous sheets of metal have been comprehensively studied, both theoretically and experimentally, by various authors, and their driving point characteristics are reviewed in section 6.2.1. The driving point characteristics of matched conical monopoles are investigated experimentally

---

<sup>1</sup>Usually abbreviated to log-periodic.

in section 6.3.1, where a comparison is made between a cone made of wires and a sheet metal cone. The effect on the input impedance of inserting a phase correcting lens into the aperture is investigated in section 6.3.2. The results are discussed in section 6.4.1.

Another wideband antenna of simple construction, but which has received little attention in recent years, is the triangular fan antenna<sup>2</sup>. This antenna is made from a continuous sheet of flat metal, and has similarities with the conical antenna. It is commonly used as a VHF television antenna (Jasik 1961, section 24.8). The fan monopole has been comprehensively studied experimentally by Brown and Woodward (1952). Theoretical investigations appear to be limited to determining its characteristic impedance (Carrel, 1958; Hall, 1971). The driving point characteristics of the sheet metal fan are reviewed in section 6.2.2.

It is impractical to use a fan antenna made from a continuous sheet of metal at frequencies where its physical dimensions are greater than about a metre or so, because its weight and wind resistance would be too great. Consequently it is of interest to examine the characteristics of fan antennas which are made from discrete wires. The simplest construction is a radial wire fan (all the wires emanate from the driving point). Measurements were made on several shapes of radial wire fan, and the results are presented in section 6.3.3. These measurements supplement those of Brown and Woodward (1952). Some sheet metal fans were also measured for comparison, and close agreement with the c.w.

---

<sup>2</sup>Sometimes called a fin.



measurements of Brown and Woodward is obtained. Measurements of the surge impedance were made to verify the theories of Carrel (1958) and Hall (1971). The results are discussed in section 6.4.2.

A discussion of the measurement errors is given in section 6.3.4.

## 6.2 THEORETICAL CONSIDERATIONS

### 6.2.1 Conical Monopoles

The characteristic impedance is constant along the length of a conical monopole which is constructed from a continuous sheet of metal. The relation between the core characteristic impedance  $Z_0$  (which would equal the input impedance if the cone was infinitely long) and the cone half flare angle  $\varphi$  is

$$Z_0 = 60 \ln \cot \varphi / 2. \quad (6-1)$$

The flare angle is defined in Fig. 6.1.  $Z_0$  is resistive, and equals 50 ohms when  $\varphi = 46.9^\circ$ <sup>3</sup>. If the cone is made of a cage of constant diameter wires then  $Z_0$  is not constant, but increases as the distance from the driving point increases. This is demonstrated by experiment in section 6.3.1.  $Z_0$  is constant only if the wires themselves are conical (Schelkunoff and Friis 1952, section 4.11; Schelkunoff 1943, section 8.14).

The input impedance of a conical monopole depends only on the TEM wave (Jordan and Balmain 1968, p572). This is the basis of Schelkunoff's ingenious solution for the input impedance, in which he represents the cone as a section of

---

<sup>3</sup>From now on this is referred to as a 50 ohm cone.

transmission line with an appropriate terminal impedance. However, the approximations he made in calculating the terminal impedance make his results valid only for small flare angles ( $\phi \ll 1$  radian) (King 1956, section VIII.9; Hurd 1969, p23).

The input impedance for wide angle ( $\phi \gg 30^\circ$ ) conical monopoles capped with sections of spheres has been obtained theoretically by Papas and King (1949). Results are presented for half flare angles ranging from  $30^\circ$  to  $70^\circ$ , and reasonable agreement with the experimental measurements made by Reich (1947) was obtained. In most of the theoretical treatments the effect of the discontinuity at the driving point is neglected<sup>4</sup>. Papas and King (1949) point out that there must be an upper limit to the flare angle for which their results are valid, for as the flare angle increases the discontinuity becomes more severe, thereby making the evanescent modes there significant<sup>5</sup>. It is also interesting to note that the theoretical solutions of the conical antenna do not give results which are as accurate as solutions of the thin cylindrical antenna, even for very small flare angles and in spite of the analytically convenient shape of the cone (King 1956, section VIII.10).

Brown and Woodward (1952) have published a set of curves of the measured input resistance and reactance of conical monopoles plotted against electrical length for a wide range of flare angles. These curves also appear in Jasik (section

---

<sup>4</sup>It has apparently been analysed by Ess (1951) (Hurd 1969, p60).

<sup>5</sup>All higher than the TEM (Jordan and Balmain 1968, section 14.13).

3.2). They noticed that the measured input impedance of hollow (i.e. open ended) cones is the same as that obtained theoretically by Papas and King (1949) if the slant heights were the same<sup>6</sup>. The spherical cap thus makes no difference to the measured input impedance (although they found that it affected the radiation pattern slightly).

The input impedance of the wide angle conical monopole is close to the characteristic impedance at resonance and at antiresonance, and the impedance variations are slight providing the slant height is greater than about  $\lambda/4$ . The conical monopole can therefore be matched to the coaxial line which feeds it over a wide bandwidth by choosing  $\phi$  so that the cone characteristic impedance is the same as that of the coaxial line. The only reflections from the base then are caused by the discontinuity at the junction of the feed-line and the cone.

Ross et al. (1966a, 1966b) use Papas and King's expressions for the input impedance to infer the shape of the impulse response of a 50 ohm matched conical monopole by a graphical inverse Fourier transform. Their result is reproduced in Fig. 6.2, plotted with respect to the input of the cone as a function of  $L/c$ , the propagation delay along the cone. They substantiated this result experimentally by a narrow pulse (400 ps)<sup>7</sup> measurement of a 15 cm slant height cone.

The impulse response, and hence the narrow pulse response, is seen to consist only of a single reflection from the rim. Its duration is long (about  $4L/c$ ), and its rise-time and falltime are about  $0.4L/c$  and  $2L/c$  respectively.

---

<sup>6</sup>The slant height is defined in Fig. 6.1.

<sup>7</sup>This is the duration of the pulse as defined in section 4.1, and not the half-power pulse width which Ross et al. quote.

This is because the reflection contains mainly the low frequency content of the input pulse spectrum since the cone radiates nearly all the energy in the pulse (or impulse) for frequencies above about  $c/4L$  (i.e. when  $L$  is greater than about  $\lambda/4$ ). Consequently the peak amplitude of the reflection is small (typically about one-quarter of the peak amplitude of the input pulse: see section 6.3.1). The shape of the impulse response can be explained by the following simple physical argument. The current pulse (as a TEM wave) travels onto the cone and to the rim without distortion. At the rim the pulse is reflected. No current flows around the rim. Some current travels over the rim and into the cone, but its amplitude is small compared with that which is reflected, because when a spherical cap is fitted to divert the current which would have flowed inside onto the cap, there is no sensible change in the input impedance (Brown and Woodward, 1952). The current travelling back down the core induces current on the surface of the ground plane which is directed towards the driving point (after a time delay which allows for the effect of the current, propagating at the speed of electromagnetic waves, to be felt at the ground plane). This follows from the relation between the induced surface current density  $\underline{K}$  and the magnetic intensity  $\underline{H}$  at the surface of a perfect conductor:

$$\underline{K} = \underline{n} \times \underline{H} \quad (6-2)$$

where  $\underline{n}$  is a unit vector directed normal to the conductor surface (the underlining denotes a vector quantity), and  $\times$  denotes the vector cross product. Practically, many metals

are effectively perfect conductors. The induced current then reinduces current on the surface of the cone, and so on. The current travels into the feedline without reflection from the driving point. The signal observed in the feedline is a relatively long pulse which corresponds to the arrival of the reflected current and the induced current at the feedpoint. It has a slow decay because the magnitude of  $\underline{K}$  decreases as the distance from the feedpoint increases, and the weaker current induced far from the feedpoint arrives later in time than the current induced near the feedpoint.

If the characteristic impedance of the cone is not equal to that of the transmission line then there is a reflection from the base. The amplitude of the reflection is determined by the surge impedance of the cone, which is simply equal to the characteristic impedance. Some measured pulse responses of mismatched cones are given by Ross et al. (1966a, 1966b).

### 6.2.2 Fan Monopoles

Two geometries of sheet metal fan monopole are shown in Fig. 6.3 and four geometries of radial wire fans are shown in Fig. 6.4. Like the cone, the characteristic impedance of the sheet metal fan is constant (Carrel, 1958). Expressions for the characteristic impedance of fans are given by Carrel, but they contain elliptic integrals and are thus not as simple as the expression for the cone (eqn 6-1). Brown and Woodward (1952) present the measured input impedance of straight ended fan monopoles made of sheet metal, such as the

one shown in Fig. 6.3(b). Measurements were made for flare angles ranging from  $5^\circ$  to  $90^\circ$ . They found that the straight ended fan exhibited resistance and reactance variations similar to those of the cone, but that the fluctuations were greater than for a cone with the same flare angle. For a fan then,  $v(t)$  should be similar to  $v(t)$  for a cone which has a smaller flare angle than the fan. This is confirmed later in section 6.4.2.1.1.

The characteristic impedance of fan antennas which are constructed from thin constant diameter radial wires lying in a plane is not constant (by analogy with the cone, section 6.2.1). Also, because the current is constrained to flow only on the wires, significant differences can be expected between the performance of the wire fans and the continuous sheet fans. Current flowing on the surface of a flat, perfectly conducting, sheet metal fan only induces current on the edge of the sheet. If the current is flowing away from the driving point then the induced current also flows away from the driving point. This follows from eqn(6-2). On a radial wire fan however, current flowing on one wire induces current on adjacent wires which flows both towards and away from the driving point (from eqn 6-2, the current induced on the far side of the adjacent wire flows in the same direction as the inducing current and the current induced on the near side in the opposite direction). No net current is induced on a wire situated between two adjacent wires carrying equal currents, provided the wires are equally spaced in angle and their diameter is small compared with their spacing. Thus the net current induced on the

wires near the centre of the fan is contributed by the edge wires, and, the net induced current is greatest on the edge wires. This is not unlike the current flow on the continuous sheet fan. It follows that significant differences can be expected between sheet metal fans and fans made of only a few wires. It also follows that as the number of wires increases the characteristics of the wire fan will tend to those of the sheet metal fan.

### 6.3 MEASURED RESPONSES

#### 6.3.1 Conical Monopoles

Reflection coefficients were computed from measured signals from two hollow cones (each of 50 ohm characteristic impedance when mounted above a ground plane) of 0.71 m slant height. One cone was constructed from 0.33 mm thick tin plated steel sheet, and the other from 26 equally spaced wires of 0.32 cm diameter. The ends of the wires were not connected together. The reflected signals, due to the test pulse shown in Fig. 4.5, are shown in Fig. 6.5(a). The computed  $\rho(f)$  are presented in Fig. 6.5(b). The sampling parameters are given in Appendix 4.

#### 6.3.2 Phase-Corrected Conical Monopoles

Measurements of the far field characteristics of phase-corrected conical monopoles are reported later in section 9.4. The measurements were made on hollow 50 ohm cones which were made from thin brass sheet. The slant height was 7.6 cm. The geometry of the cones, and of the phase-correcting lens, is given in Fig. 9.8. The measurement of the driving point characteristics of these cones is reported here.

The reflected signal, due to the test pulse shown in Fig. 4.12, and the computed  $\rho(f)$  and  $Z(f)$  for the cone without phase correction are shown in Fig. 6.6. The phase correcting lens was inserted into the aperture and the measurement repeated. The results are shown in Fig. 6.7.

These measurements were made using the experimental apparatus (which was designed for measuring bends) described in section 3.3. The sampling parameters are given in Appendix 4.

### 6.3.3 Fan Monopoles

Reflection coefficients and input impedances were computed from measured signals from each of the four configurations of 6 wire fan monopole shown in Fig. 6.4. Measurements were made for flare angles of  $60^\circ$  and  $90^\circ$ . Sheet metal fans (made of 0.33 mm thick tin plated steel sheet with  $L = 30.5$  cm) were also measured for flare angles of  $60^\circ$  and  $90^\circ$  so that a direct comparison could be made with the wire fans. Notice that the slant height is kept constant as the flare angle is changed. This is in contrast to the measurements reported by Brown and Woodward (1952) in which the vertical height was kept constant.

The reflected signals, due to the test pulse shown in Fig. 4.5, and the computed  $\rho(f)$  and  $Z(f)$  are shown in Figs 6.8(a) to 6.8(l). Points selected from the measurements made by Brown and Woodward (1952) are superimposed on the corresponding curves in Figs 6.8(c) and 6.8(d). For convenience, the different shapes of fan are given an identification number. The meaning of this identification is illustrated with some examples. A CE-60 fan is a sheet metal fan with a



circular end and a flare angle  $2\phi = 60^\circ$ . A 6W-SE-90 fan is a 6 wire fan with a straight end, a  $90^\circ$  flare angle and no end wire. The same fan with an end wire is designated 6W-SE-90-E. The measurements were made with the apparatus described in section 3.2, and the sampling parameters are given in Appendix 4. The measurements were repeated for fans made of 5 wires, and these results can be found in a separate report (Burrell, 1972).

The graphs of  $Z(f)$  were forced to be normalised to 250 ohms so that each vertical division conveniently corresponds to 25 ohms. This was done by limiting  $|Z(f)|$  to 250 ohms and setting the phase of  $Z(f)$  to zero for frequencies less than 100 MHz where  $|Z(f)|$  is large (corresponding to  $\rho(f)$  approaching 1). However, for some of the antennas measured,  $|Z(f)|$  is larger than 250 ohms at some higher frequency, so that all the graphs are not normalised to the same value.

Measurements of the pulse reflection coefficient (see section 5.4.2) were made on sheet metal and 6 wire fans for a range of flare angles. The surge impedance  $Z_s$  was then calculated. This is simply equal to the characteristic impedance for the sheet metal fan. Because  $Z_s$  was likely to be dependent on the spectrum of the pulse (as it is for a thin cylindrical monopole; section 5.4.2), the measurements were made with two different test pulses. They both had risetimes of 100 ps but their durations were 500 ps and 1 ns. The apparatus described in section 3.3 was used to make the measurements, and the pulse duration was altered by adjusting the short circuited stub. To the accuracy with

which the pulse reflection coefficient could be measured from the oscilloscope screen (an estimated error of  $\pm 0.02$ ) no difference could be detected in the values of the pulse reflection coefficients measured using the two test pulses, although some distortion was evident on the tail of the 1 ns pulse reflected from the 6 wire fan when  $\phi = 80^\circ$  (the angular spacing of the wires was then  $32^\circ$ ). This means that the characteristic impedance is an insensitive function of frequency. The results are shown in Table 6.1 and the values of  $Z_s$  are plotted against  $\phi$  in Fig. 6.9. The characteristic impedance of a conical monopole is included for comparison.

Half flare angle	Sheet metal fan		6 wire fan	
	Pulse reflection coefficient	Surge impedance (ohms)	Pulse reflection coefficient	Surge impedance (ohms)
$17.5^\circ$	$0.50 \pm 0.02$	$150 \pm 8.3$	$0.51 \pm 0.02$	$155 \pm 8.7$
$30^\circ$	$0.40 \pm 0.02$	$117 \pm 5.8$	$0.44 \pm 0.02$	$128 \pm 6.6$
$45^\circ$	$0.31 \pm 0.02$	$95 \pm 4.3$	$0.36 \pm 0.02$	$106 \pm 5.0$
$60^\circ$	$0.18 \pm 0.02$	$72 \pm 3.0$	$0.31 \pm 0.02$	$95 \pm 4.3$
$70^\circ$	-	-	$0.26 \pm 0.02$	$85 \pm 3.8$
$77.5^\circ$	$0.0 \pm 0.02$	$50 \pm 2.0$	-	-
$80^\circ$	-	-	$0.20 \pm 0.02$	$75 \pm 3.2$
$87.5^\circ$	$-0.20 \pm 0.02$	$33.2 \pm 1.4$	-	-

Table 6.1: Pulse reflection coefficients and surge impedances for fan monopoles.

#### 6.3.4 Discussion of Errors

Estimates of the error in the computed spectra due to noise can be made using the expressions given in section 2.3.3.2. This is now done for the spectrum of the test pulse used for the measurements reported in this chapter.

The error due to quantisation can be estimated using eqn(2-17). When the 3-point scanning method of sampling is used the conversion accuracy is 14 bits (see Appendix 2). After making proper allowance for the sampling oscilloscope scales and the attenuators used in the experiment, this corresponds to a quantising interval  $\delta$  of 2.06 mV referred to the signal level at the pulse generator. The peak value of the pulse was 14 volts. Substituting the values of N and T which were used for the experiments reported in this chapter (see Appendix 4) into eqn(2-17), the noise amplitude exceeded by not more than 1% of the frequency domain ordinates ( $\xi = 0.01$ ) is  $\epsilon_{1,Q} = 0.28 \times 10^{-11}$  V/Hz. From Fig. 4.5,  $|U(f)|$  is  $0.8 \times 10^{-8}$  V/Hz at 0 MHz falling to about  $0.46 \times 10^{-8}$  V/Hz at 800 MHz. However, because of the loss introduced by the connecting cables  $|U(f)|$  at 800 MHz is  $0.28 \times 10^{-8}$  V/Hz when  $u(t)$  is measured in the way described in section 3.2.1.1.  $\epsilon_{1,Q}$  is negligible compared to this.

3-point scanning removes amplitude and timing drift from the measured signal. Thus the remaining noise is amplitude noise and jitter and timing jitter. The error due to amplitude noise can be estimated using eqn(2-14). When  $u(t)$  for the fan measurements was being measured, the maximum difference between the sampled values of the old average and the updated average of  $u(t)$  (see Appendix 2)

after four scans had been made was 40 mV referred to the signal level at the pulse generator. The experiment described in Appendix 2 shows that the standard deviation of the differences in all the sample values is about one quarter of the maximum difference when four scans are made. Assuming that all the noise is additive,  $\sigma_N$  is estimated to be 10 mV. Thus, from eqn(2-14), the noise amplitude exceeded by not more than 1% of the frequency domain ordinates ( $\xi = 0.01$ ) is  $\epsilon_{1,N} = 0.48 \times 10^{-10}$  V/Hz, which is about 0.6% of  $|U(f)|$  at 0 MHz and 1.7% of  $|U(f)|$  at 800 MHz. A similar calculation using  $|V(f)|$  would give an error estimate for  $V(f)$ . If the same  $\sigma_N$  is used then the error in the computed  $\rho(f)$  follows a Cauchy distribution (section 2.3.5). However, it is doubtful if the error obtained by evaluating the area under this distribution would be realistic. The assumption that all the noise is amplitude noise is not really valid. Just how much of the noise is due to timing jitter and amplitude jitter is unknown.

As already discussed in section 2.3.5, error analyses as involved as this are seldom carried out in practice, and some simpler method is usually sought. When  $f$  is less than 100 MHz, the computed  $|\rho(f)|$  tends to 1. Therefore an estimate of the error can be made simply by inspecting the computed  $\rho(f)$  at low frequencies (neglecting the results for  $f < 1/NT$ , for truncation errors and slight errors in the zero levels of  $u(t)$  and  $v(t)$  manifest themselves there). It is seen to be about 3-4% for the reflection coefficients reported in this chapter. The error in the input impedance can be estimated from eqn(2-9b).

## 6.4 DISCUSSION

### 6.4.1 Conical Monopoles

Figure 6.5 shows that the characteristics of a cone made of discrete wires are similar to those of a cone made of a continuous sheet of metal. There are however, noticeable differences. Both reflection coefficients exhibit similar fluctuations with frequency, but that of the wire cone is slightly higher than that of the sheet cone. However, for both cones  $|\rho(f)|$  is less than 0.33 above about 100 MHz, which means that both cones are good wideband antennas<sup>8</sup>. Notice that the leading edge of the reflection of the test pulse from the rim of the wire cone has a faster risetime and a higher amplitude than has the corresponding part of the reflection from the rim of the sheet cone. This indicates that the high frequency components in its spectrum are of greater amplitude; hence its higher reflection coefficient. There are small reflections from the base of each cone, and because of this some multiple reflections are evident. The match could have been improved with a vertical adjustment of the cones. Ross et al. (1966a) reduced the reflection by adjusting the vertical height of the cone by fitting thin washers under the mounting screw. This was not attempted because the reflection was already small, and the cones were heavy so that the risk of breaking the small mounting screw was great. Notice that for the sheet metal cone there are only reflections from the base and the rim

---

<sup>8</sup>  $|\rho|=0.33$  corresponds to a VSWR of 2. HF and VHF radio transmitters are usually designed to operate with antennas whose VSWR  $\leq 2$ .

but there is a continuous low amplitude reflection from the whole length of the wire cone. This means that the characteristic impedance is not constant, but increases (because the reflection is positive) as the distance from the driving point increases. This agrees with Schelkunoff's theory (see section 6.2.1). Notice also that there is a small negative reflection, which indicates a lowering of the characteristic impedance, from the region near the ends of the wires. This is similar to the end effect which is known to occur for cylindrical antennas (Jordan and Balmain 1968, p394).

It is seen in Fig. 6.6(a) that there is a significant reflection from the base of the 7.6 cm slant height cone. This cone was carefully constructed so that its apex was in the plane of the ground plane, which means that the only discontinuity is the abrupt change at the junction of the coaxial line and the cone. The discontinuity is large enough (the diameter of the coaxial line is one sixth the slant height of the cone) to give a significant reflection, and  $|\rho(f)|$  shows that this cone is not as well matched as the larger sheet metal cone (although the match is still acceptable above about 1 GHz).  $Z(f)$  (shown in Fig. 6.6(c)) exhibits the same behaviour as the theoretical input impedance calculated by Papas and King (1949).

When the phase correcting lens is introduced into the aperture of the cone there is a strong reflection from the inner surface of the lens. This is seen in Fig. 6.7(a), where  $v(t)$  exhibits a negative reflection (because the intrinsic impedance of the lens material is lower than that of air) corresponding to the arrival time of the test pulse

at the inner surface of the lens. Inspection of  $\rho(f)$  shows that the lens spoils the match although it is still within the acceptable limit ( $VSWR = 2$ ) above 1 GHz. Notice that  $Z(f)$  remains inductive above 600 MHz when the lens is introduced. Possible means of improving the match are discussed later in chapter 10.

#### 6.4.2 Fan Monopoles

##### 6.4.2.1 Reflected Pulse Responses

###### 6.4.2.1.1 Sheet metal fans

The measured values of  $Z_s$  (which is equal to the characteristic impedance) agree, within experimental error, with the values obtained theoretically by Carrel (1958) and Hall (1971). These theories are thus verified. The curve presented in Fig. 6.9 can be used to choose an optimum fan to match a given transmission line, just as eqn(6-1) is used for a cone.

The similarity between the signals reflected from a sheet metal fan and a cone with a smaller flare angle than the fan, predicted in section 6.2.2, is shown in Fig. 6.10 where the narrow pulse responses of the circular ended sheet fans are shown with the narrow pulse responses of mismatched cones. The cone responses are reproduced from Ross et al. (1966a). There is a greater similarity between the cones and the circular ended fans than there is between the cones and the straight ended fans (see Figs 6.8(c) and 6.8(d)). This is because large currents flow along the end of the straight ended fan because the end does not coincide with the wavefront of the current pulse (remember that no current flows around the rim of the cone).

#### 6.4.2.1.2 Wire fans

It is shown in Fig. 6.9 that  $Z_s$  for a 6 wire fan is higher than  $Z_s$  for a sheet metal fan of the same flare angle, but the difference decreases as the flare angle decreases. This is because the angular spacing of the wires is also decreasing so that the characteristics of the wire fan tend towards those of the sheet metal fan, in agreement with the basic considerations presented in section 6.2.2.

The value of  $Z_s$  for an antenna depends on the characteristics of the antenna near its base. In section 5.4.2 it is demonstrated that  $Z_s$  for a cylindrical monopole is a strong function of the shape of the pulse, because the characteristics of the monopole near its base are frequency dependent. For the cone and sheet metal fan  $Z_s$  is simply equal to the characteristic impedance  $Z_0$ , which is resistive and frequency independent. Hence  $Z_s$  is independent of the pulse shape. It was observed in section 6.3.3 that the measured values of  $Z_s$  for the 6 wire fans were the same (as far as could be detected) for the two different test pulses used (recall however that some distortion was perceptible on the reflection of the 1 ns pulse when  $\phi$  was  $80^\circ$ ). This means that the properties of the base region of the 6 wire fans are approximately independent of frequency for the range of frequencies in the spectra of the test pulses used (up to a few GHz). Thus Fig. 6.9 can be used to choose an optimum 6 wire fan to match a given transmission line, just as eqn(6-1) is used for a cone.

The leading edge of the reflection of the test pulse from the end of the wire fans has a higher amplitude and a faster risetime than has the corresponding part of the



reflection from the end of the sheet fans (e.g. compare  $v(t)$  in Figs 6.8(f) and 6.8(h) with  $v(t)$  in Fig. 6.8(b), remembering that the reflection from the base of a wire fan is stronger than that from the base of a sheet fan). This effect was also noticed in the reflection from the rim of the wire cone (section 6.4.1), but its effect there was not as pronounced. Notice that the strength of the initial reflection increases as the distance between the tips of the wires increases (e.g. it is higher for a 6 wire,  $90^\circ$  flare angle than it is for a 6 wire,  $60^\circ$  flare angle fan). Notice also that for a fan with an end wire this initial reflection is unaltered in shape, but is delayed approximately by the time required for the current pulse to travel along the end wire between two adjacent radial wires. A small negative reflection which corresponds in time to the instant at which the pulse arrives at the end wire is also observed. A wire fan with an end wire appears to be longer than the same fan without an end wire, and a wire fan with an end wire appears to be the same length as a sheet metal fan with the same overall dimensions. Thus an end wire is desirable on a wire fan because it increases the electrical length of a fan of a given physical length.

#### 6.4.2.2 Frequency responses

##### 6.4.2.2.1 Sheet metal fans

The agreement between the measurements reported by Brown and Woodward (1952) and those reported here (see Fig. 6.8(c) and 6.8(d)) is good. However, there appears to be a slight error in the calibration of the frequency scales. This could have been caused by a drift in the time calibration of

the sampling oscilloscope. Notice however that the frequency calibration error is greater at low frequencies than it is near 800 MHz (the frequency of the second resonance agrees exactly with Brown and Woodward's measurement but the first and second resonant frequencies do not). This suggests that the measurement method used by Brown and Woodward introduces errors when the electrical length of the fan is small. They made their measurements at a constant frequency of 500 MHz by varying the electrical length of the fans, which were mounted on a ground plane 2.45 m (i.e. four wavelengths) in diameter (it would have been better if it had been square; Kraus 1950, section 15-7). The outer diameter of the 50 ohm coaxial line which fed the fans was 0.75 cm. An antenna with an electrical length of  $20^\circ$  at 500 MHz is 3.33 cm long, which is only 4.4 times the diameter of the coaxial line. The base discontinuity has an appreciable effect on the characteristics of a small antenna, as was illustrated in section 6.4.1.

$Z(f)$  for the sheet metal fans with straight ends (Figs 6.8(c) and 6.8(d)) exhibits similar behaviour to  $Z(f)$  for the circular ended fans (Figs 6.8(a) and 6.8(b) respectively) except that the resonant and antiresonant frequencies are slightly higher for the straight ended fan than for the corresponding circular ended fan. For a  $90^\circ$  flare angle, the vertical height of the circular fan is 40% greater than the vertical height of the straight ended fan, but the resonant frequency has only dropped by 17%. Thus the resonant frequency is a function both of the vertical height and the shape of the fan. However, the input impedance at resonance

depends mainly on the flare angle (it is about 21 ohms for the  $60^\circ$  fans and 16 ohms for the  $90^\circ$  fans).

Voltage standing wave ratios for fan dipoles, calculated from the results shown in Fig. 6.8, are presented in Fig. 6.11 for several feedline impedances. The match is seen to be optimum when the feedline impedance is selected from Fig. 6.9. Wide bandwidths ( $> 2.6:1$ ) are achieved with sheet metal fans.

#### 6.4.2.2.2 Wire fans

The 6 wire fans exhibit greater variations of impedance with changing frequency than the corresponding sheet metal fans (compare Figs 6.8(a) to 6.8(d) with Figs 6.8(e) to 6.8(1)), in agreement with the basic considerations presented in section 6.2.2. Thus the wire fans are not as well matched as a sheet metal fan (see Fig. 6.11). Some trends are noticeable in the characteristics of the different shapes of wire fan. These trends also apply to the characteristics of the 5 wire fans which are presented in a separate report (Burrell, 1972).

1) The 5 wire fans have higher resonant and antiresonant frequencies, and have higher impedances at antiresonance, than the 6 wire fans.

2) Fitting an end wire to a fan lowers its resonant and antiresonant frequencies.

3) A straight ended fan has higher resonant and antiresonant frequencies than the corresponding circular ended fan. For fans with end wires, the straight ended fans have higher antiresonant impedances than the corresponding circular ended fans. For fans without end wires, the straight ended fans have lower antiresonant impedances than

the corresponding circular ended fans.

4) The  $90^\circ$  flare angle fans with circular ends have lower resonant and antiresonant frequencies, and lower antiresonant impedances, than the corresponding  $60^\circ$  fans. The  $90^\circ$  flare angle fans with straight ends have higher resonant and antiresonant frequencies than the  $60^\circ$  straight ended fans. Thus the resonant and antiresonant frequencies are dependent both on the vertical height, the flare angle, and the number of wires in the fan.

#### 6.5 A SUGGESTION FOR FURTHER WORK

The graphs of resistance and reactance of continuous sheet fans for a wide range of flare angles published by Brown and Woodward (1952) are valuable design data for antenna engineers. When large fans are required they must be made from wires. Consequently a comprehensive set of design data for wire fans would be invaluable. Measurements should cover a wide range of flare angles and wire numbers from 2 to about 15. The measurement method described in this thesis makes such a task feasible.

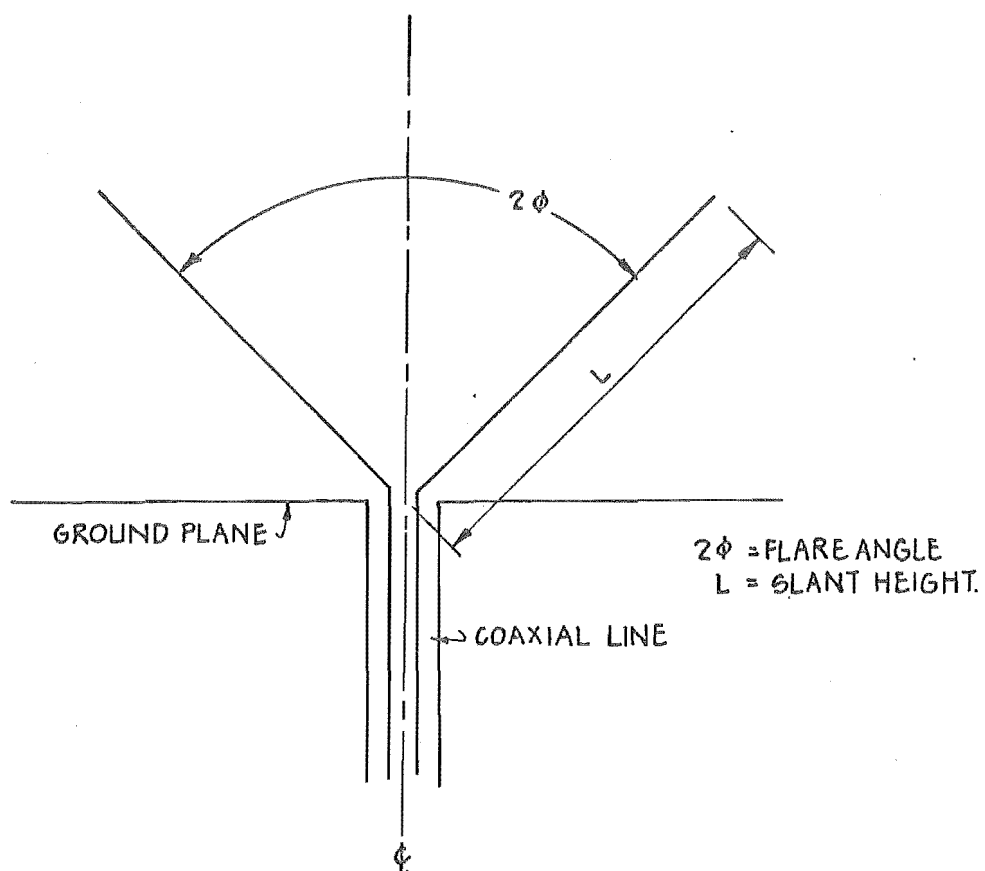


FIGURE 6.1: CROSS-SECTION OF CONICAL MONOPOLE

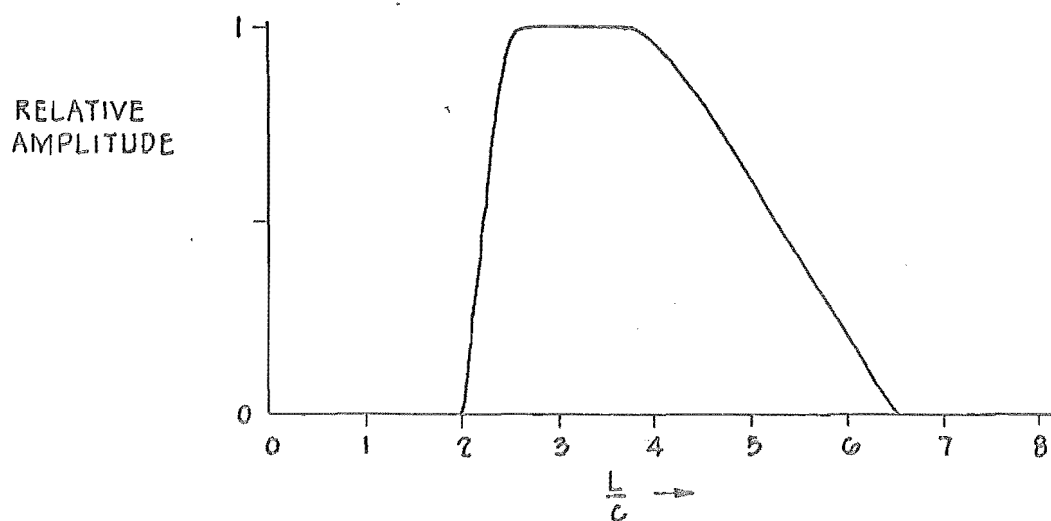
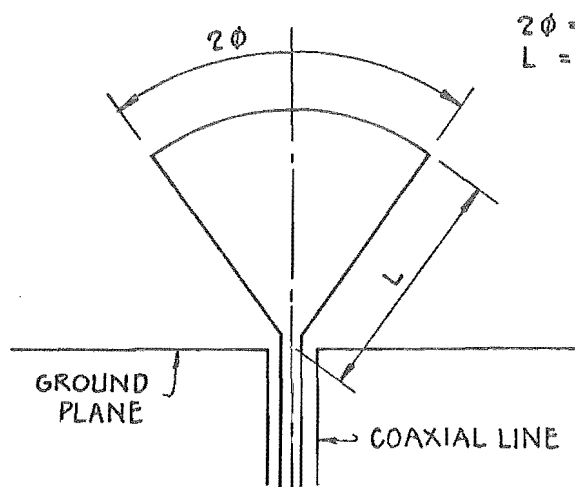
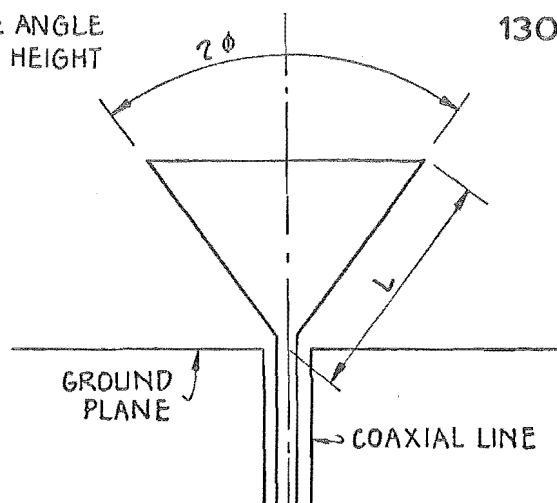


FIGURE 6.2: THEORETICAL IMPULSE RESPONSE OF 50 ohm CONICAL MONOPOLE (reproduced from Ross et al., 1966a).

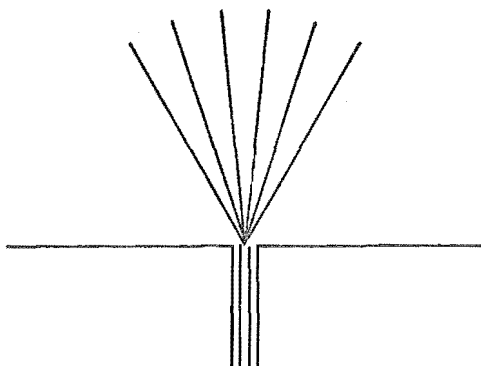


(a) FAN WITH CIRCULAR END

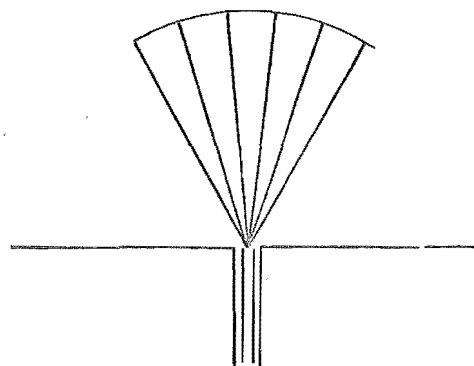


(b) FAN WITH STRAIGHT END.

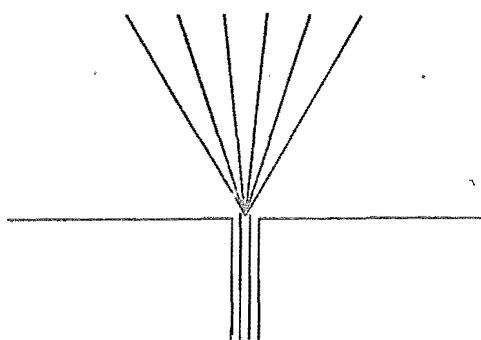
FIGURE 6.3: GEOMETRY OF SHEET METAL FAN MONOPOLES



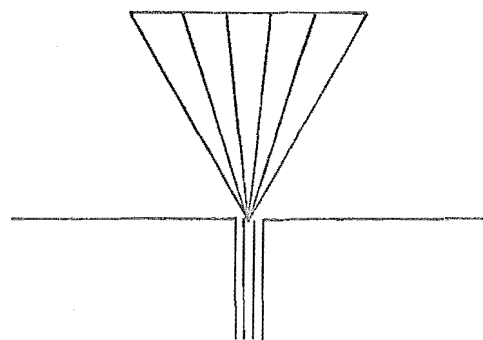
(a) CIRCULAR END, NO END WIRE



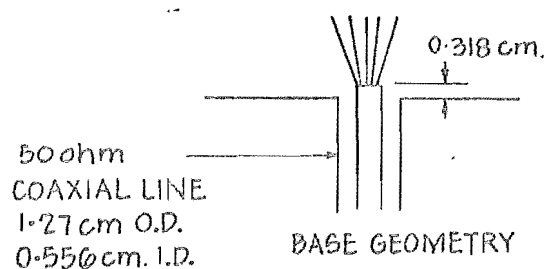
(b) CIRCULAR END, WITH END WIRE



(c) STRAIGHT END, NO END WIRE

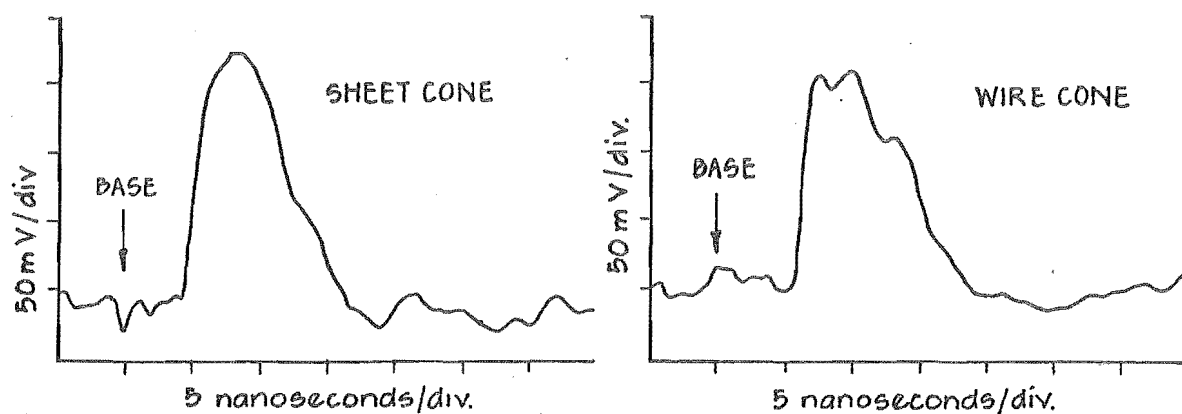


(d) STRAIGHT END, WITH END WIRE

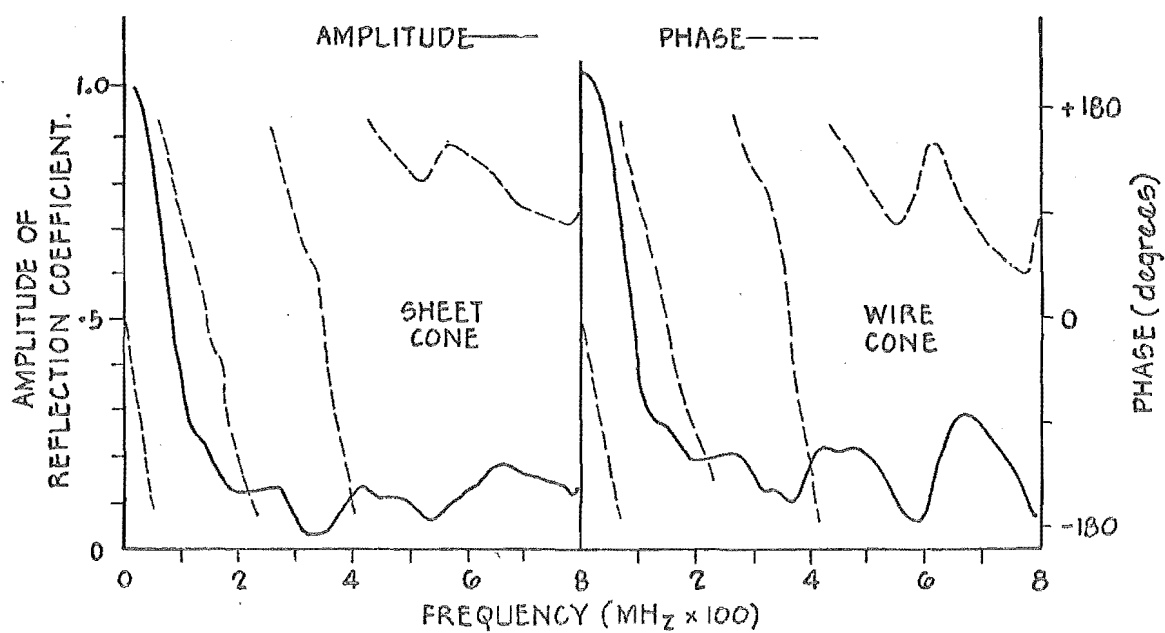


0.78 mm DIA WIRES  
 $L = 30.5$  cm.  
 THE ANGLES BETWEEN  
 THE WIRES ARE EQUAL.

FIGURE 6.4: FAN MONOPOLES CONSTRUCTED FROM 6 WIRES.



(a) RESPONSES TO 665 mV AMPLITUDE, 1 ns LONG TEST PULSE



(b) REFLECTION COEFFICIENTS.

FIGURE 6.5: DRIVING POINT RESPONSES OF 0.71 METRE SLANT HEIGHT 50ohm CONICAL MONOPOLES

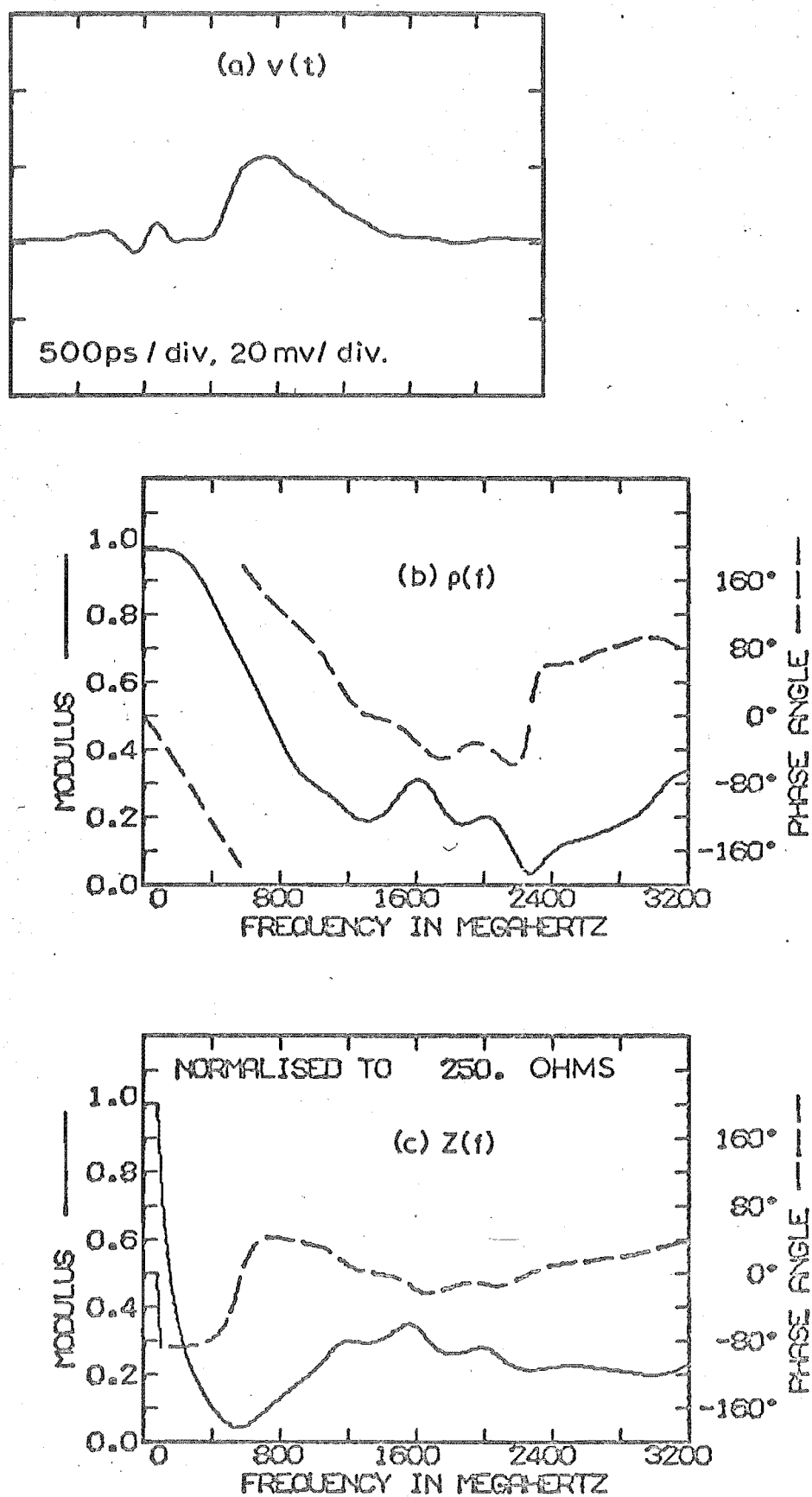


Figure 6.6: RESPONSES OF 7.6cm SLANT HEIGHT 50 OHM CONE



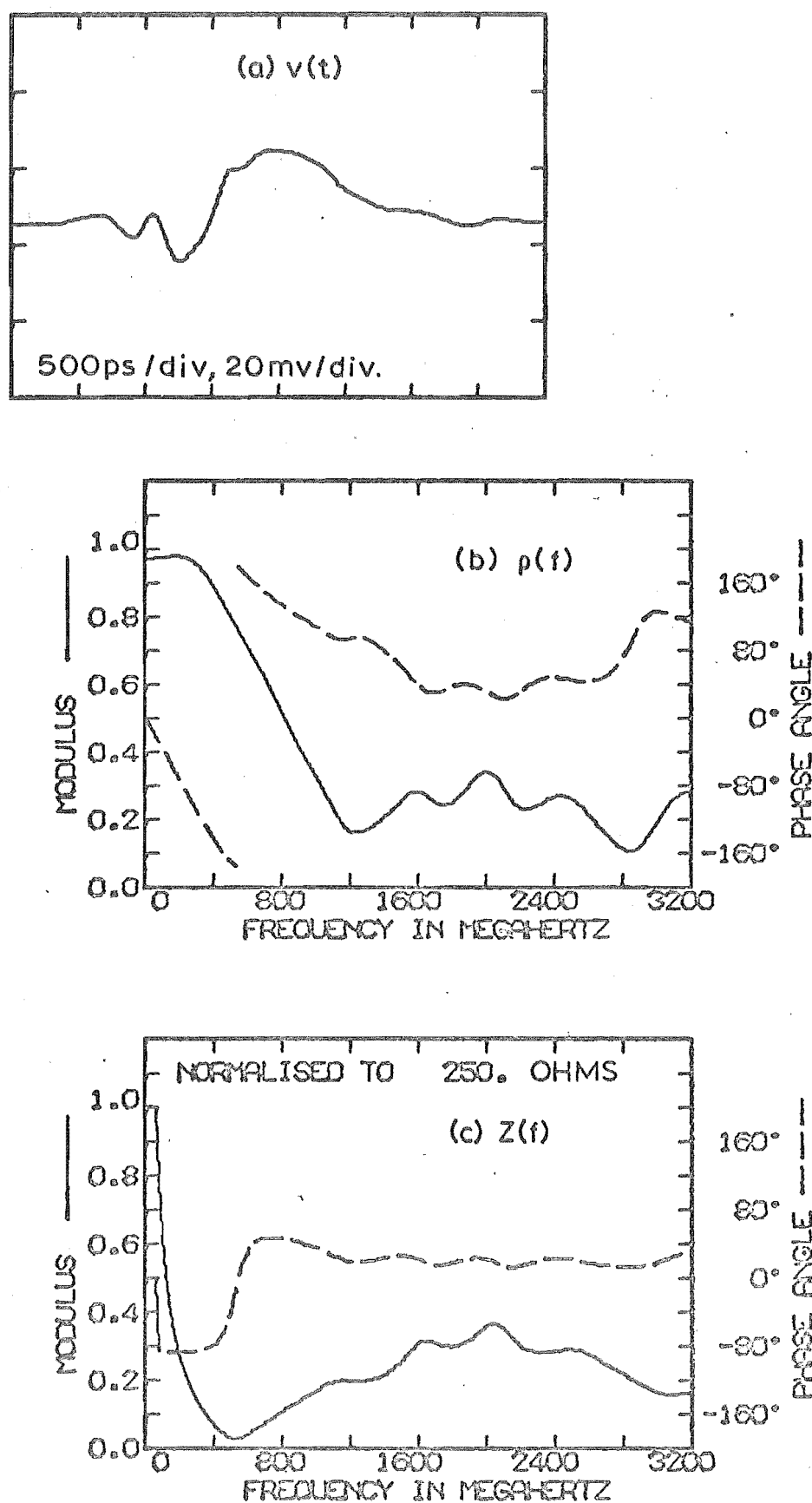
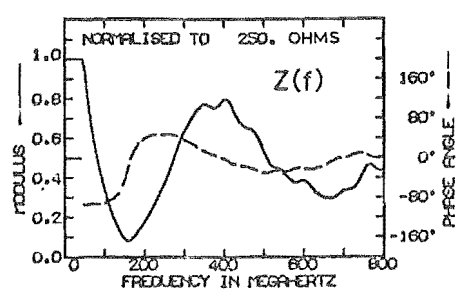
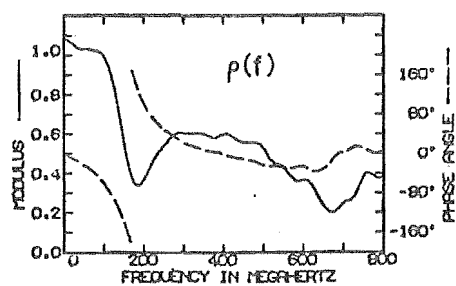
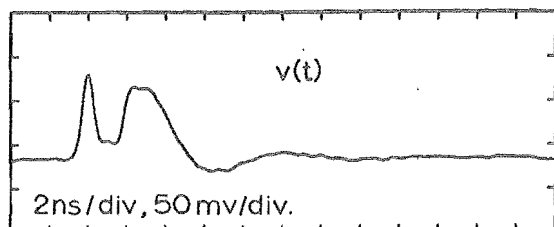
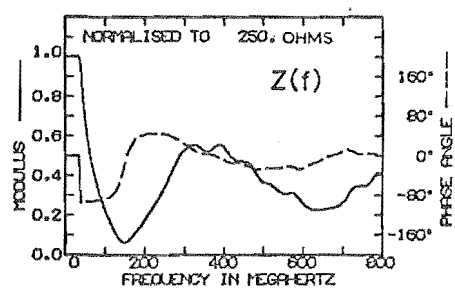
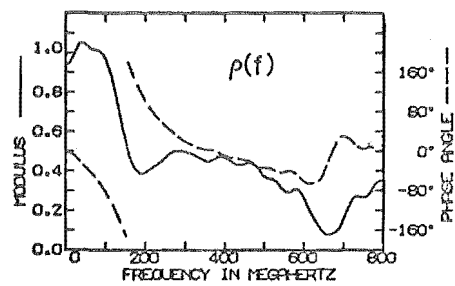
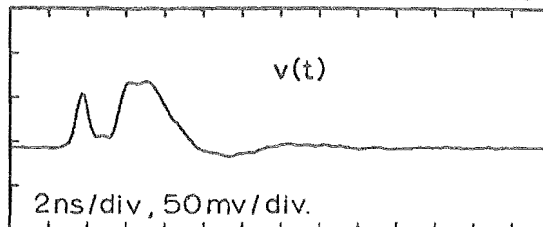


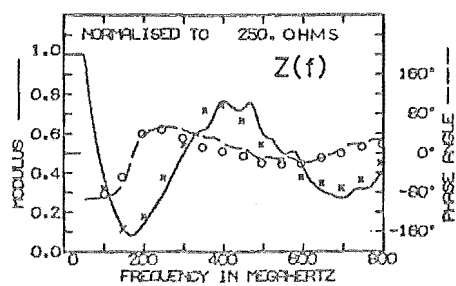
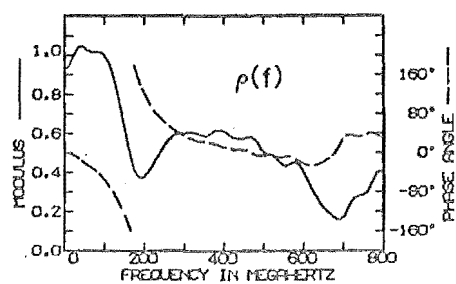
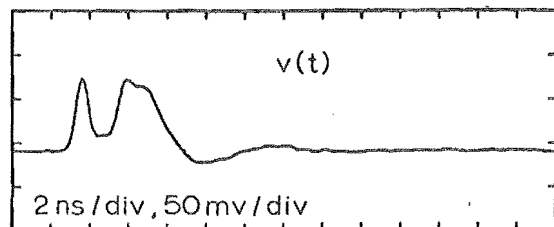
Figure 6.7: RESPONSES OF 7.6cm SLANT HEIGHT 50 OHM  
PHASE CORRECTED CONE



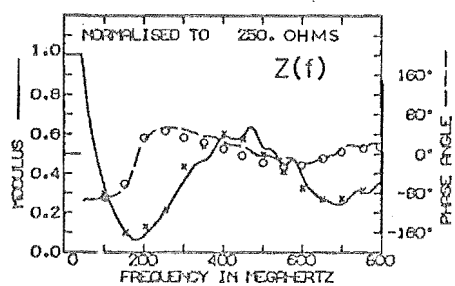
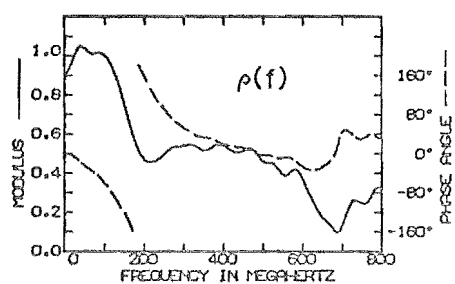
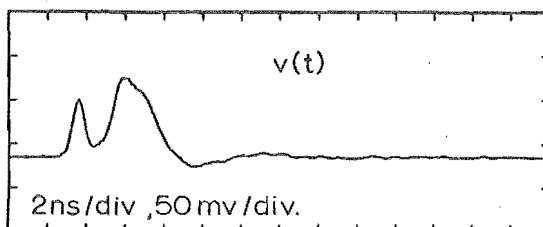
(a) CE-60



(b) CE-90



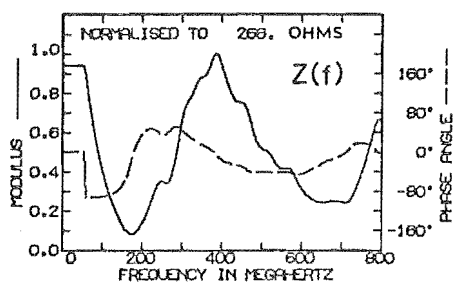
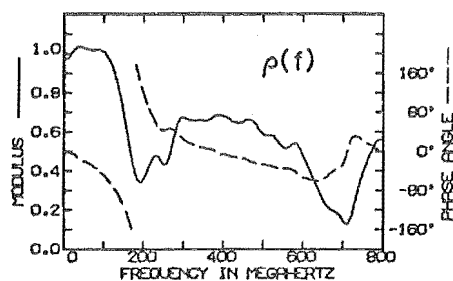
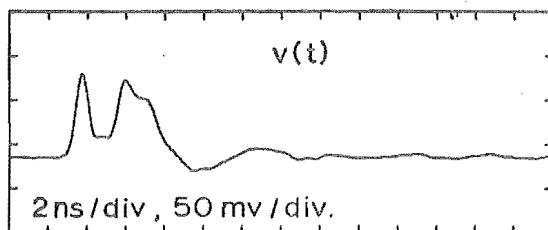
(c) SE-60



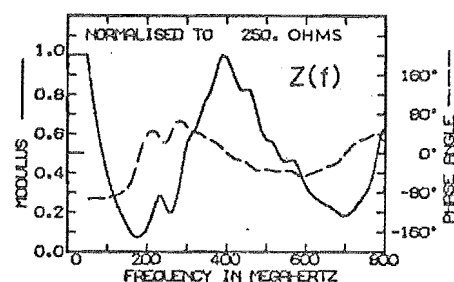
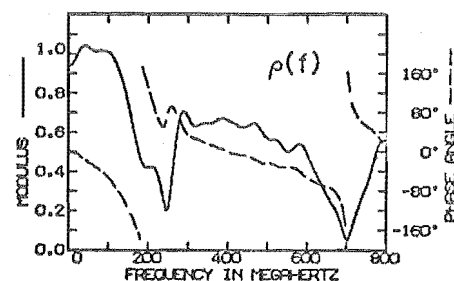
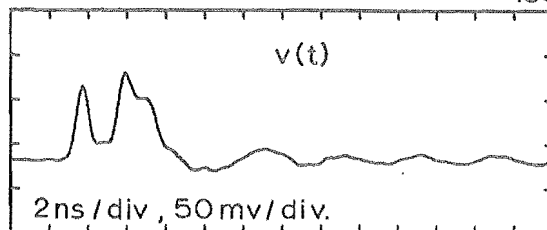
(d) SE-90

BROWN &  
WOODWARD  
Modulus x  
Phase o

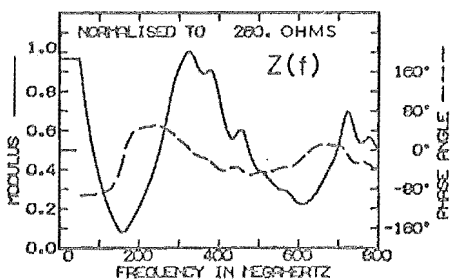
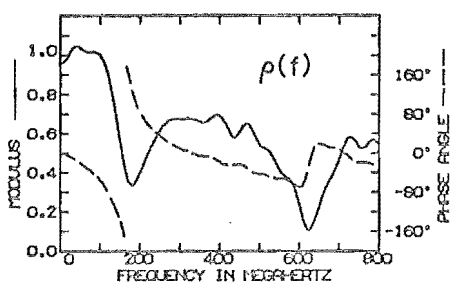
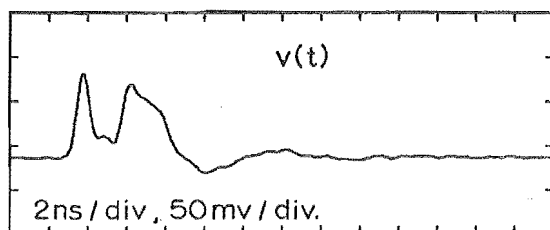
Figure 6.8: RESPONSES OF SHEET METAL FAN MONOPOLES.



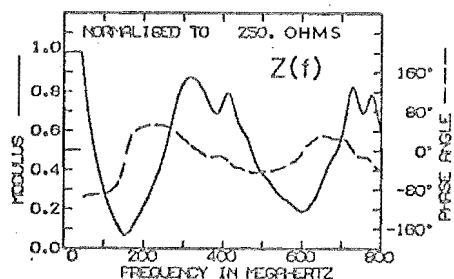
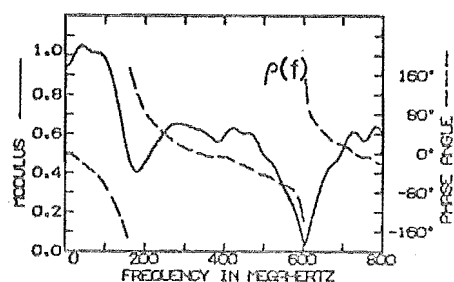
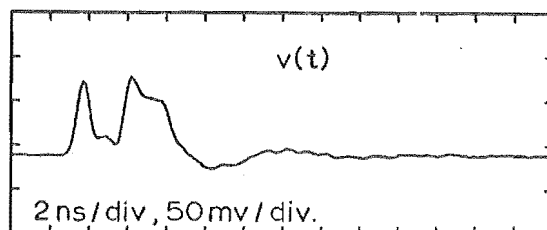
(e) 6W-CE-60



(f) 6W-CE-90

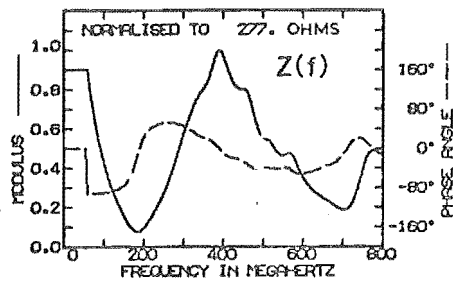
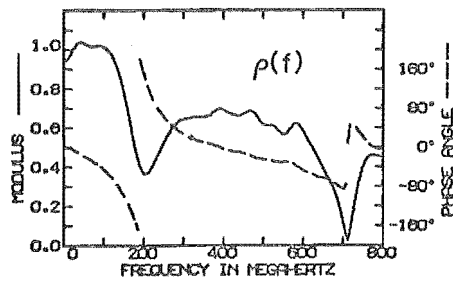
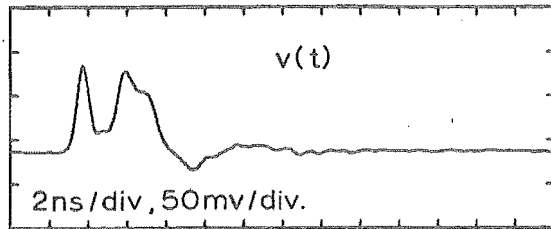


(g) 6W-CE-60-E

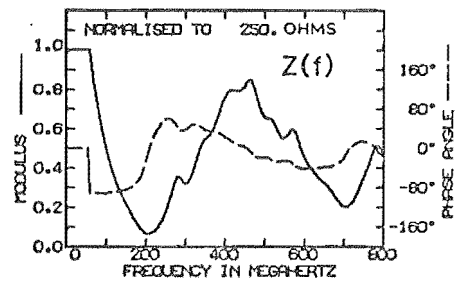
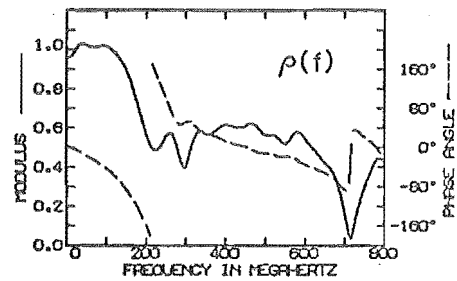
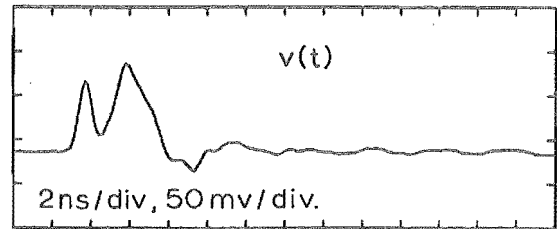


(h) 6W-CE-90-E

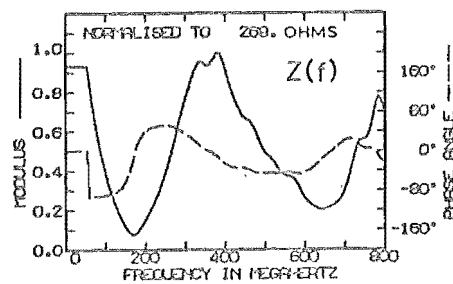
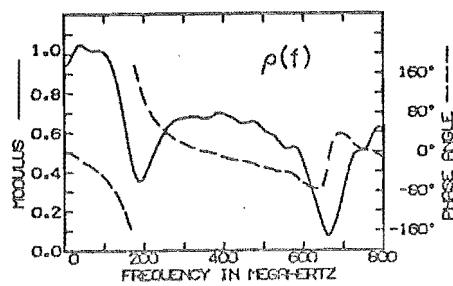
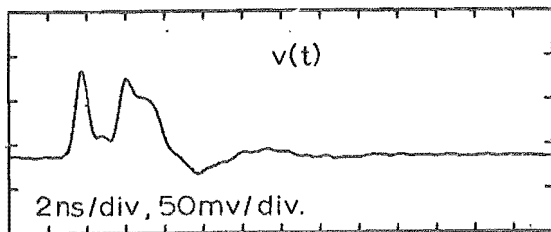
Figure 6.8(cont'd): RESPONSES OF WIRE FAN MONOPOLES



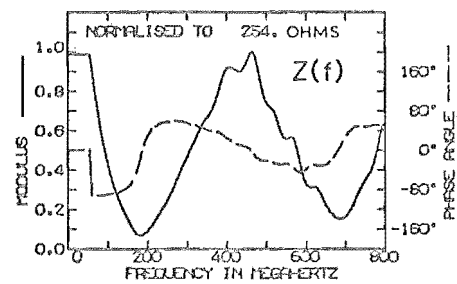
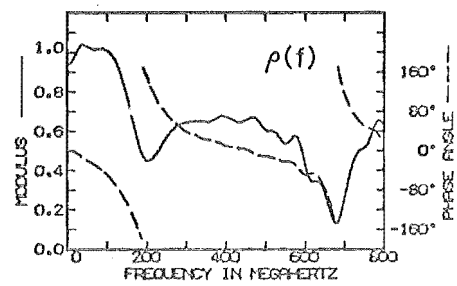
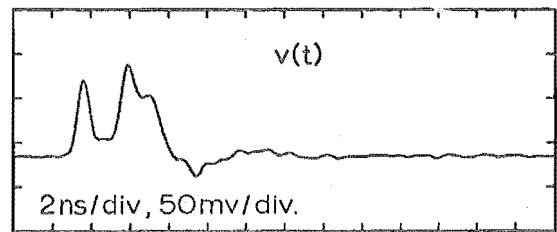
(i) 6W-SE-60



(j) 6W-SE-90

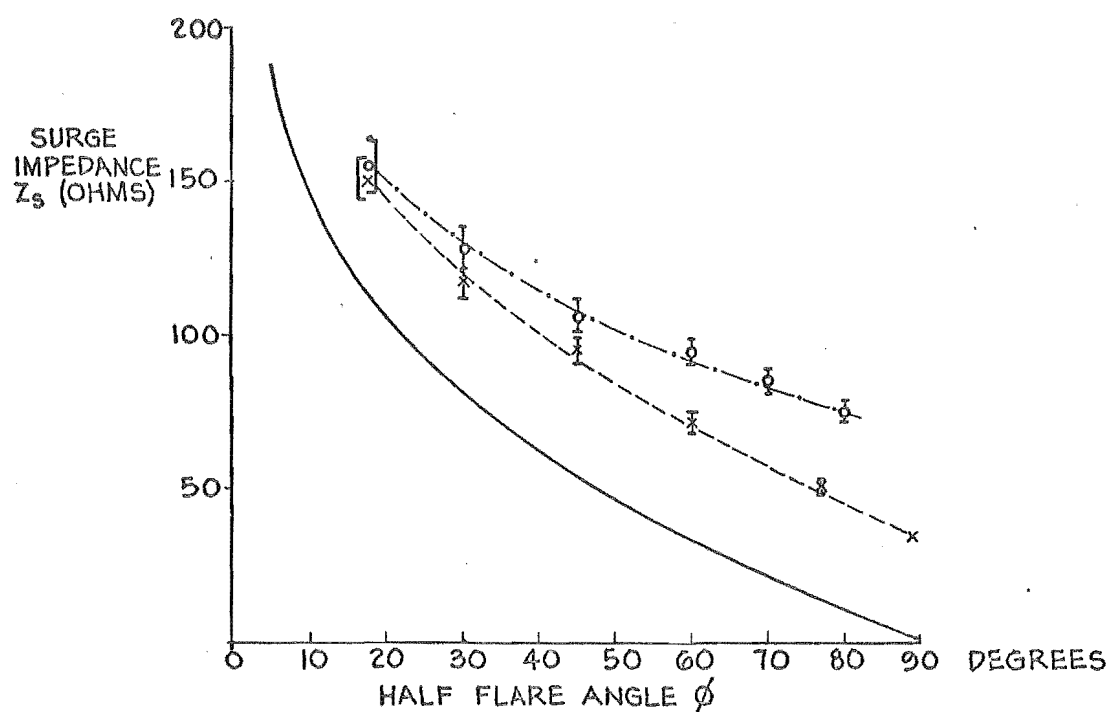


(k) 6W-SE-60-E



(l) 6W-SE-90-E

Figure 6.8(cont'd): RESPONSES OF WIRE FAN MONOPOLES



— · — · — 6 WIRE FAN MONOPOLE

$\begin{array}{c} \text{I} \\ \text{O} \\ \text{I} \end{array}$  EXPERIMENTAL POINTS WITH ERROR LIMITS

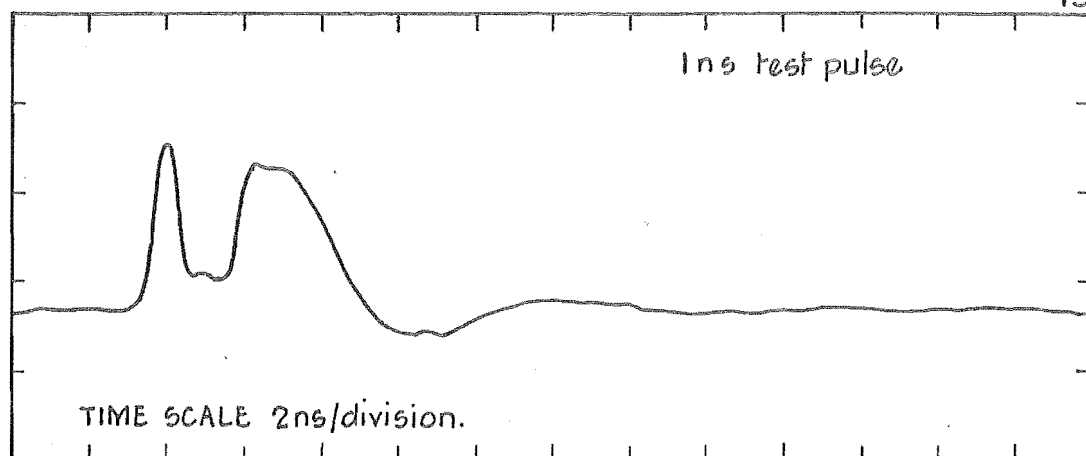
----- SHEET METAL FAN MONOPOLE

$\begin{array}{c} \text{I} \\ \text{X} \\ \text{I} \end{array}$  EXPERIMENTAL POINTS WITH ERROR LIMITS

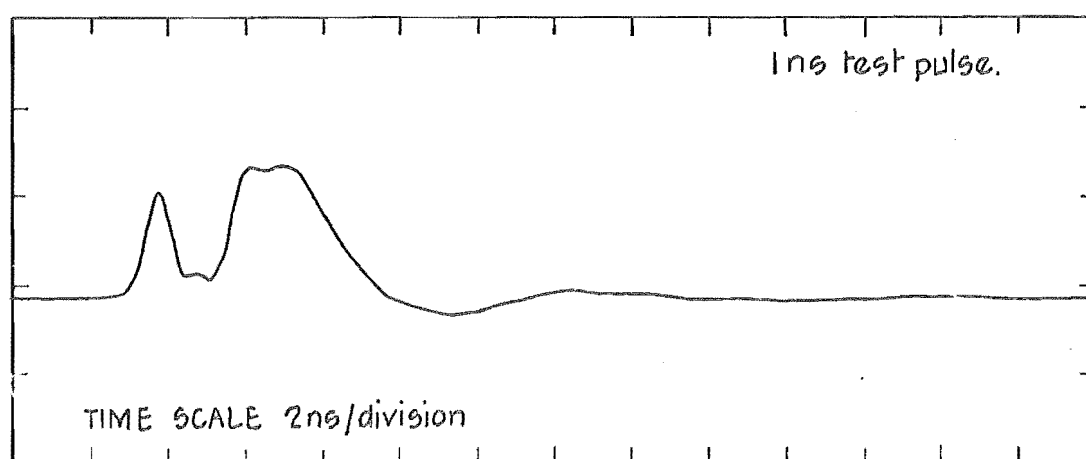
———— CONICAL MONOPOLE

$$Z_s = Z_o L_M \cot \frac{\phi}{2}$$

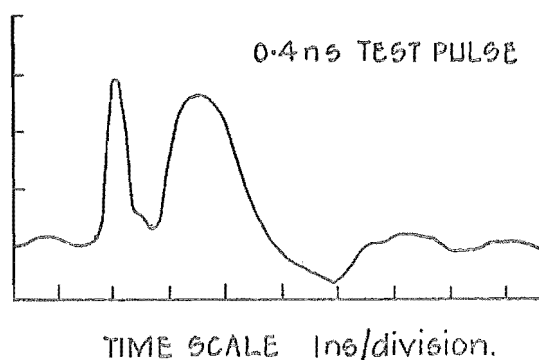
FIGURE 6-9: SURGE IMPEDANCES OF FAN MONOPOLES.



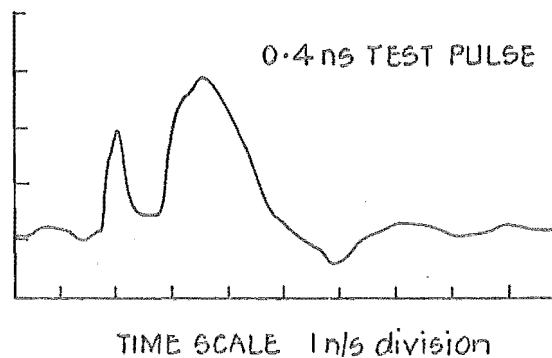
(a) FAN, 60° FLARE ANGLE,  $L = 30.5 \text{ cm}$ ,  $Z_g = 117 \text{ ohms}$ .



(b) FAN, 90° FLARE ANGLE,  $L = 30.5 \text{ cm}$ ,  $Z_g = 95 \text{ ohms}$ .



(c) CONE, 36° FLARE ANGLE,  
 $L = 15 \text{ cm}$ ,  $Z_g = 93 \text{ ohms}$ .



(d) CONE, 50.4° FLARE ANGLE  
 $L = 15 \text{ cm}$ ,  $Z_g = 75 \text{ ohms}$ .

(CONE RESPONSES REPRODUCED FROM  
ROSS et al. 1966a)

FIGURE 6.10: COMPARISON OF SHAPES OF DRIVING POINT PULSE RESPONSES  
OF SHEET METAL FANS WITH CIRCULAR ENDS AND MISMATCHED CONES.

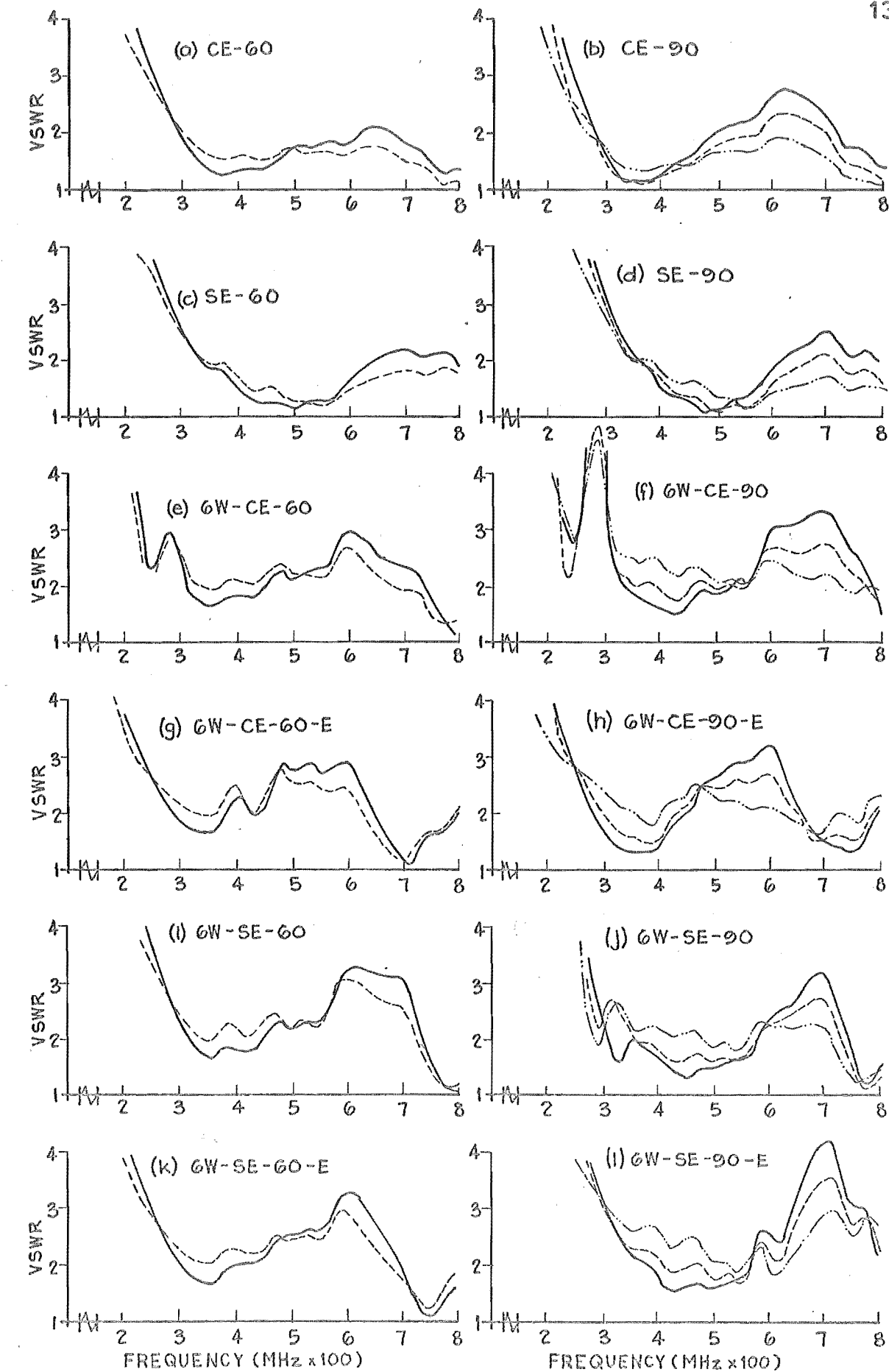


FIGURE 6.11 : VOLTAGE STANDING WAVE RATIOS FOR FAN DIPOLES.

## CHAPTER 7: SOME WIDEBAND WIRE ANTENNAS FOR HF

### 7.1 INTRODUCTION

The operating frequency of high frequency (HF) band radio-telephone services between two points on the earth's surface which are separated by several hundred miles must be changed several times during the day to take advantage of changing propagation conditions<sup>1</sup>. The frequencies used may span a 4:1 range. Wideband antennas must be used if switching between a number of single frequency antennas (e.g. dipoles) is to be avoided. Also, occasional changes in frequency allocations often results in the single frequency antennas being used at frequencies well removed from their design frequencies.

Radio-telephone services are generally used for communicating with geographically isolated settlements. Violent storms and icing are often experienced. Reliability is essential so that the antennas must be strongly constructed to withstand severe weather conditions. A mechanically simple antenna is desirable because it is cheaper to construct and is more reliable. In New Zealand the distance between the stations is seldom more than 500 miles, so that a minimum radiation angle of about  $30^{\circ}$  above the horizontal is required. Horizontal polarisation is used. For safe operation of the transmitter the VSWR on the feedline should be less than 2.

A rhombic antenna (Schelkunoff and Friis 1952, chapter 14) has about a 3:1 bandwidth but is physically large, requires four poles, and has a radiation angle of about  $10^{\circ}$ .

---

<sup>1</sup>The HF band is 3-30 MHz.



There is also a power loss in the terminating resistance.

A simple travelling wave antenna, called a Delta antenna, operates over a 25:1 bandwidth (Cones et al., 1950). However, because it was developed for ionospheric studies its radiation is directed essentially vertically and it is unsuitable for a radio telephone service.

A wide angle biconical dipole has a nearly constant input impedance over a wide bandwidth (see chapter 6) but it would be awkward to support if it was constructed large enough to operate in the HF band. However, vertically polarised wire conical monopoles with conical caps have been used at HF (Mason, 1963).

Frequency independent antennas based on the principle first suggested by Rumsey (1957), and experimentally developed by Dyson (1959a; 1959b) are also impractical because they would be awkward to support if constructed large enough to operate in the HF band. However, log-periodic antennas (Du Hamel and Isbell 1957, Jordan and Balmain 1968, chapter 15) can be built for the HF band. Log-periodic antennas can be designed to have specified bandwidths, specified vertical radiation angles (which are frequency independent), and about 13 dB of directivity relative to a dipole (Jasik 1961, section 18.5). However, they are mechanically complex which means that they are expensive to erect and their reliability is reduced. Tall and therefore costly poles are required<sup>2</sup>.

---

<sup>2</sup>e.g. for the log-periodic specified in Jasik (1961), the poles are  $1.1\lambda$  high at the lowest design frequency. Thus for a lower limit of 5 MHz the poles need to be 67 m high.

A bandwidth of about 1.4:1 has been obtained from 3-wire fan antennas mounted on aircraft (Meir, 1945) and from vertical 2-wire fan monopoles used for broadcasting (Brownless, 1955). The virtue of the fan antenna is its mechanical simplicity. In the last chapter measurements were made on some VHF fan monopoles made of wires. In this chapter the HF wire fan antenna is developed further by inferring the input impedance from measurements made on scale models using the experimental method described in Part I of this thesis. A discussion and bibliography of scale modelling techniques is given by IEEE (1965, section 1.7).

It is difficult to achieve perfect scaling, especially with such items as transmission lines and screw fastenings. It is impossible to scale the conductivity of the conductors. These disparities affect the input impedance much more than the radiation pattern. In particular, the input impedance is greatly affected by the dimensions of the region where the transmission line terminates at the ground plane (Brown and Woodward, 1945). It is wise then to regard measurements of the input impedance of scaled models as being primarily qualitative in nature, and to use them only to determine the general trends of the impedance of HF antennas. In this chapter a direct comparison is made between the measured input impedance of an HF fan antenna and a 1/50th size scale model. Differences of up to 40% are observed. The reasons for the differences are explained.

A fan antenna made from a continuous sheet of flat metal can be matched to its feedline over more than an octave bandwidth (see chapter 6). It was also shown in

chapter 6 that the variations in impedance with frequency when the fan is made from wires are greater than those of a sheet metal fan. In this chapter it is shown that these variations are reduced if the fan is made asymmetrical about its axis. Measurements have been made on a number of asymmetrical fan monopoles, and these are reported in this chapter. The shapes of all the antennas tested were such that they could be supported by only two poles if they were constructed to operate in the HF band.

At HF it is impractical to mount an antenna so far above the earth that the mutual coupling between the antenna and its image in the earth can be neglected. It is also impractical to accurately scale the highly variable and sometimes unknown properties of the soil (IEEE 1965, section 1.7). Since it represents a worst case (maximum mutual coupling) the earth was modelled by an aluminium sheet which was placed at right angles to the ground plane on which the antennas under test were mounted. Two preliminary designs of HF fan dipoles were constructed. The measured input impedances of these antennas are presented in this chapter. A bandwidth of 5:1 is obtained.

The criterion used for the acceptance of the antennas in this chapter is the VSWR on the feedline. The vertical radiation angle is also important, but it depends upon the height of the antenna above the earth in wavelengths, and the conductivity of the soil (Jordan and Balmain 1968, sections 11.09, 16.02).

The vertical radiation pattern changes with frequency and is multilobed when the phase centre of the antenna is

greater than a half wavelength above the earth. This problem is, however, common to most antennas which are mounted above the ground. The variations of the radiation pattern with elevation angle can only be reduced by using highly directive arrays such as the log-periodic array described above.

## 7.2 THE ASYMMETRICAL TRIANGULAR FAN

The geometry of the asymmetrical triangular fan monopole is shown in Fig. 7.1. Measurements were made only for the two special cases in which the triangle is isosceles. These are when  $\theta_1 = \theta_2 = 45^\circ$  which is designated the A type, and when  $\theta_1 = 45^\circ$  and  $\theta_2 = 90^\circ$  which is designated the B type. The vertical height is L. An asymmetrical fan made of wires is shown in Fig. 7.2. The way in which the wire antennas are identified is illustrated with some examples. An A3E antenna is type A, made from three wires, with an end wire (such as the one pictured in Fig. 7.2). An A5 fan is type A, made from 5 wires, without an end wire.

### 7.2.1 Scale Model Measurements

With the exception of the aluminium sheet used to model the earth, the experimental and computational procedures used for these measurements were the same as those used for the measurements reported in section 6.3.3. The aluminium sheet measured 0.92 m by 1.22 m. It was mounted at right angles to, and with its longer side contacting the ground plane on which the antennas under test were mounted (see Fig. 7.1). The distance between the antenna axis and the

earth plane is denoted  $h$ . For most of the measurements  $h$  was 30.5 cm. The A fans were all constructed with  $h = 30.5$  cm and the B fans with  $h = 21.55$  cm (the slant height is then 30.5 cm so that a B fan is equivalent to an A fan rotated through  $45^\circ$ ).

Reflection coefficients and input impedances were computed from measured signals from A and B fans. The fans were made from tin plated steel sheet (0.33 mm thick), and were measured both with and without the earth plane. The results are shown in Figs 7.3(a) to 7.3(d). Compare these results with those for the symmetrical sheet fans shown in Figs 6.8(a) to 6.8(d). The antiresonant impedance is higher but the second resonance (which occurs at about 700 MHz) has become very indistinct. Another important point is that the earth plane reduces the variations of impedance with frequency (for the A fan measured with the earth plane the impedance is nearly constant from 300 MHz to 800 MHz), so that this geometry of antenna is potentially useful in the HF band where it is impractical to mount an antenna many wavelengths above the ground. The low VSWR of the A and B type dipoles are shown in Fig. 7.4 for two feedline impedances. Notice that for both antennas the lower frequency limit is reduced by the presence of the earth plane, and that the A type is better matched than the B type. Also, wire A antennas (see Fig. 7.2) are simpler to erect if made large enough to operate in the HF band. Consequently development centred on the A type.

Reflection coefficients and input impedances were computed from measured signals from wire A type antennas. In

section 6.4.2.1.2 it was shown that the electrical length of a wire fan is increased (hence lowering its frequency band of operation) by fitting an end wire. Consequently the investigation was mainly limited to fans with end wires. The measurements for A3E, A4E, A5E and A6E antennas with  $h = 30.5$  cm (see Fig. 7.2) are shown in Figs 7.5(a) to 7.5(d). The effect of reducing  $h$  for the A5E antenna is shown in Fig. 7.6. Fig. 7.7 shows the measured characteristics of an A6E antenna without the earth plane and an A3 antenna for  $h = 30.5$  cm. VSWR plots (calculated from the computed results) for the wire antennas are shown in Fig. 7.8.

The most prominent characteristic of the A3 antenna (see Fig. 7.7(b)) is that the measurable duration of  $v(t)$  is longer than the measurement interval, which was 29.5 ns. The measurable duration of  $v(t)$  for this antenna could not be determined because the viewing window of the measurement apparatus was set at 30 ns (see section 3.2). Notice that the tail of  $v(t)$  is approximately a 300 MHz sinusoid. This means that  $\rho(f)$  and  $Z(f)$  are frequency sensitive in the vicinity of 300 MHz (an extended pulse response indicates a frequency sensitive frequency response): this is observed in Figs 7.7(b) and 7.8(h). Also, because  $v(t)$  was truncated, significant errors can be expected in the computed  $\rho(f)$  and  $Z(f)$ , especially near 300 MHz. The extra truncation introduced by the data window (see Appendix 4) also contributes to this error. Consequently the rapid fluctuations in  $\rho(f)$  and  $Z(f)$  near 300 MHz will actually be more severe than indicated in Fig. 7.7(b). The frequency sensitivity disappears when an end wire is fitted (see Fig. 7.5(a)). Thus

end wires are essential on asymmetrical wire fans. It is interesting to note that the characteristics of the A3 fan are more frequency sensitive than the characteristics of the thin monopole shown in Figs 2.5 and 2.6. Some frequency sensitivity around 300 MHz is also noticed for symmetrical wire fans without end wires, see e.g. Fig. 6.11(f).

The characteristics of the asymmetrical wire fans (see Fig. 7.5) exhibit a particularly interesting behaviour when compared to the characteristics of the symmetrical wire fans presented earlier in chapter 6. Instead of exhibiting distinct antiresonances, the input impedance of the asymmetrical wire fans oscillates about some mean value. For the A5E and the A6E the mean is about 175 ohms. For this reason the asymmetrical wire fans can be matched over more than 2.5:1 bandwidths (see Figs 7.8(c) and 7.8(d)). The second resonance (at about 700 MHz) is more distinct than it is for the sheet metal fan (see Fig. 7.3(b)) but it still does not spoil the match. Figs 7.7(a) and 7.8(g) demonstrate that removing the earth plane spoils the match. As  $h$  is reduced, a peak appears in the input impedance at 380 MHz (see Fig. 7.6). This spoils the match at low frequencies (see Figs 7.8(e) and 7.8(f)). However, there is a slight improvement at about 600 MHz (see Figs 7.8(c) and 7.8(e)). The conclusion is that the optimum value of  $h$  is slightly less than 30.5 cm for the wire fans.

### 7.2.2 An HF Asymmetrical Triangular Fan Dipole

An A5E dipole was constructed to the dimensions shown in Fig. 7.9, which are 50 times the dimensions of the model. The height of the masts corresponded to an  $h$  of 30.5 cm in

the model, so that, after allowing for some sag, the average height of the antenna was about optimum. A length (about 18 m) of low loss, nominal 300 ohm TV antenna feedline was connected to the centre of the dipole<sup>3</sup>. Measurements were made of the impedance at the end of the feedline with a Wayne-Kerr VHF admittance bridge, and the antenna input impedance was calculated using the lossless transmission line equation (Jordan and Balmain 1968, section 7.15). The electrical length of the feedline was determined by short circuiting the far end and measuring the frequency at which its input admittance was zero (as measured on the bridge). This corresponds to an electrical length of an odd multiple of  $\lambda/4$ , and the ambiguity was resolved by calculating the approximate electrical length from the physical length by assuming a velocity factor of 0.88. The feedline used was a wavelength long at 14.0 MHz. The characteristic impedance, determined from open and short circuit measurements, was 320 ohms.

The criterion for accepting or rejecting the antenna was whether the VSWR is less than, or greater than 2. Standard 300 ohm TV feedline has a loss of 0.14 dB/30 m at 1 MHz and 0.43 dB/30 m at 10 MHz. For an 18 m length at a frequency of 10 MHz, a VSWR of 2 at the antenna would be measured as 1.91, and a VSWR of 4 at the antenna would be measured as 3.6. Thus the error increases with VSWR. The scale model measurements indicate that a feedline of about 300 ohms will give the best match (see Figs 7.8(c) and

---

<sup>3</sup>Low loss 300 ohm feedline is perforated so that most of the plastic dielectric separating the conductors is removed. This also causes an increase in the characteristic impedance.



7.8(e)), which means that the measurement error caused by neglecting the feedline loss is a minimum when the measurements are made using 300 ohm feedline. Also the error will be smaller than indicated because the feedline used had lower loss than the standard feedline (although no specification could be found). Consequently the feedline loss was neglected.

The measured input impedance (plotted on a resistance-reactance diagram) is shown in Figs 7.10(a) and 7.10(b). The circle for a VSWR of 2 on a 300 ohm feedline is superimposed (the VSWR is less than 2 for all the frequencies for which the input impedance lies within the circle; Reich 1947, chap. 3). The VSWR calculated from the measured input impedance is also plotted in Fig. 7.10(b). Comparison with Fig. 7.8(c) shows that the match is not as good as that of the model, although the VSWR is less than 2.4 from 7 MHz to 24 MHz.

### 7.2.3 Comparison of Measured Input Impedances of HF Dipole and Scale Model Monopole

The measured input impedances of the HF A5E dipole and the scale model A5E monopole (for  $h = 30.5$  cm) are shown superimposed in Fig. 7.11. The agreement is reasonably good (about 10%) when  $|Z(f)|$  is less than 150 ohms, with the exception of phase errors of about  $40^\circ$  above 700 MHz. Significant differences (up to 40%) are observed when  $|Z(f)|$  is large, although the shapes of the impedance/frequency characteristics are the same. The differences are more than can be expected from errors in the computed  $\rho(f)$ , e.g. if  $\rho(f)$  is real and equal to 0.65 (giving  $Z(f) = 236$  ohms), then

a 4% error in  $\rho(f)$  (see section 6.3.4) only causes a 10% error in  $Z(f)$ .

There are three main reasons for the differences. The first is the effect of base capacitance on the model measurements. The length of the model fans were only 24 times the outer diameter of the coaxial line which fed them, so that the driving point dimensions cannot be ignored (Brown and Woodward, 1945). From experimental data, King (1955; 1965, section 5-22) infers values for an end correction (shunting) capacitance for thin ( $a < \lambda/250$ ) cylindrical monopoles driven from coaxial lines. The value of the capacitance depends upon the coaxial line gap  $b-a$ , and upon the ratio  $b/a$ . The effect of this shunting capacitance is greatest when  $|Z(f)|$  is large, in agreement with the observed differences in Fig. 7.11. An improvement could have been made by reducing the diameter of the sections of coaxial line which fed the model antennas, but then it would have been difficult to manufacture the test antennas. Also the HF dipole is fed by a two wire transmission line. Strict observation of scaling demands that the model be fed by a single wire (above the image plane). It would be difficult to arrange a reflection free junction between a single wire transmission line and a coaxial line.

The second reason is that the diameter of the wires from which the models were made was not scaled exactly. Experiments conducted recently by Sharp and Tanner (1969) on scaled log-periodic antennas show that incorrect scaling of the wire diameter (by 200 times) causes large errors in the current distribution (and hence in the input impedance) and

in the radiation pattern. It was not possible to scale the wire diameter exactly and have a self-supporting model (exact scaling demands 0.066 mm diameter wire). Consequently the fan length to wire diameter ratio is smaller (11 times) for the model than for the HF dipole. This reduces the input impedance at antiresonance (cf. the monopole, for which the input impedance at resonance is a strong function of the length/diameter ratio; Jordan and Balmain 1968, pp566-567). Thus the errors due to thicker wires and the increased base capacitance tend to add.

The third reason is that the aluminium sheet representing the earth for the model antennas is not an accurate representation of the true earth. The effect of the imperfect earth is unknown, but it is reasonable to expect the characteristics of the antenna near an imperfect earth to lie somewhere between those with no earth and those with a perfect earth. The phase/frequency characteristics of the input impedances shown in Figs 7.5(d) and 7.7(a) indicate that removing the earth plane increases the phase angle. Thus the phase differences observed in Fig. 7.11 can be (at least partly) attributed to the imperfect earth.

Fig. 7.11 shows that the scale models cannot be used to accurately predict the input impedance of an HF antenna. However, the shape of the impedance/frequency characteristics are the same so that the model measurements are useful for determining trends in the input impedance. Also, the full scale version of the model is a satisfactory HF antenna. Consequently, the short pulse model measurement technique introduced in this thesis has been shown to have practical value.

### 7.3 THE FOLDED SQUARE FAN

An improved match was sought by adding a second fan in such a way that the antenna is a square fan folded about its axis to include an angle  $2\psi$ . This antenna is designated the 2A5E, and its geometry is shown in Fig. 7.12.

#### 7.3.1 Scale Model Measurements

Reflection coefficients and input impedances were computed from measured signals from a 2A5E antenna for  $h = 30.5$  cm, 25.4 cm and 20.3 cm. The apex angle  $2\psi$  was  $45^\circ$ . The results are shown in Fig. 7.13. The second fan greatly reduces the fluctuations of input impedance with frequency (e.g. compare Fig. 7.13(a) to Fig. 7.5(c)). The optimum value of  $h$  is the same as for the A5E antenna. It is interesting to note that the characteristics of this configuration of wire fan roughly approximate those of the A type sheet metal fan (Fig. 7.3(b)).

#### 7.3.2 An HF Folded Square Fan

The HF A5E antenna shown in Fig. 7.9 was converted into a 2A5E, and the apex angle of  $45^\circ$  was obtained by placing anchor posts 6.3 m either side of the centre line (a straight line between the two masts). The input impedance (measured using the method described in section 7.2.2) is plotted on a resistance-reactance diagram in Figs 7.14(a) and 7.14(b). The circle for a VSWR of 2 on a 300 ohm feedline is superimposed. The VSWR calculated from the measured input impedance for a 300 ohm feedline is also plotted in Fig. 7.14(b), and a 2.8:1 bandwidth is obtained (7.5 MHz - 21 MHz).

The input impedance of this antenna is predominantly inductive, and the match can be improved by adding series capacitive reactance. Following the matching procedures described by Reich (1947, chapter 3) the optimum match shown in Fig. 7.15 was obtained with a series capacitor of  $130 \text{ pf}^4$ . The bandwidth exceeds 5:1.

#### 7.4 FURTHER DEVELOPMENTS

The results presented in this chapter demonstrate that horizontal wire fan dipoles are potentially good wideband HF antennas. However, the investigation reported in this chapter was restricted to two specific values of  $\theta_1$  and  $\theta_2$  and to one value of  $\psi$ . The numbers of wires from which the fans were made also occupied a restricted range. The performance of the HF dipole might be improved by varying the fan angles, the number of wires, and the angles between the wires. Also, satisfactory performance might be obtained from a fan contained in a single plane if enough wires are used. A disadvantage of the particular geometry of antenna presented in this chapter is that the masts need to be spaced about 30% greater than the antenna length so that the antenna can be rigged properly. A modification to the geometry is necessary to utilise the mast spacing more efficiently. A comprehensive experimental investigation using scale models would enable the design to be optimised. The experimental technique developed in this thesis is ideal

---

<sup>4</sup>In practice two 260 pf capacitors (one connected in series with each side of the feedline) would have to be used to preserve symmetry, hence preventing out-of-balance currents flowing on the feedline.

for this purpose. In any further investigation however, the dimensions of the coaxial line feeding the model antennas should be reduced. Also, the models should be made of thinner wires so that the scaling conditions are more closely approximated, provided that it is found that (to provide proper mechanical support) thin wires glued to foam polystyrene (which has a dielectric constant very near to that of air) are electromagnetically equivalent to thin wires in air (it is doubtful if this can be assumed from existing knowledge without further experiment).

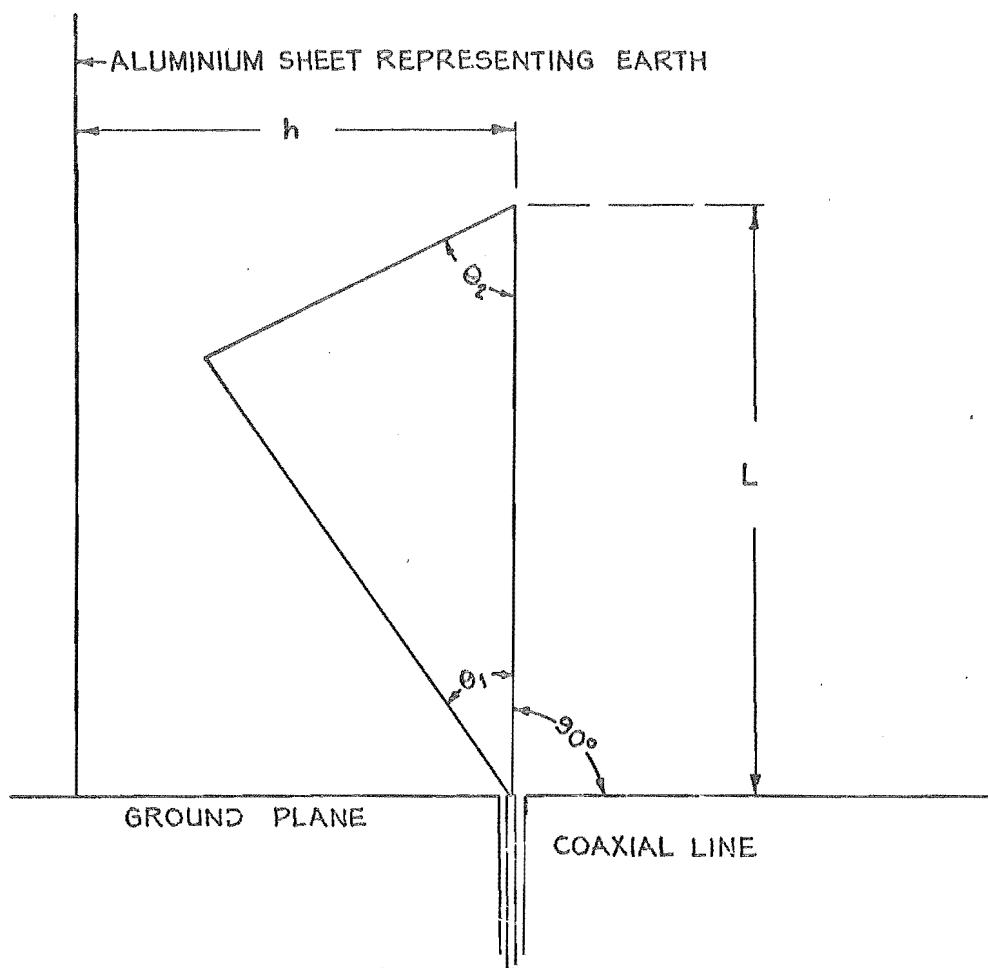
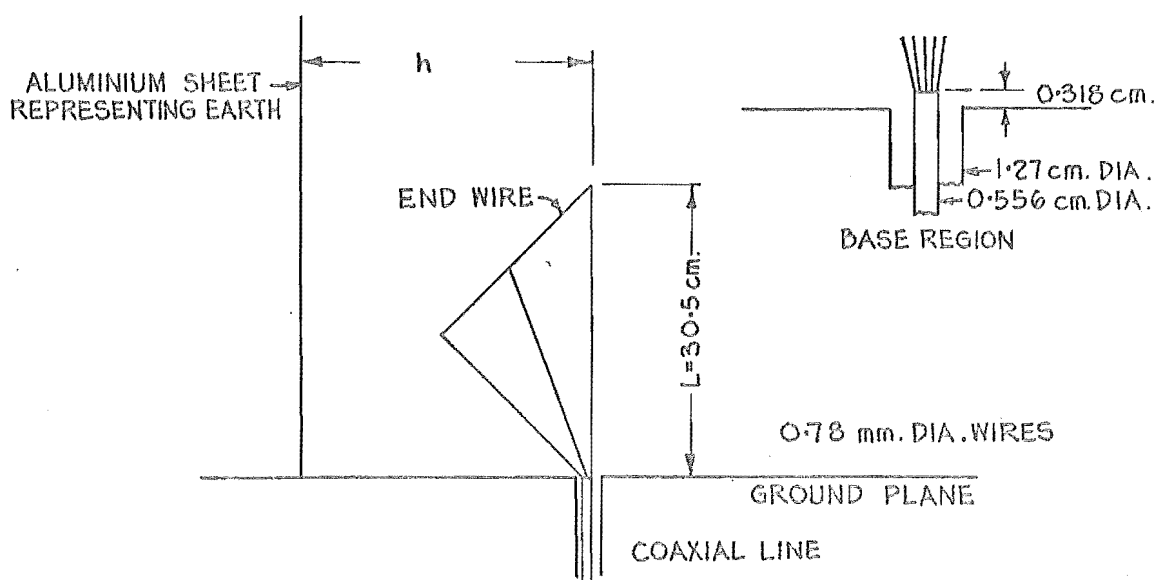


FIGURE 7.1: GEOMETRY OF ASYMMETRICAL TRIANGULAR FAN MONOPOLE



A TYPE :  $\theta_1 = \theta_2 = 45^\circ$

PICTURED IS AN A3E FAN i.e. 3 WIRES WITH END WIRE.  
THE ANGLES BETWEEN THE WIRES ARE EQUAL.

FIGURE 7.2: GEOMETRY OF ASYMMETRICAL WIRE FAN MONOPOLES

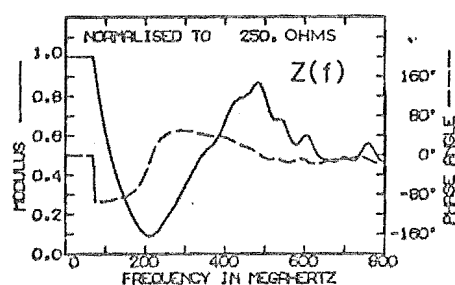
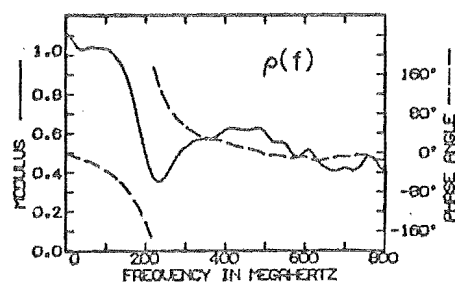
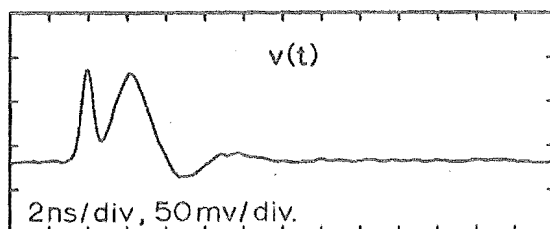
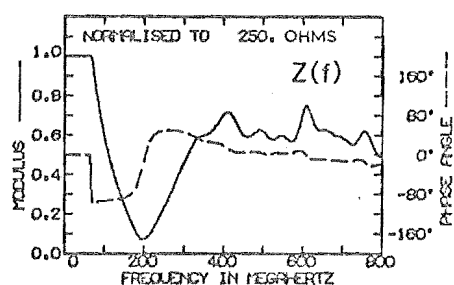
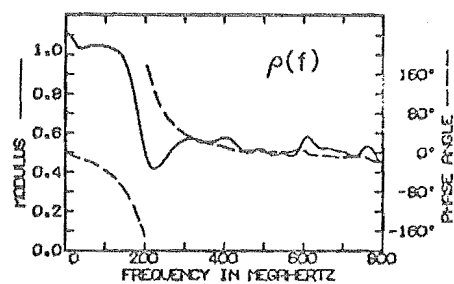
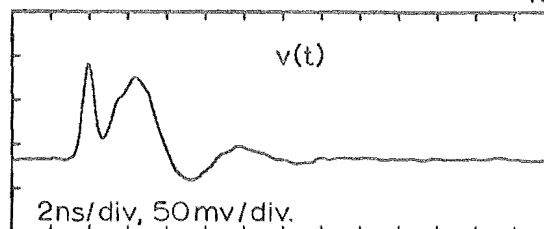
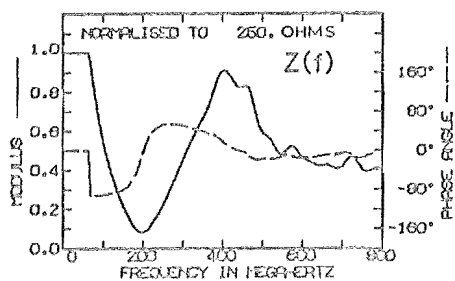
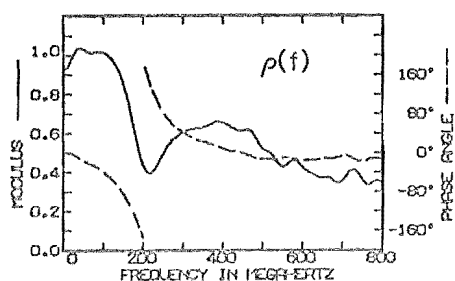
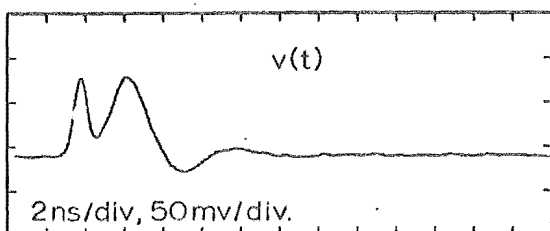
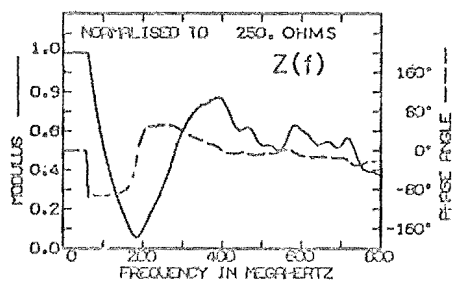
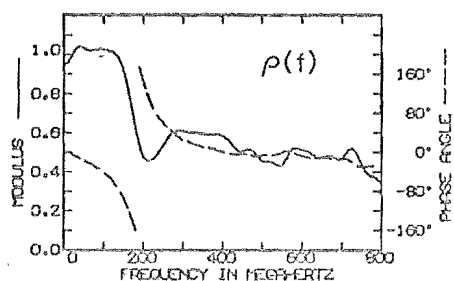
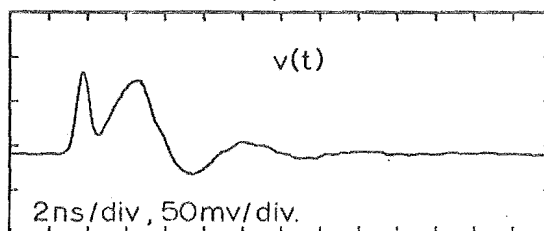
(a) A TYPE,  $h=\infty$ (b) A TYPE,  $h=30.5\text{cm}$ .(c) B TYPE,  $h=\infty$ (d) B TYPE,  $h=30.5\text{cm}$ .

Figure 7.3: RESPONSES OF ASYMMETRICAL SHEET METAL FAN MONOPOLES



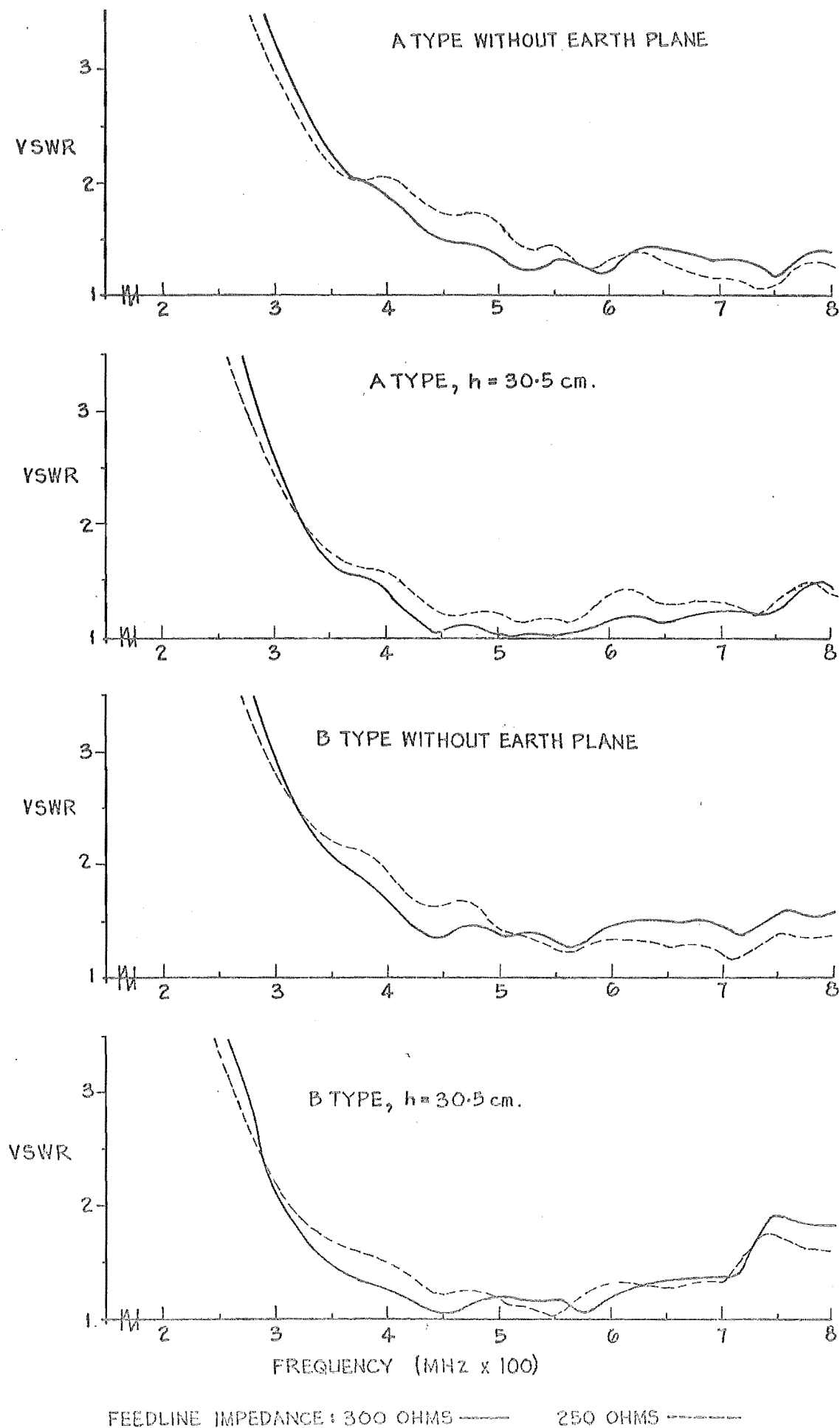


FIGURE 7.4: VSWR FOR ASYMMETRICAL SHEET METAL FAN DIPOLES

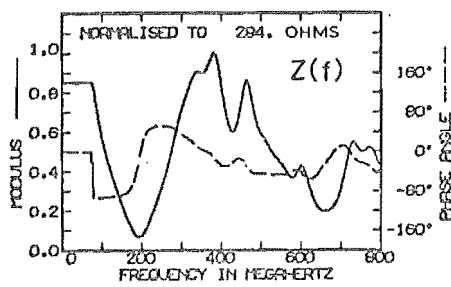
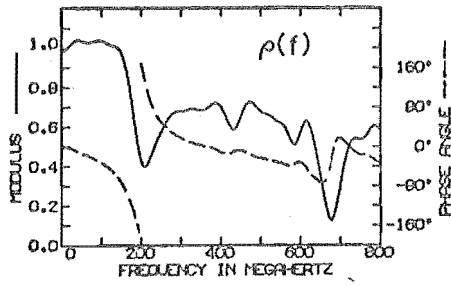
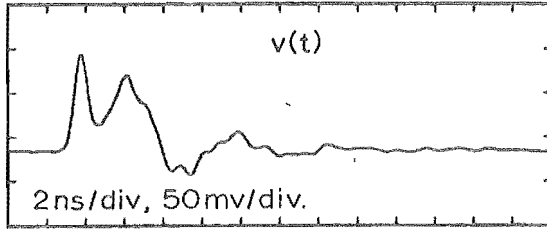
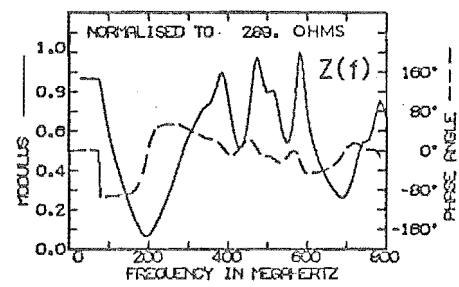
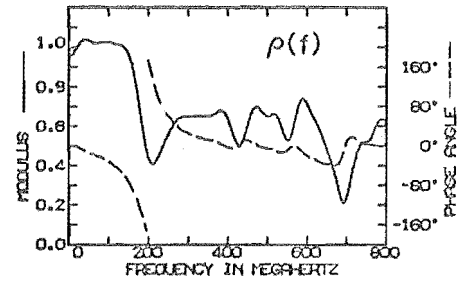
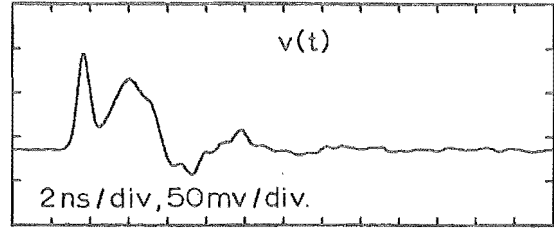
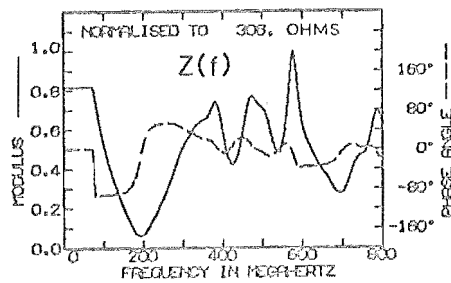
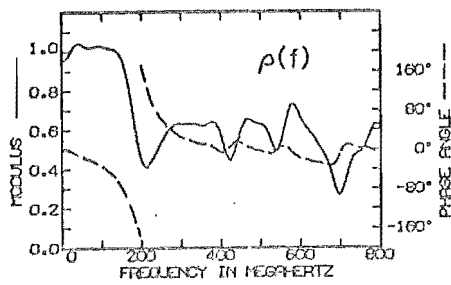
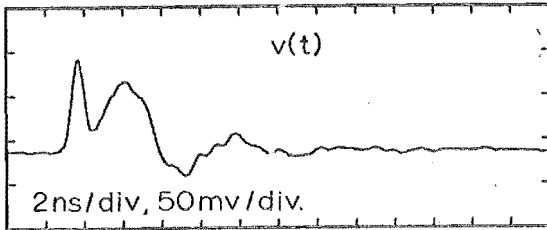
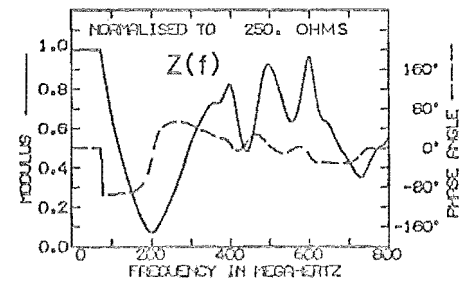
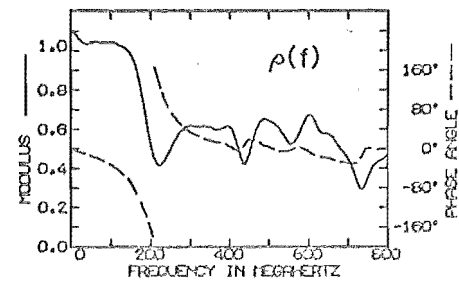
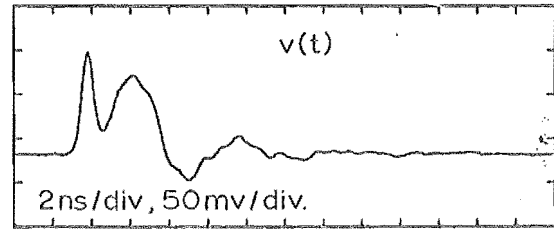
(a) A3E,  $h = 30.5$  cm.(b) A4E,  $h = 30.5$  cm.(c) A5E,  $h = 30.5$  cm.(d) A6E,  $h = 30.5$  cm.

Figure 7.5: RESPONSES OF ASYMMETRICAL WIRE FAN MONOPOLES

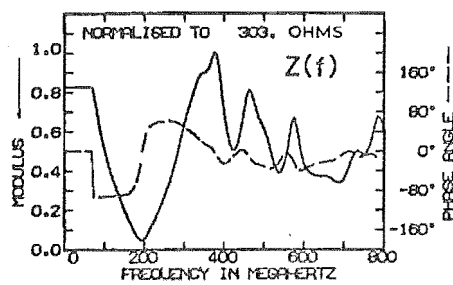
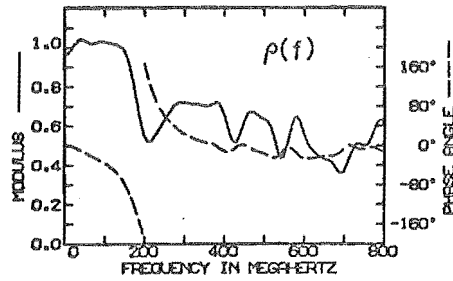
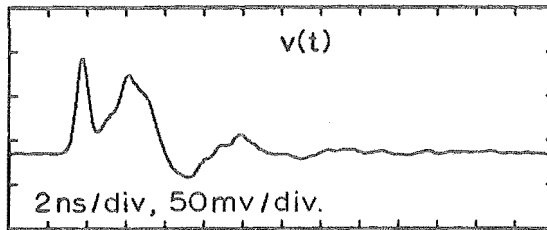
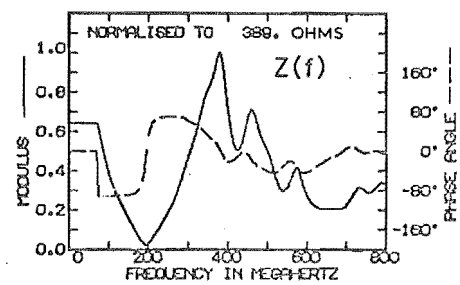
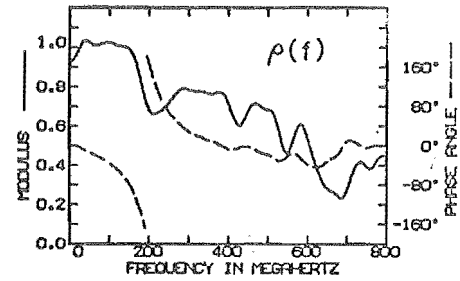
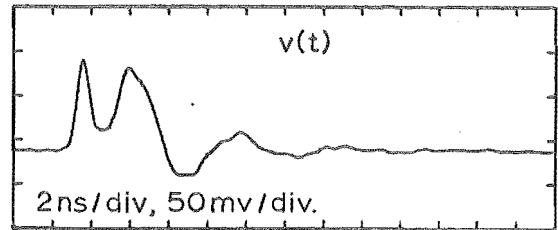
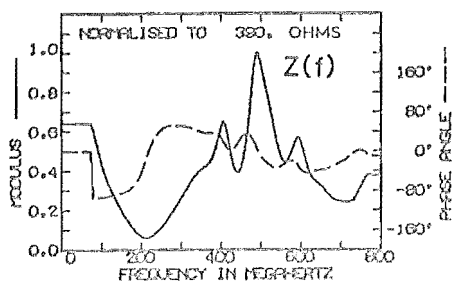
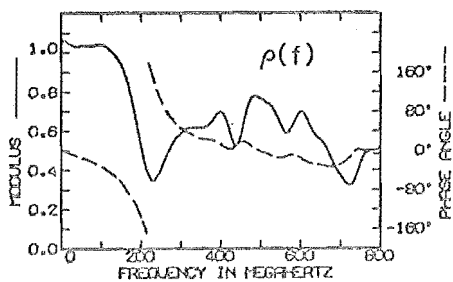
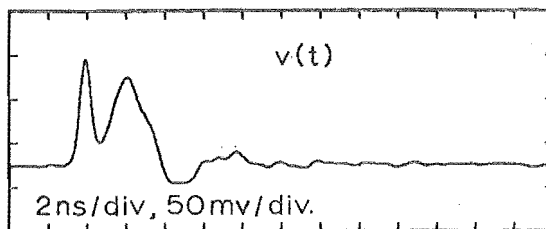
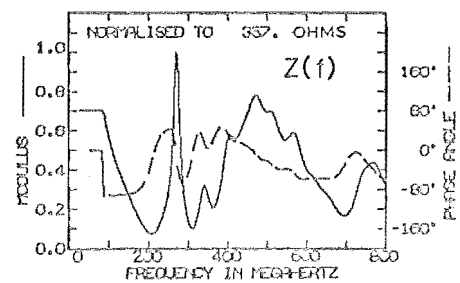
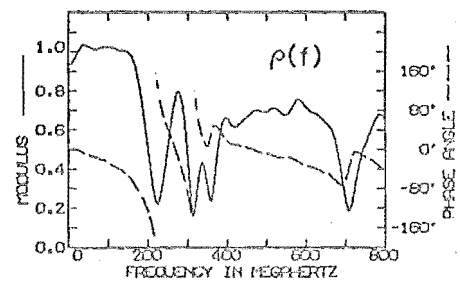
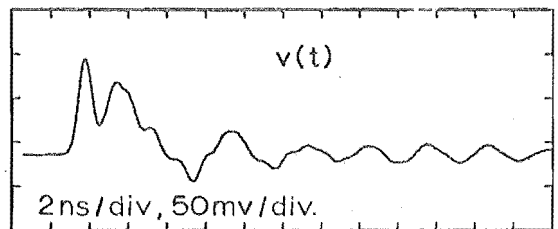
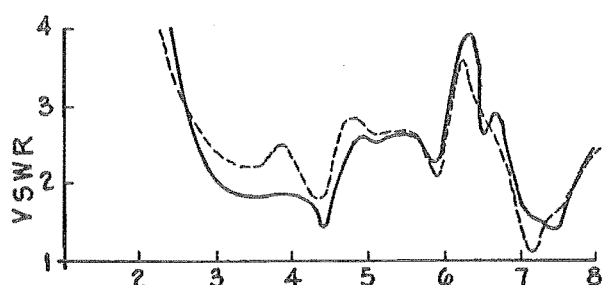
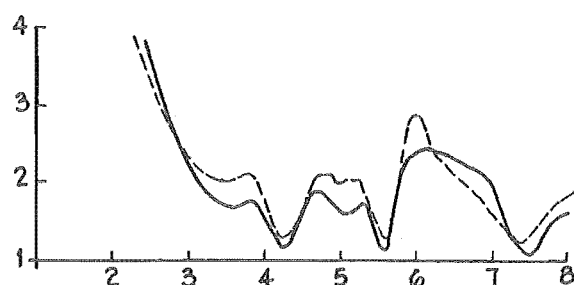
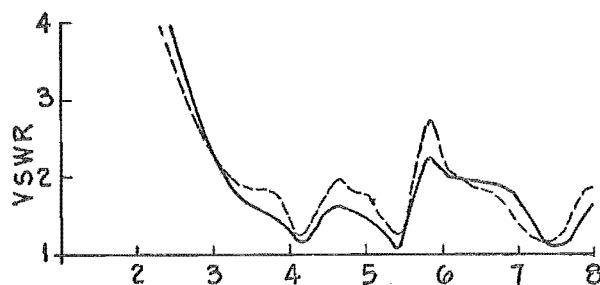
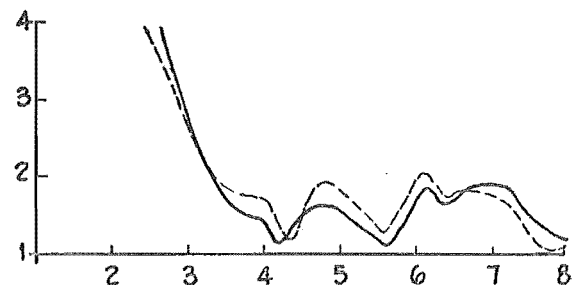
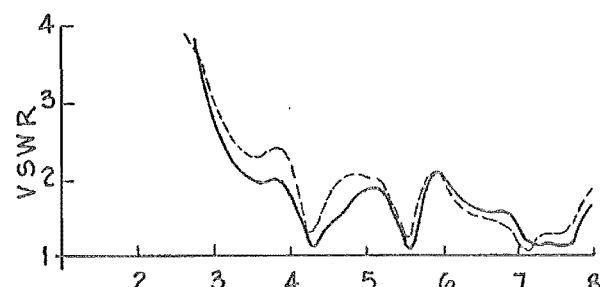
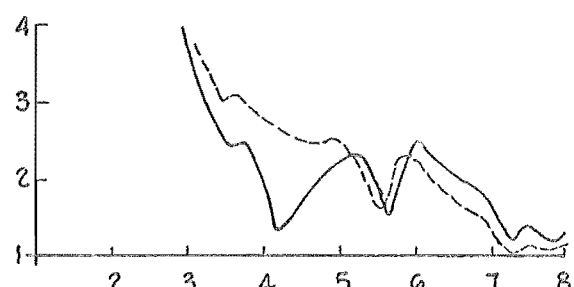
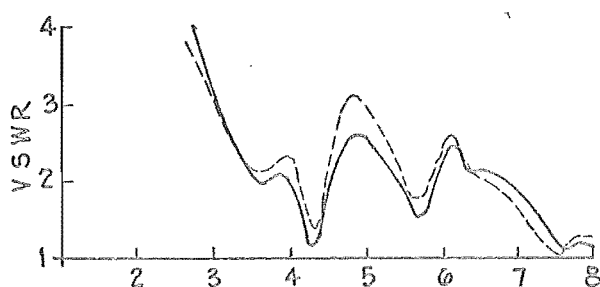
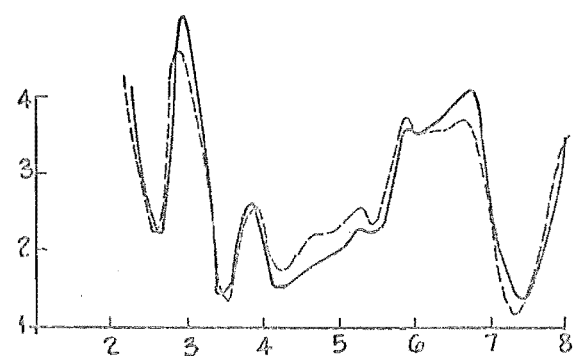
(a) A5E,  $h=25.4\text{cm}$ .(b) A5E,  $h=20.3\text{cm}$ .Figure 7.6: EFFECT OF REDUCING  $h$  ON A5E ANTENNA RESPONSES(a) A6E,  $h=\infty$ (b) A3,  $h=30.5\text{cm}$ .

Figure 7.7: RESPONSES OF ASYMMETRICAL WIRE FAN MONOPOLES

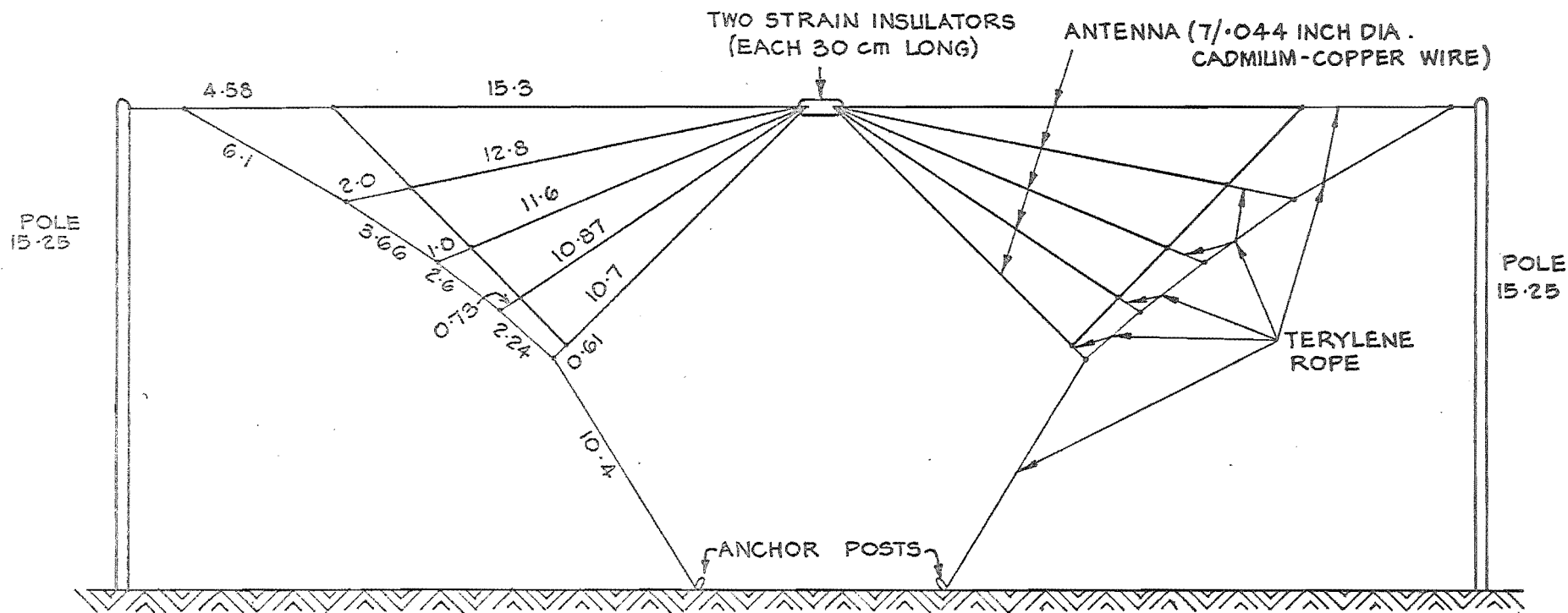
(a) A3E,  $h=30.5$  cm.(b) A4E,  $h=30.5$  cm.(c) A5E,  $h=30.5$  cm.(d) A6E,  $h=30.5$  cm.(e) A5E,  $h=25.4$  cm.(f) A5E,  $h=20.3$  cm.(g) A6E,  $h=\infty$ (h) A3,  $h=30.5$  cm.

FREQUENCY SCALE IS HUNDREDS OF MEGAHERTZ.

FEEDLINE CHARACTERISTIC IMPEDANCE: 300 OHMS ———

250 OHMS - - - - -

FIGURE 7-8: VSWR OF ASYMMETRICAL WIRE FAN DIPOLES



ALL ANTENNA DIMENSIONS ARE IN METRES UNLESS OTHERWISE SPECIFIED

FIGURE 7-9: DIMENSIONS OF HF A5E DIPOLE

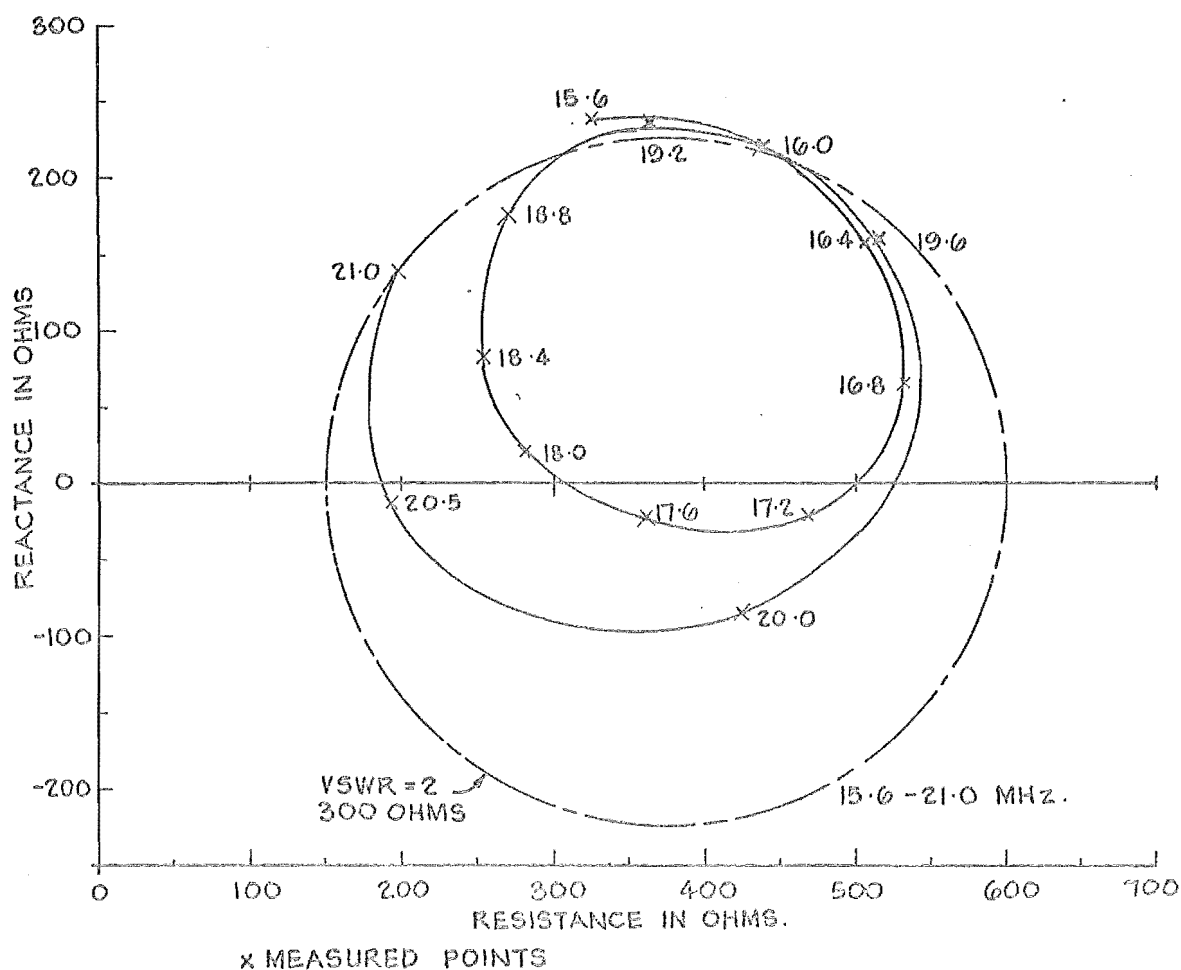
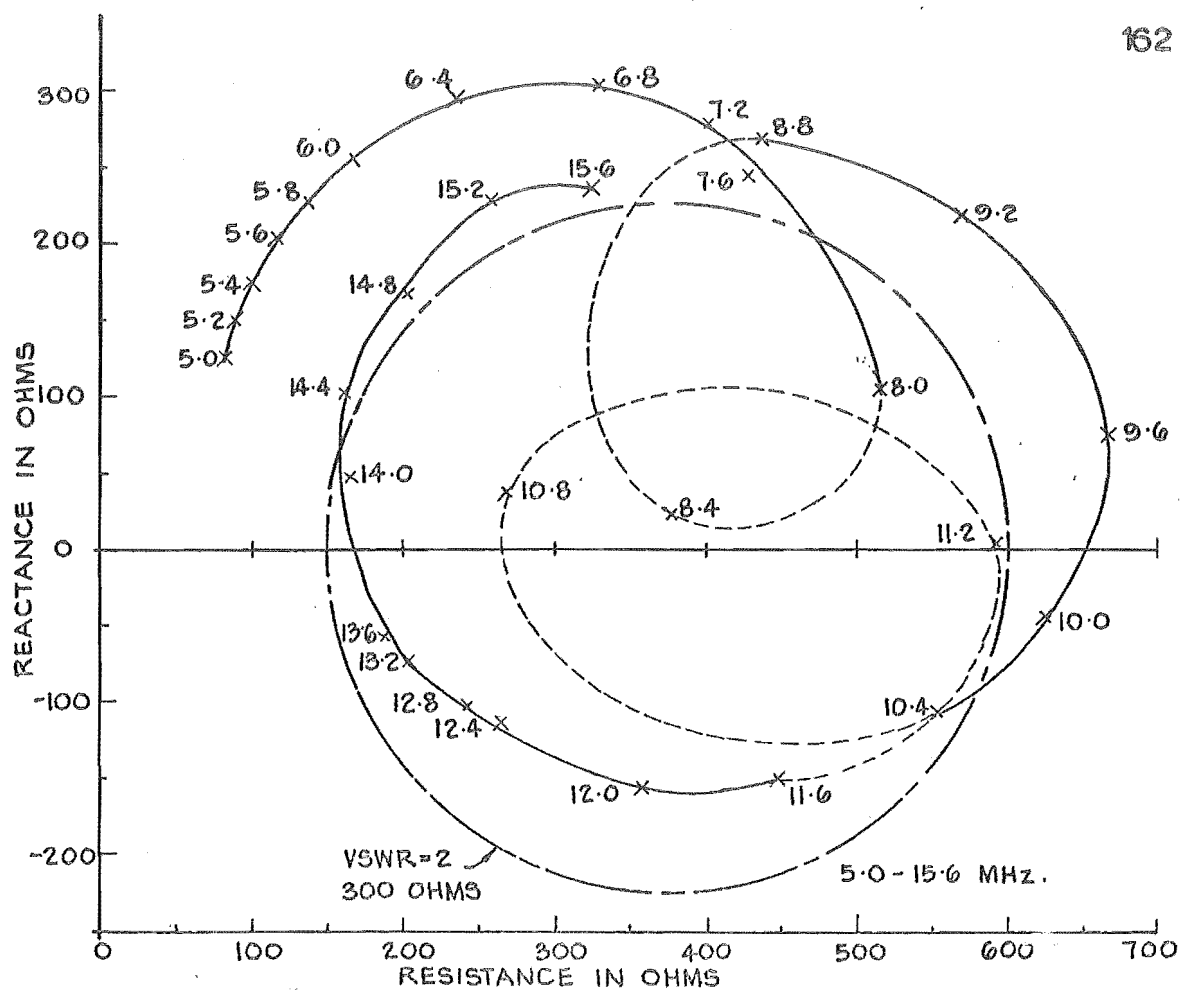
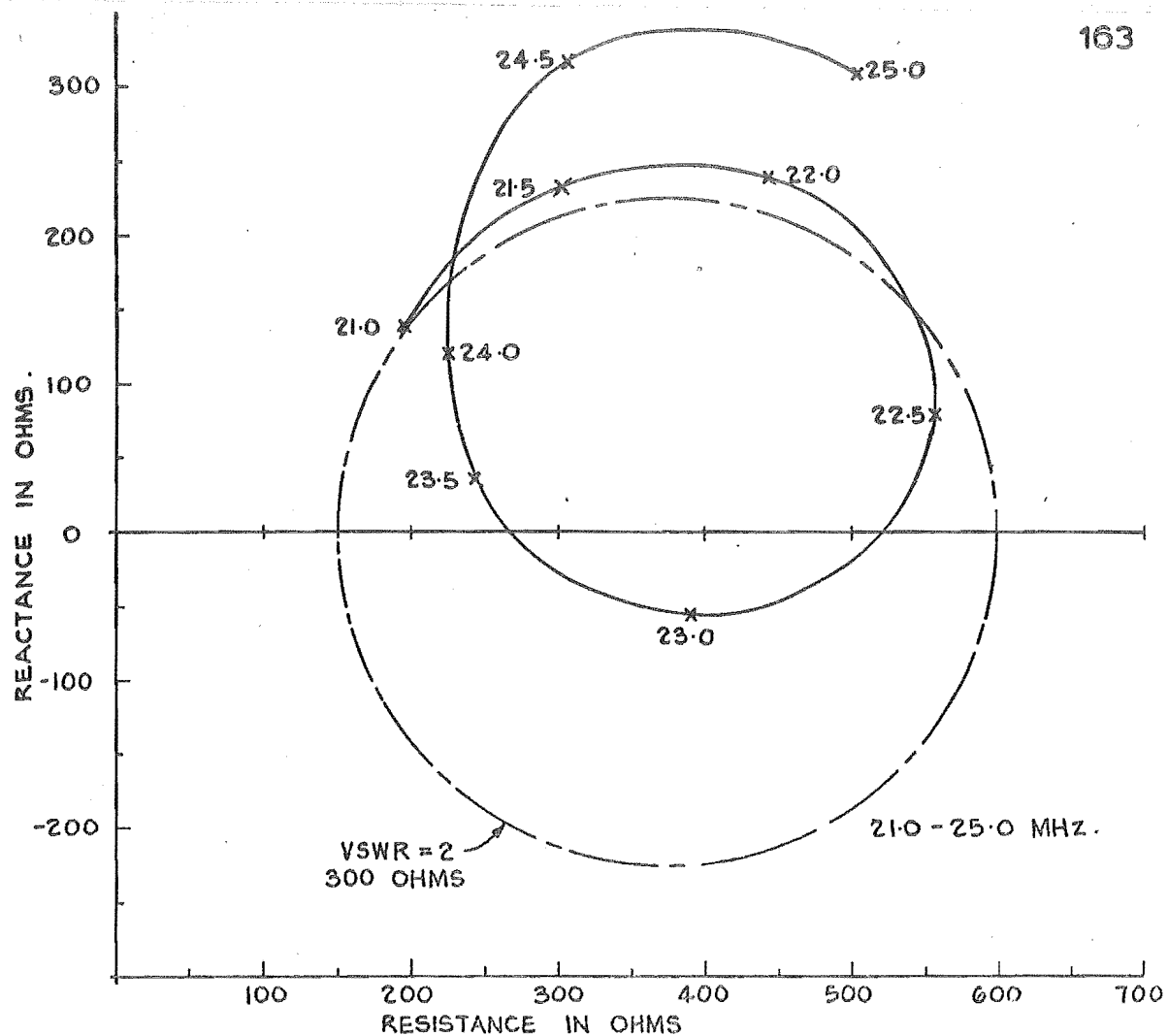


FIGURE 7-10 (a) : MEASURED INPUT IMPEDANCE OF HF ABE DIPOLE



x MEASURED POINTS

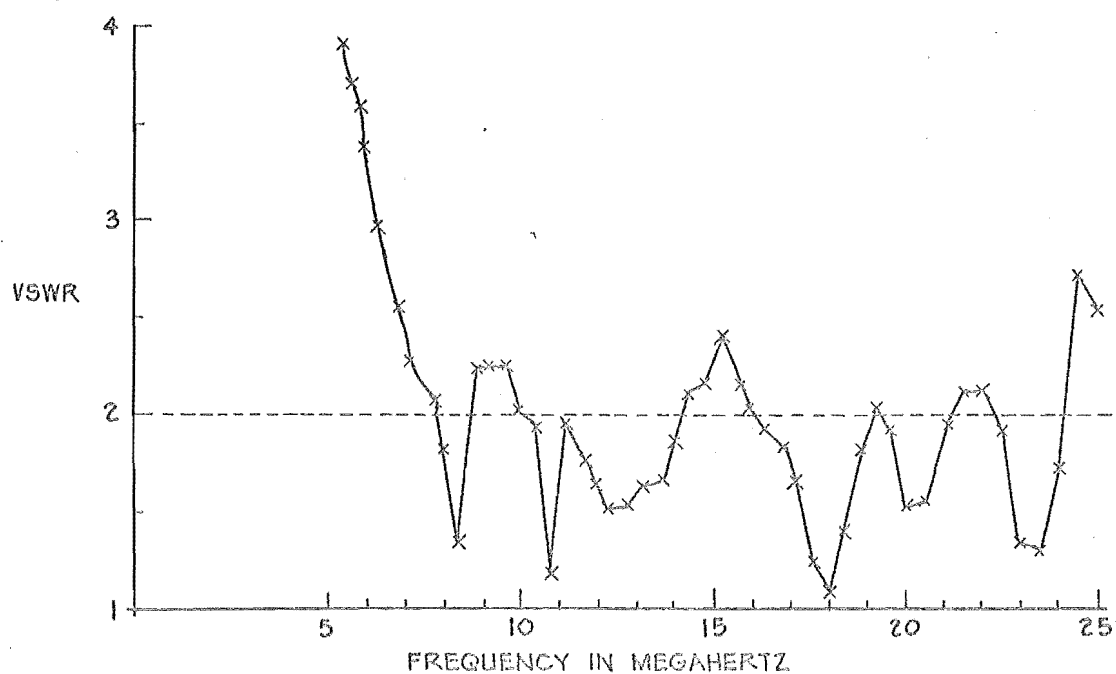


FIGURE 7-10 (b) : MEASURED INPUT IMPEDANCE AND VSWR ON 300 OHM FEEDLINE FOR HF A5E DIPOLE

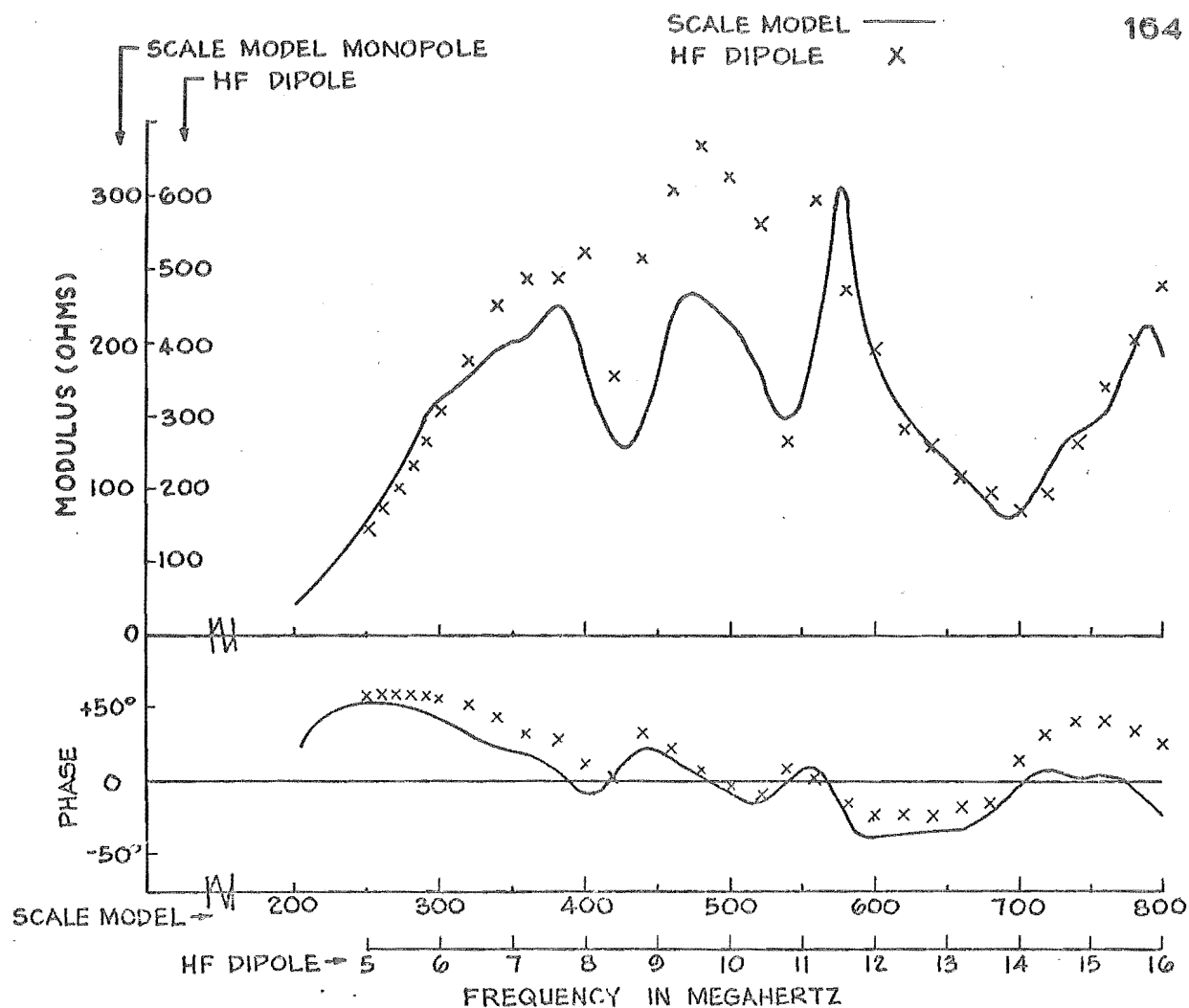
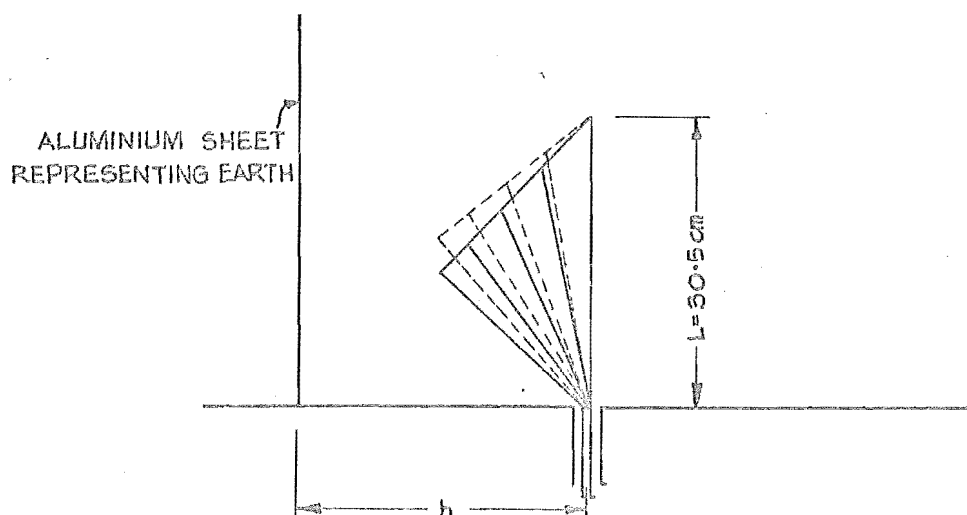


FIGURE 7-11: COMPARISON OF MEASURED INPUT IMPEDANCES OF HF ABE DIPOLE AND SCALE MODEL MONOPOLE

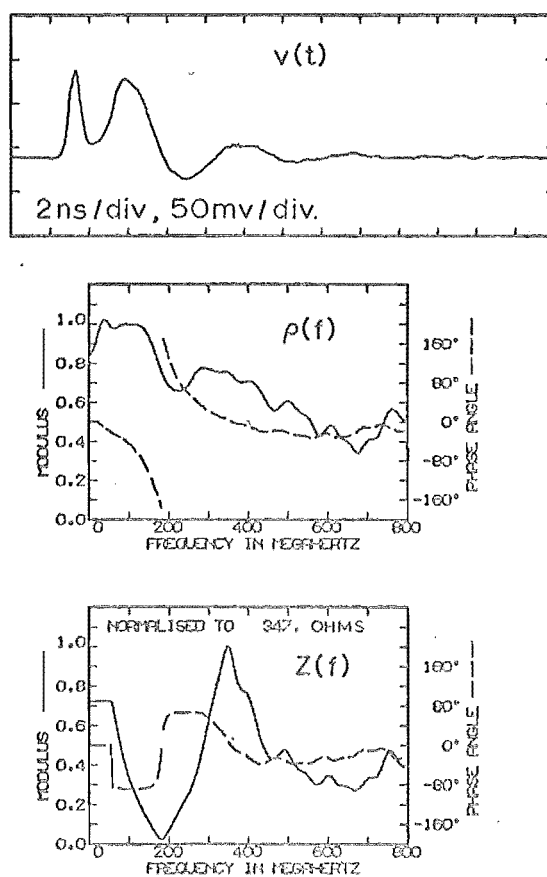
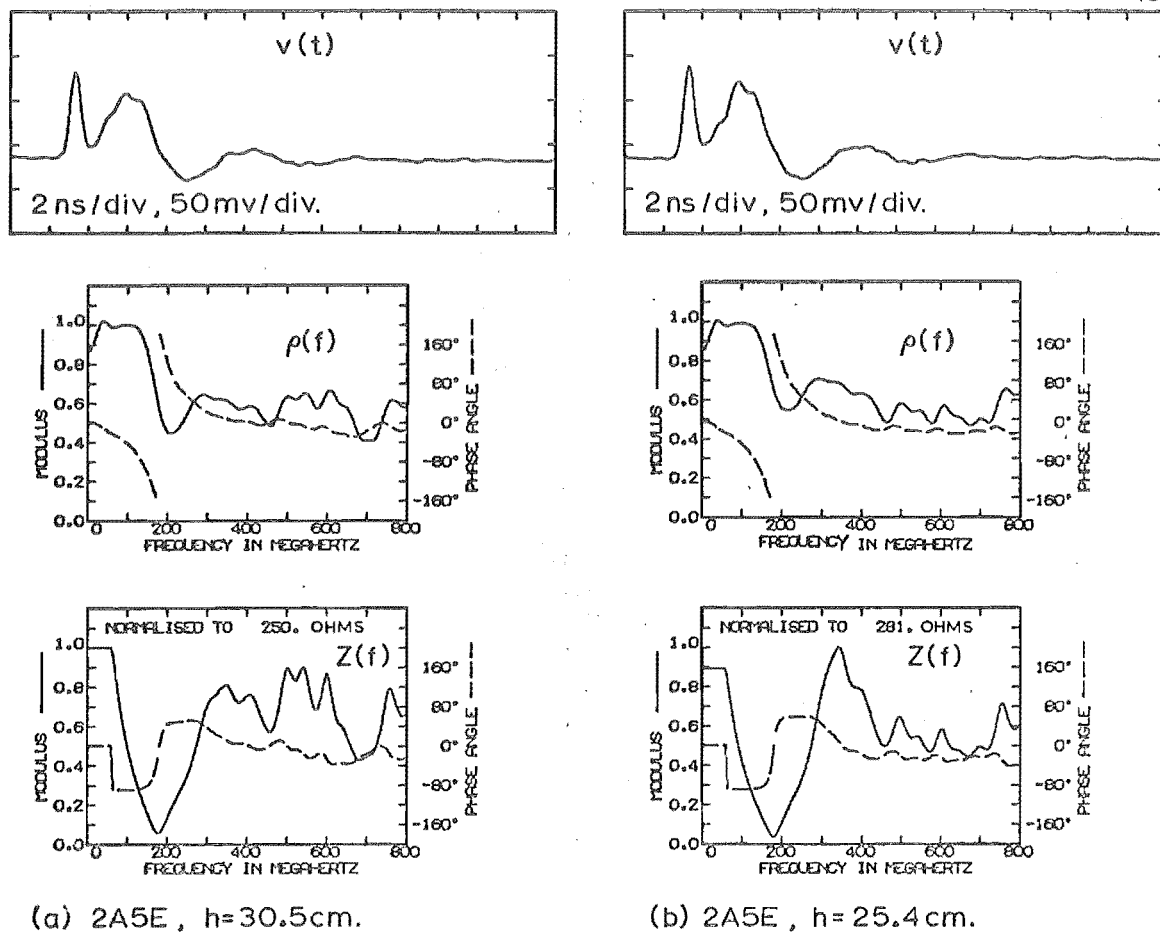
THE INCLUDED ANGLE BETWEEN THE FANS IS  $2\psi$



THE REAR FAN IS DRAWN WITH A BROKEN LINE FOR CLARITY

FIGURE 7-12: GEOMETRY OF 2A5E FOLDED SQUARE MONOPOLE





(c) 2A5E,  $h=20.3$  cm.

Figure 7.13: RESPONSES OF SCALE MODEL 2A5E MONOPOLE

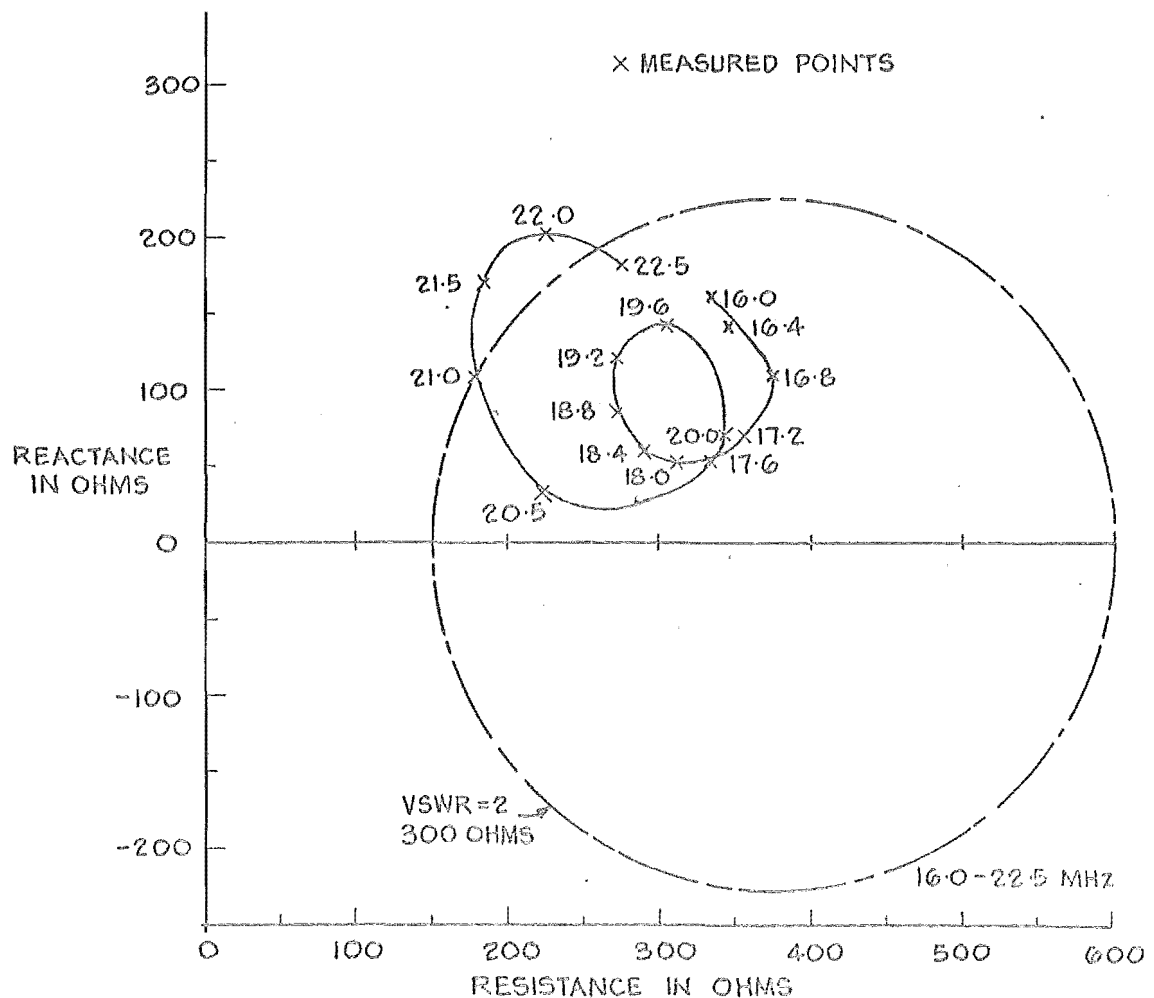
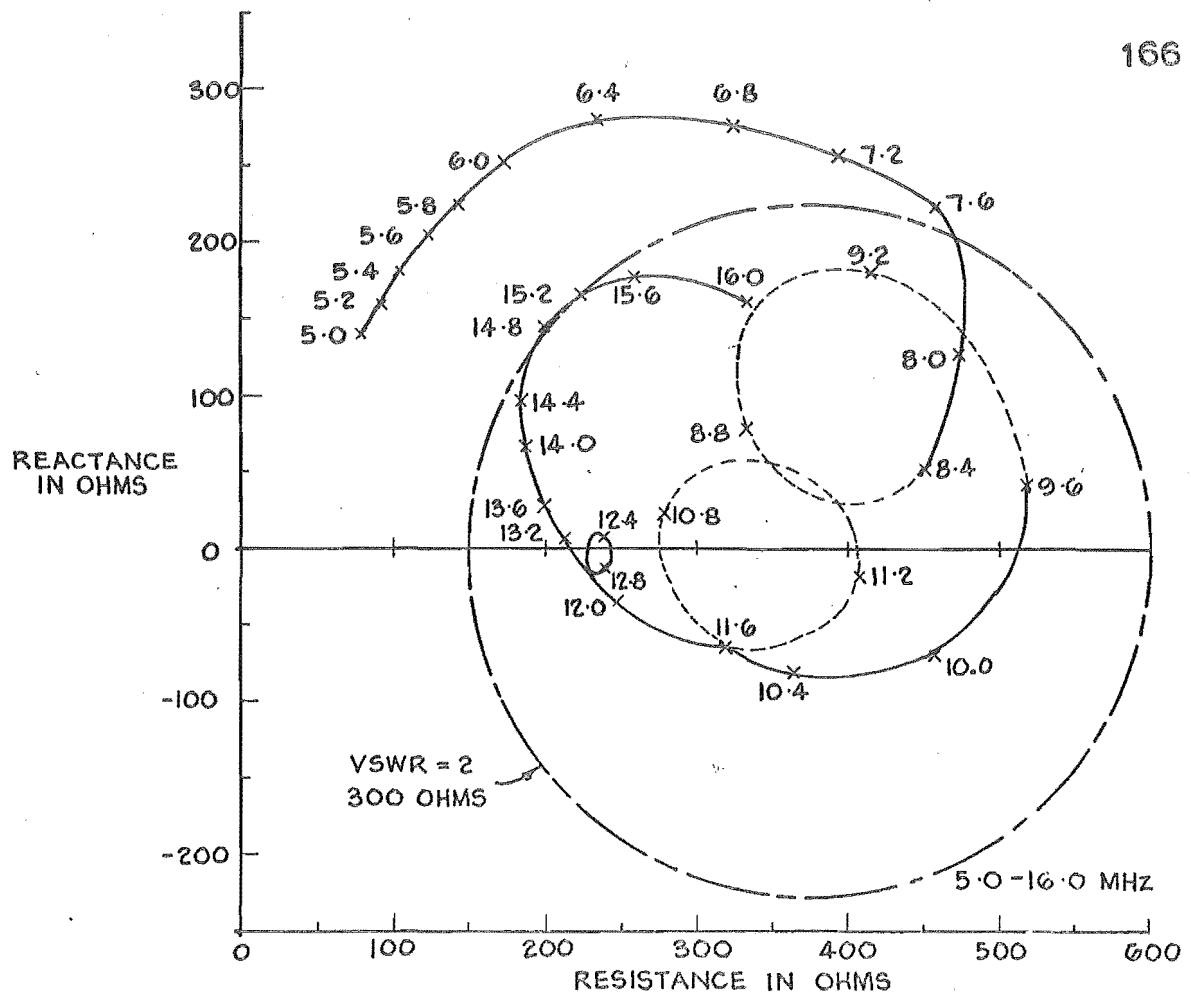
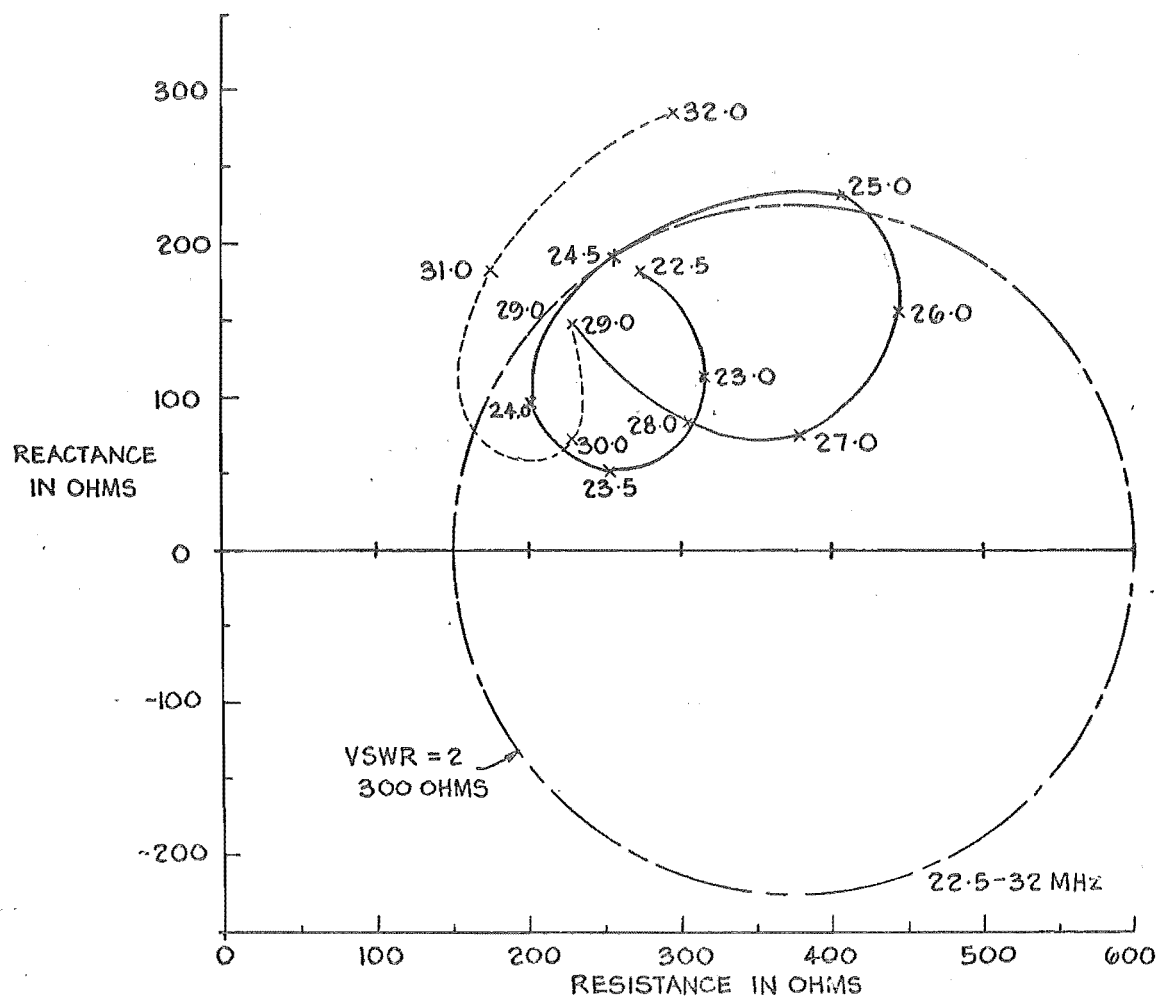


FIGURE 7-14 (a): MEASURED INPUT IMPEDANCE OF HF 2A5E DIPOLE



X MEASURED POINTS

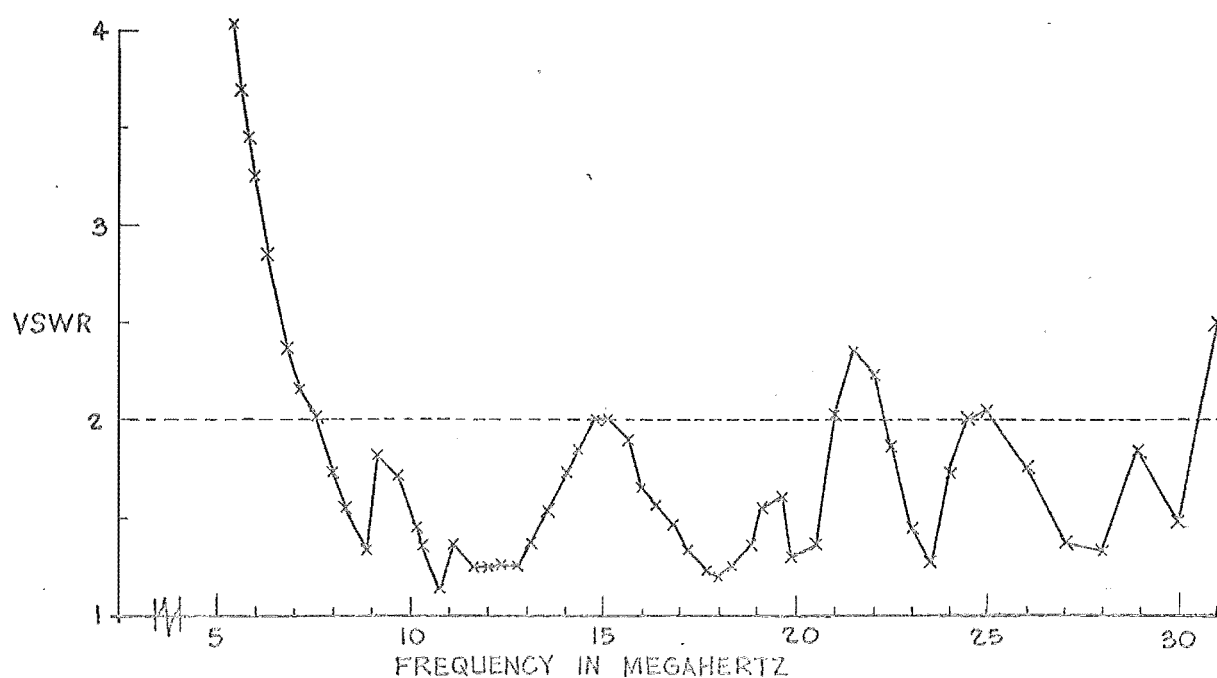


FIGURE 7.14 (b): MEASURED INPUT IMPEDANCE AND VSWR ON 300 OHM FEEDLINE FOR HF ZASE DIPOLE

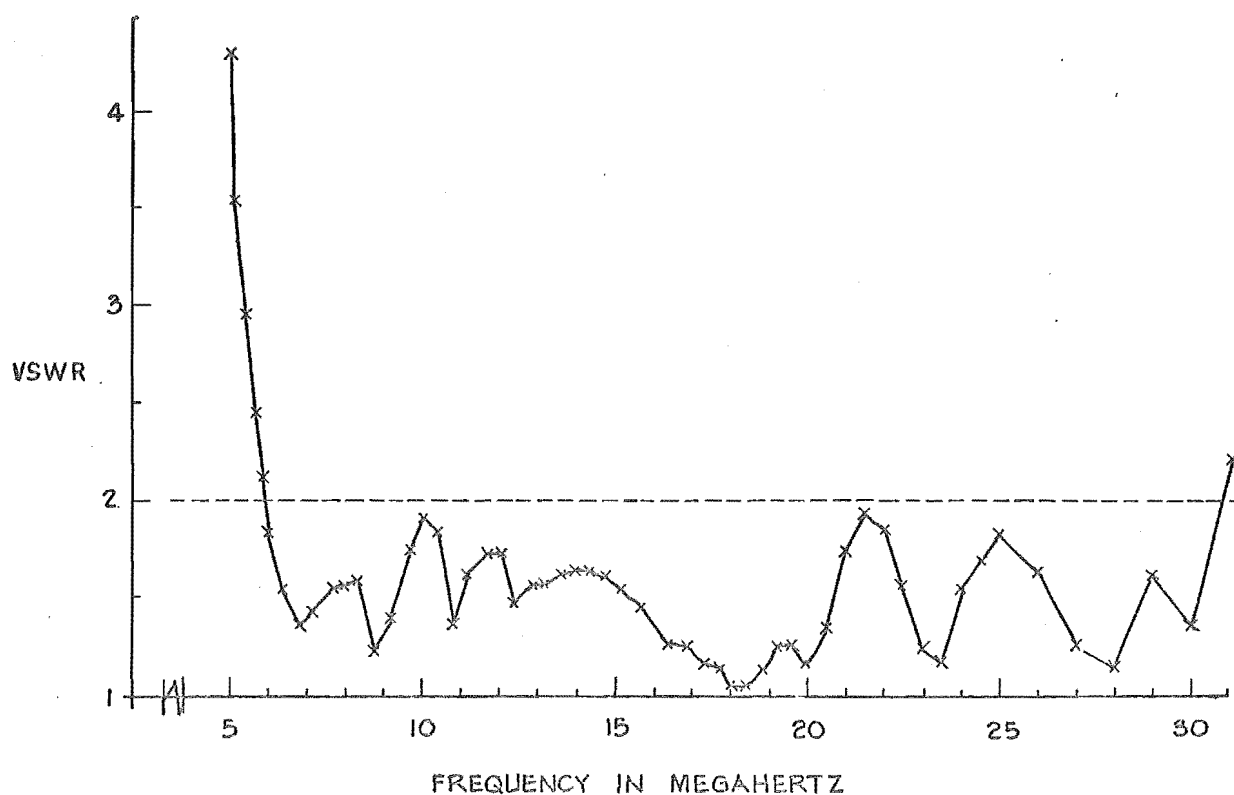


FIGURE 7-15: VSWR ON 300 OHM FEEDLINE FOR HF 2A5E DIPOLE  
MATCHED WITH 130 PFD SERIES CAPACITOR

PART III

FAR FIELD RESPONSES

## CHAPTER 8: THE FAITHFUL TRANSMISSION OF VERY WIDE BANDWIDTH SIGNALS

### 8.1 INTRODUCTION

Suppose that it is desired to obtain faithful radio transmission of a signal having a bandwidth of an octave or more. Even neglecting the vagaries of the propagation path between the transmitting and receiving antennas, the desired result cannot be achieved with existing antenna designs, unless complicated compensating filters are inserted in the transmission lines feeding the antennas. The discussion in section 8.2 indicates the magnitude of the problem. The mathematical description of wideband radiation is extremely complicated, and it has not been found profitable to proceed much beyond basic theoretical considerations of the kind outlined in section 8.3, and section 8.4 discusses suitable types of antenna.

### 8.2 GENERAL THEORETICAL CONSIDERATIONS

An efficient antenna system must consist of individual antennas which are properly matched to their feedlines. There are two ways in which a radiating element can be matched. These can be seen by considering the behaviour of the radiating element on transmission:

- 1) The reflections from the driving point and the various physical discontinuities on the element are made to cancel in the transmission line which feeds the element (a dipole is the simplest example of this).

- 2) The element is constructed so that there is a smooth

transition from the feedline into free space. Consequently only outward travelling waves exist on the antenna when it is transmitting (a horn is the simplest example of this).

Narrow band antennas are usually matched by the first method. The way in which a resonant dipole is matched to its feedline for monochromatic excitation is illustrated by Ross (1966c). Wideband antennas can be matched by both the above methods because the first method can be made effective over a wide frequency range<sup>1</sup>. A thick dipole is an example of a wideband antenna which is matched by the first method.

When very wide bandwidth signals, which necessarily possess the character of transients, are transmitted then the first method of obtaining a match cannot be used because it will be impossible to cancel the first reflection from the driving point. It follows then that travelling wave antennas must be used. Horns and spirals are examples of radiating elements which support only outward travelling waves during transmission. Now the faithful transmission of signals depends on the antenna system having a flat amplitude response and a linear phase response. A transmitting horn has a nearly linear phase response over a wide bandwidth but its amplitude response is not flat because its radiation pattern varies rapidly with frequency (Schelkunoff and Friis 1952, chapter 16). A spiral radiating element (Dyson, 1959a, 1959b) has a nearly flat amplitude response but its phase response is not linear because the effective phase centre of

---

<sup>1</sup>The term wideband is commonly used to mean an antenna which can transmit (or receive) a narrow band signal whose centre frequency may be anywhere within the passband of the antenna.

the radiation changes position rapidly with frequency (Pulfer 1961; Collin and Zucker 1969, section 22.5).

The problem is complicated further by differences between transmission and reception. An essentially spherical wave is transmitted while the receiving antenna is illuminated by a wave which is essentially plane. Thus, for frequencies above that for which the smallest linear dimension of the physical aperture of a horn is about half a wavelength, the effective aperture of the horn is nearly constant so that the amplitude response of the horn is flat on reception. This reasoning does not contravene reciprocity, but follows necessarily from it, as is demonstrated in the next section.

A time domain criterion for the design of elements for faithfully transmitting and receiving transients has been suggested by Ross (1968). The criterion states that the impulse response (the inverse Fourier transform of  $T(f)$  or  $R(f)$ ) shall be time-limited. The distortion introduced by the antenna then cannot exceed the duration of the impulse response. The design objective is to make the impulse response short compared to the duration of the transient. Several elements for receiving transients with minimum distortion have been designed and built on the basis of this criterion. Ross (1967a) limits the impulse response of a monopole by suppressing the reflection from the base. This is done by matching the surge impedance at the base with a



tapered line transformer<sup>2</sup>. Fenster and Ross (1968) suppress the reflection from the tip with a matched termination<sup>3</sup>.

The duration of the impulse response of these elements is twice the propagation time of electromagnetic waves along the monopole. Thus, if a step modulated monochromatic wave is incident upon the monopole, and if the monopole is  $\lambda/4$  long at the frequency of the monochromatic wave, then the distortion of the received signal is limited to one half cycle.

The duration of the impulse response of an antenna is proportional to the size of the antenna (Polk, 1960). It follows that signals which have step changes in amplitude, frequency, or phase can only be faithfully received (or transmitted) by infinitesimal antennas. Hence signals containing step changes cannot be efficiently and faithfully transmitted.

Earlier in this section it was shown that travelling wave antennas must be used in a wideband transmission system. The impulse response of a travelling wave antenna is (approximately) time limited. Therefore Ross' criterion is satisfied. The transient receiving elements previously reported have effective apertures which are approximately constant over a wide frequency range (Ross 1967a, Ross 1968).

---

<sup>2</sup>The match is only approximate. Table 5.1 shows that the surge impedance is different for different shapes of input signal. Therefore the match is optimum only for a specific input signal. Fig. 5.3 shows that the characteristics of the base region are frequency dependent. Thus the match is not perfect which means that the impulse response is not strictly time limited. The approximation is however good enough for most engineering applications.

<sup>3</sup>The termination is described in section 3.4.3.

Thus they are faithful receivers, but are not faithful transmitters of transients. It follows that Ross' criterion is necessary but not sufficient to characterise the antennas of a wideband transmission system.

### 8.3 A DESIGN PRINCIPLE FOR A FAITHFUL TRANSMISSION SYSTEM

Consider a pair of antennas, as in Fig. 8.1, the one at P transmitting a signal  $u(t)$  and the one at Q receiving. The signal observed at the terminals of the antenna at Q is  $v(t)$ . Assume that the two antennas are in their respective far fields and define:

$\alpha$  = free space voltage attenuation factor for isotropic radiation from P to Q.

$G(f)$  = gain of antenna P in direction of antenna Q.

$A(f)$  = effective area of antenna Q in direction of antenna P.

Recall that "gain" and "effective area" refer respectively to the power radiated and received by antennas. Thus:

$$G(f) A(f) = |H(f)|^2 / \alpha^2 \quad (8-1)$$

so that the condition for faithful transmission is

$$G(f) A(f) = K \quad (8-2)$$

where K is some constant. It is convenient to appeal to reciprocity and make use of the well known connection (Kraus 1950, section 3-12) between  $A(f)$  and the gain, denoted by  $\Lambda(f)$ , of antenna Q in the direction of P. So eqn(8-2) becomes

$$G(f) \Lambda(f) = \frac{4\pi K}{c^2} f^2. \quad (8-3)$$

Notice that eqn(8-3) implies that faithful transmission is obtained if one antenna is a perforated horn or reflector having a gain constant with frequency (Rumsey 1957, Parker and Anderson 1957, Ferris and Zimmerman 1966) and the other antenna is a conventional horn having a gain proportional to  $f^2$ . If the perforated horn is used for transmitting then the shape of the radiated field is also a replica of the transmitted signal. In certain applications, such as a broadband bistatic radar, or communication between just two points, these two antennas might form an ideal pair. For a communication system involving many arbitrarily placed antennas it is convenient if they are all identical, in which case  $\Lambda(f) = G(f)$  so that eqn(8-3) gives

$$G(f) \propto f \quad (8-4)$$

#### 8.4 SUITABLE TYPES OF ANTENNA

The first thing to notice about eqn(8-4) is that an antenna system consisting of conventional horn antennas or parabolic reflector antennas will not transmit very wide bandwidth signals faithfully because their gains are proportional to  $f^2$ . Antennas similar to the perforated horns suggested by Rumsey (1957) and Parker and Anderson (1957), or the perforated reflectors suggested by Ferris and Zimmerman (1966) would be suitable provided they were fed by transmission lines supporting TEM modes. Neither single tube waveguides nor surface waveguides can be used because they are dispersive and distort transient signals (Elliot, 1957). Dihedral horns (Schelkunoff and Friis 1952, p528) or rudimentary horns (Sengupta and Ferris, 1971) can be fed

conveniently by TEM transmission lines. Limited finance and experimental facilities made it impossible to investigate perforated horns, or perforated reflectors. None of the pulse generators which were constructed could produce pulses with large energy above 1 GHz (see chapter 4), so that enormous horns or reflectors would have had to be constructed to be able to obtain meaningful experimental results.

As shown in the previous section, antennas with radiation focussed in two perpendicular planes are not suitable. But consider an antenna which radiates isotropically in one plane and, in all perpendicular planes, radiates a beam with a width which is inversely proportional to frequency. Such an antenna has a gain which satisfies eqn(8-4), by definition, and it is most easily realised if its radiating aperture is cylindrically symmetric. If the aperture dimension, parallel to the axis of symmetry, is somewhat greater than half a wavelength (quarter of a wavelength if the antenna is mounted above a ground plane) for all frequencies for which the spectrum of the transmitted signal has significant energy, then eqn(8-4) will be satisfied at least approximately if the radiation is focussed in all the planes containing the axis of symmetry.

Suppose that one wishes to design a pair of identical antennas which will form a faithful transmission system between any two points on the earth's surface (assuming that the points are not so far separated so that  $\alpha$  is excessive). It is clearly convenient if the antennas radiate isotropically in the horizontal plane. The conclusion drawn in the previous paragraph indicates that the radiation from the antennas must be focussed in all the vertical planes.

If the flare angle of a conical monopole is correctly chosen then the monopole will be well matched over a wide bandwidth and it will support virtually only outward traveling waves on transmission. But, the gain of the monopole will oscillate about a constant value for frequencies for which the vertical height of the cone is greater than a quarter wavelength, and assuming TEM wave excitation (Barrow et al., 1939). However, if the monopole is looked upon as a horn, and a cylindrical phase-correcting lens is inserted in its aperture, then for all frequencies above a particular frequency, the gain will be almost proportional to  $f$  as demanded by eqn(8-4). This is discussed further in chapter 9, in which a preliminary experimental evaluation of the concept is reported.

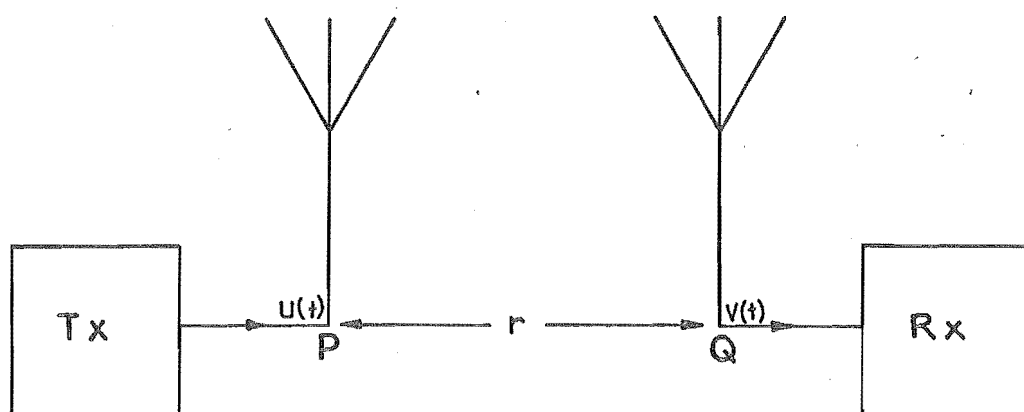


FIGURE 8-1: TRANSMITTING AND RECEIVING ANTENNAS.

## CHAPTER 9: MEASURED RESPONSES

### 9.1 INTRODUCTION

To obtain a proper understanding of antenna behaviour it is necessary to be able to isolate the radiation from different parts of an antenna, as has been recognised before (Schmitt 1960, King and Schmitt 1962). The experimental technique described in Part I of this thesis permits the frequency response of the radiation from individual parts of an antenna to be obtained easily. To illustrate this, section 9.2 contains a plot of the frequency dependence of the radiation which occurs when a current pulse is reflected from the tip of a monopole. The same is done for the radiation emanating from the base of the monopole when it is excited by a transient. This result is compared with previous theories.

Conical monopoles are potentially suitable antennas for the efficient radiation of very wide bandwidth signals (chapter 8). The far field responses of conical monopoles are presented in section 9.3. The experimental results are compared with the theory of Harrison and Williams (1965). An experimental evaluation of phase-corrected conical monopoles is presented in section 9.4. Section 9.5 contains the far field transfer functions of a wire fan antenna.

The frequency responses presented in this chapter were computed from measured signals radiated between two antennas. The measurements on the small (7.6 cm slant height) cones reported in section 9.4 were made with the cones mounted on the ground plane which was used for the

driving point measurements (see section 3.2).

The experimental procedure is given in section 9.4. For the remainder of the measurements the antennas were mounted on the far field antenna range described in section 3.4. The experimental procedure followed when determining the transmission and reception transfer functions,  $T(f)$  and  $R(f)$  respectively, is given in section 3.4.2. The system transfer function  $H(f)$  was computed using eqns (2-7) and (2-9a) from a measurement of the signal radiated between two identical antennas. The experimental procedure is the same as for  $T(f)$  and  $R(f)$ . The upper limit of the measurement bandwidth for these measurements is set at 600 MHz in section 3.4. The sampling parameters for the results presented in this chapter can be found in Appendix 4.

## 9.2 RADIATION FROM THE BASE AND TIP OF MONOPOLE

The far field of a thin monopole of length  $L$  consists of a series of transients, provided the monopole is excited by a narrow pulse. The times at which the transients occur correspond to the instants at which the pulse is reflected successively from the base and the tip. The narrow pulse driving point response, which demonstrates the multiple reflections of a pulse on a long thin monopole, is discussed in chapter 5.

The experimental arrangement is shown in Fig. 9.1. Fig. 9.2(a) shows the received signal when the pulse shown in Fig. 3.7 is transmitted. The transients, considered individually, characterise the radiation from the base and the tip. Consequently, by only accepting one of the



transients, the radiation from either the base or the tip of the monopole can be measured.

Figs 9.2(b) and 9.2(c) show  $T(f)$  for radiation from the tip and the base respectively. If the monopole were infinitely long the only radiation would be that represented by the  $T(f)$  shown in Fig. 9.2(c). A rectangular data window (section 2.3.3.1.2), 3.7 ns long, was used to separate the transients radiated from the base and the tip (see Fig. 9.2(a)) from the rest of the received signal. The time origin of the window separating the tip transient was delayed by 4 ns to allow for the time taken for the test pulse to propagate from the base to the tip. Proper allowance was made for the different distances and angles between the standard monopole and the tip and base of the 1.2 m monopole (see Fig. 9.1). The plots of  $T(f)$  are only continued out to 400 MHz because severe ripples were observed above this frequency. These were caused by the sharp edge of the data window (see section 2.3.3.1.2), and because the test pulse has little energy above 400 MHz (see Fig. 3.7).

Fig. 9.2(c) also shows  $T(f)$  calculated from three previous theories. Manneback (1923) states, and Schelkunoff (1952, section 2.24) discusses the following expression for the transverse component  $E_\theta$  of the electric field radiated from one end of an infinitely thin wire extending to infinity:

$$E_\theta = \frac{(1+\cos\theta)\eta}{4\pi r \sin\theta} i(t-r/c) \quad (9-1)$$

where  $i(t)$  is the current flowing from the end, and  $\theta$  is angle between the direction of the radiation and the wire.

Taking the Fourier transform of eqn(9-1), substituting  $\theta = \pi/2$  and  $\eta = 120\pi$  ohms, and using eqns (3-6) and (3-7), we obtain for an infinite wire driven above an infinite ground plane

$$E_1(f) = \frac{120 U(f) e^{-jkr}}{[50 + Z(f)]r} \quad (9-2)$$

where  $E_1(f)$  is the radiated electric field intensity a distance  $r$  from the antenna, and  $Z(f)$  is the input impedance. By comparison with eqn(2-20) we obtain:

$$T(f) = \frac{120}{50 + Z(f)} \quad (9-3)$$

Values calculated from eqn(9-3) are plotted in Fig. 9.2(c).  $Z(f)$  was taken from Fig. 5.3.

Harrison and King (1967) have discussed a formula (due to Papas, 1949) for the transfer function of an infinite cylindrical dipole antenna when it is transmitting:

$$\frac{rE_1(f)}{V_a(f) \exp(-jkr)} = \frac{j}{\pi H_0^{(2)}(ka)} \quad (9-4)$$

where  $V_a(f)$  is the voltage discontinuity exciting the infinite dipole, and  $H_0^{(2)}(ka)$  is the Hankel function of zero order and second kind. From the equivalent circuit for transmission (Fig. 3.8), and using eqns (3-6), (3-7) and (2-20), we obtain, for an infinite monopole:

$$T(f) = \frac{j 4 Z(f)}{\pi [50 + Z(f)] H_0^{(2)}(ka)} \quad (9-5)$$

Values calculated from eqn(9-5) are also shown in Fig. 9.2(c). The Hankel function was calculated from formulas and tables in Abramowitz and Stegun (1965, chapter 9).

Andersen (1968; 1971, p28) has also derived a formula for the radiated field of an infinite monopole driven above an infinite ground screen:

$$E_1(f) = \frac{-V_a(f)}{\ln\left[\frac{ka \sin\theta \Gamma}{2j}\right]} \frac{e^{-jkr}}{r}, \quad ka \ll 1 \quad (9-6)$$

where  $V_a(f)$  is the voltage exciting the monopole,  $\Gamma = 1.781\dots$ , and the time dependence (suppressed) is  $\exp(-j\omega t)$ . Simplifying eqn(9-6), and using eqns (3-7) and (2-20) we obtain

$$T(f) = \left\{ \frac{-2Z(f)}{[50+Z(f)][\ln(0.89ka) - j\pi/2]} \right\}^* \quad (9-7)$$

where the asterisk denotes the complex conjugate. The phase factor is then  $\exp(-jkr)$  so that eqn(9-7) is consistent with eqn(2-20). Values calculated from eqn(9-7) are also shown in Fig. 9.2(c).

The  $T(f)$  determined by experiment is seen to differ by up to 15% from the theories of Harrison and King and Andersen. This is attributed to experimental error (it was difficult to obtain satisfactory separation of the transients radiated from the base and the tip, see Fig. 9.2(a)). Phase differences of  $20^\circ$  are also within experimental error. Manneback's result differs significantly from the other theories and the experiment. However, his result is true only for infinitely thin wires. The following is a check on the consistency of eqns (9-3), (9-5) and (9-7) for very thin wires. King and Schmitt (1962) derive a formula (which is due to a theory by Wu, 1961a) for  $Z(f)$  of an infinitely long monopole driven above an infinite ground plane:

$$Z(f) \approx \frac{\eta}{2\pi} \Omega - j \frac{\eta}{4}, \quad ka \ll 1 \quad (9-8)$$

where

$$\begin{aligned} \Omega &= \ln(1/ka) - 0.557 \\ &\approx -\ln(ka), \quad ka \ll 1. \end{aligned} \quad (9-9)$$

Thus, from eqns (9-9) and (9-8) with  $\eta = 120\pi$  ohms (9-10)

$$Z(f) \approx -60 \ln(ka), \quad ka \ll 1. \quad (9-11)$$

Substituting eqn(9-11) into the expression for  $T(f)$  derived from Manneback's theory (eqn 9-3), we obtain

$$T(f) \approx \frac{-2}{\ln(ka)}, \quad ka \ll 1. \quad (9-12)$$

since  $Z(f) \gg 50$ . For large  $Z(f)$ , the expression for  $T(f)$  derived from Harrison and King's result (eqn 9-5) reduces to

$$T(f) = \frac{j4}{\pi} \left[ \frac{1}{H_0^{(2)}(ka)} \right]. \quad (9-13)$$

By substituting the asymptotic form for  $H_0^{(2)}(ka)$  for small arguments:

$$H_0^{(2)}(ka) \approx -j \frac{2}{\pi} \ln(ka). \quad (9-14)$$

eqn(9-13) readily reduces to eqn(9-12). For large  $Z(f)$  and small  $ka$ , the expression for  $T(f)$  derived from Andersen's theory (eqn 9-7) also readily reduces to eqn (9-12). Thus the three theories are consistent for very thin wires.

A short receiving monopole produces an output voltage proportional to the time differentiation of the received electric field intensity (Schmitt et al., 1966). The time response shown in Fig. 9.2(a) indicates that  $T(f)$  for the

base is positive and constant, and  $T(f)$  for the tip is negative and constant, because the transients which characterise the radiation from the base and the tip are approximately proportional to the time derivative and the negative of the time derivative respectively of the transmitted pulse (see Fig. 3.7). This is in agreement with the computed results shown in Figs 9.2(b) and 9.2(c).

### 9.3 CONICAL MONOPOLES

It was suggested in section 8.4 that the conical monopole could form the basis of the design of radiators suitable for faithful transmission systems. Measurements were made on two hollow cones (each of 50 ohm characteristic impedance when mounted above a ground plane) of 0.71 m slant height. One was made of a continuous sheet of metal and the other was made of wires. The construction of these cones, and their driving point properties, is given in section 6.3.2.

Fig. 9.3(a) shows the signal received by the standard monopole when the test pulse is radiated from the sheet metal cone. The computed  $T(f)$  and  $R(f)$  are shown in Fig. 9.3(b). The antenna gain  $G(f)$  is related to  $T(f)$  by

$$G(f) \propto |T(f)|^2 / [1 - |\rho(f)|^2] \quad (9-15)$$

because the gain refers to the power radiated by an antenna. There is only a small error in assuming that  $|\rho(f)|^2 = 0$  (see Fig. 6.5(b)), so that Fig. 9.3(b) shows that  $G(f)$  is effectively constant over the measurement bandwidth, in agreement with the basic considerations presented in section 8.4.

$T(f)$  and  $R(f)$  were smoothed by convolving their values at intervals of  $1/2NT$  with the weights  $\frac{1}{4}$ ,  $\frac{1}{2}$  and  $\frac{1}{4}$  (see section 2.3.3.1.2). The effect of smoothing is shown in Fig. 9.3(c) where the smoothed transfer functions are superimposed upon the transfer functions which were computed from  $v(t)$  gated with a rectangular data window. The effect of the sharp edge of the truncation is seen to be quite severe.

Theoretical transmission and reception transfer functions for a matched conical monopole capped with a section of a sphere are presented by Harrison and Williams (1965).  $T(f)$  and  $R(f)$  were transcribed from their graphs for a 0.71m slant height 50 ohm cone and are shown with the experimental transfer functions in Fig. 9.4(a). Proper allowance was made for the antenna separation and source impedance so that the transfer functions were consistent with eqns (2-20) and (2-21). There is an estimated error of 10% in transcribing the theoretical transfer functions (the relevant parts of the published graphs measured 2 cm square).

There are significant differences in the shapes of the curves, even after allowing for measurement and transcription errors<sup>1</sup>. The measured responses appear to fall off rapidly below 150 MHz, in contrast to the theoretical predictions. The differences are attributed to the measured cone being hollow while the theoretical transfer functions are for a spherically capped cone. In calculating the transfer functions Harrison and Williams used a solution for the radiation field derived by Papas and King (1951). A

---

<sup>1</sup>The measurement error was estimated at 5% in section 3.4.2.

step in this solution was equating the electric field tangential to the cap to zero. This is not true if the cone is hollow, and affects in particular the lowest "useful" frequency. Notice that the first peaks in the experimental and theoretical  $T(f)$  differ by a frequency ratio of about 1.9. This is nearly equal to the ratio of the slant height plus half the distance across the cap of the spherically capped cone to the slant height of the hollow cone (which is  $1.3/0.71 = 1.83$ ). Thus the lowest "useful" frequency of a spherically capped cone depends upon an "effective" length which equals the slant height plus half the distance across the cap. The magnitude of the first peak of the measured  $T(f)$  is larger than the magnitude of the first peak of the theoretical  $T(f)$  because the gain of the cone is larger at the higher frequency (at 190 MHz the vertical dimension of the aperture is  $0.304\lambda$ , and at 100 MHz it is  $0.16\lambda$ : the gain of a cone falls off when the vertical dimension of the aperture is less than  $0.25\lambda$  when the cone is mounted above a ground plane, Barrow et al. 1939).

Brown and Woodward (1952) noticed that the theoretical radiation pattern of a cone with a spherical cap (from Papas and King, 1951) was the same as the measured pattern of an open ended (i.e. hollow) cone, or a cone with its end closed by a plane sheet, if the overall vertical heights of the cones (i.e. including the height of the spherical cap) were equal<sup>2</sup>. In Fig. 9.4(b) the experimental transfer functions

---

<sup>2</sup>This measurement was only made for a 79 ohm cone ( $2\phi = 60^\circ$ , see Fig. 6.1). They also noticed that adding a spherical cap to a cone did not sensibly alter its input impedance. Therefore the input impedance is a function of the slant height only.

are shown with Harrison and Williams' results transcribed for a 0.5 m slant height, spherically capped, 50 ohm cone. The vertical height of this cone is equal to that of the measured cone. There is better alignment of the frequency scales above 300 MHz (observe  $R(f)$ ) but the lowest "useful" frequencies of the two cones are different because this depends on the "effective" length defined in the previous paragraph.

Fig. 9.5(a) shows the signal radiated between the two cones when the test pulse is transmitted from one of the cones.  $H(f)$  for the two cones, shown in Fig. 9.5(b), has approximately linear phase (one requirement of a faithful transmission system) but its amplitude falls off rapidly with increasing frequency, also in agreement with both the results shown in Fig. 9.3(b) and the arguments given in section 8.4.

#### 9.4 PHASE CORRECTED CONICAL MONOPOLES

Suppose a phase correcting lens were introduced into the aperture of a conical monopole. The basic geometry is shown in Fig. 9.6. The inner surface of the lens is described by

$$r' = \frac{(n-1)x}{n \cos \phi - 1} \quad (9-16)$$

where  $n$  is the refractive index, given by  $n = \sqrt{\epsilon_r}$  where  $\epsilon_r$  is the relative permittivity of the lens material. If the lens is to be physically realisable then  $x/y$  must be positive. Elementary algebra shows that  $n$  must be greater than 1.37 for this to be so, which is convenient since



conventional, comparatively cheap lens material, such as polythene and polystyrene, have refractive indexes of about 1.6.

A complete lens of the size required, constructed from even the cheapest available lens material, would have exceeded the financial resources of this research project. However, it was decided that it was worthwhile investigating the effect of limited phase-correction. Crude lenses were formed from stacks of computer cards placed in the apertures of the two cones. The thickness of each lens at its base was about  $OB/2$ . The refractive index of the lenses would have been about 1.7 if they had consisted of solid paper, but stacked cards contain many air spaces which reduce the effective refractive index considerably. The refractive index was estimated to be 1.5 by observing the time delay of signals passing from one short, thin monopole through a pile of stacked cards to another short, thin monopole.

The received signal, and the computed system transfer functions for these partially phase-corrected conical monopoles is shown in Fig. 9.7. There is considerable improvement over the transfer function shown in Fig. 9.5, especially above 300 MHz, but extra phase correction is clearly required. The signal delay caused by the lens shows as an increase in the average slope of the phase/frequency characteristic. The experimental and computational procedure used for this measurement was the same as that used for the measurement shown in Fig. 9.5. Both the plots shown in Figs 9.5 and 9.7 were continued out past the upper limit of the measurement bandwidth (600 MHz) to show the

benefit obtained by the partial phase correction. Although the absolute values are likely to be in error, a direct comparison can be made since the values of  $U(f)$  stored in computer memory were the same for both measurements.

Some time after the measurements described above were made, a Tektronix 1S2 TDR became available. It was realised that with this measurements could be made on phase-corrected cones which were small enough to be within the financial resources of this project.

Two hollow 50 ohm cones, each with a slant height of 7.6 cm, were constructed from thin sheet brass. The lenses were made from perspex which was found to possess a sufficiently low loss factor to permit meaningful measurements to be made<sup>3</sup>. Polythene and polystyrene have almost negligible loss but in New Zealand they are not as easy to procure or to fabricate<sup>4</sup>. The dimensions of the cones and the lenses are given in Fig. 9.8. The cones were placed 0.61 m apart on the ground plane which is described in section 3.2.

The magnitude of the induction field was less than 10% of the magnitude of the radiation field for frequencies above 1 GHz. The Fraunhofer condition, eqn(3-4), was satisfied provided the frequency was less than 4.6 GHz. However, estimates of  $H(f)$  could be made up to 9 GHz with less than 10% error due to phase differences from the edge of the aperture (Montgomery 1947, p902).

---

<sup>3</sup>For perspex  $\tan \delta = 0.0067$  at 10 GHz.

<sup>4</sup>For polystyrene  $\tan \delta = 0.00041$  at 10 GHz and for polythene  $\tan \delta = 0.00066$  at 10 GHz (Moreno, 1948).

The peak amplitude of the transmitted pulse was 120 mV (it is shown in Fig. 4.12) and the peak amplitude of the received signal was about 1.5 mV. Accurate measurements of signals as small as this can only be made using the 3 point scanning method of sampling (Nicolson, 1969) which is described in section 2.3.6. All the responses of these cones were measured by this method. By averaging 24 scans of the received signal (which took about 14 minutes) the effective noise level of the measuring equipment could be reduced to about 10  $\mu$ V. The RMS noise level of the sampling oscilloscope was about 1 mV referred to the input (section 2.3.3.2.1), so that the 3-point scanning method gave an improvement of 40 dB.

The reflection coefficients of these cones are presented in section 6.3.2, where it was observed that they are not as well matched as a larger 0.71 m slant height sheet metal cone. Since we are interested in the system transfer function between two cones matched to their respective transmission lines, the modulus of the computed system transfer functions have been corrected for the power lost due to the mismatch. The correction applied was

$$|H(f)|_{\text{matched}} \approx |H(f)|_{\text{measured}} / [1 - |\rho(f)|^2] \quad (9-17)$$

The corrected system transfer functions for these cones are presented in Fig. 9.9, which shows that the modulus is flatter and the phase is more linear when phase correction is applied. The difference between the slopes of the phase curves shown in Fig. 9.9 and those shown in Figs 9.5 and 9.7 are due to different time origins for the test pulse and the

received signal. For faithful signal transmission all that is required is linear, or as near linear as possible, phase. The actual average slope of the phase/frequency characteristic is immaterial.

For cones having the dimensions shown in Fig. 9.8 the benefit of phase correction is only fully apparent at frequencies appreciably higher than 4 GHz. For instance, when an uncorrected (no lens) cone is transmitting the signals at points  $B_1$  and  $B_2$  (see Fig. 9.8) are out-of-phase at 7.3 GHz, and the gain is a minimum. So, at 7.3 GHz phase-correction of the cones should result in a considerable increase in  $|H(f)|$ .

Time domain measurements could not be made above 4 GHz because no suitable equipment was available. Larger phase-corrected cones were too expensive to make. However, reasonably accurate, though very tedious, continuous wave (c.w.) measurements of  $|H(f)|$  could be made in the range 4 GHz to 8 GHz. A microwave oscillator was used as a transmitter and a heterodyne detector was used as a receiver. The following procedure was used to allow for reflections from the walls, ceiling and objects in the laboratory. For each measurement frequency the ground plane (which was mounted on a trolley fitted with castors) was wheeled about within a roughly circular area in the middle of the room, and the maximum and minimum received signals were searched for. The circle was several tens of wavelengths in diameter at 4 GHz. The maximum and minimum signals were then averaged and the system transfer function was calculated by comparing the averaged received signal with the signal

measured by connecting the two cables feeding the antennas together (thus allowing for cable loss). A simple check was made on the accuracy of this method. The measurement made at 4 GHz on the cones without phase-correction was repeated and 120 readings of the received signal were taken with the ground plane positioned at random within the allotted area. Because the measured signals exhibited many maxima and minima within that area, and because the ground plane was positioned at random, the measured signals could be assumed to be normally distributed about some mean value which was a good approximation to the value that would be obtained in an ideal anechoic chamber. The magnitude of the system transfer functions obtained by the c.w. measurements is presented in Fig. 9.10, together with that obtained from the time domain measurements.

The difference between the mean of the maximum and minimum measurements and the mean of the 120 random measurements is seen to be about one quarter of the RMS error in the random measurements, from which it can be concluded that the measurement method used was satisfactory. There is also about 12% error at 4 GHz in the frequency response inferred from the time domain measurements, which is an estimate of the accuracy of the time domain measurements. The system response of the phase-corrected cones is seen to be considerably flatter than that of the uncorrected cones. The measurements verify that the gain of the uncorrected cones has a minimum near 7.3 GHz.

A lens with a cylindrical aperture, such as the ones shown in Figs 9.6 and 9.8, tapers the amplitude distribution across the aperture (Silver 1949, section 11.3). This

reduces the antennas gain. For cones with large flare angles (i.e. low characteristic impedance) the amount of taper is less and hence the gain is higher for a given aperture size. Less phase correction is required. A more uniform amplitude distribution across the aperture for a given cone could be obtained by using a lens with both its inner and outer surfaces convex (Silver 1949, section 11.3).

### 9.5. FAN MONOPOLES

Figs 9.11(a) and 9.11(b) show  $T(f)$  and  $R(f)$  for a  $60^\circ$  flare angle, 6 wire fan antenna with a circular end and an end wire. The geometry of this antenna is shown in Fig. 6.4. The transfer functions are given for two orientations of the antenna: when it is broadside on and when it is edge on. The  $H(f)$  for transmission between two of these antennas are given for the same orientations. It is clear from Fig. 9.11 that two fan antennas form a system of wider bandwidth when they are arranged to be broadside than when they are arranged to be edge-on to each other (remember however, that this antenna is not matched to a 50 ohm feedline over the whole of the measurement bandwidth).

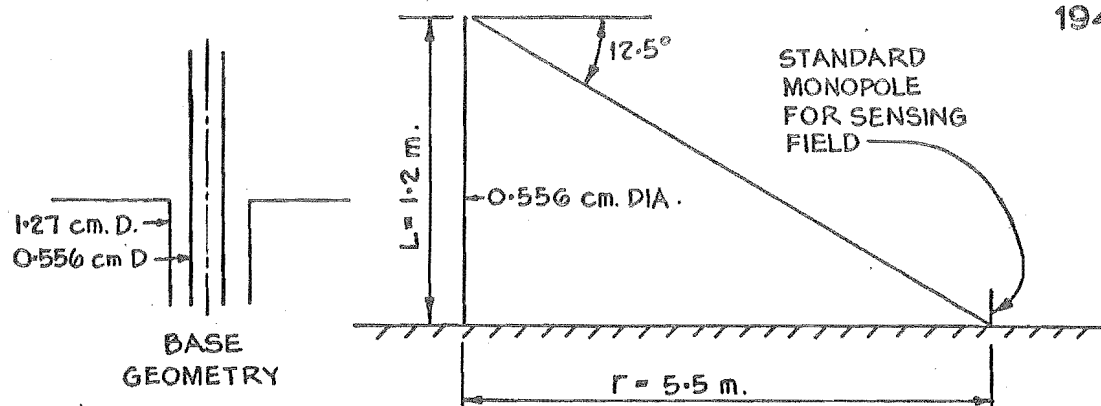


FIGURE 9-1: GEOMETRY OF MONOPOLE RADIATION EXPERIMENT.

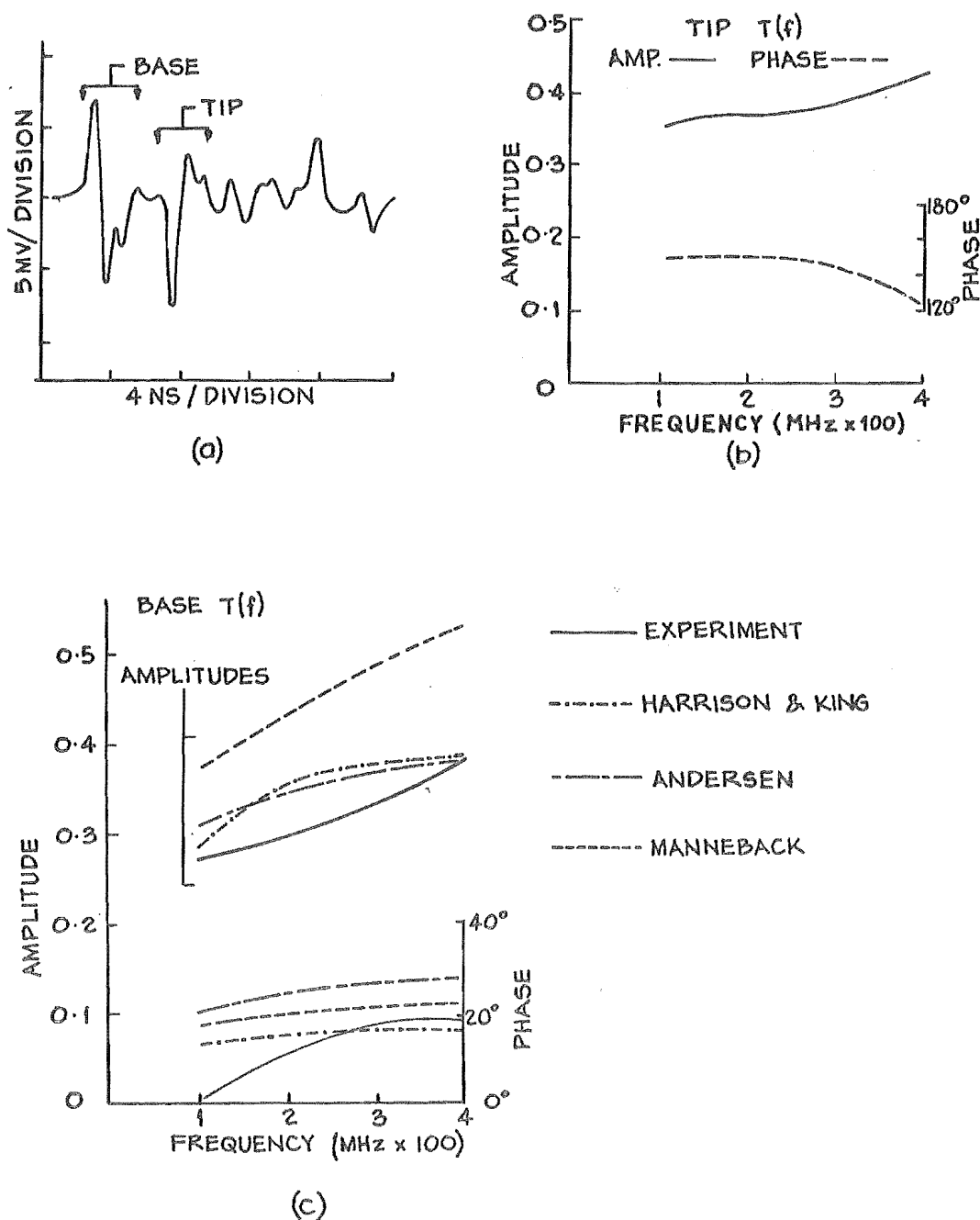


FIGURE 9-2: (a) RECEIVED SIGNAL RADIATED FROM 1.2 METRE MONOPOLE.  
(b) & (c) TRANSFER FUNCTIONS FOR RADIATION FROM TIP & BASE

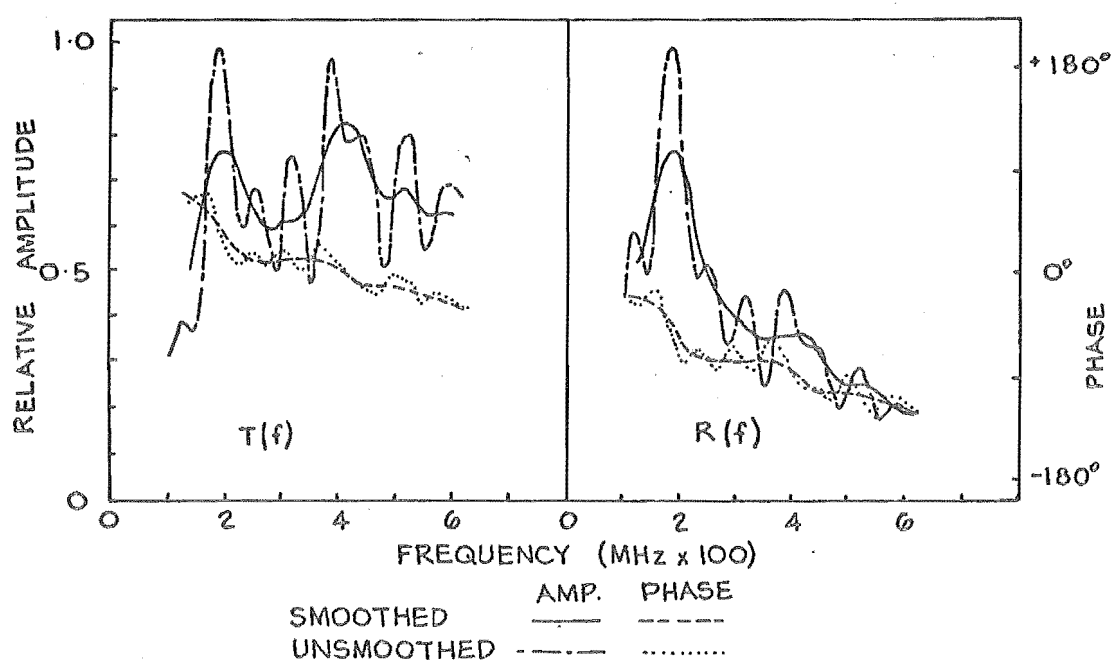
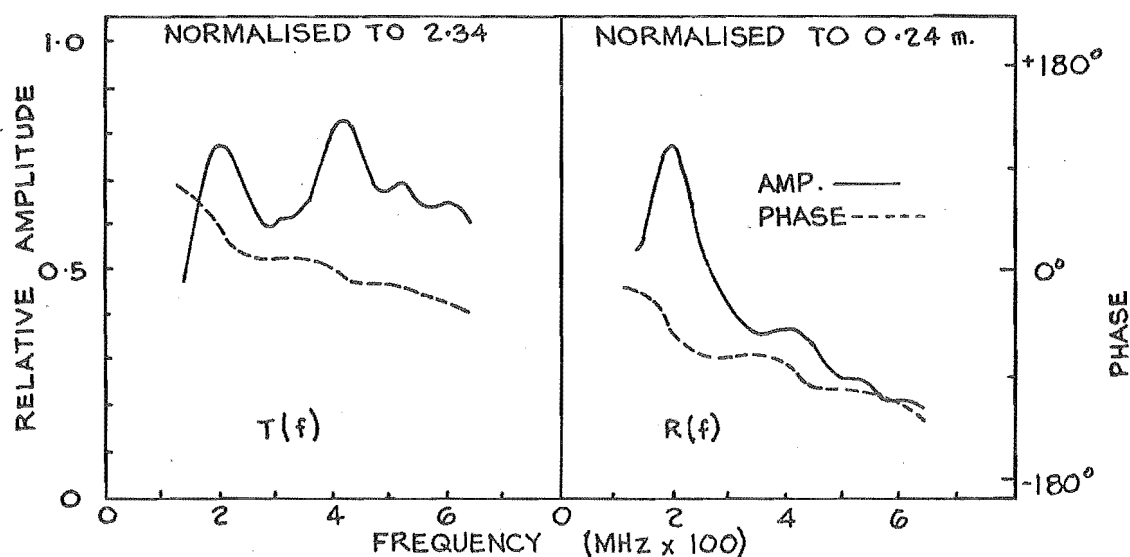
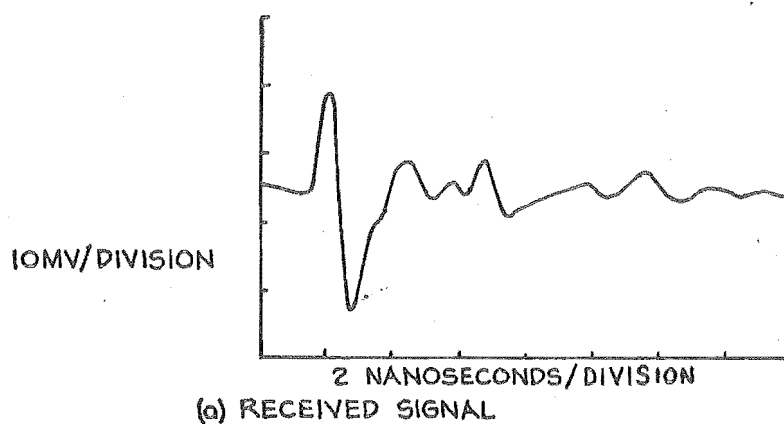


FIGURE 9-3: FAR FIELD RESPONSES OF 0.71 METRE SLANT  
HEIGHT 50 OHM CONICAL MONOPOLE.



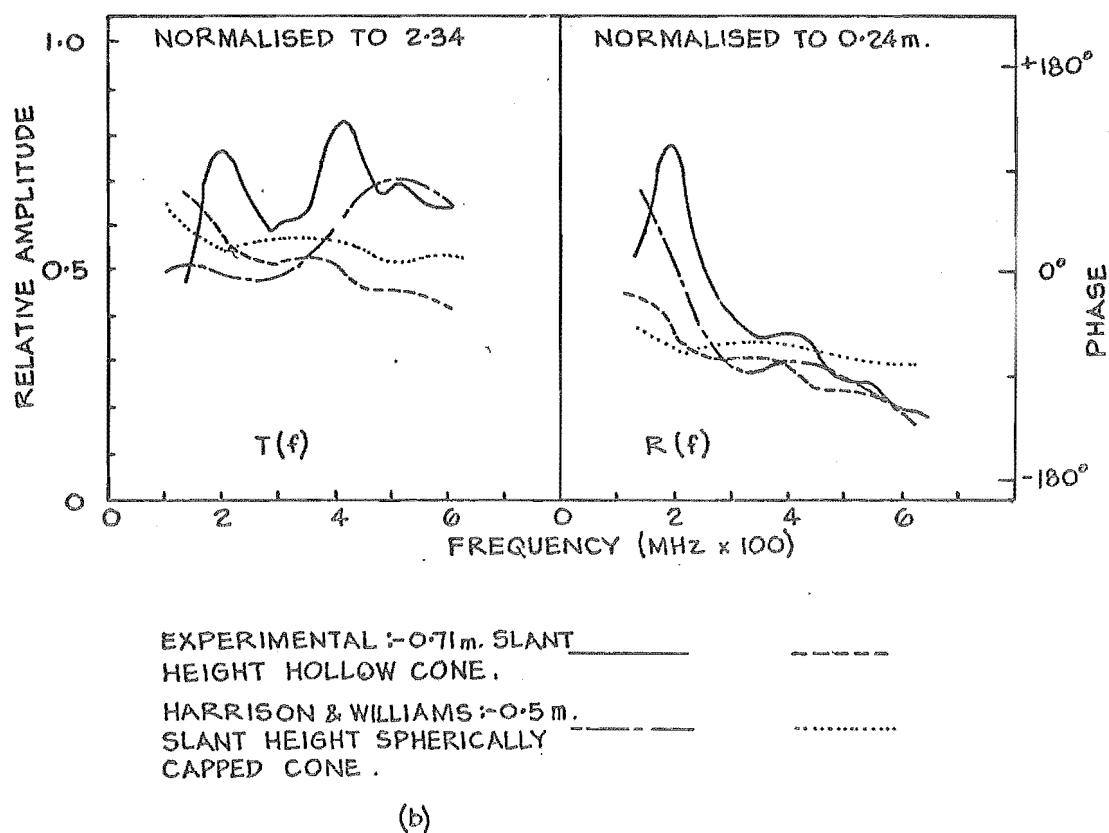
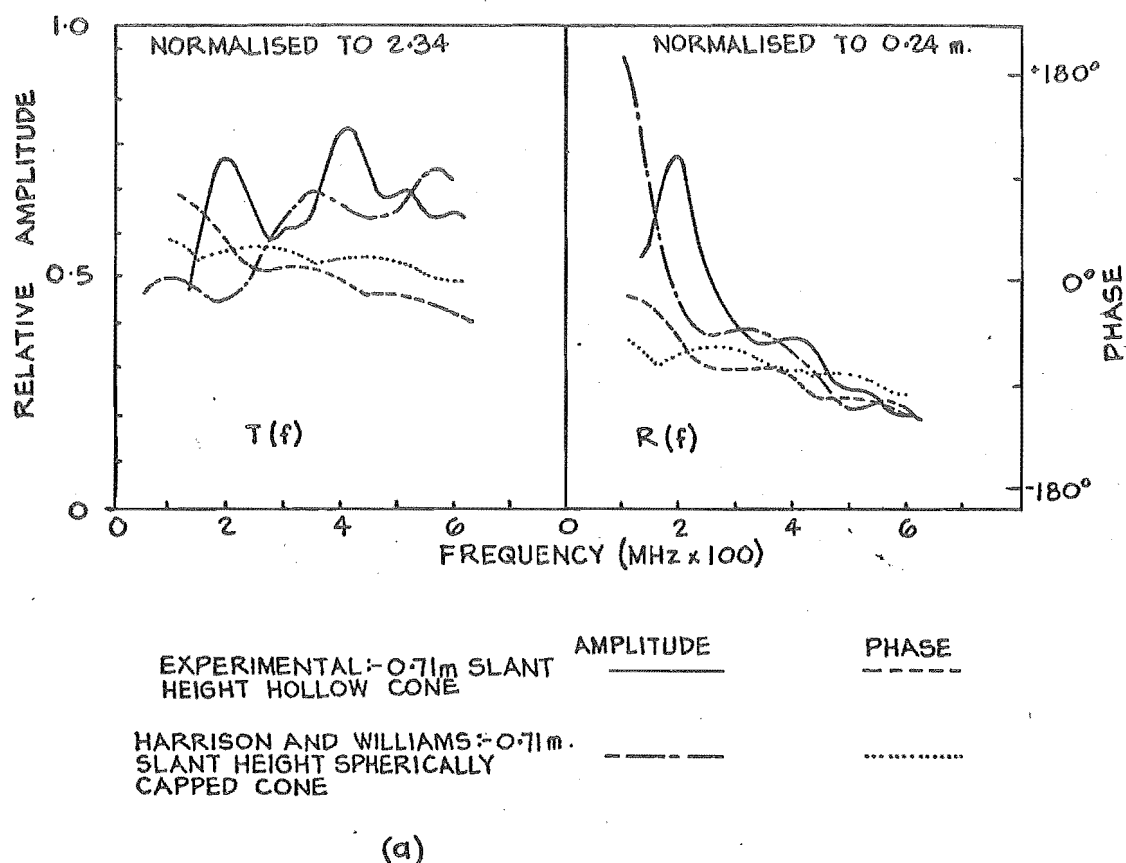
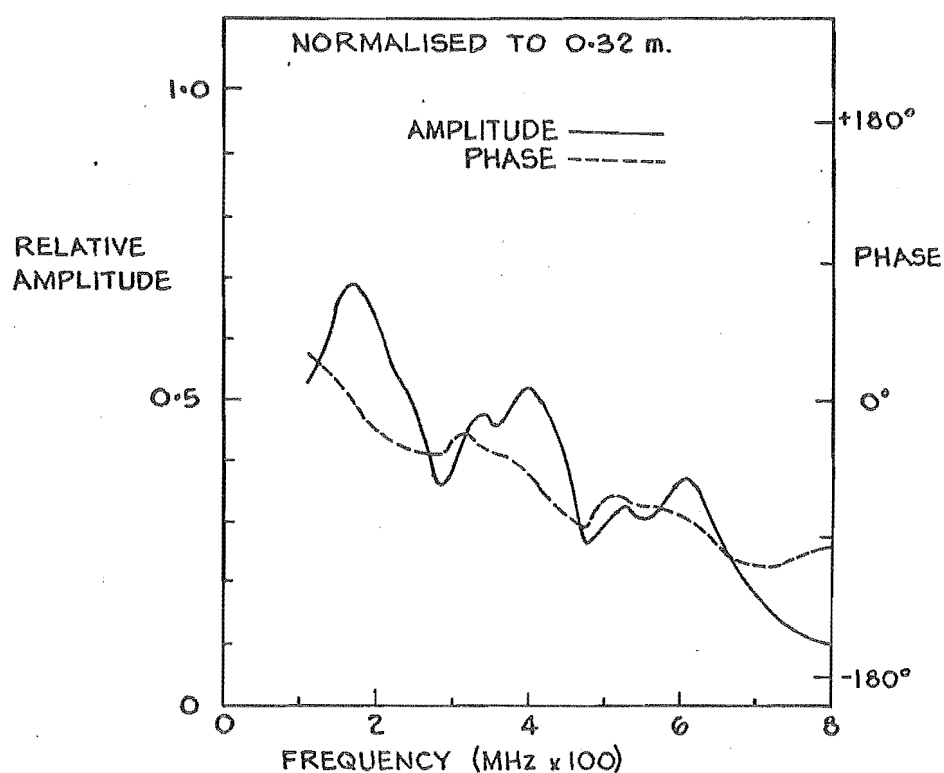
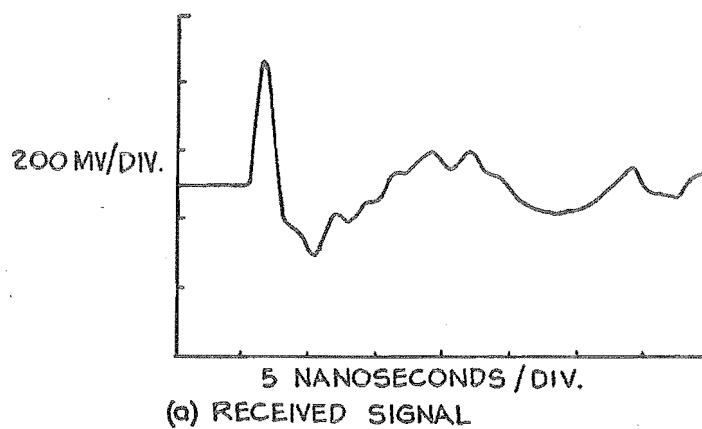


FIGURE 9.4: COMPARISON OF EXPERIMENTAL AND THEORETICAL TRANSMISSION AND RECEPTION TRANSFER FUNCTIONS FOR 50 OHM CONICAL MONOPOLES.



(b) COMPUTED SYSTEM TRANSFER FUNCTION

FIGURE 9.5 : SYSTEM RESPONSES FOR TWO 0.71 METRE SLANT HEIGHT 50 OHM CONICAL MONOPOLES.

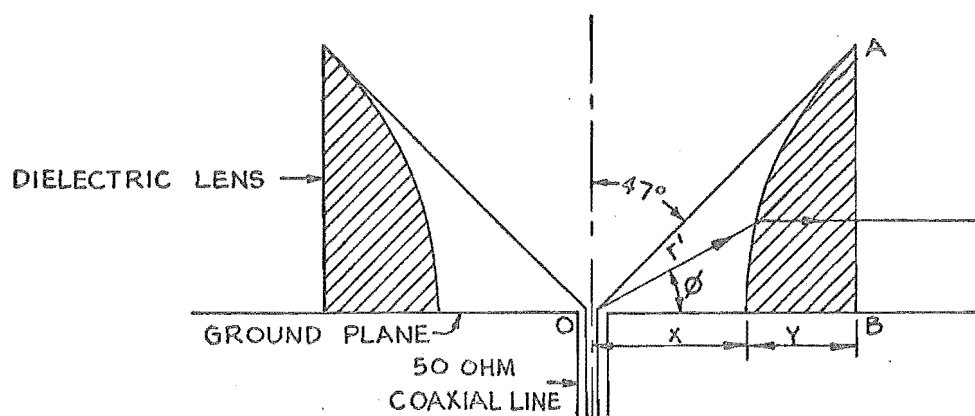


FIGURE 9.6 : GEOMETRY OF PHASE CORRECTING LENS FOR CONICAL MONOPOLE.

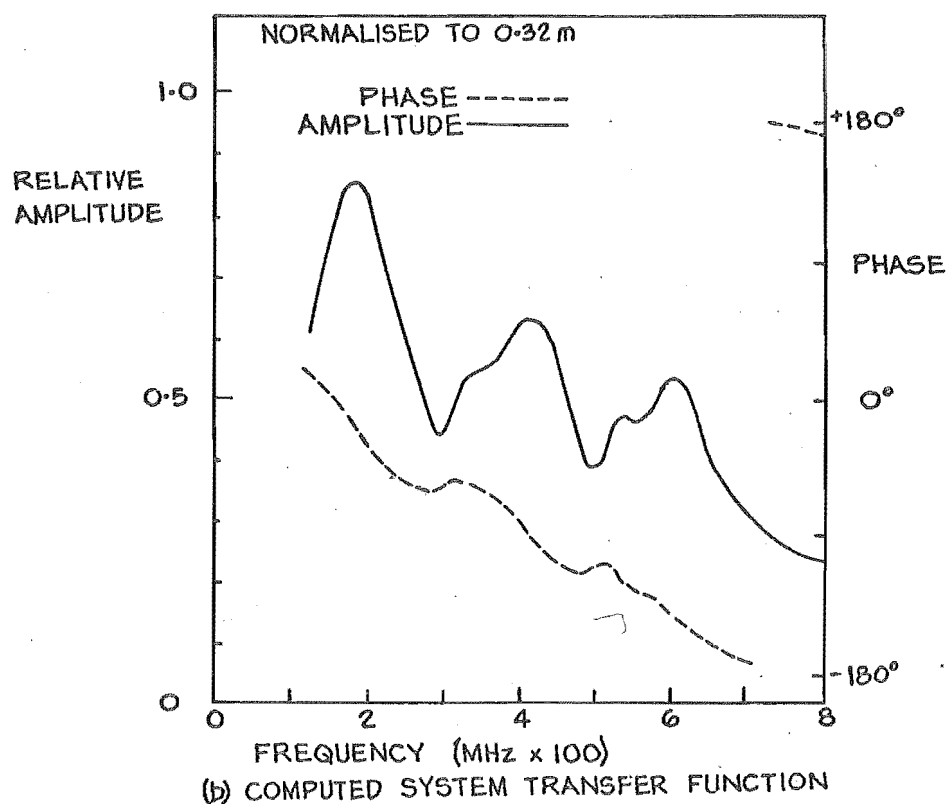
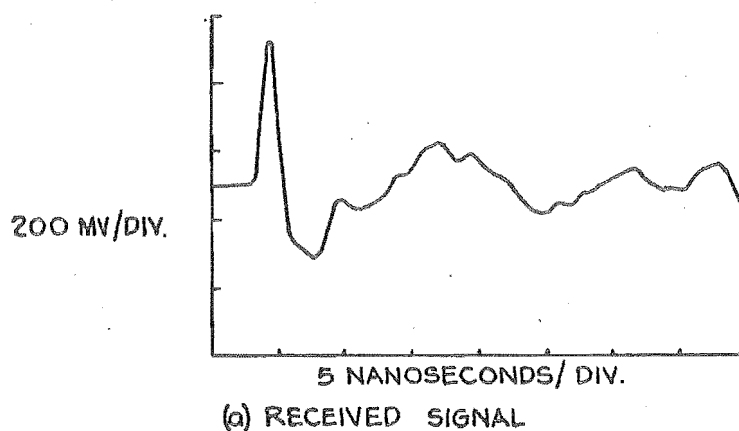


FIGURE 9.7: SYSTEM RESPONSES FOR TWO PARTIALLY PHASE CORRECTED, 0.71 METRE SLANT HEIGHT, 50 OHM CONICAL MONOPOLES.

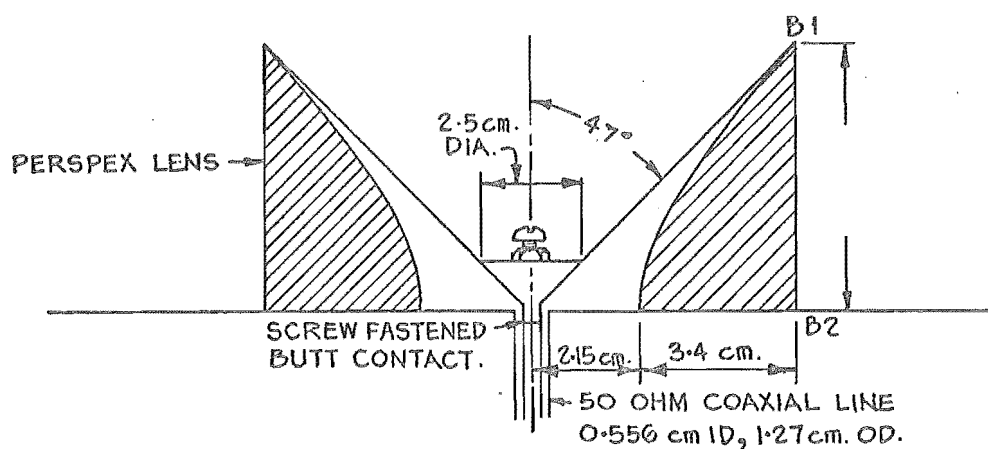
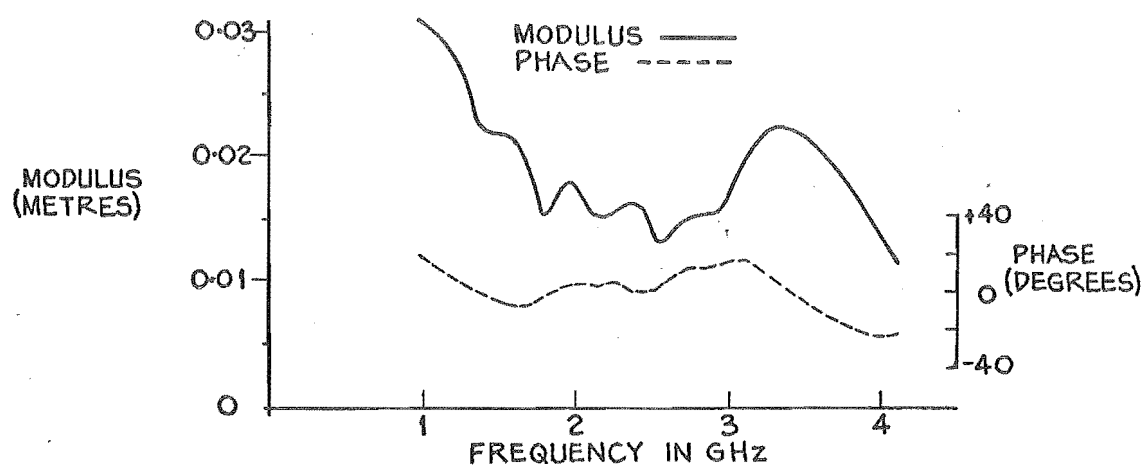
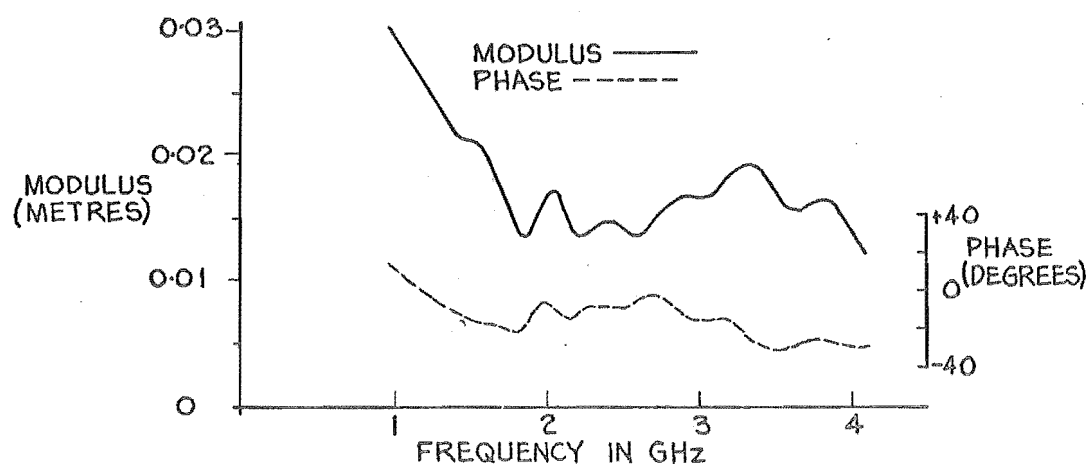


FIGURE 9.8: DIMENSIONS OF 7.6 cm. SLANT HEIGHT CONICAL MONOPOLE WITH PHASE CORRECTING LENS.



(a) WITHOUT PHASE CORRECTION



(b) WITH PHASE CORRECTION

FIGURE 9.9: CORRECTED SYSTEM TRANSFER FUNCTIONS FOR TWO 7.6 cm. SLANT HEIGHT 50 OHM CONICAL MONOPOLES.

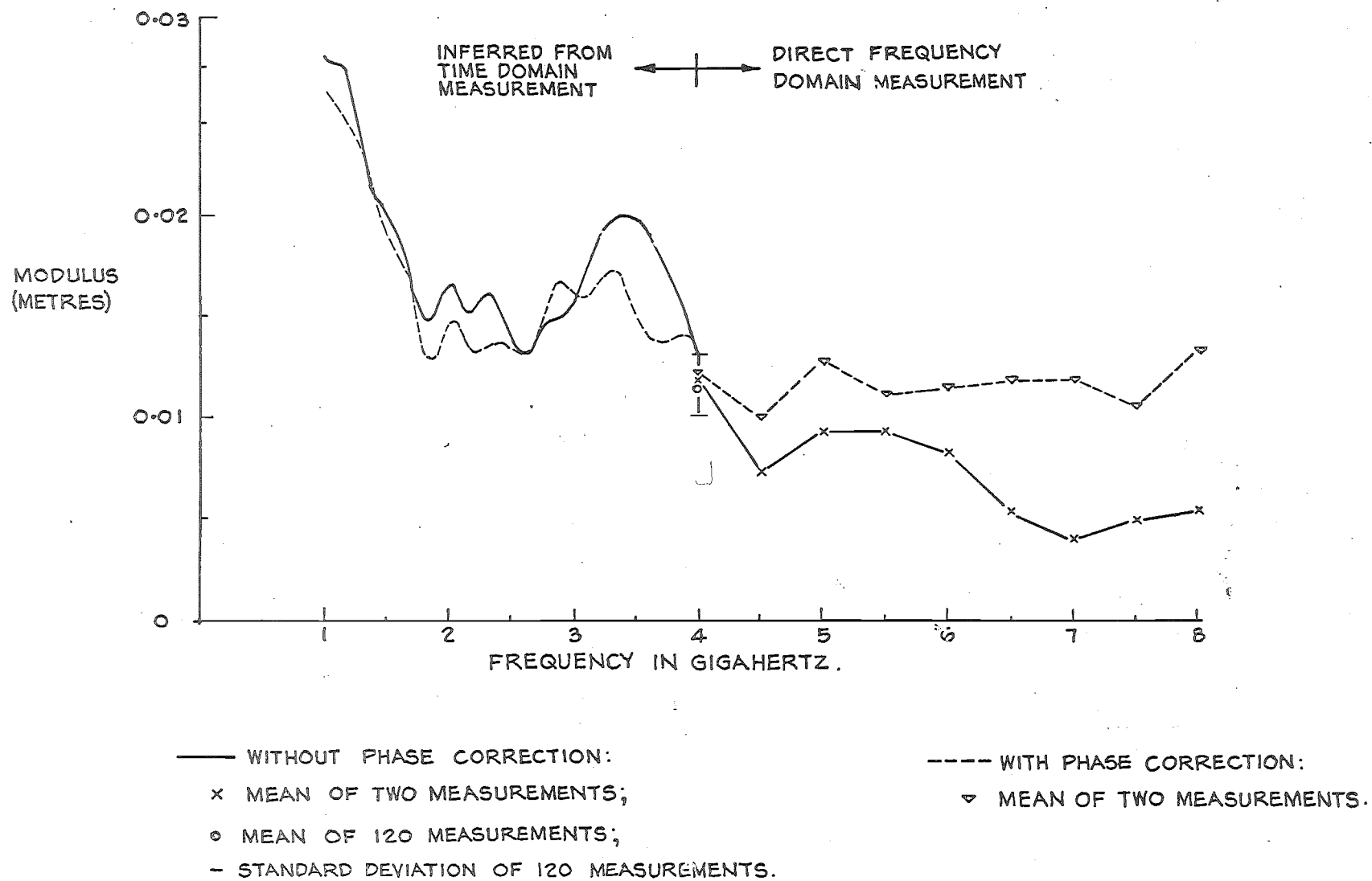


FIGURE 9.10: MODULUS OF SYSTEM TRANSFER FUNCTIONS FOR TWO 7.6cm. SLANT HEIGHT 50 OHM CONICAL MONOPOLES.

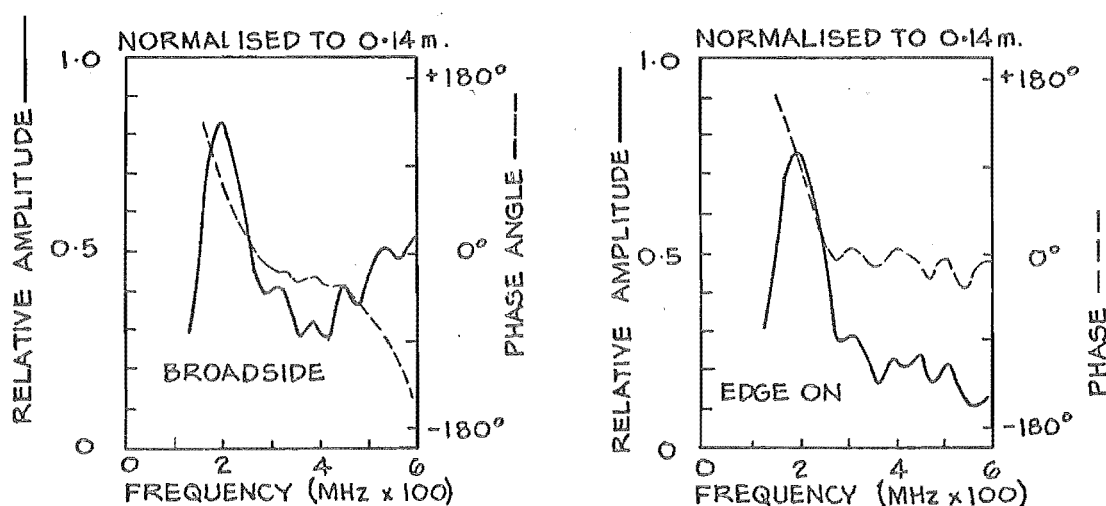
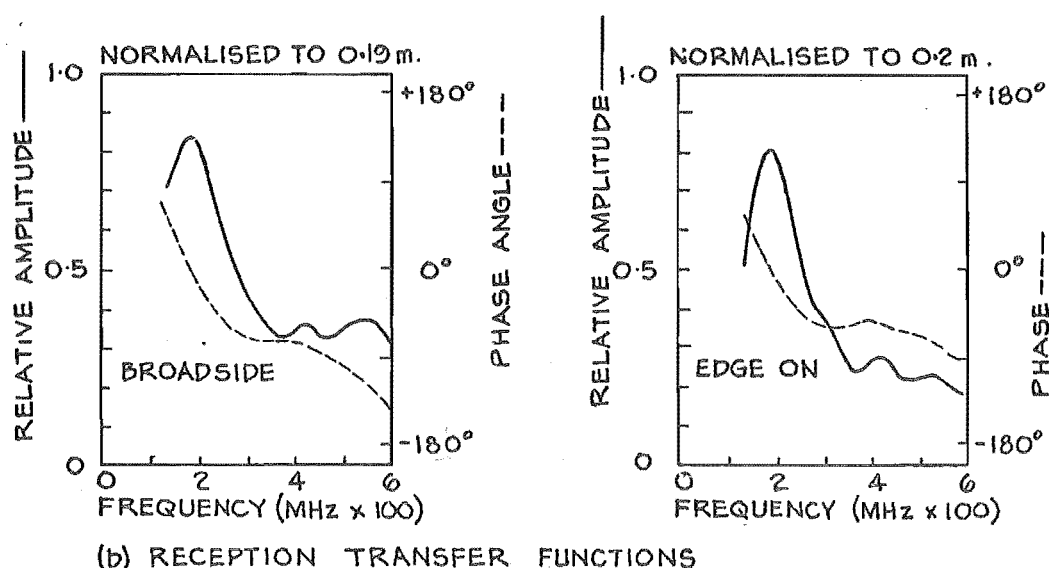
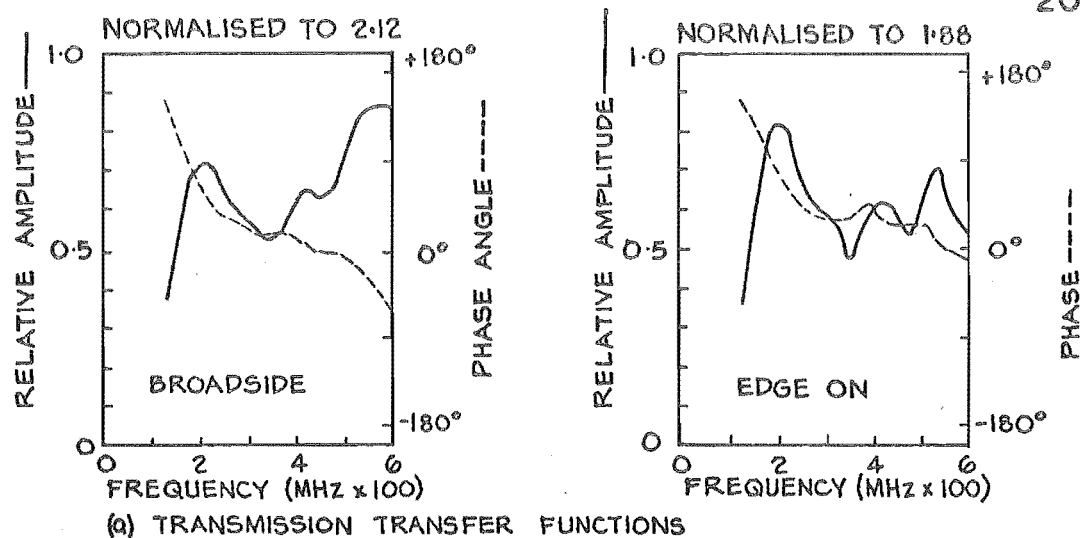


FIGURE 9-11: FARFIELD TRANSFER FUNCTIONS FOR 60° FLARE ANGLE 6 WIRE FAN ANTENNAS WITH END WIRES.

## CHAPTER 10: DISCUSSION OF FAR FIELD RESPONSES

### 10.1 RADIATION FROM A MONOPOLE

The results presented in section 9.2 show that the fields radiated when signals are incident upon the base and the tip of a thin monopole are essentially frequency independent. The shape of the time domain field is therefore essentially a replica of the input pulse shape. The measurement also shows that the radiation emanates mainly from the points of discontinuity, i.e. the base and the tip (see Fig. 9.2) (radiation occurs when charge accelerates; Jones 1964, section 3-2). The radiation which occurs as the propagation velocity of the current increases along the monopole (see section 5.2) is too small to be detected in the experiment reported in section 9.2.

Schmitt et al. (1966) have also experimentally verified that the radiation which occurs when a transient signal is incident upon the base and the tip of a thin monopole is frequency independent. They verified it with a time domain measurement. Their result, and the one presented in section 9.2, is at variance with King's and Schmitt's (1962) qualitative discussion of the radiation mechanism of a dipole which was presented in order to explain the theoretical and experimental results given by Schmitt (1960). King's and Schmitt's argument was based on the assumption that the far field of the antenna is proportional to the time derivative of the local current density. It is pointed out by Ross et al. (1966a) that this is incorrect, and that the far field of a dipole is given by

$$E \propto \frac{\cos\theta}{1-\sin\theta} \left[ i\left(t-\frac{r}{c}\right) - i\left(t-\frac{r}{c}-\frac{L}{c}[1-\sin\theta]\right) \right] \quad (10-1)$$

where  $\theta$  is the angle between the wire axis and the direction of the radiation and  $L$  is the dipole half-length. Eqn(10-1) means that the far field is directly proportional to the current, and not its time derivative, at times corresponding to the instants when the current appears at the base of the dipole, and is reflected from the end and the base. Eqn(10-1) corresponds to differentiation only when  $L \rightarrow 0$ , i.e. for an infinitesimal dipole. This agrees with the findings of Katayama and Mushiake (1967).

Schmitt (1960) calculated theoretically the far zone field of a monopole when it is excited by a step-function of voltage by performing a graphical inverse Fourier transform of its frequency response. Unfortunately he was forced to truncate his integration prematurely because values of the effective height of the monopole were only known up to about the second antiresonance whereas the spectrum of the excitation extends to arbitrarily large frequencies. The loss of the small but significant amount of high frequency information results in the risetime of the radiated field depending upon the monopole length  $L$  and not upon the risetime of the step (as we would expect it to). He was not able to substantiate this result experimentally because he did not have a broadband receiving probe. The time domain receive response of an antenna is proportional to the integration of the transmit response (section 2.4). Schmitt integrated the transmit response to obtain the time dependence of the received signal when a step change in electric field is incident upon the antenna, and then calculated the received



signal when a step-function of voltage excites an identical, distant (i.e. in the far field) antenna). This latter result was substantiated experimentally. The inaccuracies in the calculated transmit response were masked by the integration required to obtain the receive response. It appears that King and Schmitt were led to their erroneous conclusion in attempting to explain the transmit response.

More accurate calculations made by Schmitt et al. (1966) for various pulse durations show that the field risetime is equal to the excitation risetime, even for the fastest risetime pulse for which computations were made ( $t = 0.05 L/c$ ). These results were substantiated experimentally. The shape of the response to approximate step function excitation can be obtained by integrating their result for narrow pulse excitation. For ideal (zero-risetime) step function excitation we would expect the field risetime to depend only on the dimensions of the base region, just as the risetime of the signal reflected from the base was limited by the base geometry (Wu and King, 1963).

It is worth mentioning that Ross et al. (1966a, 1966b) experienced difficulty in inferring the time domain transmission and reception characteristics from the frequency response because of incomplete knowledge of the frequency response. Instead they postulated simple transmission line models for the dipole and deduced the time domain radiation characteristics from them<sup>1</sup>. The time dependence of the received voltage when an impulsive field is incident upon a

---

<sup>1</sup> A simple transmission line model presented by Ross to explain the observed driving point characteristics of a dipole is described in section 5.4.2.

dipole of half length  $L$  is deduced from a model by Ross (1969a). This response has the same shape as the field radiated from the dipole when it is excited by a step function (section 2.4). His result, together with that of Schmitt (1960), is reproduced in Fig. 10.1. The differences are seen to be characteristic of truncation errors (e.g. see Fig. 9.3(c)), as suggested above. It must be remembered that the simple models which Ross uses are only approximate because he assumes that the driving point characteristics of the base region are frequency independent. It is shown in chapter 5 that this is not true. However, the results obtained are good enough for most engineering applications if the characteristic impedance of the feedline is low (e.g. 50 ohms, section 5.4.2).

If a thin dipole is excited by a step modulated monochromatic wave then the transient buildup of the radiated field can be obtained by superimposing the waves radiated from the feedpoint and the tips as the monochromatic wave is successively reflected up and down the dipole. The amplitude of each radiated wave is given approximately by the amplitude of the radiated transients when the dipole is excited by a narrow pulse: these were taken from Schmitt et al. (1966). The step modulated response is pictured in Fig. 10.2. For clarity the waves emanating from the base and the tip are shown separately in Figs 10.2(a) and 10.2(b), and the resultant radiated wave is shown in Fig. 10.2(c). It is implied that for times long after the arrival of the excitation the radiated field has a phase advance of  $90^\circ$  on the excitation, in agreement with the field radiated by a current element

(Jordan and Balmain 1968), p319). The response pictured in Fig. 10.2 is in close agreement with the measurement reported by Schmitt et al. (1966).

The field of a thin dipole with an exactly sinusoidal current distribution can be represented as the field due to an array of three isotropic radiators, two located at the tips and one at the base (Jordan and Balmain 1968, section 10.09). When the dipole is an odd number of half wavelengths long the strength of the source at the base is zero (in the steady state). Notice that the waves pictured in Fig. 10.2 agree with this representation.

## 10.2 FAITHFUL TRANSMISSION OF WIDEBAND SIGNALS

It is shown in section 9.4 that phase-corrected conical monopoles are suitable antennas for a system required to faithfully transmit signals having a bandwidth of an octave or more, provided the monopoles can be well matched. As mentioned in section 6.3.2, the cones shown in Fig. 9.8 exhibited appreciable reflections from the base and from the surfaces of the lens. The base reflections can be made negligible, as has been shown (Ross et al., 1966b), by reducing the dimensions of the coaxial feed-line but retaining the same characteristic impedance, so that there is a smooth transition from the feed-line to the cone.

It is impossible to compensate for lens reflections over an octave bandwidth. However, a variable refractive index lens could be used; the refractive index tapering to unity at the apex of the cone and its cylindrical aperture. The lens could be fashioned from coaxial cylinders of

differing refractive index. It would be inconvenient to attempt to use a number of different materials for such a lens, but it could be constructed using artificial dielectrics (Collin and Zucker 1969b, p104), which can be designed to operate satisfactorily over bandwidths of much greater than one octave.

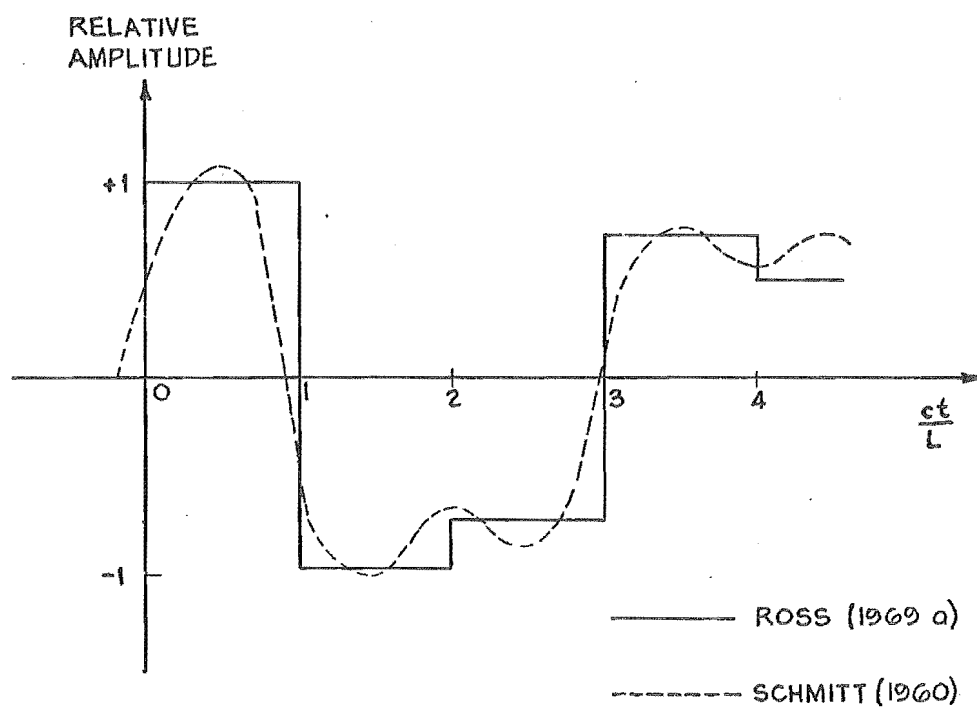


FIGURE 10.1: FIELD RADIATED BY DIPOLE OF HALF-LENGTH  $L$  WHEN EXCITED BY A STEP FUNCTION

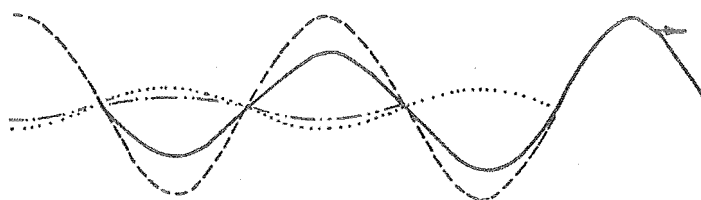
(a) WAVES RADIATED FROM BASE:

----- FIRST WAVE

..... SECOND WAVE

----- THIRD WAVE

———— RESULTANT



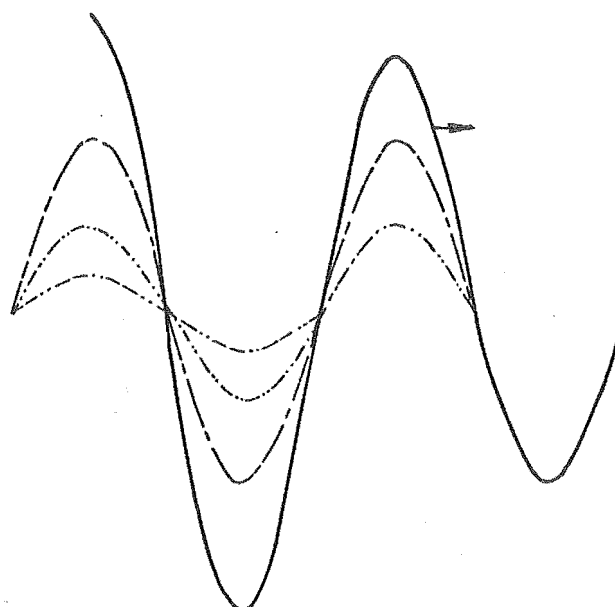
(b) WAVES RADIATED FROM TIP:

----- FIRST WAVE

..... SECOND WAVE

----- THIRD WAVE

———— RESULTANT



(c) RESULTANT RADIATED WAVE

→ DIRECTION OF TRAVEL

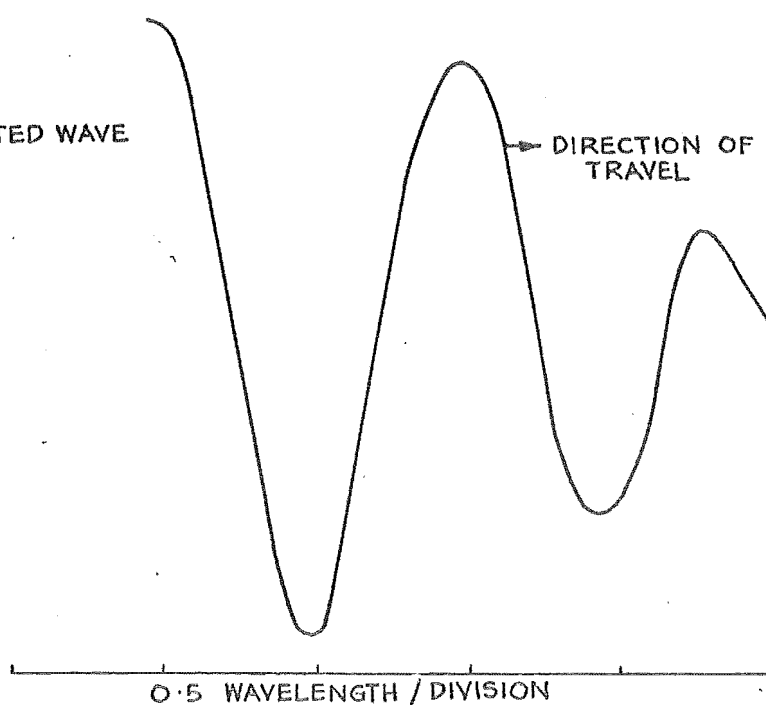


FIGURE 10.2 : WAVES RADIATED BY A HALF WAVELENGTH LONG DIPOLE EXCITED BY A STEP MODULATED MONOCHROMATIC WAVE .

PART IV

PROPAGATION OF CURRENT ON BENT WIRE ANTENNAS

## CHAPTER 11: PROPAGATION OF CURRENT ON BENT WIRE ANTENNAS

### 11.1 INTRODUCTION

The propagation of current on bent wires was first studied by Pocklington (1897). He demonstrates that current propagates along the surface of a perfectly conducting wire of circular cross section approximately with the velocity of light. There is effectively no attenuation, dispersion or reflection provided the wire is not too sharply bent. He also demonstrates that the phase velocity of monochromatic current waves propagating along sharply curved (in terms of wavelength) circular loops and helices is virtually constant and greater than the velocity of light. Pocklington's theory is of practical significance, even though it is only approximate. The assumption that the current propagates at the velocity of light is valid only in the limit for infinitely thin straight wires (Hallén 1962, p446). The propagation of current on wire antennas has been reviewed by Hallén (1962, chapter 35) and Jones (1964, sections 3.14 and 3.15). Very little has been done on bent wires. Carson (1928) deals only with straight wire transmission lines at distances far from the feedpoint. However, Brundell (1960b) has shown that the phase velocity of a current wave propagating around a circular loop of thin cross section is approximately constant and greater than the velocity of light. This behaviour is also apparent in the theoretical input impedances of circular arc and helical antennas presented by Tang (1964).



Hallén (1962, chapter 35) examines the vector potential at the surface of a straight, perfectly conducting antenna of arbitrary, but constant, cross section which is excited symmetrically with respect to its axis, and shows that it propagates exactly at the velocity of light, without attenuation, dispersion or reflection. This is not true for a bent antenna. Bates (1966) (also in Ross et al. 1966a, 1966b) has analysed theoretically the propagation of the vector potential along the surface of a strip (i.e. a flat wire of zero thickness) which is bent in the plane containing itself. When the width of the strip is small and constant, so that there is negligible current flow across the strip, the component of the vector potential along the strip propagates virtually without reflection and almost at the velocity of light, provided that the radius of curvature of the strip remains constant. The major effect of the curvature of the strip is to introduce attenuation: there is only a small amount of dispersion. Reflection occurs from points where the radius of curvature changes.

The current can only be obtained from the vector potential by solving an integral equation. In general, the behaviour of the current is different from that of the vector potential. A current wave propagating along a straight wire antenna is advanced in phase with respect to the potential, but the phase difference diminishes as the distance from the driving point (or any discontinuities such as sharp bends) increases (Hallén 1962, chapter 35). This means that the phase velocity of the current wave is slower than that of light, which it approaches asymptotically as the distance

from the driving point increases (see section 5.2). This distance depends upon the electrical thickness of the wire (Andersen, 1968). Thin wires are only dispersive near their driving points or near sharp bends. Consequently by assuming that the behaviour of the current and the vector potential are similar Bates (1966) was able to obtain qualitative confirmation of his theory for the vector potential by observing the reflections of narrow pulses from thin bent wires (consisting of two straight segments joined by a circular arc) of circular cross section. Measurements were made of the pulse reflection coefficient of sharp bends ( $< 2$  cm radius) (Bates 1966, Ross et al. 1966b, section III) and the pulse attenuation coefficient of gradual bends ( $> 2$  cm radius) (Ross et al. 1966b, section III). The measured coefficients were calculated by dividing the peak amplitudes of the pulses reflected from the bend and the tip respectively by the peak amplitude of the pulse reflected from the tip of a straight wire.

Both of Bates' measured coefficients were observed to be strong functions of the pulse duration. Inspection of the oscilloscope waveforms presented in Ross et al. (1966b, section III) shows that the shape of the pulse reflected from the tip of a wire changes as the wire is bent. Thus the reflection and transmission characteristics of current on bent wire antennas are frequency sensitive. It was shown earlier in this thesis in section 5.4.2 that a pulse reflection coefficient for frequency sensitive discontinuities can be misleading. Further, the spectrum of the pulse which is actually applied to the bend depends upon the electrical

dimensions of the base region (see section 5.3). Changing the wire diameter but feeding the wire with the same test pulse from the same coaxial line results in a pulse with a different spectrum being applied to the wire. It is unlikely that the reflection and transmission characteristics for the bent wires have the same dependence on the wire diameter as the base region, hence pulse reflection and transmission coefficients for different wire diameters cannot be directly compared.

An accurate method of measuring the reflections of a narrow pulse from a bent wire antenna is described in section 11.2. Measurements of the reflections from both sharp and gradual bends in thin wires are presented in sections 11.2.1 and 11.2.2. In section 11.2.3 careful examination of the shape of the pulse reflected from the tip of a bent wire and the wire geometry show that the distortion of the reflected pulse is caused both by attenuation of the pulse as it travels around the bend and by current induced on the bent section due to radiation from the base. Reflection coefficients and transmission coefficients which describe the propagation of monochromatic current waves on bent wire antennas are presented in section 11.3. How to compute these frequency responses was demonstrated with the aid of a simple model of a bent wire in section 2.5. Section 11.4 discusses the responses and presents a physical explanation of the mechanism of the current flow on a bent wire antenna. The section concludes with suggestions for continuing the work reported in this chapter.

## 11.2 THE DRIVING POINT PULSE RESPONSES OF BENT WIRE ANTENNAS

The geometry of a bent wire or strip antenna driven above a ground plane is shown in Fig. 11.1<sup>1</sup>. Notice that  $r$  is used to denote the radius of curvature in this chapter and should not be confused with the  $r$  meaning antenna separation elsewhere in this thesis. Measurements were made of the driving point responses up to the first tip reflection of a number of bent wire and strip antennas. The geometries of these antennas (with the exception of two measurements reported later in section 11.2.2) are summarised in Tables 11.1 and 11.2. The wires were machined to exactly the same length before bending: the length of the wire axis changes negligibly during bending (a measurement indicated that the axis of a 0.64 cm diameter wire lengthened by less than 0.01 cm for a 10 cm radius, 80° bend). The strips were cut from 0.33 mm thick tin plated steel sheet. Careful measurement ensured that the axes of the strips were all the same length. The spatial length of the test pulse ( $c\tau_1$  where  $\tau_1$  is the pulse duration) was much less than the wire or strip length (Fig. 4.12 shows the test pulse:  $c\tau_1 \approx 9$  cm).

The 3-point scanning method of sampling (see section 2.3.6) was used to measure the signals. The program described in Appendix 2 was used for the measurements identified by an A (called measurements A) in Tables 11.1 and 11.2. Four scans of the reflected signal were averaged (taking about four minutes) which reduced the RMS noise level to about 200  $\mu$ V. An improved program (see section A2.7) was

---

<sup>1</sup>From now on a wire is assumed to have a circular cross section.

Wire diameter D (cm)	Distance to bend l (cm)	Bend radius r	3 mm					5 cm				10 cm				15 cm				20 cm			
		Bend angle $\theta$ Wire length L (cm)	20°	40°	60°	80°	90°	20°	40°	60°	80°	20°	40°	60°	80°	20°	40°	60°	80°	20°	40°	60°	80°
0.32	61 ± 2	91.5	A	A	A	A	A	A	A	A	A	A	A	A	A					A	A	A	A
0.32	30.5 ± 2	91.5	A	A	A	A	A					A	A	A	A								
0.32	90.3 ± 0.1	153	B	B	B	B	B																
0.64	61 ± 2	91.5						A	A	A	A	A	A	A	A					A	A	A	A
0.64	47.5 ± 2	75.7														B	B	B	B				
0.64	79.5 ± 1	121.3														B	B	B	B				

Table 11.1: Summary of measurements of bent wire antennas. A and B denote measurements. The meanings of A and B are defined in section 11.2.

Strip width W (cm)	Bend configuration	Distance to bend $\ell$ (cm)	Bend radius r	20 cm	
			Bend angle $\theta$ Strip length L (cm)	40°	80°
2.54	bent in plane of strip	$48 \pm 2$	92 cm	A	A
2.54	bent 90° to plane of strip	$48 \pm 2$	92 cm	A	A

Table 11.2: Summary of measurements of bent strip antennas.

A denotes a measurement. The meaning of A is defined in section 11.2.

used for the measurement identified by a B (called measurements B). These signals were scanned and averaged until the RMS noise level was reduced to 10  $\mu$ V: this required about 17 scans taking about 12 minutes. The experimental apparatus and the procedure followed when making all the measurements is described in sections 3.3 and 3.3.1. The sampling interval T was 25 ps.

The signals reflected from the tips of some of the 0.32 cm diameter wires were measured with the bend in two positions, near the base and near the tip (see Fig. 3.5). This was done simply by mounting the wire by its other end. The effect of the bend position could then be evaluated. The centre of the bend is  $L_1 + r\theta/2$  from the base: this distance is denoted  $\ell$  (see Fig. 11.1). The reason for placing the bends in the positions indicated in Fig. 3.5 is to prevent

overlap of primary and secondary reflections: this was discussed earlier in section 3.3.

The amplitude of most of the signals reflected from the bends are too small to be measured directly. The following example illustrates the difficulty. The test pulse amplitude is 120 mv and the peak amplitude of the signal reflected from a  $\theta = 60^\circ$ ,  $r = 3$  mm bend in a  $D = 0.32$  cm wire is 1.08 mv or -41.6 dB of the test pulse amplitude when received by the sampling oscilloscope. The VSWR of GR-874 air line (which was used for the experiment) is specified to be better than 1.025 up to 4 GHz. This means that the amplitude of reflections caused by line mismatch are equal to or smaller than -38 dB of the amplitude of the input signal. Thus the reflection from the bend is immersed in the ripples caused by reflections of the test pulse (and the first base reflection which arrives earlier than the bend reflection) from line irregularities. Even if GR-900 precision air line had been available the improvement would only have been about 20 dB.

The reflected signal from the bend can however be obtained indirectly. The reflections of the test pulse and the first base reflection from the line irregularities are the same whether the wire is bent or not. Hence the reflection from the bend can be obtained by subtracting the signal reflected from a long straight wire from the signal reflected from the bent wire. The disadvantage of this procedure is that it increases the effective noise level of the measurement (because the signal being subtracted is also contaminated by noise). However, the reflection cannot be

isolated satisfactorily unless the ripples are subtracted. The improvements obtained by subtracting the ripples are shown in the next two sections.

#### 11.2.1 Reflections From Sharp Bends

When a signal is incident upon a bend in a wire antenna it is partially reflected. Fig. 11.2 shows the reflected signals from straight and sharply bent ( $r \approx D$ ;  $r\theta \ll c\tau_1$ ) wires. The wires were 0.32 cm diameter brass rods which were threaded at the end and screwed directly into the mounting sections shown in Fig. 3.2. The radius of curvature  $r$  of the bend was 3 mm and the midpoint of the bend was 90.3 cm from the surface of the ground plane. The bends were made by clamping the wire in a vice and striking it with a hammer. The reflections from the bends for  $\theta < 80^\circ$  are seen to be smaller than the ripple amplitude as discussed in the previous section (some of the ripples were also attributed to reflections from the mounting sections, see Fig. 3.2). The improvement obtained by subtracting the ripples (i.e. the response shown in Fig. 11.2(a)) is shown in Fig. 11.3. The RMS noise level on the measured signals was 10  $\mu\text{V}$  so that the RMS noise level on the "ripple reduced" signals is 20  $\mu\text{V}$ . Notice that the residue of the base reflection is everywhere less than 250  $\mu\text{V}$  in magnitude. The slope of the leading edge of the pulse reflected from the base is 342 mv/ns: thus timing jitter is estimated to be about 0.75 ps.

The amplitude and durations (measured at the -6 dB points) of the pulses reflected from the wires are summarised in Table 11.3. The pulse durations show that the pulse



	Pulse amplitude (millivolts)	Pulse duration measured between -6 dB points (picoseconds)	Current pulse reflection coefficient
base of wire	50.5	$257 \pm 12$	-
Tip of straight wire	19.85	$306 \pm 12$	-
$\theta=20^\circ$ bend	-0.2	$208 \pm 12$	0.01
$\theta=40^\circ$ bend	-0.48	$208 \pm 12$	0.024
$\theta=60^\circ$ bend	-1.08	$208 \pm 12$	0.054
$\theta=80^\circ$ bend	-2.18	$208 \pm 12$	0.110
$\theta=90^\circ$ bend	-2.71	$208 \pm 12$	0.136

Table 11.3: Parameters of pulses reflected from straight and sharply ( $r = 3$  mm) bent 0.32 cm diameter wires.

reflected from the end of the straight wire is longer than the pulse reflected from the base. Thus dispersion at the base stretches the pulse, in agreement with Ross (1966c). A particularly interesting result is that the pulses reflected from the bends are narrower than both the base reflection and the tip reflection. Thus sharp bends exhibit pulse compression characteristics. Observe the small positive peaks (marked S) following the main negative reflection in Fig. 11.3(e) and 11.3(f). These are similar to the side-lobes exhibited by pulse compression radar signals (Cook and Bernfeld 1967, chapter 6).

The current pulse reflection coefficients included in Table 11.3 (which are obtained by dividing the peak amplitude of the reflection from the bend by the peak amplitude of the voltage pulse reflected from the tip of a straight wire and changing its sign) are in good agreement with those reported by Bates (1966). However, they are only valid for the particular input signal shown in Fig. 4.12 (see the discussion in section 5.4.2 and Bates, 1966).

#### 11.2.2 Reflections from Gradual Bends

Fig. 11.4 shows the reflected signals from gradually bent ( $r \gg D$ ,  $r\theta \approx c\tau_1$ ) wires after the ripples have been subtracted. The wire geometries are summarised in Table 11.4.

Figure number for measurement	Radius of curvature $r$	Bend angle $\theta$	Distance to bend $L_1$ (see Fig 11.1)	Arc length $r\theta$
11.4 (a)	15.0 cm	$20^\circ$	78.5 cm	5.1 cm
11.4 (b)	15.0 cm	$40^\circ$	77.0 cm	10.25 cm
11.4 (c)	15.0 cm	$60^\circ$	73.5 cm	15.4 cm
11.4 (d)	15.0 cm	$80^\circ$	71.5 cm	20.5 cm
11.4 (e)	13.5 cm	$120^\circ$	18.9 cm	28.3 cm
11.4 (f)	20.2 cm	$120^\circ$	16.0 cm	42.4 cm

Table 11.4: Geometries of wires for reflection measurements shown in Fig. 11.4.

The signals from the  $\theta = 120^\circ$  bends were scanned and averaged until the RMS noise was reduced to  $1.5 \mu\text{V}$  (requiring 120 scans taking one hour with the improved 3-point scanning program described in section A2.7): thus the RMS noise on

the "ripple reduced" signals is about  $3 \mu\text{V}$ . Notice that a small amount of ripple remains on the signals: this is probably caused by minute expansion and contraction of the delay lines due to temperature changes. Notice also that the residue of the base reflection still indicates that timing jitter is about  $0.75 \text{ ps}$  (see section 11.2.1). However, the quantising error in the voltage scanning the sampling oscilloscope was found to be  $0.3 \text{ ps}$ , so it is unlikely that this error could have been reduced.

The arrival times of signals corresponding to the points P and Q (see Fig. 11.1) are marked  $t_P$  and  $t_Q$  in Fig. 11.4 (the times were calculated by taking the velocity of propagation along the wire to be the free space velocity). The measurements show that the pulse is continuously reflected as it travels around the bend. The duration of the reflection exceeds  $(t_Q - t_P)$  only by the pulse duration, and for the large bend angles the reflection is a good approximation to the impulse response (since  $r\theta > c\tau_1$ ). The shape of the impulse response is approximately an asymmetrical triangle, although Figs 11.4(d) and 11.4(e) suggest that the leading edge is slightly curved (this curvature was not caused by a non-circular bend:  $r$  was everywhere within  $\pm 0.5 \text{ mm}$ ). The negative swing following the bend reflection in Fig. 11.4(e) is caused by radiation from the wire tip (see the next section).

No significant reflections are observed at times corresponding to the rate of change of curvature of the bend (i.e. at  $t_P$  or  $t_Q$ ) as predicted by Bates (1966). However, it is

difficult to manufacture a bend (other than a sharp bend) with a very large rate of change of curvature, so that these reflections, if they exist, will be unlikely to be observed in practice.

### 11.2.3 Transmission Along Bent Wires

Figs 11.5, 11.6 and 11.7 show the reflections from the tips of straight and bent 0.64 cm diameter wires after the ripples have been subtracted. The reflections from the bends discussed in the previous section are indicated. The time  $t_s$  which is marked on all the plots marks the beginning time of the reflection from the tip of the straight wire. Notice that as the bend angle increases the leading edge of the pulse advances in time. This indicates that energy is coupled across the bend. Table 11.5 shows the distances  $L_1$  and OZ (see Fig. 11.1) for the measured wires.

Wire length $L=L_1+r\theta+L_2$ (see Fig. 11.1)	Bend angle $\theta$	20°	40°	60°	80°
75.7 cm	Distance to bend $L_1$ (see Fig. 11.1)	48.5 cm	46.0 cm	43.5 cm	38.5 cm
	Distance OZ (see Fig. 11.1)	74.8 cm	72.1 cm	68.25 cm	62.4 cm
90.92 cm	$L_1$	58 cm	56 cm	52.4 cm	51.5 cm
	OZ	89.9 cm	86.6 cm	81.6 cm	75.4 cm
121.3 cm	$L_1$	78.5 cm	77.0 cm	73.5 cm	71.5 cm
	OZ	119.9 cm	115.4 cm	108.2 cm	99.1 cm

Table 11.5: Geometries of bent wires for measurements shown in Figs 11.5-11.7.

The times corresponding to return propagation directly across OZ are marked  $t_{OZ}$  on the plots. Also marked on the plots is the arrival time of the earliest detectable signal: this is denoted  $t_a$ . Notice that  $t_a$  is about halfway between  $t_{OZ}$  and  $t_s$ . This indicates that significant energy is only coupled across OZ in one direction: propagation is essentially along the wire in the other direction (the energy received at the base at  $t_{OZ}$  is smaller than -50 dB of the peak amplitude of the pulse reflected from the tip). The radiation which occurs when a current pulse travelling at (or near) the velocity of light is incident upon a discontinuity in a wire antenna is directed essentially in the direction of propagation of the pulse (Jones 1964, p147). This effect has actually been measured by Ross et al. (1966a, section 3) for sharp bends in wire antennas. It follows that significant coupling occurs across OZ only when the pulse propagates outward from the driving point: return propagation is essentially along the wire<sup>2</sup>.

The field radiated from the base is essentially a replica of the input pulse (section 9.2, Harrison and King 1967). Fig. 11.8 shows the direction of the current pulse induced on the bent section of the wire  $\tau$  seconds after a positive current pulse (corresponding to the positive input voltage pulse used for the measurements reported in this chapter) flows onto the base of the antenna. Thus the induced current adds to the current propagating along the wire. The induced current flows both towards the wire tip

---

<sup>2</sup>If the bend angle becomes large then a sensible amount of the tip radiation (which is negative for a positive input pulse, see section 9.2) is received at the base (see Fig. 11.4(e)).

and back towards the driving point: that which flows towards the driving point is too small to be detected in the measurements reported here. The induced current flowing towards the wire tip grows in amplitude because it is continually being reinforced by the impulsive field radiated from the base whose component of velocity in the direction of the wire is near the velocity of propagation of current along the wire (provided the bend angle is not too great). As a current pulse travels around a bend it is attenuated (due to radiation loss, Ross et al. 1966b, section III) and distorted (because the radiation loss is frequency sensitive, as shown later in section 11.4). Fig. 11.9 shows an example of the signals obtained by subtracting various proportions of the tip reflection of a straight wire from the tip reflection of a bent wire. At times earlier than  $t_s$  (see Fig. 11.9) the signals represent the current induced by radiation from the base. After  $t_s$  the signals are a function of both the current induced by radiation from the base and of the distortion of the current pulse travelling around the bend. The induced current is seen to be quite strong: its peak amplitude is nearly 30% of the peak amplitude of the tip reflection. Notice that the tail of the signal is smallest when 80% of the straight wire response is subtracted: this gives a pulse attenuation coefficient of  $\sqrt{0.8} \approx 0.9$ , in agreement with Ross et al. (1966b, section III).

### 11.3 TRANSMISSION AND REFLECTION COEFFICIENTS FOR BENT WIRE ANTENNAS

In section 2.5 it was shown how a transmission coefficient  $\beta(f)$  and a current reflection coefficient  $\Gamma(f)$  describing the transmission and reflection of current on a bent wire antenna can be inferred from a measurement of the reflection of a narrow test pulse from the bend and the tip of a bent wire and a measurement of the reflection of the same test pulse from the tip of a straight wire. These coefficients can be used to relate the amplitude, of a current wave at the base of a bent wire antenna and travelling outwards on the antenna, to the amplitude of the current wave arriving back at the base of the antenna. Thus, if  $I_O(f)$  is the current at the base travelling outward along the wire and if  $I_A(f)$  is the current at the base travelling inward, then

$$I_A(f) = I_O(f) \left\{ \Gamma(f)e^{-j2k\ell} - [\beta(f)]^2 e^{-j2kL} \right\} \quad (11-1)$$

where  $\ell$  and  $L$  are defined in Fig. 11.1. The minus sign before the second term inside the braces accounts for the change in direction of the current when it is reflected from the wire tip. The coefficients are discussed further in section 11.4.

#### 11.3.1 Computing the Frequency Responses

##### 11.3.1.1 Transmission coefficients

The transmission coefficients  $\beta(f)$  were computed using eqn(2-29). The reflections of the test pulse from the tips of the wires were separated from the rest of the measured signal by applying an extended cosine bell data window (see

section 2.3.3.1.2):

$$d(t) = 0 \quad , \quad t \leq t_1, t \geq t_4;$$

$$d(t) = \frac{1}{2}\{1 + \cos[\pi(t_2 - t)/(t_2 - t_1)]\}, \quad t_1 < t < t_2;$$

$$d(t) = 1 \quad , \quad t_2 \leq t \leq t_3;$$

$$d(t) = \frac{1}{2}\{1 + \cos[\pi(t - t_3)/(t_4 - t_3)]\}, \quad t_3 < t < t_4.$$

(11-2)

The data window parameters,  $t_1$ - $t_4$ , were chosen to cut off as little as possible of the reflection. This is particularly important on the leading edge:  $t_2$  was always chosen to be less than  $t_a$  (see Figs 11.5-11.7). The data window parameters used to compute the frequency responses presented in section 11.3.2 are given in Table 11.6.

Number of figure in which result of measurement is recorded	Data window parameters (ns)			
	$t_1$	$t_2$	$t_3$	$t_4$
11.12-11.20, 11.26	5.75	6.0	8.0	9.0
11.21	5.0	5.25	8.0	8.5
11.22	6.0	6.25	9.0	9.4
11.23	8.5	8.75	11.75	12.25
11.24	6.75	7.0	7.75	8.0
11.25	6.75	7.0	8.5	8.75

Table 11.6: Data window parameters used for computing frequency responses presented in this chapter.

The relative position of a typical data window and a measured response (from measurements A) is shown in Fig. 11.10. The



effect of changing the data window parameters on the computed results is shown later in section 11.3.3.

The measurements A (see section 11.2) were made with the program described in Appendix 2. When computing  $\beta(f)$  discrepancies in the phase were noticed. These were found to be linear phase shifts caused by timing errors (section 2.3.3.1.3) introduced by drift in the reference voltage identifying the start of sampling time (see Appendix 2). The measurements were made with a sampling oscilloscope time scale of 2 ns/cm and the external horizontal deflection factor of the 1S2 sampling unit was about 1 volt/cm. Thus only a 5 mv drift causes a timing error of 10 ps corresponding to a phase error of about  $7^\circ$  at 2 GHz. This problem was eliminated in the improved program described in section A2.7, and which was used for the subsequent measurements (measurements B). The amount of timing shift in measurements A could be determined by comparing the relative time positions of the reflections of the test pulse from the bases of the straight wire and the bent wire (which were the same). This was done by time shifting one of the reflections in one picosecond steps and searching for the smallest mean square difference between the two reflections. The time shift corresponding to the smallest difference was then used to correct the phase of the computed transfer functions. The time response was shifted in one picosecond steps by interpolating the measured samples using Everett's formula to second order (N.P.L. 1961, p66). The phase errors due to timing shift are less than  $0.7^\circ$  at 2 GHz.

### 11.3.1.2 Reflection coefficients

The current reflection coefficients  $\Gamma(f)$  were calculated using eqn(2-30). The reflection coefficient of the tip  $S_{c_{11}}(f)$  (see eqn 2-28) was taken to be unity. This assumption introduces only a small error (see section 2.5). The phase of all the computed  $\Gamma(f)$  is referred to the bend centre.

To eliminate timing shift errors (section 2.3.3.1.3) from the computed  $\Gamma(f)$  for the  $r = 3$  mm bends the distance from the base of the wire to the centre of the bend ( $\ell$  in Fig. 11.1) was made the same as the length of the straight wire: the position was accurate to  $\pm 1$  mm. Thus phase errors in the computed  $\Gamma(f)$  due to timing shift are less than  $2.5^\circ$  at 2 GHz. The phase of the computed  $\Gamma(f)$  for the  $r = 15$  cm bends was referred to the bend centre by applying a correction factor for each bend. These were determined by measurement and were accurate to  $\pm 5$  mm. Thus phase errors due to timing shift are better than  $12.5^\circ$  at 2 GHz.

The reflections from the bend and from the tip of the straight wire were separated from the rest of the measured signal by applying eqn(11-2). The data window parameters used to compute the  $\Gamma(f)$  are included in Table 11.6.

### 11.3.2 Computed Responses

The moduli of the spectra of the pulses reflected from the tips of the straight wires  $|V_S(f)|$  (see eqns 2-27 and 2-28) which were used to compute the results presented in this section are shown in Fig. 11.11. The effective bandwidths of the pulses (from measurements A) whose spectra are shown in Figs 11.11(a) and 11.11(b) are about 2 GHz: hence

the frequency responses computed using these spectra are only continued out to 2 GHz. The effective bandwidths of the pulses whose spectra are shown in Fig. 11.11(c) and 11.11(d) are about 3 GHz. The reason for the difference is that a newer and improved Tektronix 1S2 TDR was used for these measurements (measurements B) and the faster pulse extended the measurement bandwidth. Also, the signals from this later series of measurements were "ripple reduced" in the way described in section 11.2 before the frequency responses were computed. This eliminated error due to the ripples (section 2.3.3.3) although the RMS noise level was increased to 20  $\mu$ V. Notice that the spectra of the pulses applied to the 0.32 cm dia. wires is different from the spectra of the pulses applied to the 0.64 cm dia. wires, in agreement with the argument presented in section 11.1.

Computed transmission coefficients  $\beta(f)$  and current reflection coefficients  $\Gamma(f)$  for different wire geometries are plotted in Figs 11.12-11.26.

### 11.3.3 Discussion of errors

It was demonstrated in section 6.3.4 that quantisation error is negligible because of the accurate ADC used in the hybrid computer (see Appendix 2). However, a specimen calculation of the error in a test pulse spectrum due to noise in the sampled signal indicated that it was small but probably significant. Following section 6.3.4, with  $T = 25$  ps,  $N = 130$  (see Table 11.6) and taking  $\sigma_N = 200$   $\mu$ V for measurements A (see section 11.2) we obtain the noise amplitude exceeded by not more than 1% of the frequency domain ordinates  $\varepsilon_{1,N} = 1.6 \times 10^{-13}$  V/Hz for the  $|V_S(f)|$

shown in Figs 11.11(a) and 11.11(b). This is about 1.9% of  $|V_S(f)|$  at zero frequency and 16% of  $|V_S(f)|$  at 2 GHz. A similar calculation for measurements B (with  $\sigma_N = 20 \mu\text{V}$ , see section 11.3.2) gives  $\epsilon_{1,N} = 1.6 \times 10^{-14}$  V/Hz for the  $|V_S(f)|$  shown in Figs 11.11(c) and 11.11(d). This is about 0.18% of  $|V_S(f)|$  at zero frequency and 2.3% of  $|V_S(f)|$  at 3 GHz. It is also possible to estimate the timing jitter error for measurements B. In section 11.2.1 the timing jitter was estimated to be 0.75 ps. Using this as an estimate of  $\sigma_T$  in eqn(2-15), the noise amplitude exceeded by not more than 1% of the frequency domain ordinates ( $\xi = 0.01$ ) is  $\epsilon_{1,T} \approx 10^{-15}$  V/Hz. This is only 0.14% of  $|V_S(f)|$  at 3 GHz: hence timing jitter error in the frequency responses computed using data from measurements B can be assumed negligible. The integration in eqn(2-15) was done graphically.

Only 1% of the frequency domain ordinates are likely to exceed the bounds calculated in the previous paragraph, and, because the frequency responses were computed from a measurement interval  $NT$  of about 3 ns, there are only about 7 ordinates (spaced at frequency intervals of  $1/NT$ ; see eqn 2-10) in the range  $0 \leq f \leq 2\text{GHz}$ . The continuous curves are obtained by joining interpolated frequency ordinates (see section 2.3.4). Thus the error bounds are quite pessimistic. A more meaningful estimate would be the 9% error bound ( $\xi = 0.09$  in eqn 2-14): this gives  $\epsilon_{9,N} = 1.13 \times 10^{-13}$  V/Hz for  $|V_S(f)|$  in Figs 11.11(a) and 11.11(b) (measurements A). The probability that the error in a particular ordinate is less than  $1.13 \times 10^{-13}$  V/Hz is 0.91, and the probability that the error in all ordinates is less than

$1.13 \times 10^{-13}$  V/Hz is  $(0.91)^7 \approx 0.52$ . Thus it is improbable that the error anywhere will exceed  $1.13 \times 10^{-13}$  V/Hz. The probability of the error in  $|V_S(f)|$  (Figs 11.11(a) and 11.11(b)) being less than 11% at 2 GHz is 0.91. A similar estimate for measurements B ( $|V_S(f)|$  in Figs 11.11(c) and 11.11(d)) is  $\epsilon_{9,N} = 1.13 \times 10^{-14}$  V/Hz, or 1.5% at 3 GHz.

A gauge of the error in the computed frequency response is best obtained from an example. From Fig. 11.12,  $\beta(f) = 0.74$  at 2 GHz, and from Fig. 11.11(a)  $|V_S(f)| = 0.9 \times 10^{-12}$  V/Hz at 2 GHz. Thus from eqns (2-27) and (2-29)  $|V_C(f)| = 0.495 \times 10^{-12}$  V/Hz. If both  $|V_S(f)|$  and  $|V_C(f)|$  are 10% in error, and the errors are such that the error in  $\beta(f)$  is maximum (i.e.  $|V_S(f)| + 10\%$  and  $|V_C(f)| - 10\%$  and vice versa) then the error in  $\beta(f)$  is +10.8% and -9.5%. Thus the error in  $\beta(f)$  is at worst about equal to the error in  $|V_S(f)|$  and  $|V_C(f)|$ . It is highly improbable that the worst case conditions in this example will occur. The error in the  $\beta(f)$  computed from measurements A is likely to be better than 5% at 2 GHz. This is supported by the observed behaviour of  $\beta(f)$  for  $\theta = 20^\circ$  in Figs 11.12-11.15 and Figs 11.18-11.20. In only one case of the seven (Fig. 11.12) is  $\beta(f)$  more than 5% different at 2 GHz from the  $\beta(f)$  for  $\theta = 20^\circ$  shown in Fig. 11.22 (which was computed from measurements B and from the arguments presented in this section its error due to noise can be assumed less than 1%).

The noise error in the computed  $P(f)$  (see Figs 11.24 and 11.25) can be assumed to be caused entirely by noise error in  $V_B(f)$  (see eqns 2-28 and 2-30), because  $V_B(f) \ll V_S(f)$ . Using eqn(2-14) with  $T = 25$  ps,  $N = 60$  (an

average for Figs 11.24 and 11.25, see Table 11.6) and  $\sigma_N = 20 \mu\text{V}$  we obtain (with  $\xi = 0.01$ )  $\varepsilon_{1,N} \approx 10^{-14} \text{ V.Hz.}$  This corresponds to an error of  $\pm 0.01$  in the computed  $\Gamma(f)$  at all frequencies. The probability that the noise error will be within  $\pm 0.01$  anywhere is  $0.99^7 \approx 0.93$ . Timing jitter error is within  $\pm 0.001$  (see the first paragraph of this section). In Fig. 11.24 the phase of  $\Gamma(f)$  for  $\theta = 20^\circ$  behaves differently to the phase for  $\theta > 20^\circ$ : this is attributed to experimental error. The same is observed for  $\theta = 40^\circ$  in Fig. 11.25 (results for  $\theta = 20^\circ$  are not plotted here because the computations of both modulus and phase had badly deteriorated due to experimental error). Thus the phase appears to be more sensitive to experiment noise than the modulus.

Fig. 11.27 shows the effect of changing the data window on the computed  $\beta(f)$ . As the data window parameters are altered to cut off more of the signal then ripples appear in the computed spectra. Fig. 11.27 indicates that truncation errors are within about 3%. Notice however, that a small amount of truncation causes large errors in the frequency locations of the peaks and nulls in the computed  $\beta(f)$ .

There is no simple way of gauging the error in the computed frequency responses for bends in wire antennas as there is for antenna reflection coefficients (see sections 2.3.5 and 6.3.4) and antenna far field transfer functions (see section 3.4.3). Hence analyses of the kind just outlined have to be used. Estimates of their credibility can then be made by examining the repeatability of a measurement. Measurements of a known slope (e.g. the reference slope used

for the 3-point scan) should always be made since estimates of the timing jitter can then be obtained from the residue after subtracting the signals, as was done in section 11.2.1.

#### 11.4 DISCUSSION OF THE RESPONSES AND SUGGESTIONS FOR FURTHER WORK

Fig. 11.24 shows that both the modulus and the phase of the current reflection coefficients for sharp bends (i.e. bends whose arc length is very much smaller than a wavelength) of a given bend angle  $\theta$  increase with increasing frequency (notice that the phase characteristic is not linear with frequency and hence it does not correspond simply to a constant time delay)<sup>3</sup>. This causes compression of the reflected pulse, as observed in section 11.2.1. The shape of the phase characteristics indicate that the phase centre of the reflection is near the beginning of the bend (the point P in Fig. 11.1) but at 2 GHz a phase advance of only about  $6^\circ$  would correspond to reflection from P. In section 11.3.1.2 the phase error due to timing shift was stated to be less than  $2.5^\circ$  at 2 GHz. The phase of  $\Gamma(f)$  is observed to be about  $22^\circ$  at 2 GHz in Fig. 11.24. This suggests that the reflection coefficient of the tip of the wire  $S_{c_{11}}(f)$  (see eqn 2-28) is not real as assumed in the computations.  $S_{c_{11}}(f)$  could be obtained simply by applying TFT procedures to Ross' (1969a) experiment. This was not done because two ground planes were required (one suspended above the other), and the cost of another plane could not be justified for

---

<sup>3</sup>The small ripples on the responses are due to truncation error.

only one measurement. From Fig. 11.24, the magnitude of the current reflection coefficient at any frequency is approximately proportional to  $\theta^{2.3}$  ( $0 \leq \theta \leq 90^\circ$ ).

The current reflection coefficients for the gradual bends (i.e. bends whose arc length is comparable to a wavelength) shown in Fig. 11.25 decrease with increasing frequency (which is logical since we expect the electrical characteristics of an antenna to depend on its size in wavelengths). The phase characteristics indicate that the phase centre of the reflection is near P (see Fig. 11.1) at low frequencies (i.e. when the bend is sharp in terms of wavelength), in agreement with Fig. 11.24. As the frequency increases the phase centre of the reflection shifts towards the point Q.

The phase angles of all the computed  $\beta(f)$  are positive. This means that energy is coupled across the bend, in agreement with the observations made in section 11.2.3. Consider the wire whose  $\beta(f)$  is shown in Fig. 11.23. The difference (denoted  $\Delta$ ) between the direct path OZ (see Fig. 11.1) and the path OPQZ following the wire axis is (from Table 11.5) 22.2 cm for a  $\theta = 80^\circ$  bend. This corresponds to a wavelength at a frequency of 1.35 GHz and a half-wavelength at 0.675 GHz. In section 11.2.3 the induced current was shown to be in phase with the current travelling along the wire. Notice that the first minimum and maximum in  $|\beta(f)|$  occur approximately at (although slightly higher than) the frequencies at which  $\Delta$  is a half-wavelength and a wavelength respectively. The slightly higher frequencies mean that the phase centre for reception corresponds to some point between P and Z indicating that the base radiation is received by the whole



length PQZ (see Fig. 11.1), also in agreement with the observations made in section 11.2.3. An exact phase centre cannot be obtained because the positions of the maxima and minima were shown in the previous section to be sensitive functions of truncation error. All  $\beta(f)$  are greater than unity at zero frequency because the average value of the signal reflected from the tip of the bent wire is higher (due to the interception of base radiation) than the average value of the signal reflected from the tip of a straight wire. Successive maxima and minima decrease in amplitude as the frequency increases. This shows that attenuation which increases with increasing frequency occurs as current travels around the bend. Comparison of Figs 11.13 and 11.14, and Figs 11.16 and 11.17 shows that there is no significant change in  $\beta(f)$  when the wire is fed from the opposite end. Comparison of the  $\beta(f)$  for  $\theta = 60^\circ$  and  $\theta = 80^\circ$  in Figs 11.15 and 11.20 show that there is significantly more attenuation of signals propagating around bends in thick wires than in thin wires: this is consistent with the known behaviour of current on straight wires (Andersen, 1968). Fig. 11.26 shows that  $\beta(f)$  for a strip antenna which is bent in the plane of the strip is greater than  $\beta(f)$  for a strip antenna which is bent at  $90^\circ$  to the plane of the strip. This is partly due to different amounts of coupling from the base to the bent section (because the antenna is not cylindrically symmetric the base radiation is not omnidirectional in azimuth).

In this chapter it has been demonstrated how the TFT technique can be used to study the propagation of current

on bent wire antennas. Careful inspection of the time domain pulse responses were necessary to correctly interpret the frequency responses: this shows the value of having simultaneous displays of pulse response and frequency response. The measurements and computed results presented in this chapter show that the simple model postulated in section 2.5 does not give an adequate representation of the behaviour of the current on a bent wire antenna, and they suggest the following physical explanation of the current propagation. Let the antenna be excited by a step modulated monochromatic wave: the current wave travelling to the antenna is denoted  $I_B(f)$ .  $I_B(f)$  is incident upon the base (point O, see Fig. 11.1) where it is partly reflected, partly transmitted onto the antenna and partly radiated. The current wave  $I_O(f)$  which is transmitted onto the antenna (see eqn 11-1) is related to  $I_B(f)$  by the forward current scattering coefficient of the base region (call it  $S_{A_{12}}(f)$  following section 2.5, but remembering that here it relates currents and not voltages).  $S_{A_{12}}(f)$  incorporates the radiation loss. The current wave travels along OP being slightly dispersed and attenuated (unless the wire is infinitely thin, sections 5.2, 11.1). As the current wave travels around the bend PQ it is continuously reflected and attenuated (and probably dispersed). The attenuation (due to radiation) is greater than for the straight sections. The base radiation induces current all along PQZ and this adds vectorially to the current travelling along the wire. When the composite current wave arrives at the tip Z it is partly reflected and partly radiated: the radiation is

directed mainly in the direction of the current before reflection (i.e. off the end of the wire) so that, unless the bend angle is great (see section 11.2.3), little of the tip radiation is received by the wire. The radiation loss is incorporated in the tip reflection coefficient  $S_{c_{11}}(f)$ . The current wave travels back down the wire experiencing the same attenuation, dispersion and reflection as it did on outward propagation (except that no sensible tip radiation is received). The current arriving at the base is  $I_A(f)$ , and the computed coefficients presented in section 11.3.2 can be used to relate  $I_A(f)$  to the outward travelling wave  $I_O(f)$  (see eqn 11-1). At the base the current is partly transmitted into the line (described by  $S_{A_{21}}(f)$ ), partly reflected back along the antenna (described by  $S_{A_{22}}(f)$ ) and partly radiated. The sequence repeats as the reflected current wave travels back up the antenna except that the current wave is of opposite sign (the current reflection coefficient of the open end of the wire is  $\approx -1$ ) and the radiation which occurs as  $I_A(f)$  is reflected from the base is of the same sign as that caused by  $I_B(f)$  incident upon the base (Schmitt et al., 1966). Thus the current induced on PQZ and the current travelling out along the wire for the second time are out of phase at frequencies where they were previously in phase. Thus the computed  $\beta(f)$  presented in section 11.3.2 only represent the first passage of current up and down the wire. A transmission coefficient representing the second (and subsequent) passages of current would have its maxima and minima transposed.

To be able to relate the currents on the antenna at the base to the currents in the feedline knowledge of  $S_{A_{21}}(f)$  and  $S_{A_{12}}(f)$  (which are equal, Montgomery et al. 1948, p148) is required. Also, knowledge of  $S_{A_{22}}(f)$  is required to relate the incident and reflected antenna currents at the base. These coefficients could be obtained simply by applying TFT procedures to Ross' (1969a) experiment. Also, if  $S_{A_{12}}(f)$  and  $S_{C_{11}}(f)$  are known precisely, then precise measurements of the first tip reflection from straight wires of different lengths might enable the attenuation, dispersion and propagation velocity of current on straight wires as functions of frequency and distance from the driving point to be computed.

The computed  $\beta(f)$  presented in this chapter represent both the attenuation of the bend and reception of energy radiated from the feedpoint. Thus  $\beta(f)$  is a function of the whole wire geometry and the feedpoint geometry, and does not describe the local effect of the bend. It would be desirable to separate these effects. Application of TFT procedures to the multiple reflections of narrow pulses on bent and straight wires seems a logical approach.

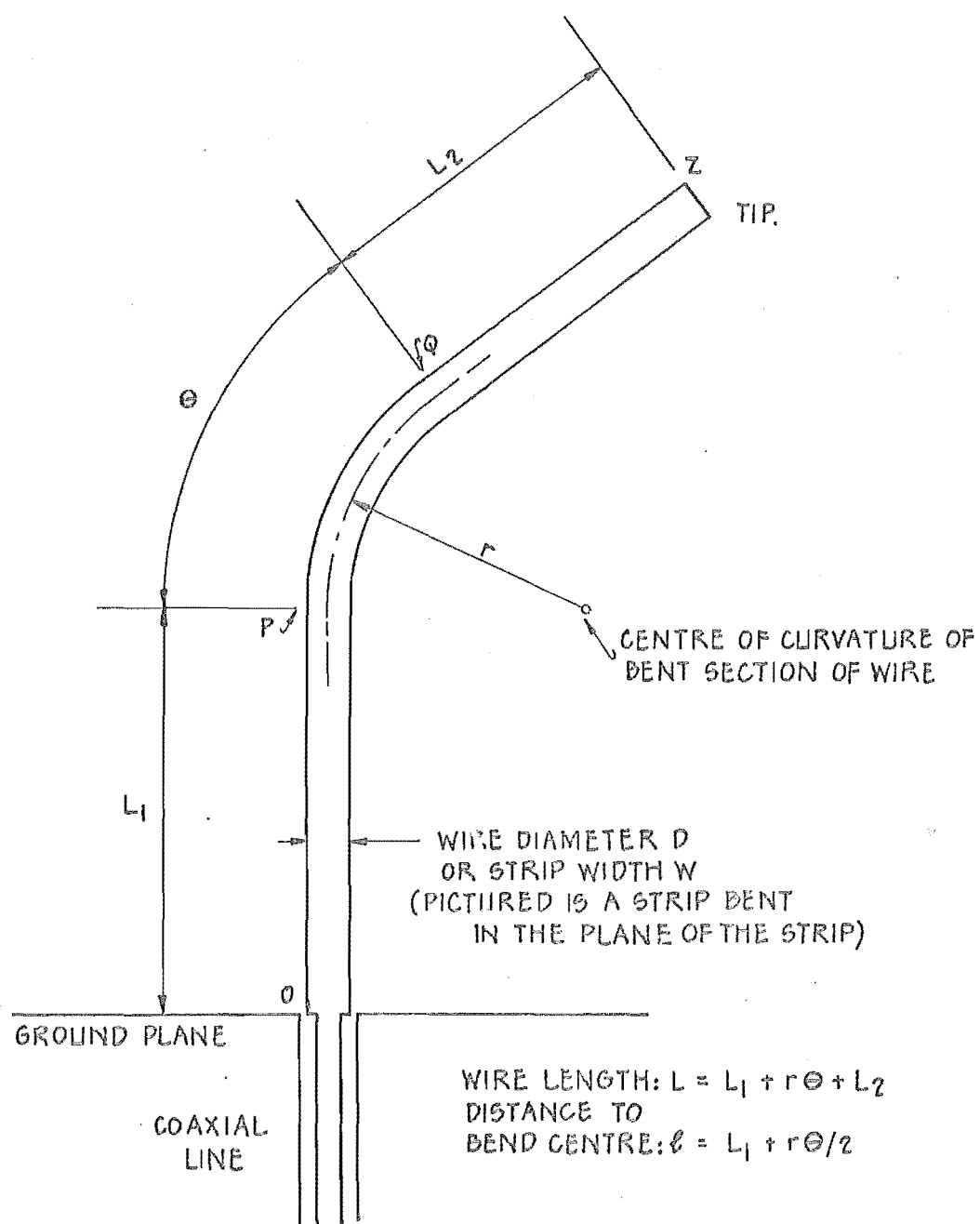


FIGURE II.1. GEOMETRY OF BENT ANTENNA ABOVE HORIZONTAL GROUND PLANE.

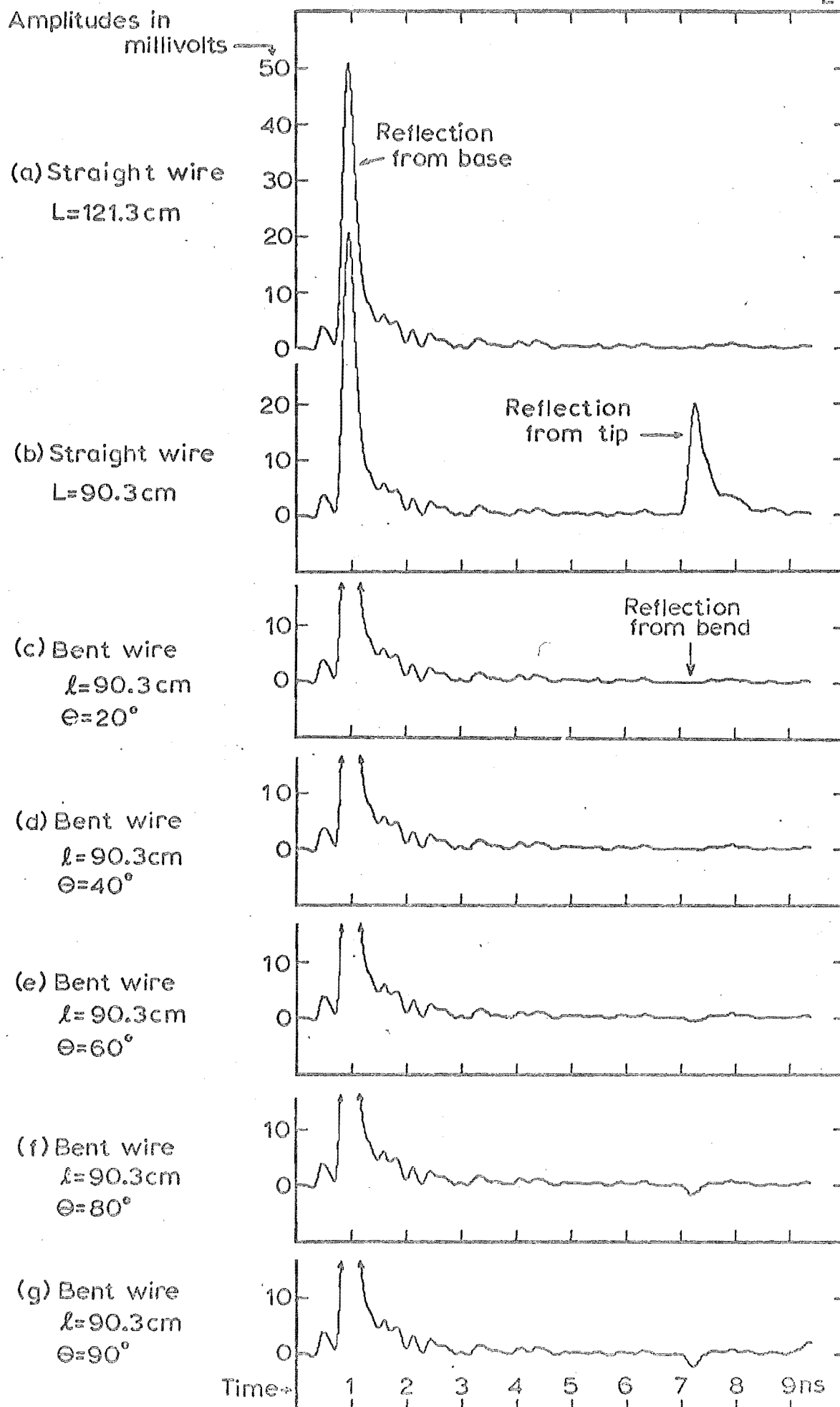


Figure 11.2: MEASURED DRIVING POINT RESPONSES OF STRAIGHT AND SHARPLY BENT( $r=3\text{ mm}$ )  $0.32\text{ cm}$  DIA. WIRES

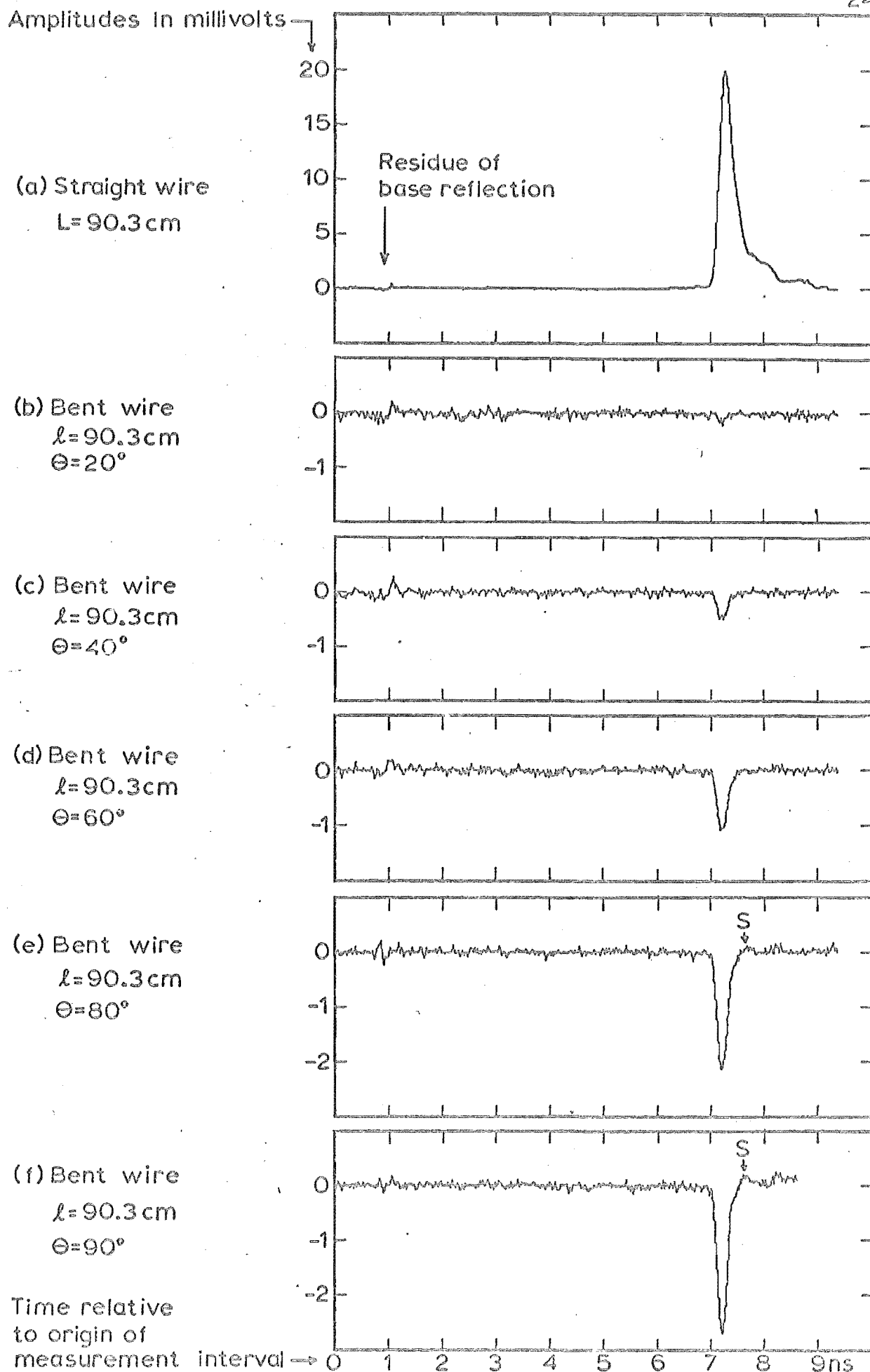


Figure 11.3: RESPONSES OF STRAIGHT AND SHARPLY BENT ( $r=3 \text{ mm}$ )  $0.32 \text{ cm}$  DIA. WIRES AFTER SUBTRACTING RIPPLES





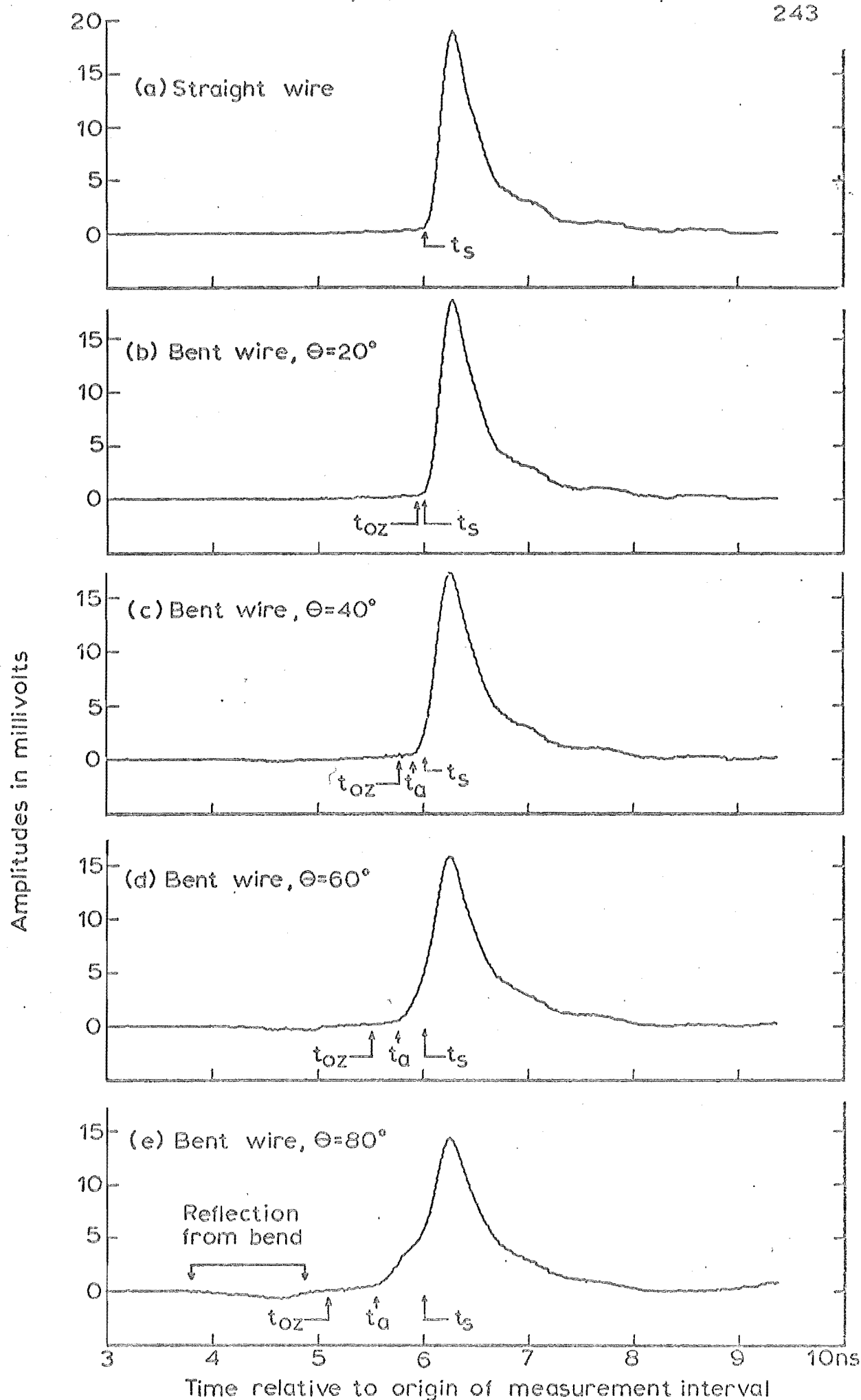


Figure 11.5: REFLECTIONS FROM TIPS OF STRAIGHT AND BENT ( $r=15\text{cm}$ ) 0.64 cm DIAMETER 75.7cm LONG WIRES

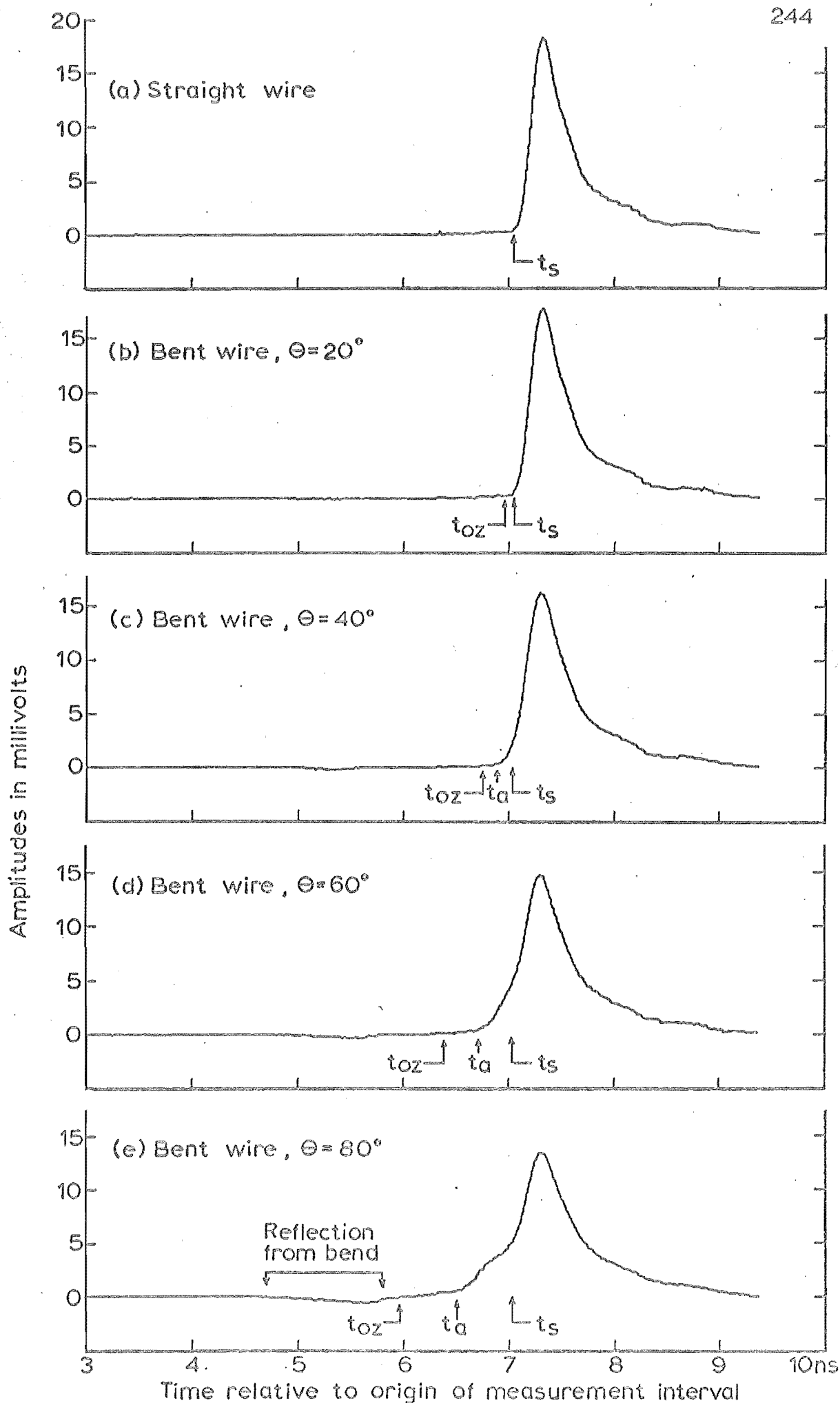


Figure 11.6: REFLECTIONS FROM TIPS OF STRAIGHT AND BENT ( $r=15\text{cm}$ ) 0.64cm DIAMETER 90.9cm LONG WIRES

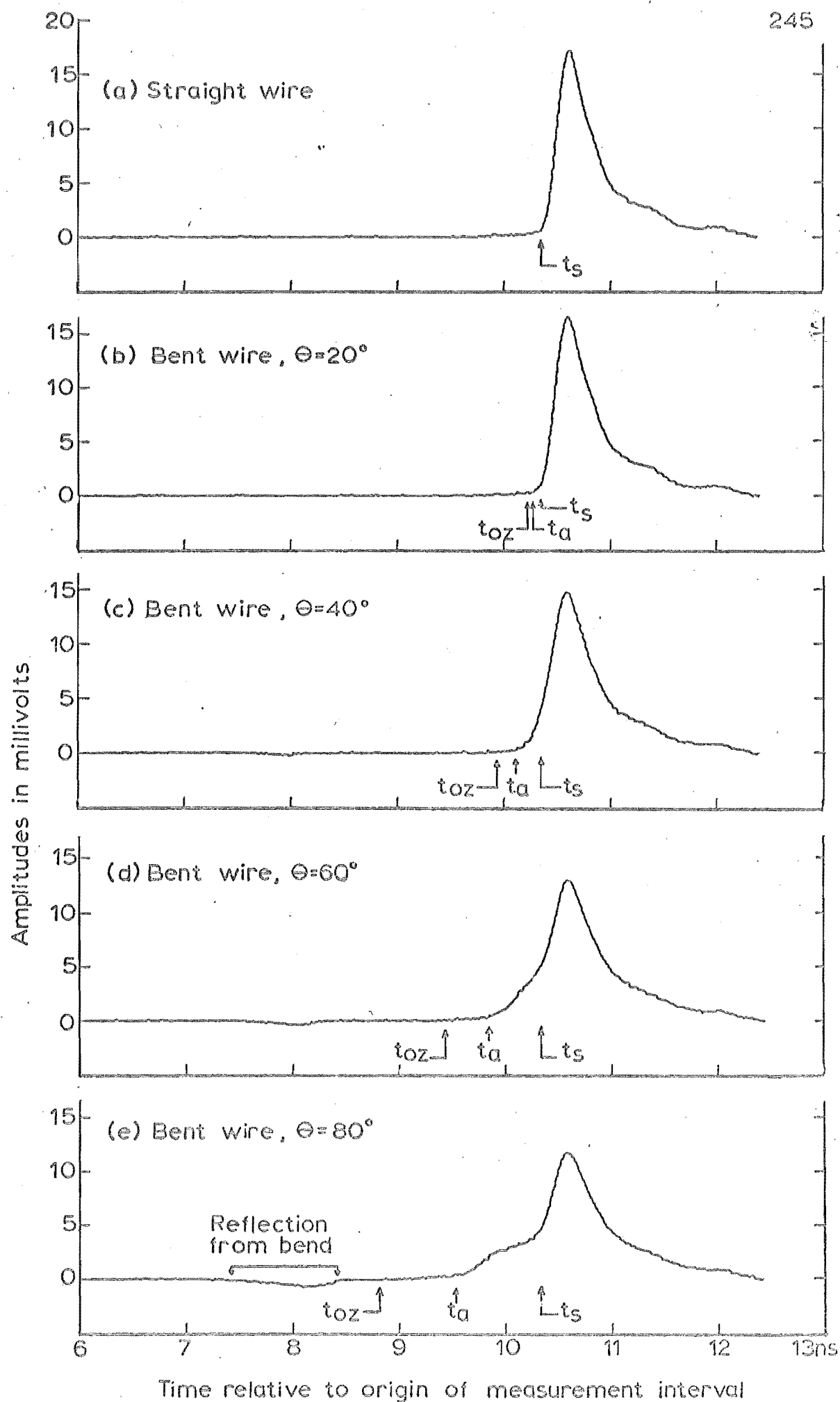


Figure 11.7 REFLECTIONS FROM TIPS OF STRAIGHT AND BENT ( $r=15\text{cm}$ ) 0.64cm DIAMETER 121.3cm LONG WIRES

$I_1(t)$  = CURRENT PULSE INDUCED ON BENT SECTION OF WIRE  
 $T$  SECONDS AFTER THE CURRENT PULSE  $I_0(t)$  FLOWS  
 ONTO THE BASE OF THE ANTENNA

246

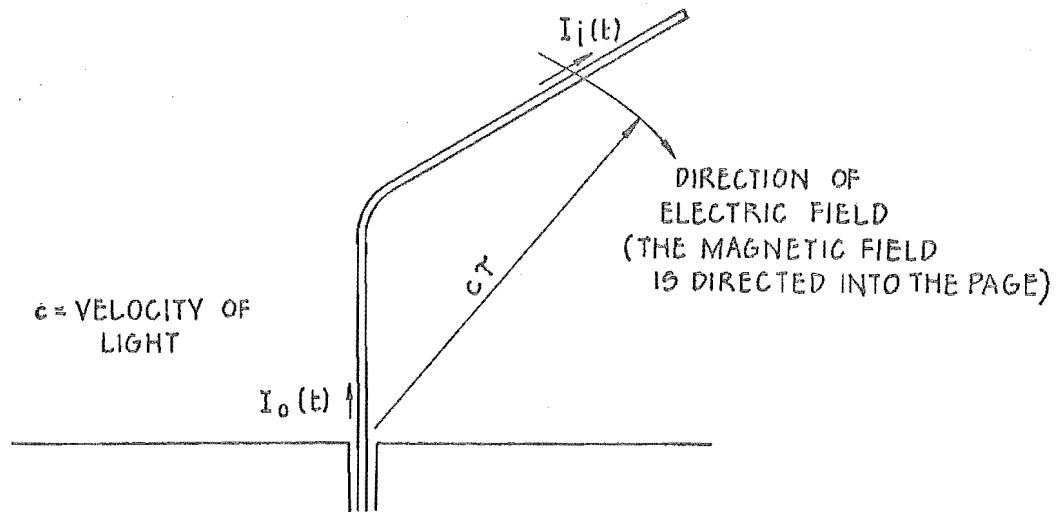


FIGURE 11.8: SHOWING THE DIRECTION OF THE CURRENT INDUCED ON BENT WIRE BY RADIATION FROM BASE.

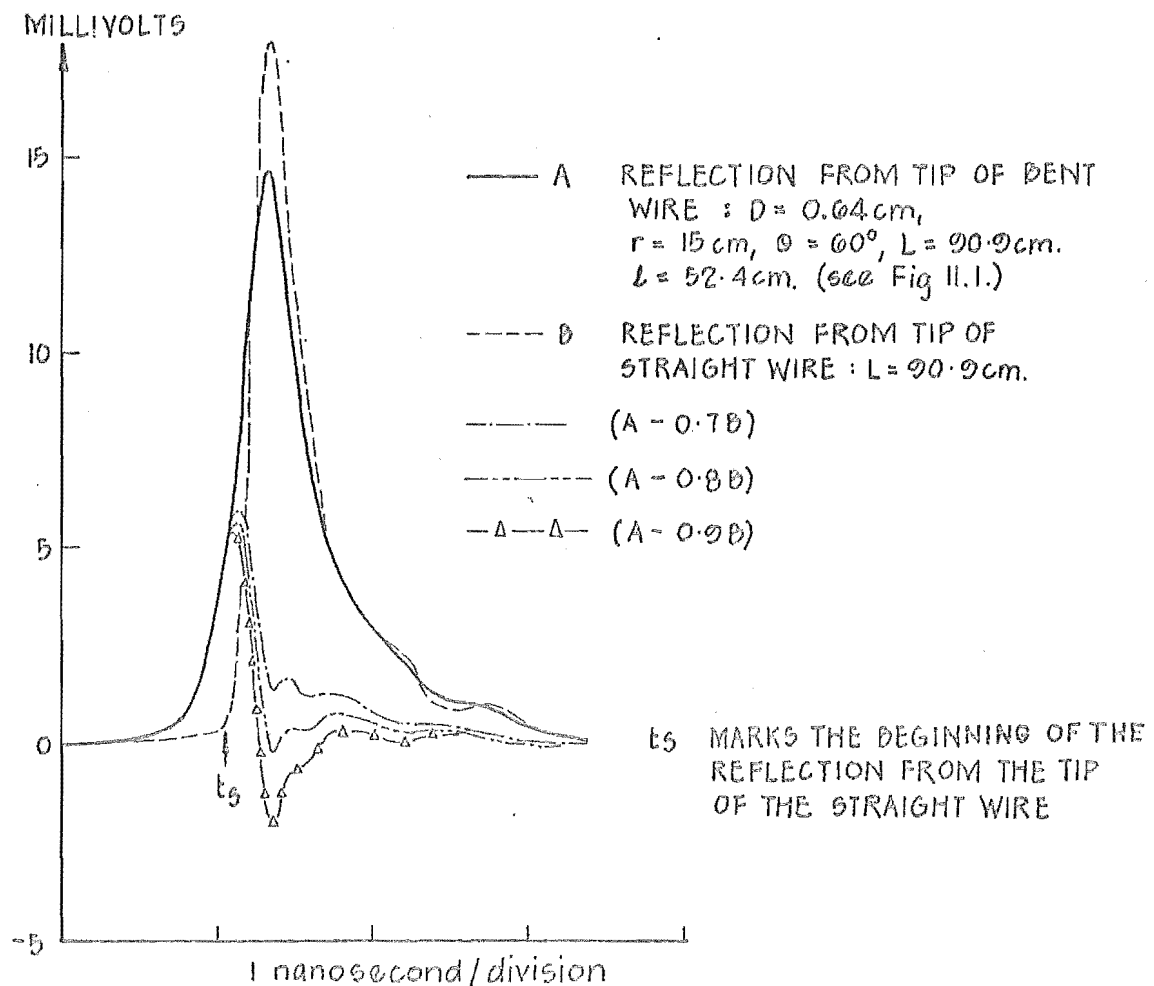


FIGURE 11.9 : EFFECT OF SUBTRACTING ATTENUATED TIP REFLECTION OF STRAIGHT WIRE FROM TIP REFLECTION OF BENT WIRE

DATA WINDOW :  $t_1 = 5.75 \text{ NS}$ ,  $t_2 = 6 \text{ NS}$ ,  $t_3 = 8 \text{ NS}$ ,  $t_4 = 9 \text{ NS}$ .

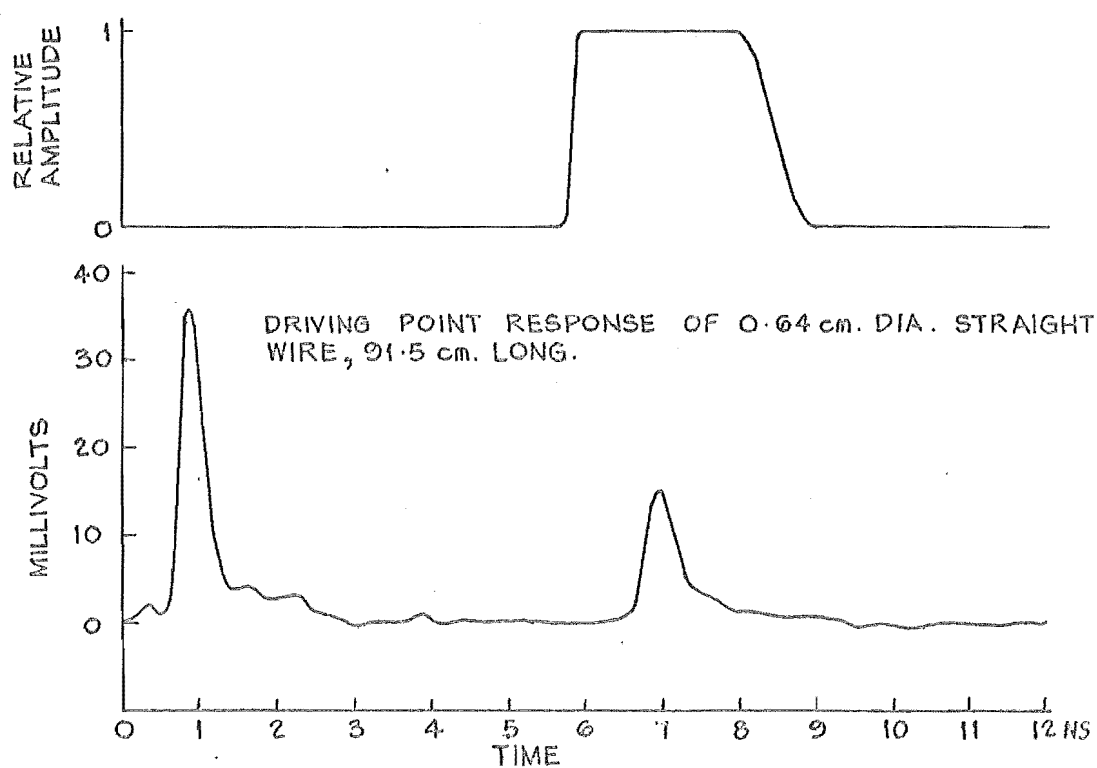
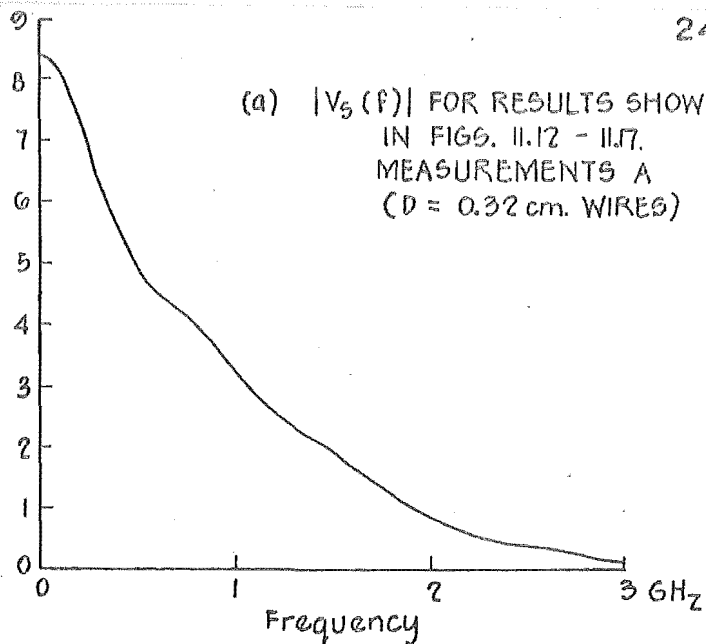


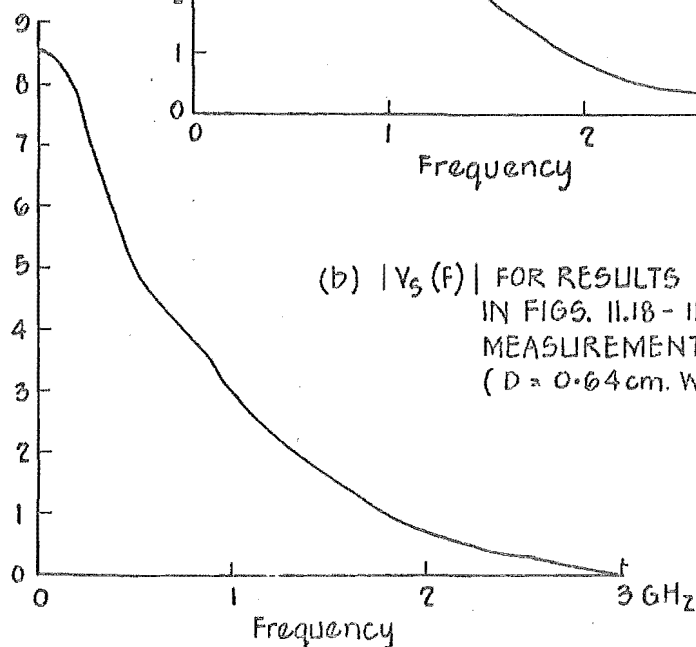
FIGURE 11-10: EXAMPLE OF DATA WINDOW USED TO SEPARATE TIP REFLECTIONS.

AMPLITUDE SCALES  
 $\times 10^{-12}$  VOLTS/Hz

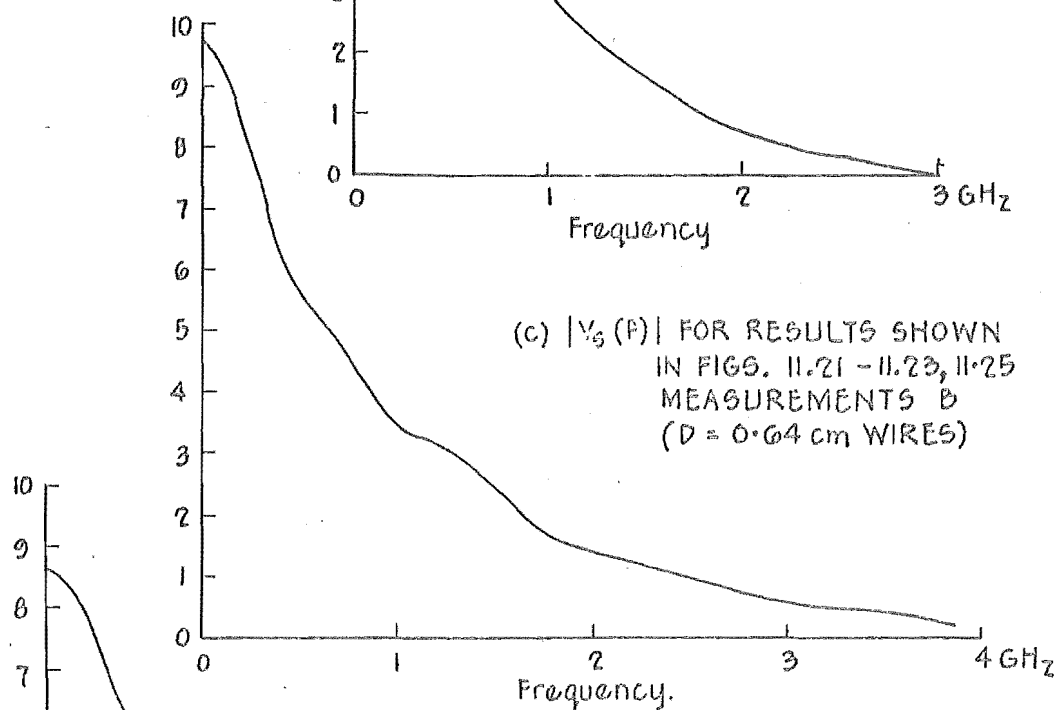
(a)  $|V_s(f)|$  FOR RESULTS SHOWN  
 IN FIGS. 11.12 - 11.17.  
 MEASUREMENTS A  
 ( $D = 0.32$  cm. WIRES)



(b)  $|V_s(f)|$  FOR RESULTS SHOWN  
 IN FIGS. 11.18 - 11.20  
 MEASUREMENTS A  
 ( $D = 0.64$  cm. WIRES)



(c)  $|V_s(f)|$  FOR RESULTS SHOWN  
 IN FIGS. 11.21 - 11.23, 11.25  
 MEASUREMENTS B  
 ( $D = 0.64$  cm WIRES)



(d)  $|V_s(f)|$  FOR RESULTS SHOWN  
 IN FIG. 11.24  
 MEASUREMENTS B  
 ( $D = 0.32$  cm WIRES)

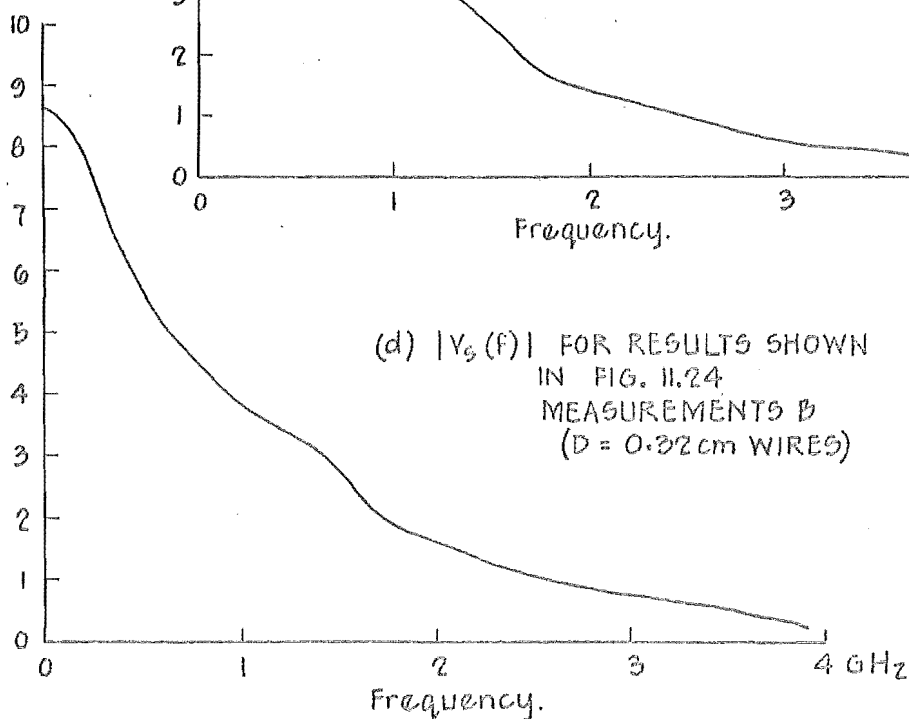


FIGURE 11.11:  $|V_s(f)|$  USED TO COMPUTE TRANSMISSION COEFFICIENTS  $\beta(f)$   
 AND CURRENT REFLECTION COEFFICIENTS  $\Gamma(f)$  FOR BENT WIRES.

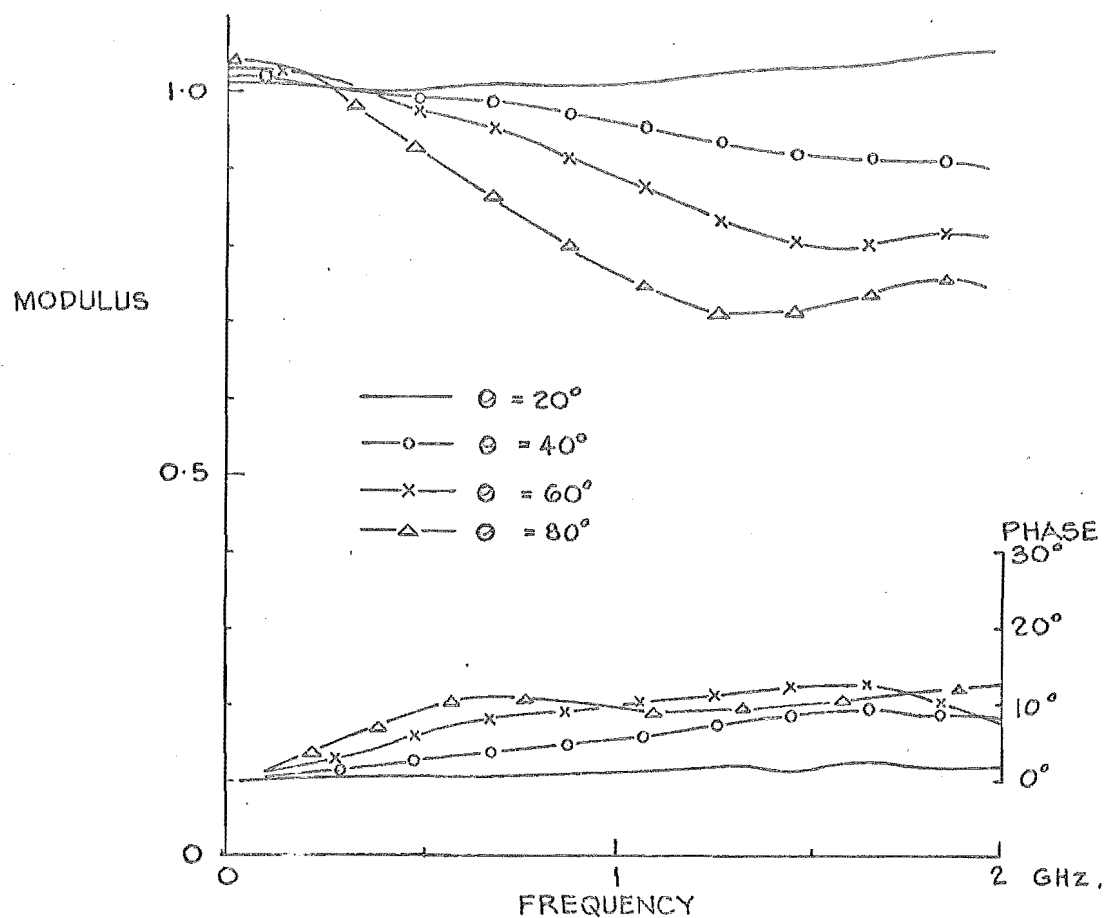


FIGURE 11-12:  $\beta(f)$ ;  $r = 20$  cm.,  $D = 0.32$  cm.,  $L = 91.5$  cm.,  $l = 61$  cm.

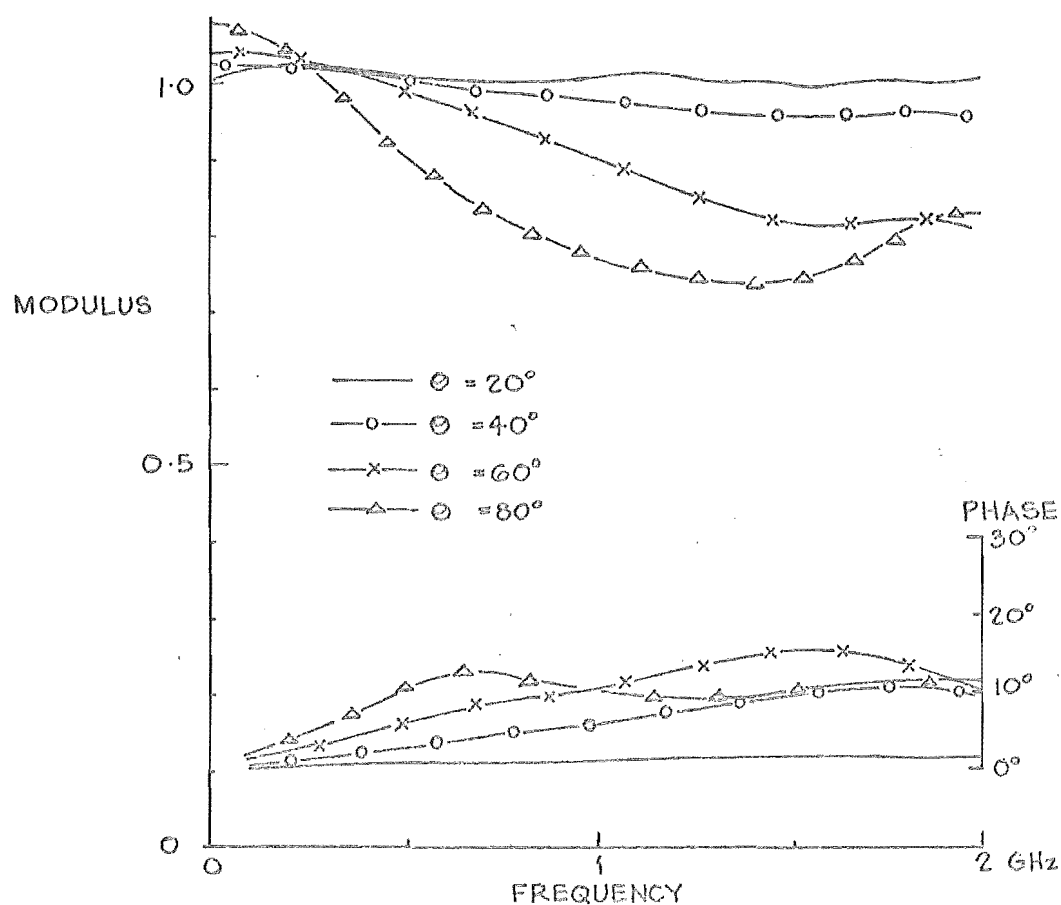


FIGURE 11-13:  $\beta(f)$ ;  $r = 10$  cm.,  $D = 0.32$  cm.,  $L = 91.5$  cm.,  $l = 61$  cm.

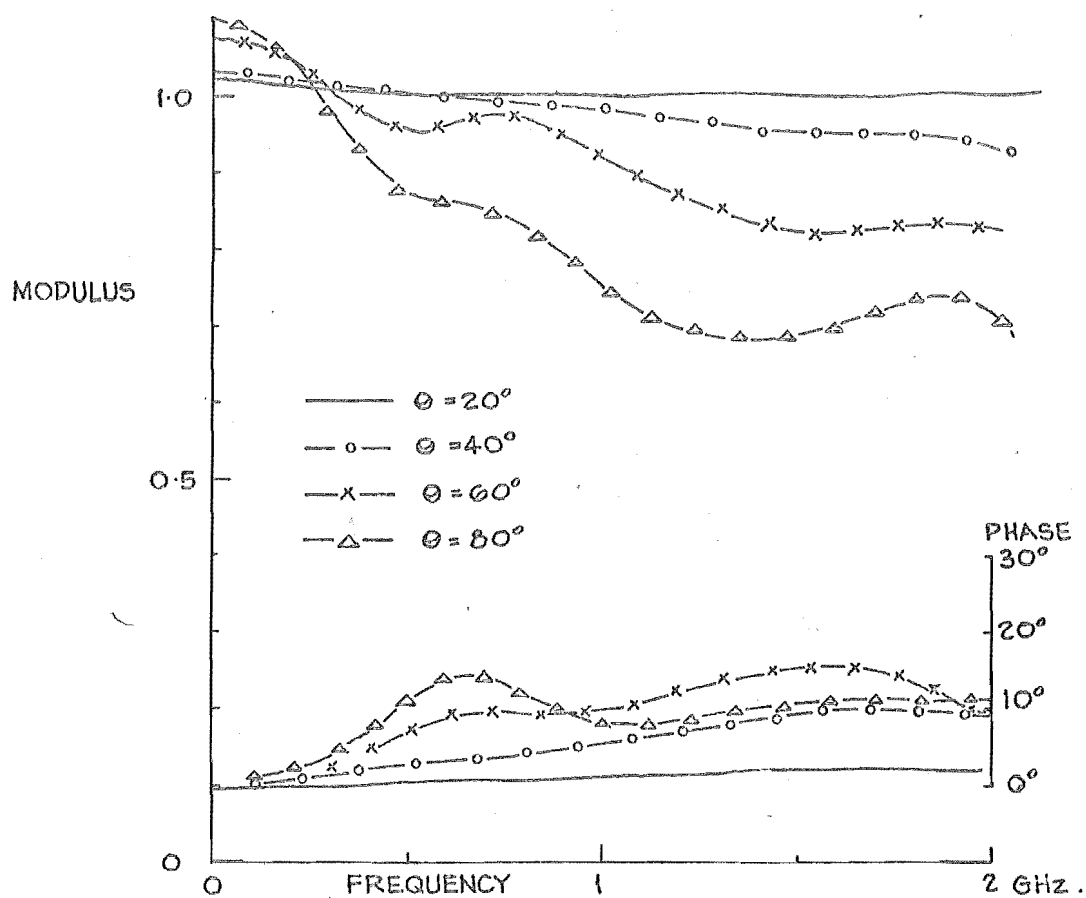


FIGURE 11.14:  $\beta(f)$ ;  $r = 10$  cm,  $D = 0.32$  cm,  $L = 91.5$  cm,  $l = 30.5$  cm.

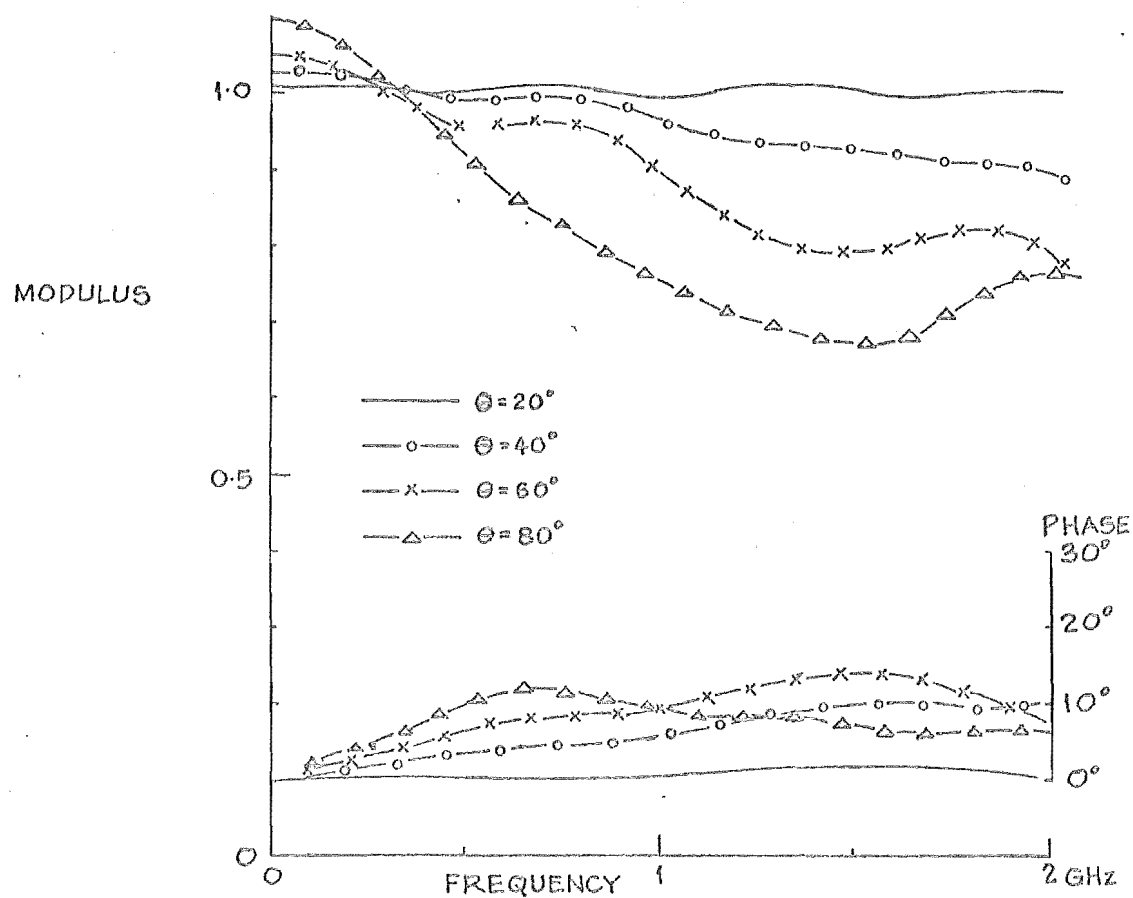


FIGURE 11.15:  $\beta(f)$ ;  $r = 5$  cm,  $D = 0.32$  cm,  $L = 91.5$  cm,  $l = 61$  cm.



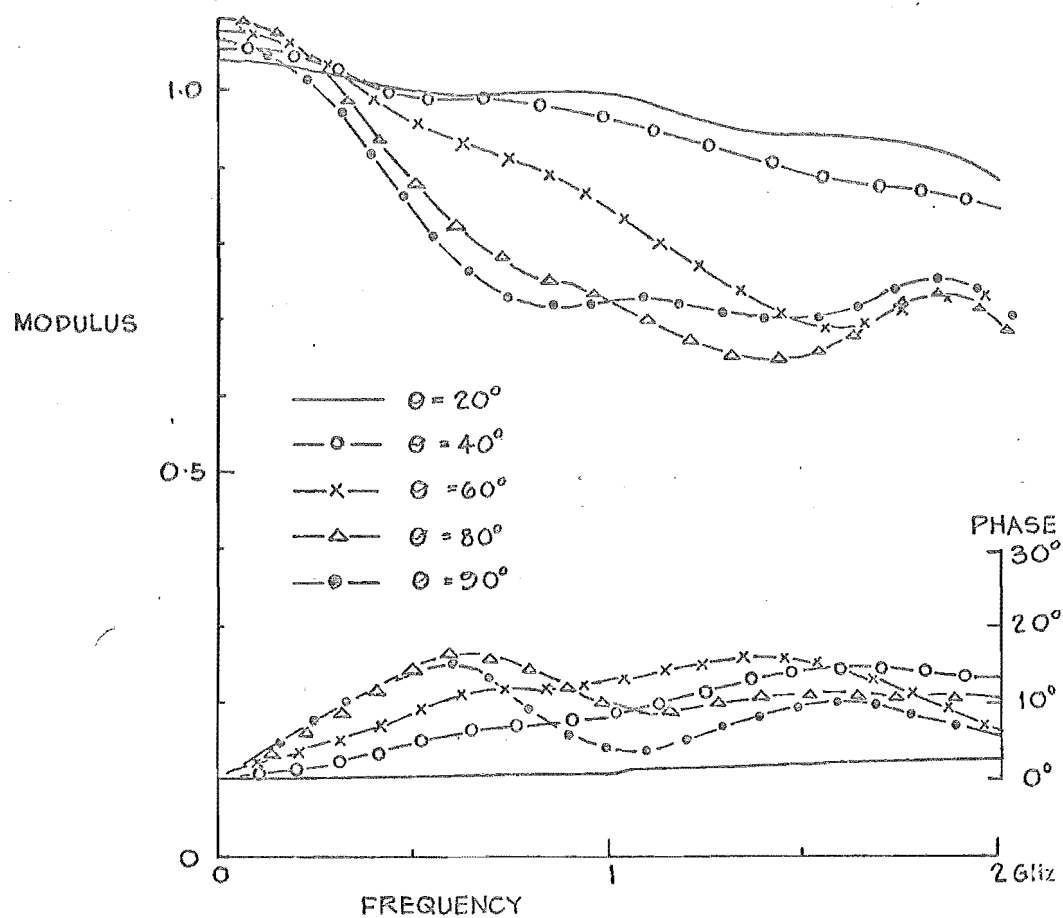


FIGURE 11.16:  $\beta(f)$ ;  $r = 3$  mm,  $D = 0.32$  cm,  $L = 91.5$  cm,  $\ell = 61$  cm.

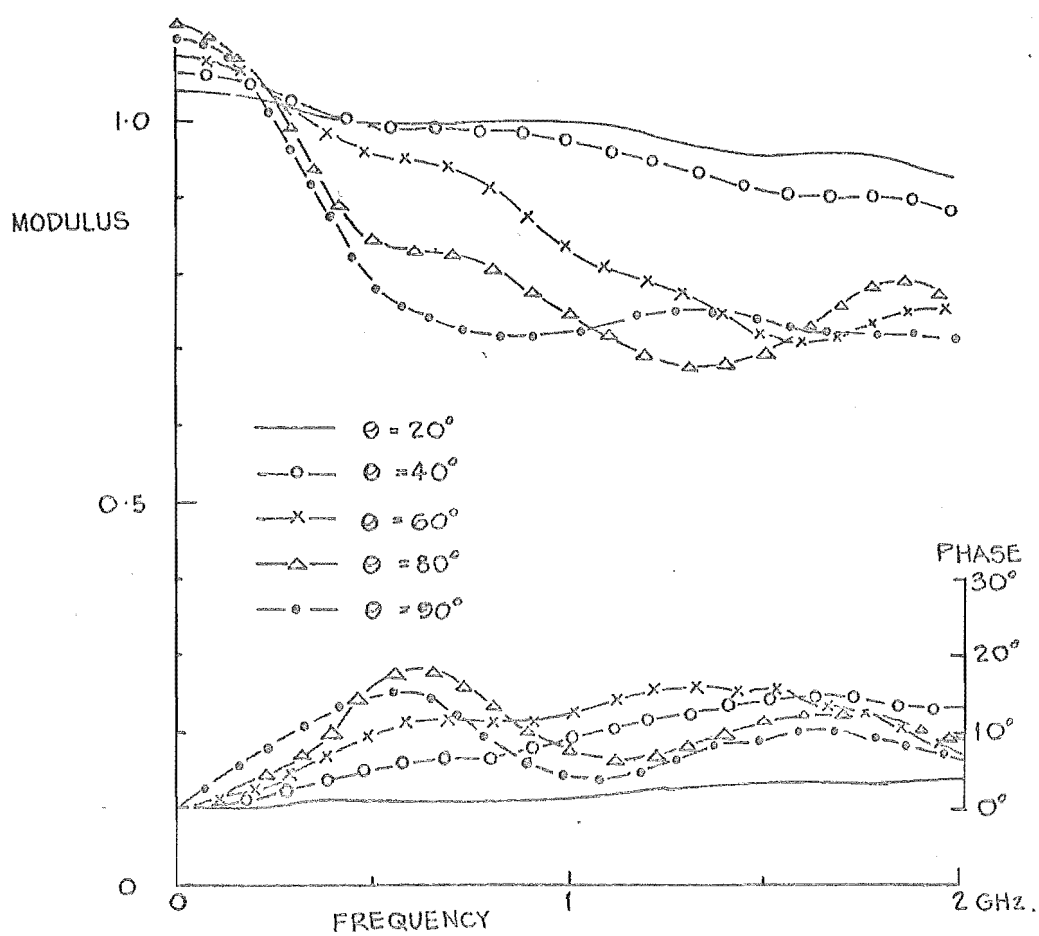


FIGURE 11.17:  $\beta(f)$ ;  $r = 3$  mm,  $D = 0.32$  cm,  $L = 91.5$  cm,  $\ell = 30.5$  cm.

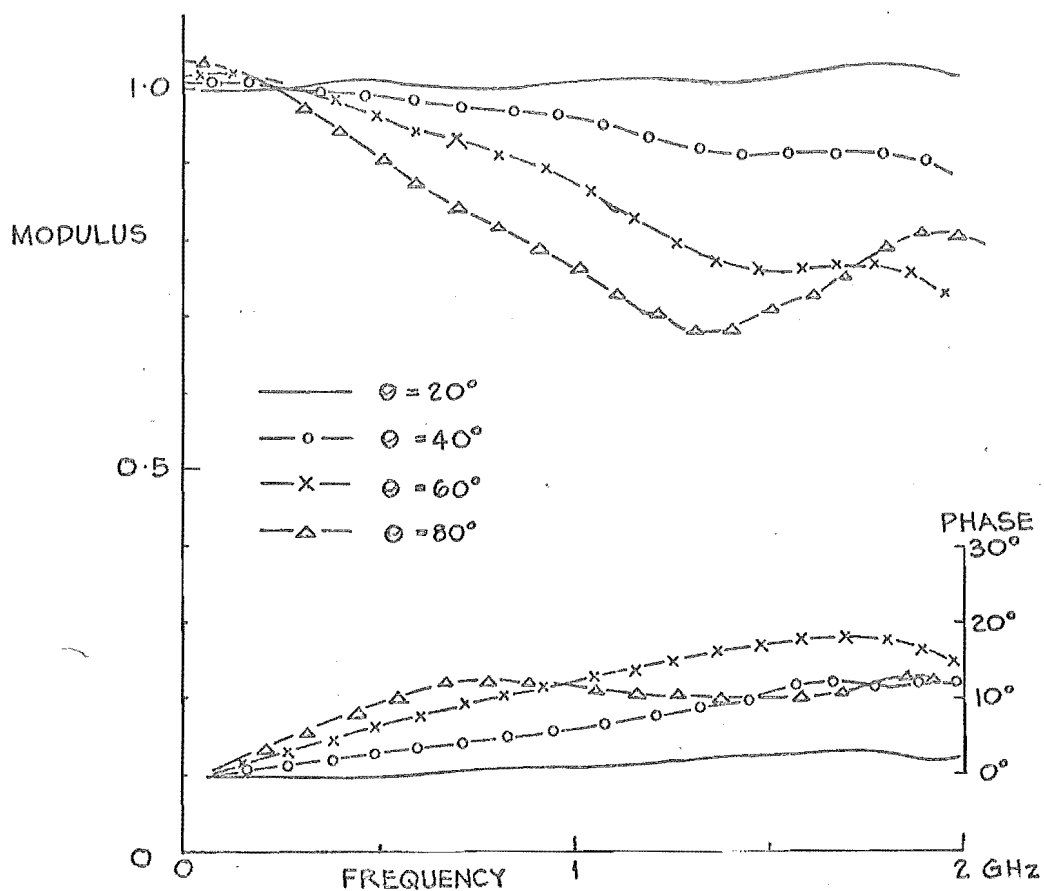


FIGURE 11-18:  $\beta(f)$ ;  $r=20\text{ cm}$ ,  $D=0.64\text{ cm}$ ,  $L=91.5\text{ cm}$ ,  $\ell=61\text{ cm}$ .

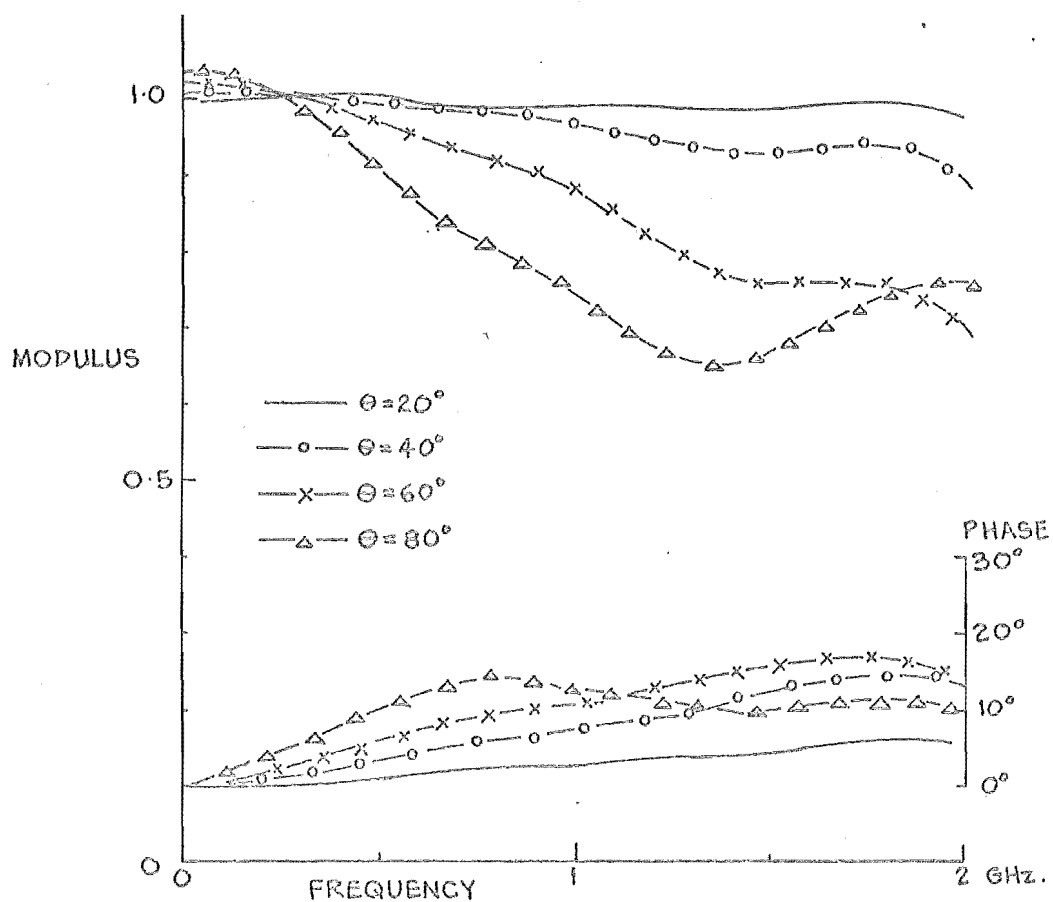


FIGURE 11-19:  $\beta(f)$ ;  $R=10\text{ cm}$ ,  $D=0.64\text{ cm}$ ,  $L=91.5\text{ cm}$ ,  $\ell=61\text{ cm}$ .

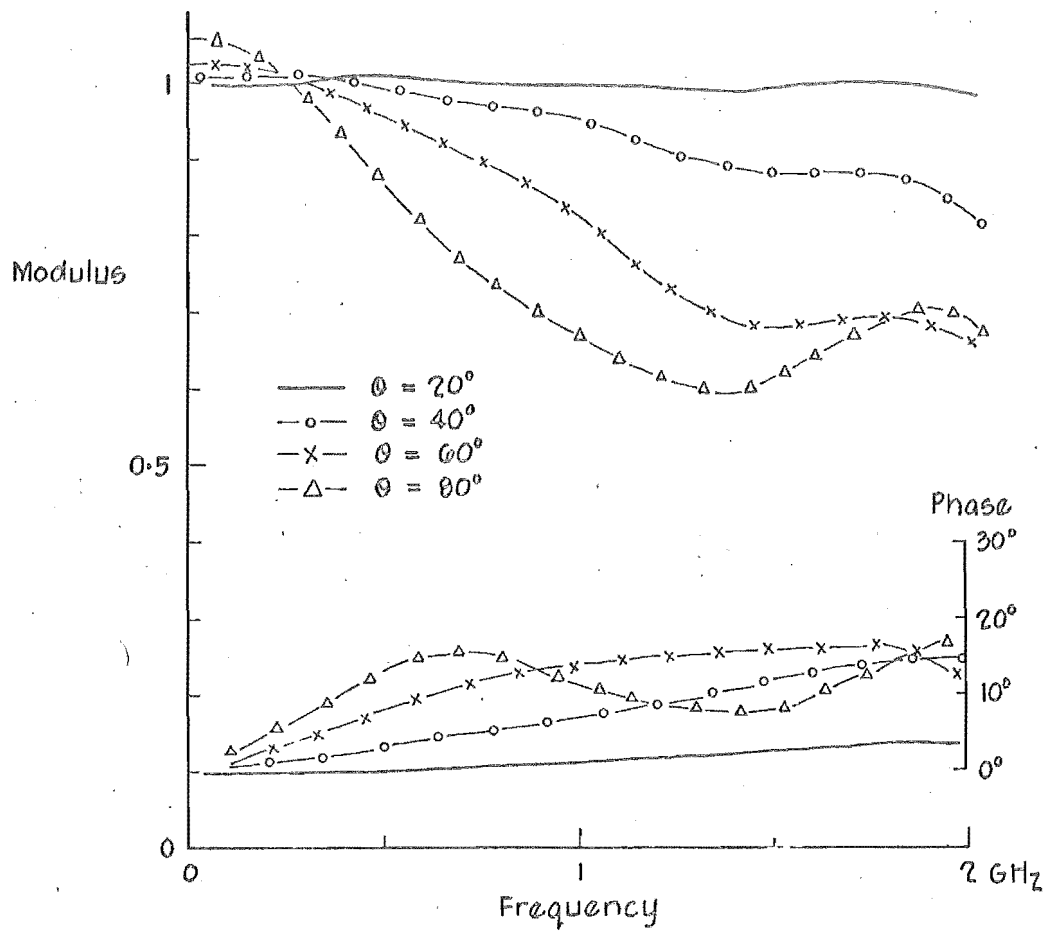


FIGURE 11.20:  $\beta(f)$ ;  $r = 5\text{cm}$ ,  $D = 0.04\text{cm}$ ,  $L = 91.5\text{cm}$ ,  $l = 61\text{cm}$ .

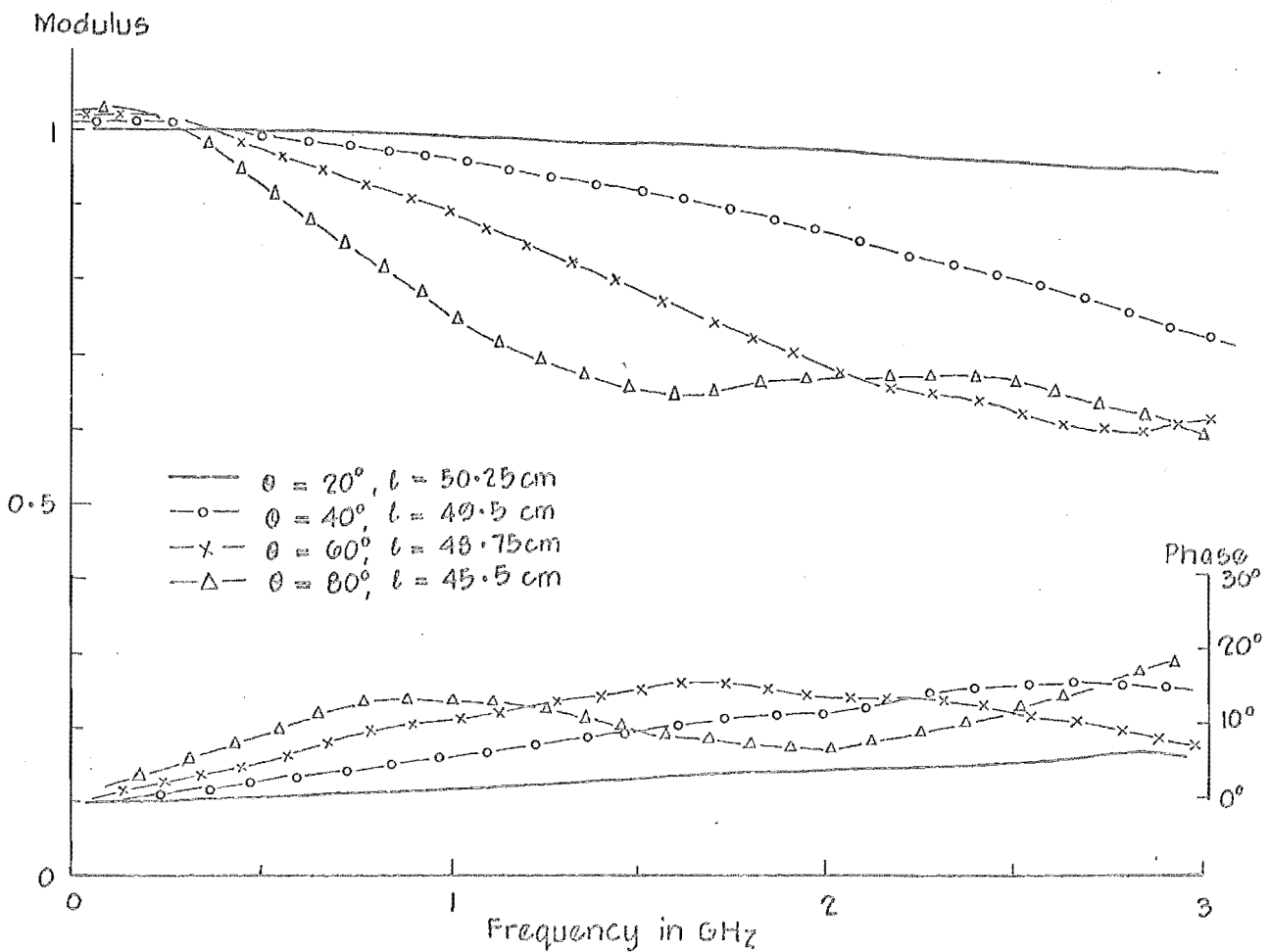
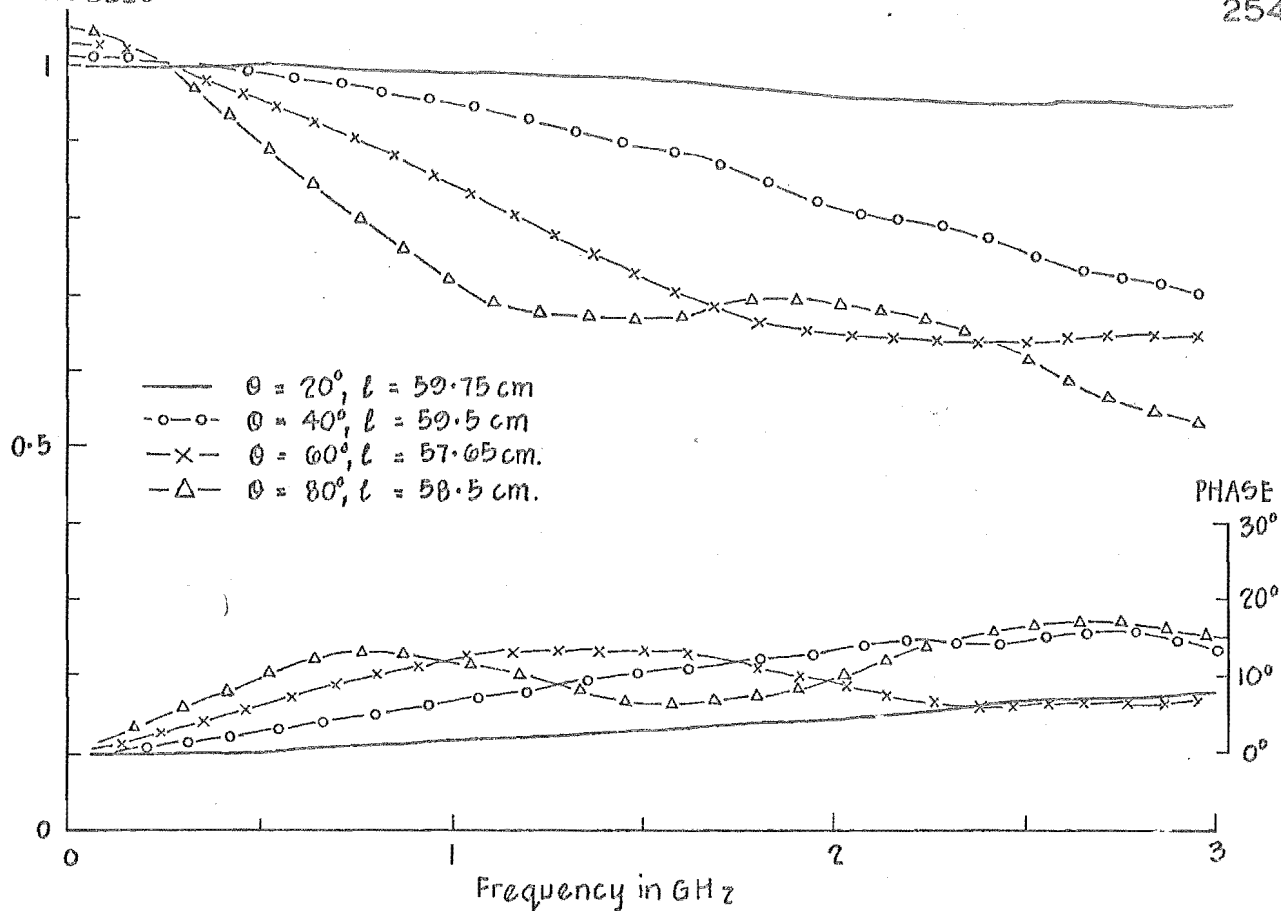
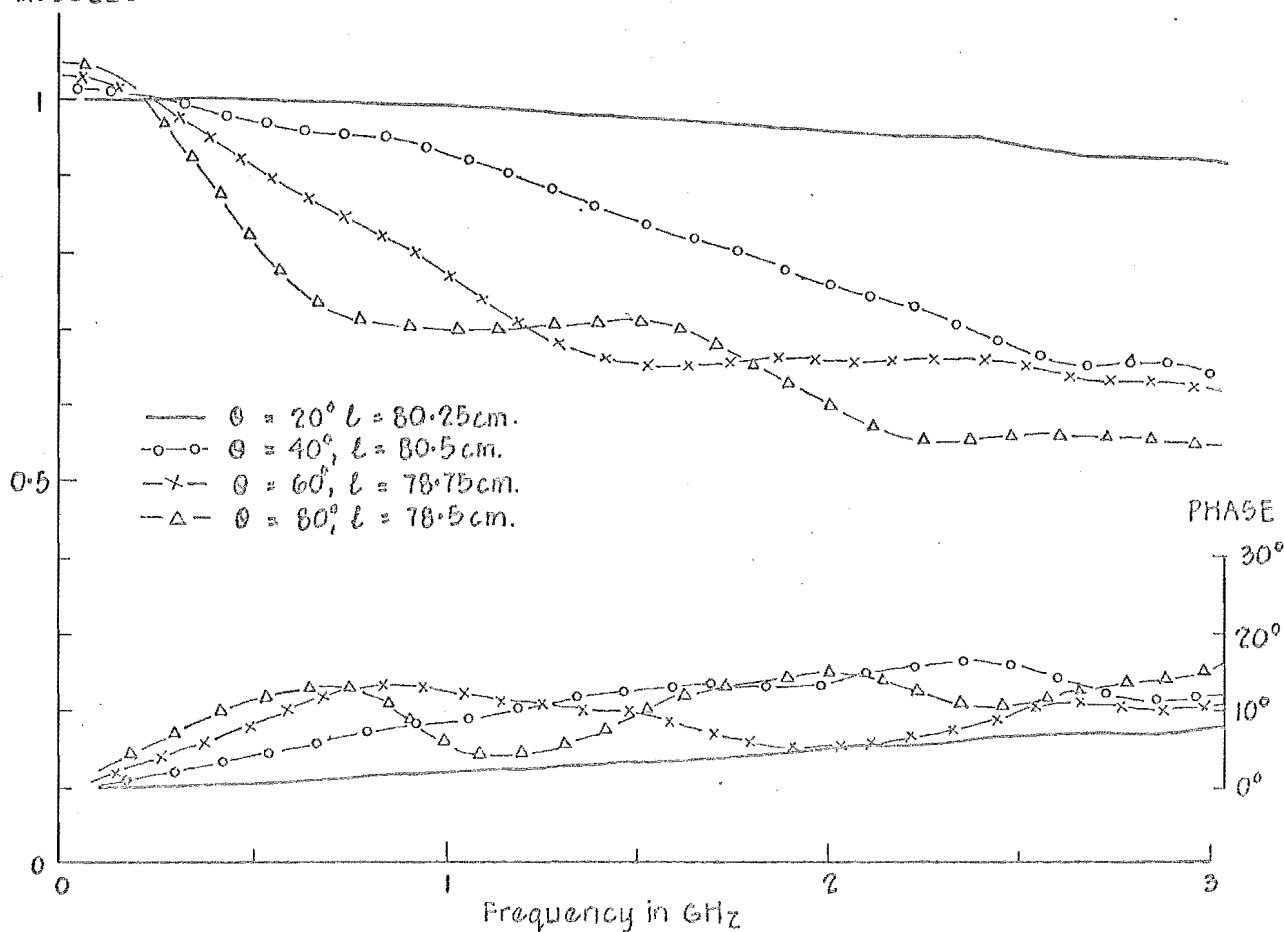


FIGURE 11.21:  $\beta(f)$ ;  $r = 15\text{cm}$ ,  $D = 0.04\text{cm}$ ,  $L = 75.7\text{cm}$ .

FIGURE 11.22:  $p(f)$ ;  $r = 15 \text{ cm}$ ,  $D = 0.64 \text{ cm}$ ,  $L = 90.92 \text{ cm}$ .FIGURE 11.23:  $B(f)$ ;  $r = 15 \text{ cm}$ ,  $D = 0.64 \text{ cm}$ ,  $L = 121.3 \text{ cm}$ .

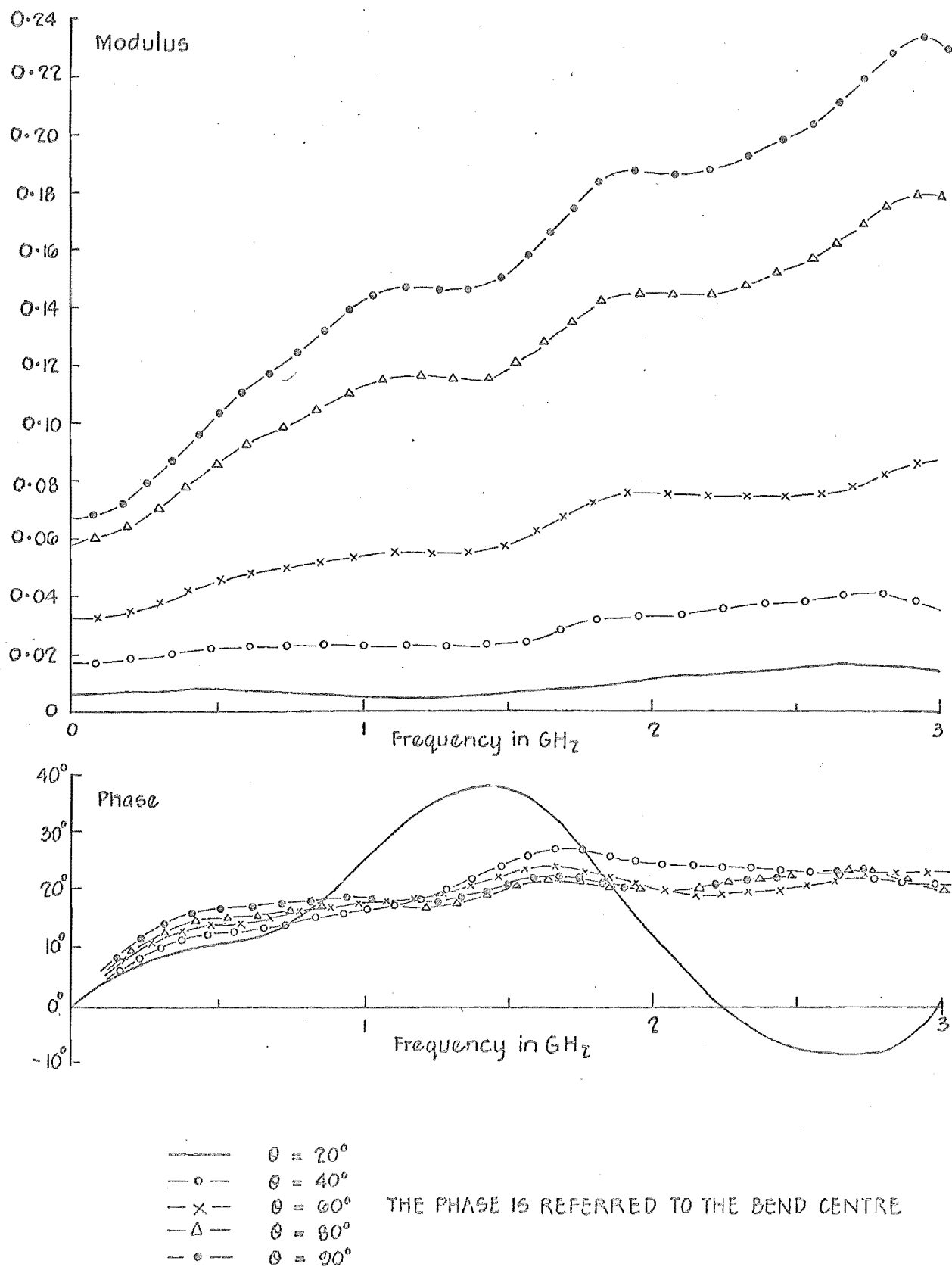


FIGURE 11.24: CURRENT REFLECTION COEFFICIENTS  $\Gamma(f)$  FOR  $r = 3\text{ mm}$  BENDS IN  $D = 0.32\text{ cm}$  WIRES.

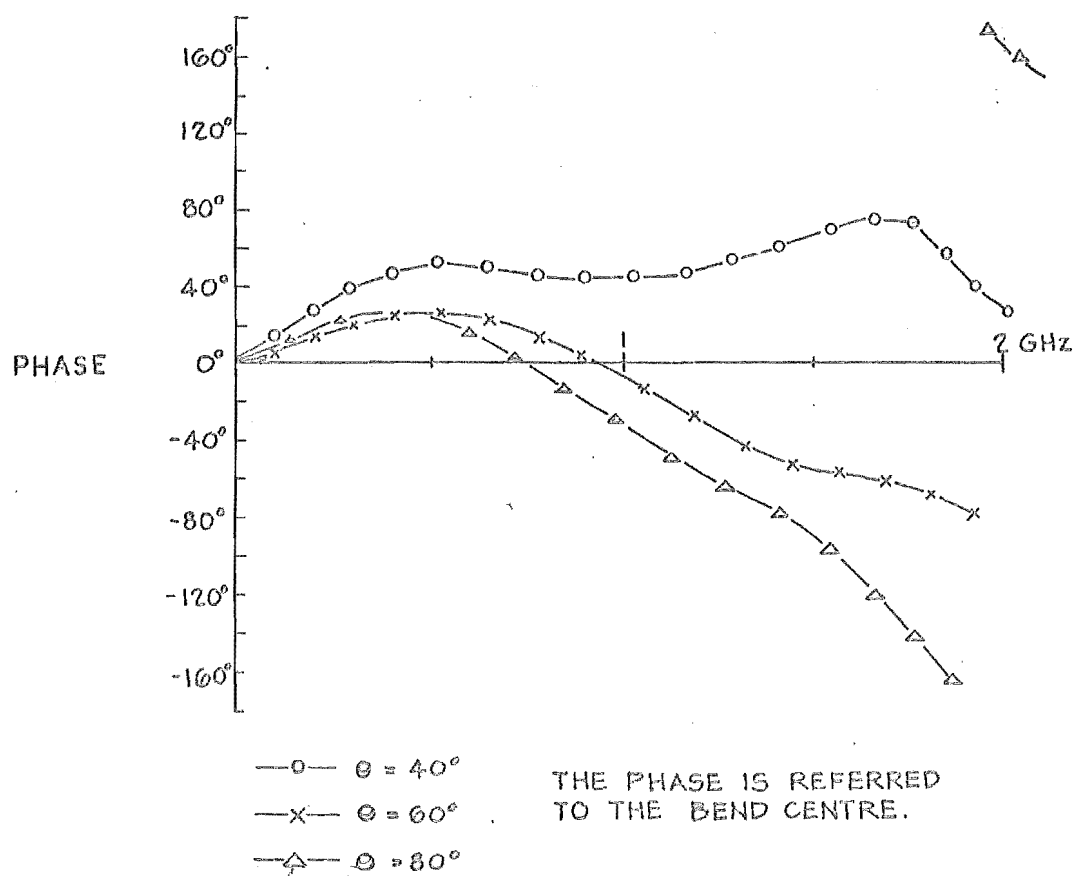
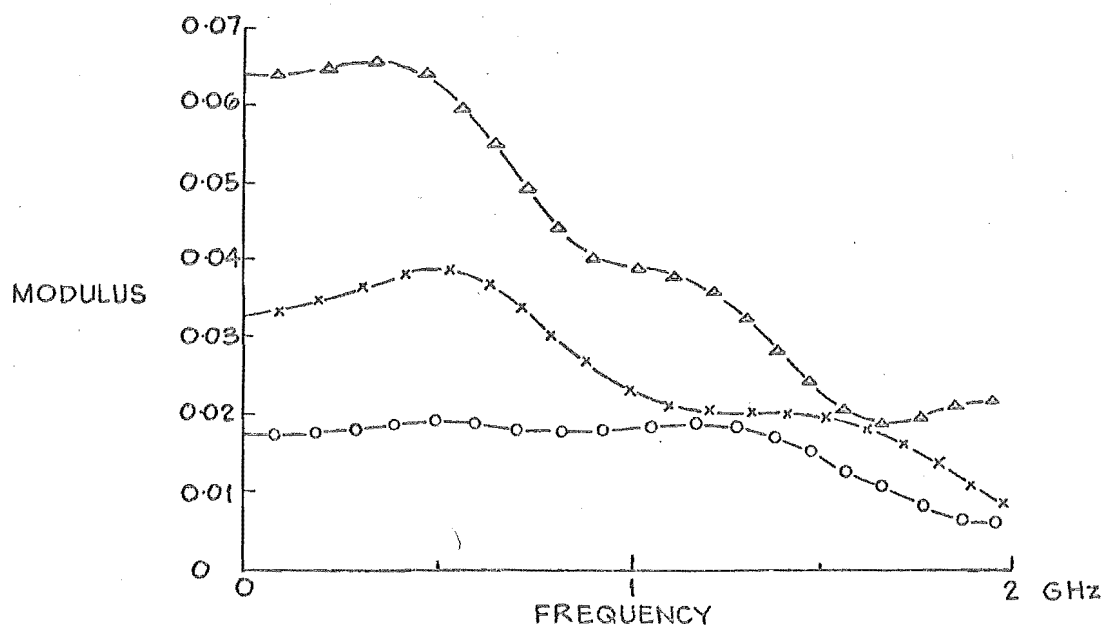
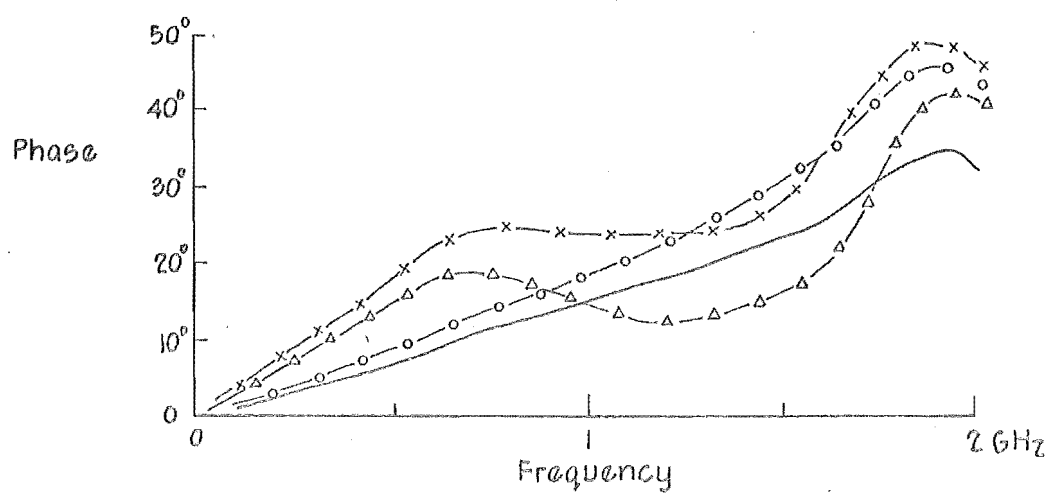
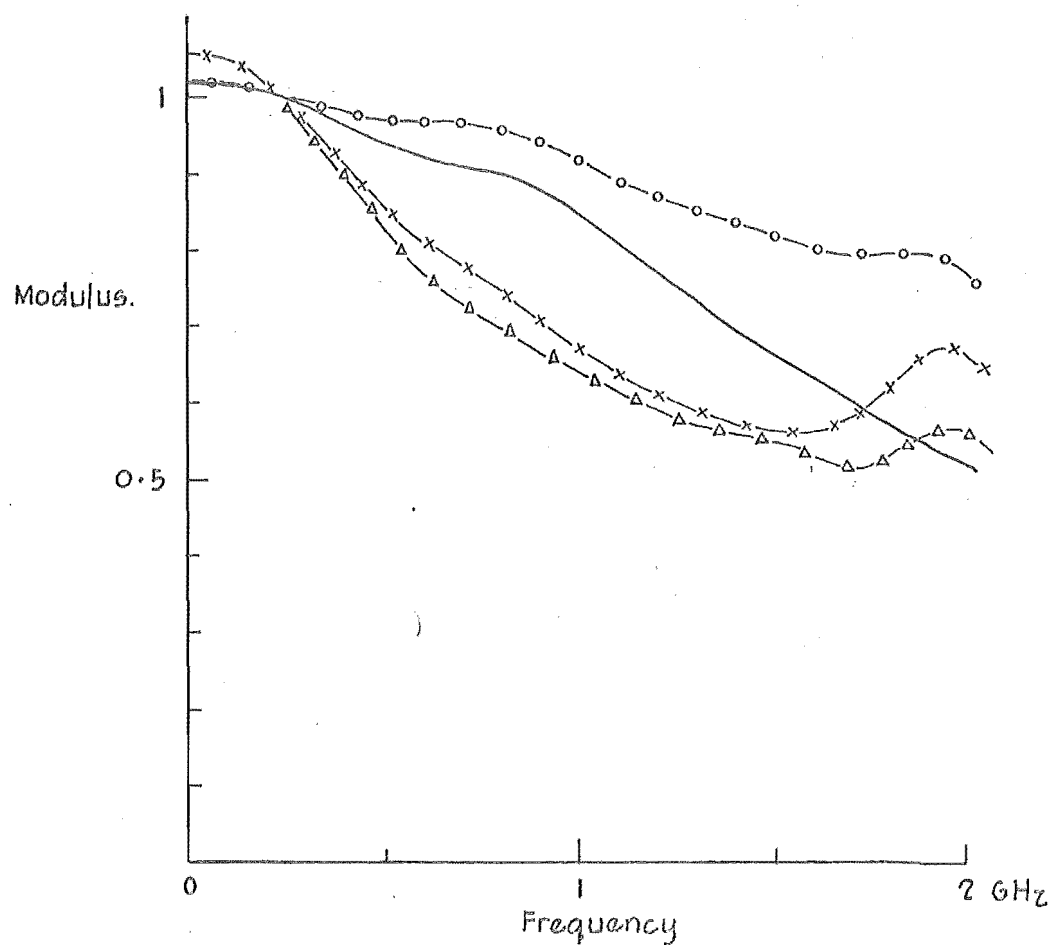
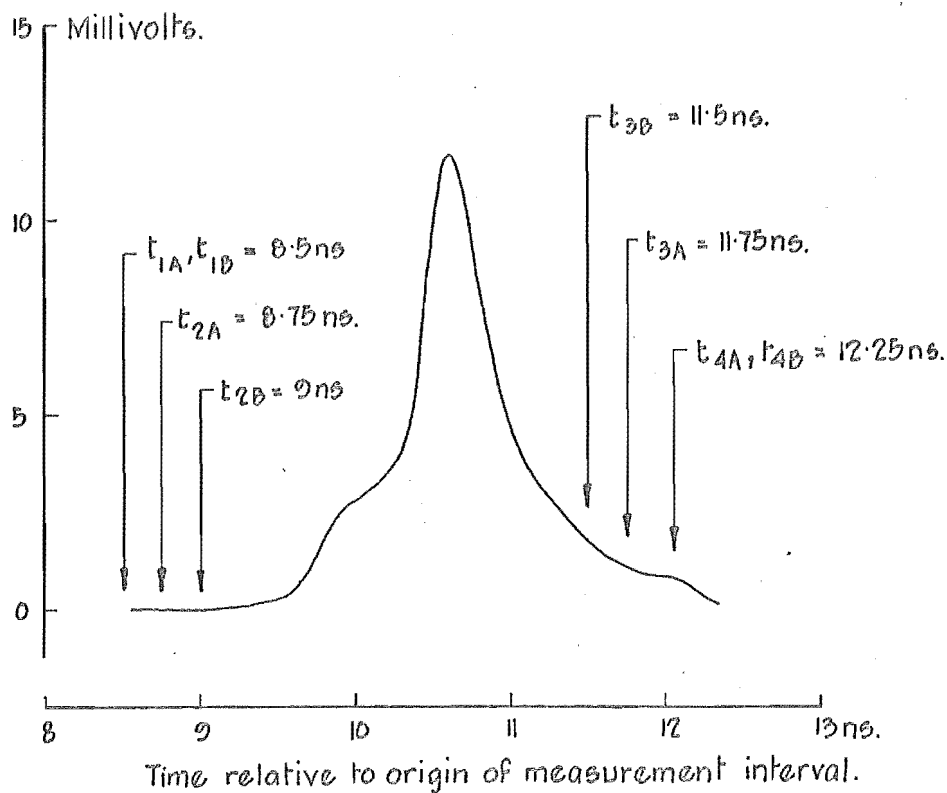


FIGURE II-25: CURRENT REFLECTION COEFFICIENT  $\Gamma(f)$  FOR  $r = 15$  cm. BENDS IN  $D = 0.04$  cm. WIRES.



- $\theta = 40^\circ$ , BEND  $90^\circ$  TO PLANE OF STRIP.  
 -o-o-  $\theta = 40^\circ$ , BEND IN PLANE OF STRIP  
 -Δ-  $\theta = 80^\circ$ , BEND  $90^\circ$  TO PLANE OF STRIP.  
 -x-  $\theta = 80^\circ$ , BEND IN PLANE OF STRIP

FIGURE 11.26:  $p(f)$  FOR BENT STRIP ANTENNAS  
 $r = 20$  cm,  $W = 2.54$  cm,  $L = 92$  cm,  $l = 48$  cm.



(a) REFLECTION FROM TIP OF BENT WIRE SHOWING DATA WINDOW PARAMETERS. (see Fig. II.10.) WIRE PARAMETERS:  $D = 0.04 \text{ cm}$ ,  $r = 15 \text{ cm}$ ,  $\theta = 80^\circ$ ,  $L = 121.3 \text{ cm}$ ,  $l = 73.5$  (see Fig II.1.)

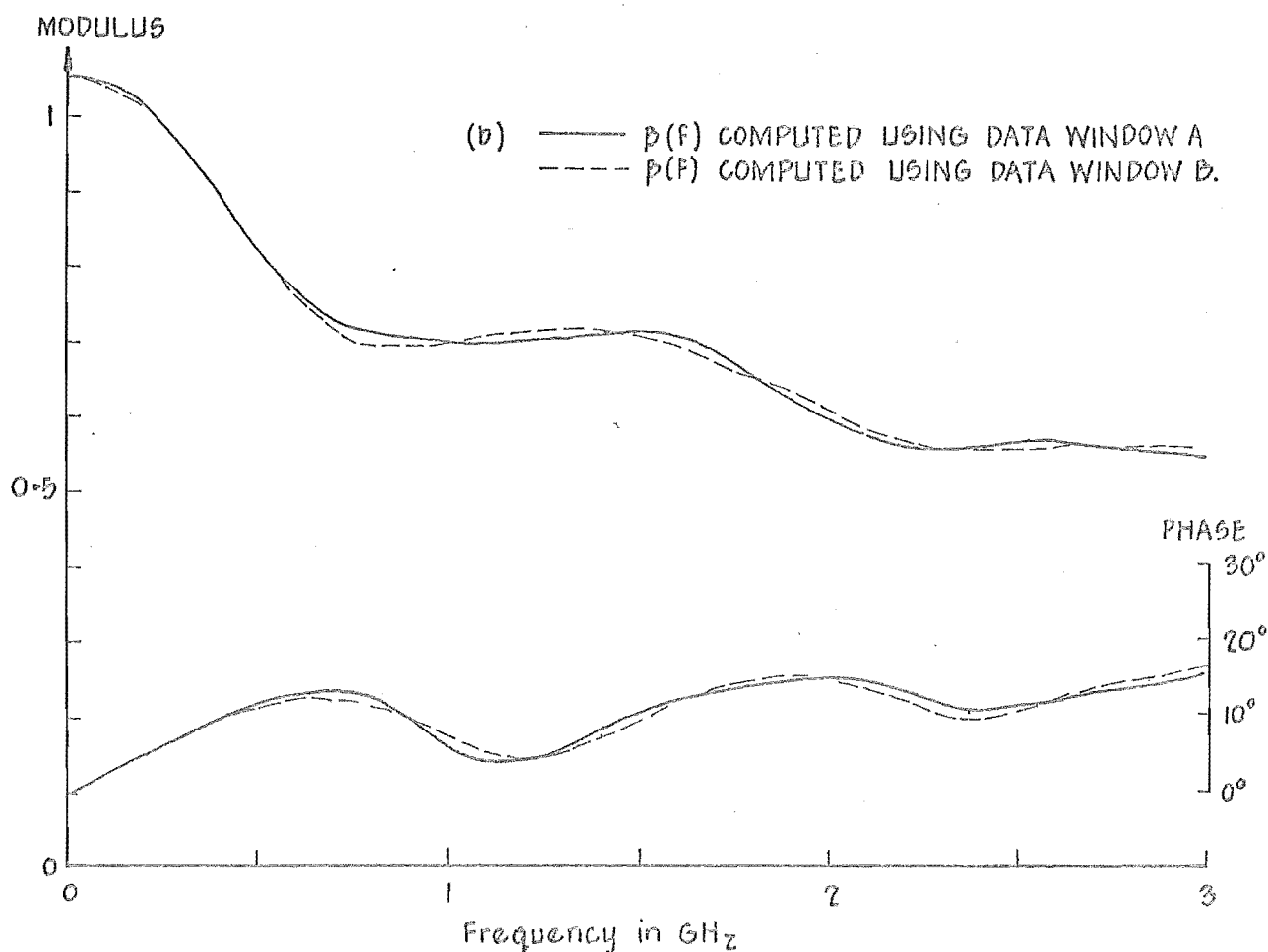


FIGURE II.27 : EFFECT OF CHANGING DATA WINDOW PARAMETERS ON A COMPUTED  $p(f)$



Appendix 1: THE ORGANISATION OF A HYBRID COMPUTER  
PROGRAM FOR SIMULTANEOUS DISPLAY OF TIME DOMAIN  
PULSE RESPONSES AND FREQUENCY RESPONSES OF ANTENNAS

The EAI-590 hybrid computing system of the Electrical Engineering Department was used. Its relevant specifications are:

EAI-640 digital computer

Storage : 16384 16 bit words<sup>1</sup>

Memory cycle time : 1.65 microseconds

I/O devices : Teletype keyboard and typer, 10  
 characters/second.

High speed paper tape reader, 300 8  
 bit characters/second.

High speed paper tape punch, 120 8 bit  
 characters/second.

EAI-260 magnetic disc memory, 360, 448  
 16 bit words<sup>2</sup>.

Tektronix 611 high resolution storage  
 display CRT with special interface.

Sense switches : 8

EAI-580 analogue computer

1 machine unit : 10 volts

Amplifiers : 28

Potentiometers : 10 manual set, 40 servo set

Function relays : 12

---

<sup>1</sup>8192 words at the time of programming.

<sup>2</sup>Not available at the time of programming.

D/A high speed switches ( $1\ \mu\text{s}$ ) : 8

AND gates : 32.

#### EAI 693 Interface

Logical control lines (D/A) : 4

Logical sense lines (A/D) : 4

ADC's (12 bit + sign)<sup>3</sup> : 16

DAC's (14 bit + sign)<sup>3</sup> : 2

DAC's (12 bit + sign)<sup>3</sup> : 3

Fig. 2.2 is a simplified block diagram of the measuring system showing the information flow. The program is used with a Tektronix 1S1 sampling unit.

#### A1.1 THE ANALOGUE COMPUTER

The logic patch panel is connected to a control box located at the antenna range. The logical condition of the sense lines can therefore be altered remotely, which allows remote control of the digital supervisory program.

A potentiometer amplifier network is used to scale the vertical output of the sampling unit so that it fits into the voltage range of the analogue computer. The sampling unit amplitude and time scale calibration factors are stored by the digital supervisory program. Three data channels are provided from the antenna range and these are multiplexed onto the ADC by high speed D/A switches in response to logical control line signals initiated by the digital supervisory program. Accurate sample timing is achieved by routing the DAC to the horizontal input of the sampling unit another potentiometer amplifier scaling network which

---

<sup>3</sup>Not available at the time of programming.

incorporates the previously determined sampling unit external horizontal deflection factor (see section 3.5). Because the high speed data transfer hardware was not installed at the time of programming, slow speed ( $> 40$  ms) A/D and D/A conversion (to 16 bit accuracy) was achieved by using the analogue component monitoring and control channels.

The signal to be analysed is displayed on the sampling oscilloscope and the measurement interval is chosen. The beginning and end of the measurement interval are identified with reference voltages supplied from the control box. These reference voltages are switched onto the horizontal input of the sampling unit and are adjusted while viewing the sampling oscilloscope screen.

#### A1.2 THE DIGITAL COMPUTER

The organisation of the program which computes Fourier transforms, reflection coefficients and system transfer functions is shown simplified in Figs A1.1 and A1.2. The required options are requested by sense switch settings. The sampling interval was chosen to be 100 pS because of aliasing error considerations (section 2.3.3.1.1). Storage is reserved for a maximum of 300 samples, which sets the maximum measurement interval at 30 nS. This was the length of the viewing window on driving point measurement range (section 3.2). The frequency response was calculated and displayed at 10 MHz intervals up to 800 MHz. The Fourier transforms are computed using the trapezoidal rule because of the limited storage available (see section 2.3).

The reference voltages which identify the beginning and end of the measurement interval are read from the control box by multiplexing the ADC onto the appropriate data channel. The ADC is then connected to the sampling unit vertical output, and the DAC scans the time-base step-wise throughout the measurement interval. One sample is converted and stored at each step. Unless computation is requested the data is erased from memory and the sampling cycle is repeated, so that a visual trace appears on the sampling oscilloscope. The sample values may be listed on the typer with a sense switch request.

Error messages are produced if error conditions arise during sampling, e.g. if the ADC attempts to convert a voltage which is greater than one machine unit, or if the measurement interval is longer than 30 ns. The error sensing routines are arranged so that no interruptions in program execution occur which require intervention at the computer console. This prevents execution being halted by the transient error conditions which often occur during oscilloscope adjustment.

A large, high resolution, graphical output display is presented on a Tektronix 611 storage display oscilloscope which has been specially interfaced to the digital computer. The display is in polar form and is normalised when it is a Fourier transform or system transfer function. Reflection coefficient displays are not normalised and each point is plotted as it is calculated. The output display is recorded by photographing it and recordings of the pulse response are made on an X-Y pen recorder.

FORTRAN was used for the calculation programming and ASSEMBLER subroutines were written for all input, output and hybrid linkage operations. In this way the advantage of problem encoding using a high level language is combined with the full instruction repertoire of the ASSEMBLER. Also significant storage space was saved by performing input-output operations from ASSEMBLER subroutines.

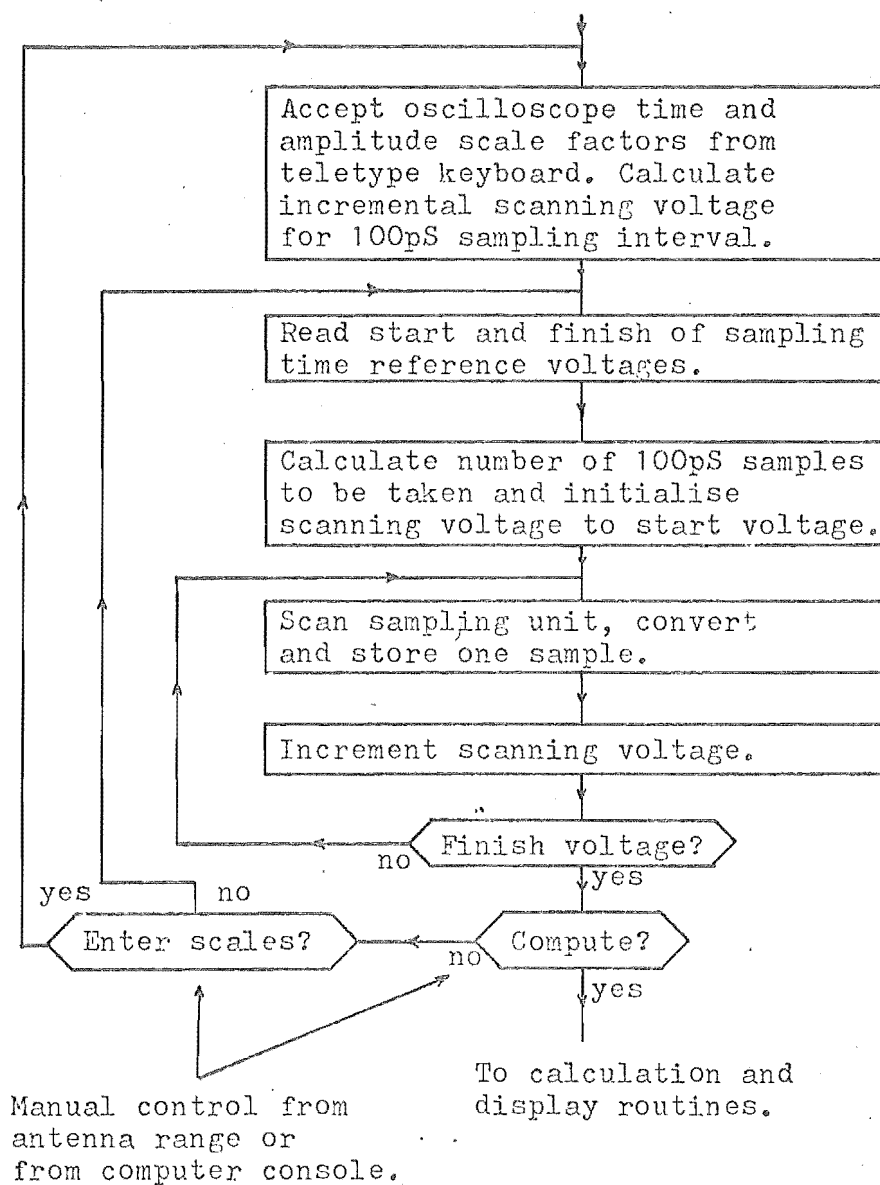
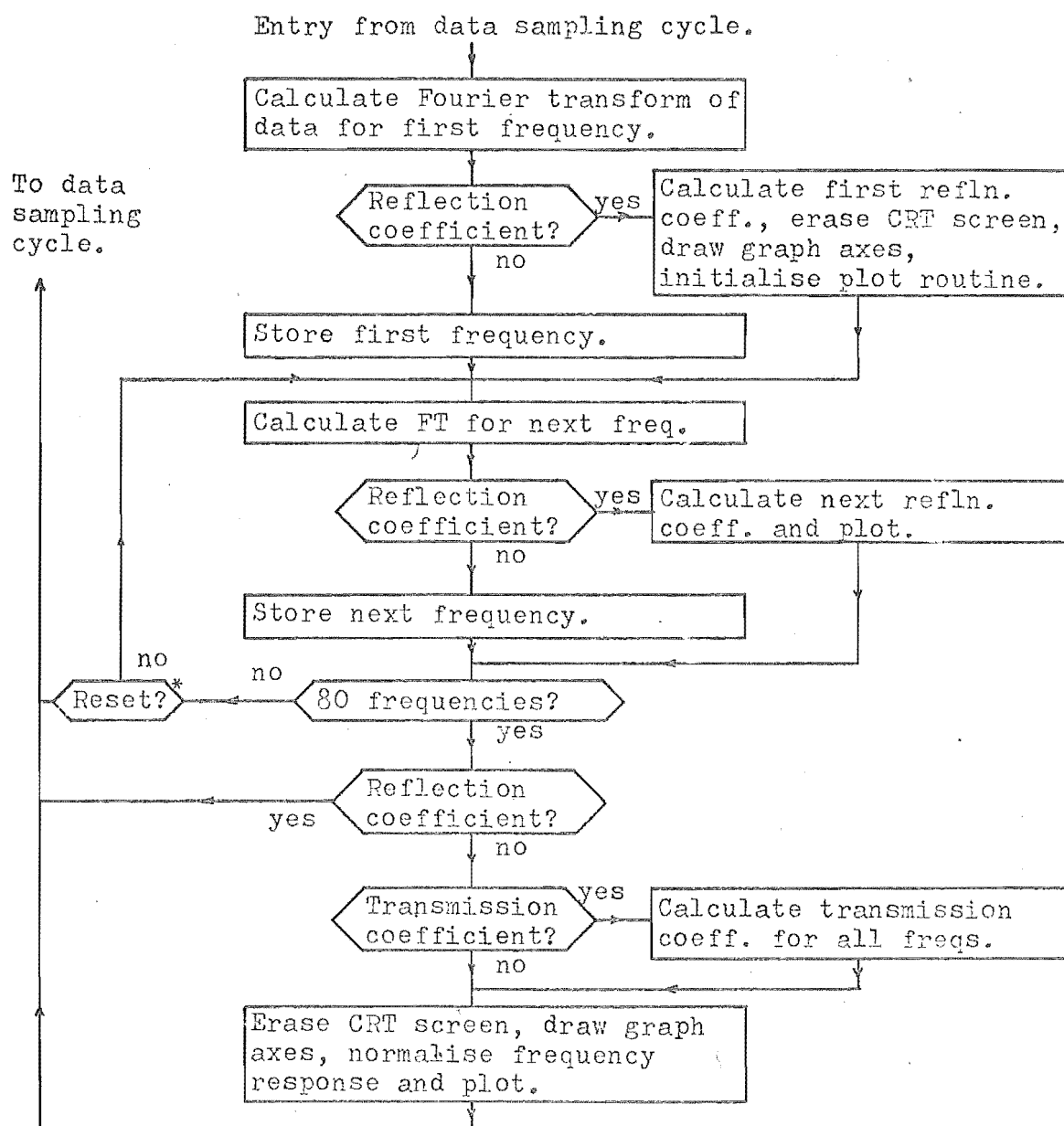


Figure A1.1: ORGANISATION OF HYBRID COMPUTER PROGRAM.

(a) THE DATA SAMPLING CYCLE.



\* Manual control from antenna range.

Figure A1.2: ORGANISATION OF HYBRID COMPUTER PROGRAM.

(b) CALCULATION AND DISPLAY.

## Appendix 2: THE ORGANISATION OF AN ON-LINE HYBRID COMPUTER PROGRAM FOR 3-POINT SCAN SAMPLING

The 3-point scanning method of sampling is described in section 2.3.6. Insufficient storage remains in the hybrid program of Appendix 1 to include a versatile 3-point scan sampling routine. Therefore a general program was written to sample any signal displayed on a sampling oscilloscope which is compatible with the voltage range of the analogue computer. The sampled data is then punched onto paper tape in a suitable format so that it may be subsequently processed on either the EAI-640 digital computer or an IBM 360/44 digital computer.

### A2.1 TIMING THE SCAN SEQUENCE

Measurements of the sampling oscilloscope noise, such as those shown in Figs 2.3 and 2.4, were used to determine the timing of the scan sequence. The risetime of the noise at the vertical output of the sampling oscilloscope was measured at about 2 ms, but was probably much faster since the pen recorder bandwidth was limited. The risetime of the low-pass filter should therefore be longer than 2 ms for effective noise filtering. The output zero level drifted significantly (1 mv referred to the input at 5 mV/cm) in times as short as 200 ms, therefore the scan sequence must occur faster than 200 ms. A scan sequence time of 150 ms was chosen (i.e. 50 ms for each measurement) and the low-pass filter risetime was set at 6.5 ms. This allows the filter output voltage to slew to 99% of a step change of input voltage before conversion.



## A2.2 THE ANALOGUE COMPUTER

The function of the analogue computer is the same as for the program described in Appendix 1. Five data channels are provided, the extra two being for voltages which represent  $t_1$  and  $t_2$  (see Fig. 2.8). The five logic signals which control the multiplexing of these channels are derived by logically decoding the four control line signals using the logic AND gates. A leaky integrator is used as a low pass filter, and a 0.068  $\mu\text{F}$  capacitor connected across the amplifier's internal 100 K ohm feedback resistor gives the required risetime.

## A2.3 THE DIGITAL COMPUTER

The program organisation is given in Fig. A2.1. The number of times the signal is to be scanned is set on the sense switches. The amplitude and time drift correction routines may be disabled by sense switch settings thus allowing faster sampling for high amplitude signals if high accuracy is not required.

The 50 ms delay between scanning the sampling unit and reading the displayed voltage is obtained by executing a delay loop in the program the required number of times. At the completion of each scan of the signal the maximum difference between the sampled values of the old average and the average updated by the latest scan is typed. The scanning may then be interrupted if the difference is acceptably small. When scanning is complete the values are punched onto paper tape.

#### A2.4 PAPER TAPE FORMAT

The sampled values are stored internally as integers in the range -16383 to 16383 (i.e. 14 bits with sign). The negative numbers are stored in twos complement form. Before punching the values are converted into 15 bit positive integers by displacing the zero level to a value of 16384. The values are then punched onto eight channel paper tape with the most significant eight bits occupying the first frame (with a hole representing a bit high), and the least significant eight bits occupying the second frame. This format is illustrated in Fig. A2.2. Because the IBM 2671 paper tape reader (used to input the data to the 360/44) ignores tape frames which have no holes punched it is necessary to ensure that at least one hole is punched in each tape frame. Bit 0 (see Fig. A2.2) is set high for every data word and bit 15 is set high if bits 8-15 are all zero. Bit 0 is then subtracted after the tape has been read and the effect of the occasional setting of bit 15 is insignificant (even if the range of data values occupy only a quarter of the allowable range, the error in any sample value with bit 15 set is only 0.025% of the maximum sample value).

#### A2.5 CARD FORMAT FOR IBM 360/44 PROCESSING

The IBM 360/44 digital computer is operated as a batch job processor with card input. Submitting input data on paper tape often delays job processing. If the data was to be used as program input more than once it was transferred to cards. The data (which was input to an integer array with a 2-byte word length) was punched onto cards in 37A2 format.

This format makes the most efficient use of the cards. The remaining six columns were used for a sequence number. This is a worthwhile insurance because it is extremely difficult to sort the cards by visually inspecting the data.

#### A2.6 THE EFFECTIVENESS OF 3-POINT SCANNING

To demonstrate the effectiveness of 3-point scanning the digital computer program described in section A2.3 was modified in the following way. After each successive scan of the signal the mean and the standard deviation, as well as the maximum value, of the difference between the sampled values of the old average and updated average of the measured signal were typed. The standard deviation (or RMS value) is a measure of the effective noise level of the measurement. A signal was then displayed on the sampling oscilloscope (it was the test pulse used for the driving point measurements of the fan antennas reported in chapter 6) and measured in three ways:

- 1) with 3-point scanning,
- 2) with normal scanning (i.e. the amplitude and time drift correction was disabled),
- 3) with 3-point scanning but with the low-pass filter connected between the oscilloscope and the ADC removed.

The peak value of the signal at the input of the sampling oscilloscope was -175 mv, and 295 samples were taken at 100 ps intervals. 12 scans of the signal were made and the improvements in accuracy obtained by averaging are shown in Fig. A2.3. Notice that by averaging only two scans of the

signal the effective noise level of the measurement is only 0.32 mv when 3-point scanning is used. This is an improvement of 10 dB (typically the RMS noise level of a sampling oscilloscope is 1 mv referred to the input; section 2.3.3.2.1). The improvement after 12 scans is 28 dB. In an experiment reported in section 9.4 an improvement of 40 dB was obtained by averaging 24 scans. Because the amplitude and time drift are corrected for in 3-point scanning the effective noise level becomes smaller more quickly than with normal scanning, which means that to obtain similar accuracy using normal scanning many more scans have to be averaged. The importance of filtering the high frequency noise is clearly shown, for, in spite of 3-point scanning, worse results than for normal scanning are obtained.

#### A2.7 SUBSEQUENT IMPROVEMENTS TO THE PROGRAM

Following the installation in the EAI-590 hybrid computing system of high speed ADC's and DAC's ( $\approx 30 \mu\text{s}$  conversion time) the program was improved by J.R. Allen, as part of his research for the Master of Engineering (M.E.) degree. The improvements made included:

- 1) Automatic measurement of reference slope.
- 2) The reference voltages identifying start and end of sampling times are measured only at the beginning of each set of experiments. This was done to eliminate timing shifts caused by drifting reference voltages (see section 11.3.1.1).
- 3) If the time drift exceeds the limits of the reference slope then measurement is interrupted until it drifts

back again (this meant that an extra point on the slope had to be measured).

- 4) Improved printout between scans includes RMS noise level, signal/noise ratio and mean value of noise.
- 6) By reducing the scan cycle time to 100 ms (permitted by the faster hardware) a noise reduction of 40 dB is attained in only 17 scans instead of the previous 24.

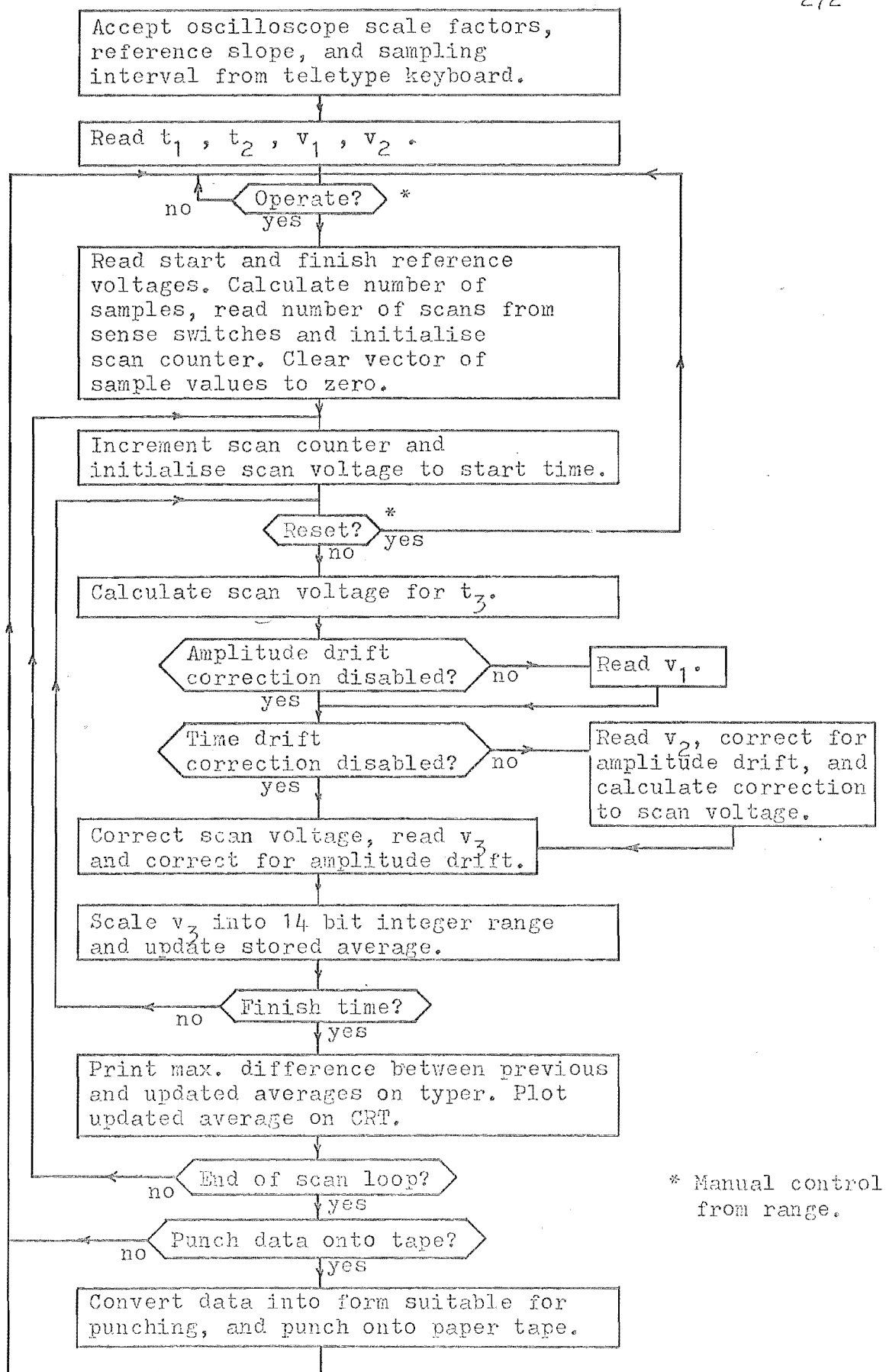


Figure A2.1: THE ORGANISATION OF AN ON-LINE HYBRID COMPUTER  
PROGRAM FOR 3-POINT SCAN SAMPLING.

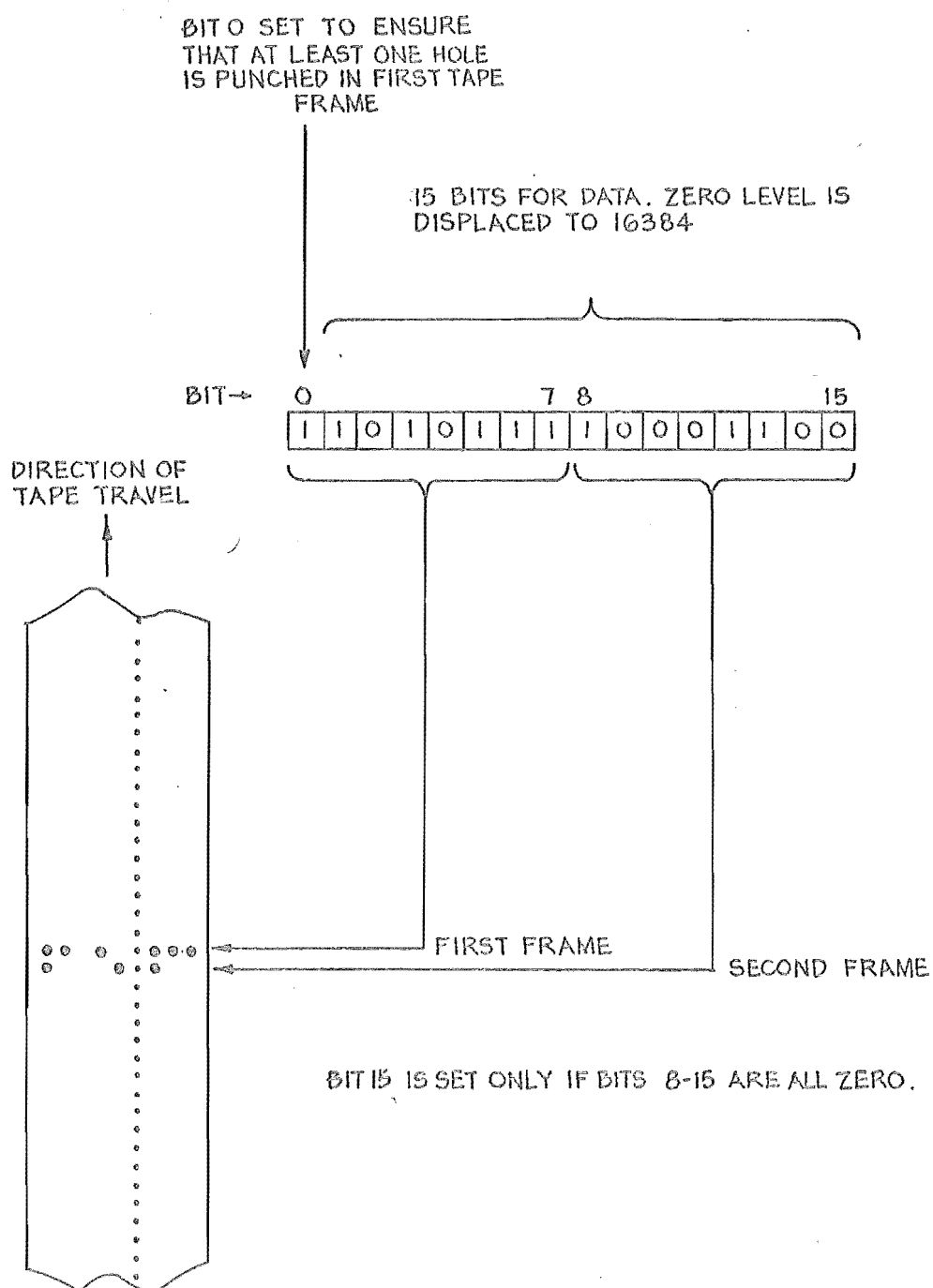


FIGURE A2-2 : ILLUSTRATION OF PAPER TAPE FORMAT FOR ONE DATA WORD.

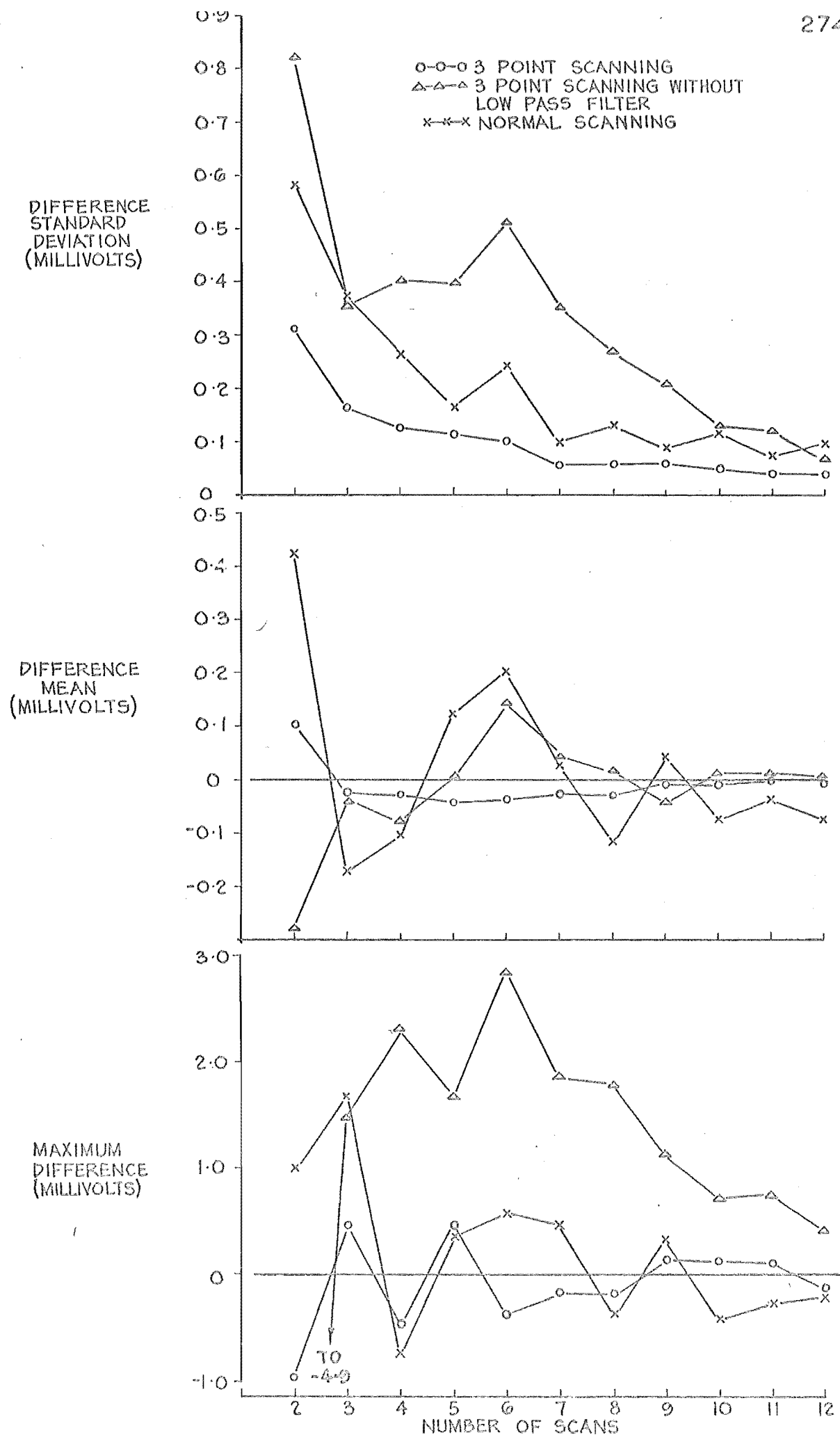


FIGURE A2.3 : EFFECTIVENESS OF 3 POINT SCANNING



Appendix 3: CALCULATION OF T(f) AND R(f) FOR A 0.45 m LONG  
MONOPOLE AT FREQUENCIES WHEN IT IS A QUARTER-WAVELENGTH  
LONG AND THREE QUARTER-WAVELENGTHS LONG

1) T(f)

The current distribution on the monopole is assumed to be, at the mth resonance,

$$I_m(z) = I_0(m) \cos(m\pi z/L), \quad m = 1, 3, 4, \dots \quad (A3-1)$$

where  $z$  is the distance along the monopole and  $I_0(m)$  is the value of the current at the base of the monopole (i.e. at  $z = 0$ ). The time dependence  $e^{j\omega t}$  is suppressed. The radiated electric field intensity in the equatorial plane a distance  $r$  from a dipole of length  $l = m\lambda/2$  is given by Silver (1949, p98):

$$E = j \sqrt{\frac{\mu}{\epsilon}} \frac{I_0(m) \sin(m\pi/2) e^{-jkr}}{2\pi r} \quad (A3-2)$$

where  $I_0(m)$  is the value of the current at the centre of the dipole,  $\mu$  is the permeability of free space and  $\epsilon$  is the permittivity of free space. Substituting  $\sqrt{\mu/\epsilon} = 120\pi$  ohms we obtain

$$E_1 = \frac{j 60 I_0(1) e^{-jkr}}{r} \quad (A3-3a)$$

for  $m = 1$ ; and

$$E_3 = \frac{-j 60 I_0(3) e^{-jkr}}{r} \quad (A3-3b)$$

for  $m = 3$ . By image theory (Harrington 1961, section 3-4) the radiated electric field intensity for a monopole is the

same as that for a dipole with the same impressed current.

From eqns (3-6) and (3-7)

$$I_0(1) = \frac{2U(f)}{50 + Z(1)} \quad (\text{A3-4a})$$

and

$$I_0(3) = \frac{2U(f)}{50 + Z(3)} \quad (\text{A3-4b})$$

where  $Z(1)$  and  $Z(3)$  are the values of  $Z(f)$  when the monopole length  $l/2 = \lambda/4$  and  $3\lambda/4$  respectively. Using  $Z(1) = 35$  ohms and  $Z(3) = 53$  ohms (Stratton 1941, p444) and substituting eqns (A3-4) into eqns (A3-3) we obtain

$$E_1 = j \, 1.41 \, U(f) \frac{e^{-jkr}}{r} \quad (\text{A3-5a})$$

and

$$E_3 = -j \, 1.165 \, U(f) \frac{e^{-jkr}}{r} \quad (\text{A3-5b})$$

Thus from eqn(2-20) the transmit transfer functions for frequencies when the monopole is a quarter-wavelength long and three quarter-wavelengths long are

$$T(1) = 1.41/\underline{90^\circ} \, , \quad (\text{A3-6a})$$

$$T(3) = 1.165/\underline{-90^\circ} \, . \quad (\text{A3-6b})$$

## 2) $R(f)$

The effective length of an antenna for receiving is the same as its effective length as a transmitting antenna (Jordan and Balmain 1968, section 11.02). Assuming the current distribution when transmitting is given by eqn (A3-1), the effective heights of the monopole at its quarter-wavelength resonance  $h_e(1)$  and at its three quarter-wavelength resonance  $h_e(3)$  are

$$h_e(1) = \frac{1}{I_0(1)} \int_0^{1/2} I_0(1) \cos(\pi z/1) dz = 1/\pi ; \quad (A3-7a)$$

$$h_e(3) = \frac{1}{I_0(3)} \int_0^{1/2} I_0(3) \cos(3\pi z/1) dz = -1/3\pi. \quad (A3-7b)$$

Using eqn(3-11), the receive transfer functions for a monopole of  $1/2 = 0.45$  m when it is a quarter-wavelength long and three quarter-wavelengths long are

$$R(1) = 0.168 \text{ metres}; \quad (A3-8a)$$

$$R(3) = -0.0464 \text{ metres}. \quad (A3-8b)$$

Appendix 4: SUMMARY OF SAMPLING PARAMETERS FOR MEASUREMENTS REPORTED IN PARTS I-III

Number of Figure in which result of measurement is recorded.	Number of Figure in which test pulse is recorded.	Tektronix oscilloscope used for receiver	Sampling interval T (ps)	Number of samples N	Method of sampling	Computer used for processing	Method of smoothing	Output display device.
2.5	4.5	1S1	100	146	Normal	EAI-590	None	CRT
3.11	3.7	1S1	100	116	Normal	EAI-590	None	CRT
3.12	3.7	1S1	100	298	Normal	EAI-590	None	CRT
5.2, 5.3	4.5	1S1	100	95	3-point (8 scans)	IBM 360/44	eqn(2-12a) w = 0.25	IBM 1627
6.5	4.5	1S1	100	207	Normal	EAI-590	None	CRT
6.6, 6.7	4.12	1S2	25	160	3-point (4 scans)	IBM 360/44	eqn(2-12a) w = 0.8	IBM 1627
6.8, 7.3, 7.5, 7.6, 7.7, 7.13	4.5	1S1	100	295	3-point (4 scans)	IBM 360/44	eqn(2-12a) w = 0.5	IBM 1627
9.2	3.7	1S1	100	37	Normal	EAI-590	None	CRT
9.3	3.7	1S1	100	185	Normal	EAI-590	eqn(2-12b)	CRT
9.5, 9.7	3.7	1S1	100	270	Normal	EAI-590	eqn(2-12b)	CRT
9.9, 9.10	4.12	1S2	25	160	3-point (24 scans)	IBM 360/44	eqn(2-12a) w = 0.5	IBM 1627
9.11a, 9.11b	3.7	1S1	100	160	Normal	EAI-590	eqn(2-12b)	CRT
9.11c	3.7	1S1	100	290	Normal	EAI-590	eqn(2-12b)	CRT

REFERENCES

- ABRAMOWITZ, M. and STEGUN, I.A. (1965): Handbook of Mathematical Functions. Dover, New York.
- ALTSHULER, E.E. (1961): "The travelling wave linear antenna", IRE Trans., AP-9, 324-329.
- ANDERSEN, J. BACH (1968): "Admittance of infinite and finite cylindrical metallic antenna", Radio Science, 3 (New series), 607-621.
- ANDERSEN, J. BACH (1971): Metallic and Dielectric Antennas. Technical University of Denmark, Lyngby; Polyteknisk Forlag.
- BARROW, W.L., CHU, L.J. and JANSEN, J.J. (1939): "Biconical electromagnetic horns", Proc. IRE, 27, 769-779; corrections and additions by CHU, L.J. (1951), Proc. IRE, 39, 434-435.
- BATES, R.H.T. (1966): "Propagation of transients of current along bent wires", IEEE International Antennas and Propagation Symposium Digest (Palo Alto, California), December, 228-233.
- BATES, R.H.T. (1967): "Comments on radiating elements which would have good transient responses", unpublished note.
- BATES, R.H.T. and BURRELL, G.A. (1970): "Simultaneous display of frequency and pulse responses of antennas", paper presented at AICA-IFIP conference, Munich, August-September, and to appear in the Proceedings.
- BEALE, J.R.A., STEPHENSON, W.L. and WOLFENDALE, E. (1957): "A study of high-speed avalanche transistors", Proc. IEE, 104, pt. B, 394-402.

- BERGLAND, G.D. (1969): "A guided tour of the fast fourier transform", IEEE Spectrum, 6, n7, 41-52.
- BLACKMAN, R.B. and TUKEY, J.W. (1958): The Measurement of Power Spectra. Dover, New York.
- BOLLE, D.M. and JACOBS, I. (1962): "The radiation pattern of long thin antennas for short pulse excitation", IRE Trans., AP-10, 787-788.
- BORGIOTTI, G. (1966): "Response of travelling wave slot arrays to non monochromatic signals", Alta Frequenza, 35, n2 (English issue), 120-129.
- BRACEWELL, R.N. (1965): The Fourier Transform and its Applications. McGraw-Hill, New York.
- BROWN, G.H. and WOODWARD, O.M. (1945): "Experimentally determined impedance characteristics of cylindrical antennas", Proc. IRE, 33, 257-262.
- BROWN, G.H. and WOODWARD, O.M. Jnr (1952): "Experimentally determined radiation characteristics of conical and triangular antennas", RCA Review, 13, 425-452.
- BROWNLESS, S.F. (1955): "Standardised transmitting aerials for medium-frequency broadcasting", Proc. IRE (Aust.), 16, 383-396.
- BRUNDELL, P.O. (1960a): "Transient electromagnetic waves around a cylindrical transmitting antenna", Ericsson Technics, 16, 137-162.
- BRUNDELL, P.O. (1960b): "Current and potential distribution on a circular loop antenna", Trans. Royal Inst. of Tech., Stockholm, Sweden, (Elec. Engrg. 4), n154.
- BURRELL, G.A. (1972): "The measured input characteristics of fan antennas constructed from wires", report to be prepared for N.Z. Post Office.

- CARREL, R.L. (1958): "The characteristic impedance of two infinite cones of arbitrary cross section", IRE Trans., AP-6, 197-201.
- CARSON, J.R. (1928): "The rigorous and approximate theories of electrical transmission along wires", Bell System Tech. J., 7, 11-25.
- CHENG, D.K. and TSENG, F.I. (1964): "Transient and steady-state antenna pattern characteristics for arbitrary time signals", IEEE Trans., AP-12, 492-493.
- COLLIN, R.E. and ZUCKER, F.J. (Eds.) (1969a): Antenna Theory, Part I. (chapters 1-15). McGraw-Hill, New York.
- COLLIN, R.E. and ZUCKER, F.J. (Eds.) (1969b): Antenna Theory, Part II. (chapters 16-28). McGraw-Hill, New York.
- CONES, H.N., COTTON, H.V. and WATTS, J.M. (1950): "A 600-ohm multiple-wire delta antenna for ionospheric studies", J. Res. NBS, 44, 475-488.
- COOLEY, J.W. and TUKEY, J.W. (1965): "An algorithm for the machine calculation of complex fourier series", Math. Comput., 19, 297-301.
- COOLEY, J.W., LEWIS, P.A.W. and WELCH, P.D. (1967): "Application of the fast fourier transform to computation of fourier integrals", IEEE Trans., AU-15, 79-84.
- COOK, C.E. and BERNFELD, M. (1967): Radar Signals - An Introduction to Theory and Application. Academic Press, New York.
- De LORENZO, J.D. (1967): "Impulse scattering measurements", Proc. 2nd GISAT Symposium, 173-176.
- DION, A.R. (1970): "Transmission of step functions by loop antennas", IEEE Trans., AP-18, 389-392.

- Du HAMEL, R.H. and ISBELL, D.E. (1957): "Broadband logarithmically periodic antenna structures", IRE National Convention Record, pt. 1, 119-128.
- DYSON, J.D. (1959a): "The equiangular spiral antenna", IRE Trans., AP-7, 181-187.
- DYSON, J.D. (1959b): "The unidirectional equiangular spiral antenna", IRE Trans., AP-7, 329-334.
- DYSON, J.D. (1962): "A survey of the very wide band and frequency independent antennas - 1945 to the present", J. Res. NBS, 66D, 1-6.
- ELLIOT, R.S. (1957): "Pulse waveform degradation due to dispersion in waveguides", IRE Trans., MTT-5, 245-257.
- ELLIOT, B.J. (1969): "Some observations on time domain measurements in the region below 25 picoseconds", WESCON, Session 22, paper 5, August.
- ELLIOT, B.J. (1970): "System for precise observations of repetitive picosecond pulse waveforms", IEEE Trans., IM-19, 391-395.
- ESS, A. (1951): Mitt. Hoch. Freq., ETH Zurich, n15.
- FARBER, A.S. and HO, C.W. (1969): "Wide-band network characterisation by fourier transformation of time-domain measurements", IEEE Journal, SC-4, 231-235.
- FENSTER, P. and ROSS, G.F. (1968): "Members of the class of TEM-mode wire antennas with a TLIR", IEEE International Antennas and Propagation Symposium Digest, September, 249-252.
- FERRIS, J.E. and ZIMMERMAN, W.E. (1966): "A broadband constant beamwidth high-gain antenna", IEEE International Symposium on Antennas and Propagation Digest, 177-181.



GIORGIS, J. (1963): "Understanding snap diodes", Electronic Equipment Engineering, 11, n11, 60-64.

HALL, C.J. (1971): "Simple method of antenna analysis leading to the mode theory results", Proc. IEE, 118, 511-514.

HALLEN, E. (1938): "Theoretical investigations into the transmitting and receiving qualities of antennae", Nova Acta Regiae Soc. Sci. Upsaliensis 4, 11, p1.

HALLEN, E. (1948): "Admittance diagrams for antennas and the relation between antenna theories", Cruft Laboratory, Harvard University, Technical Report 46, June.

HALLEN, E. (1962): Electromagnetic Theory. John Wiley, New York.

HARRINGTON, R.F. (1961): Time Harmonic Electromagnetic Fields. McGraw-Hill, New York.

HARRISON, C.W. Jnr (1964a): "Transient electromagnetic field propagation through infinite sheets, into spherical shells, and into hollow cylinders", IEEE Trans., AP-12, 319-334.

HARRISON, C.W. Jnr (1964b): "Physical limitations on the measurement of transient fields in air and in dissipative media using electric and magnetic probes", IEEE Trans., AP-12, 530-533.

HARRISON, C.W. Jnr., HOUSTON, M.L., KING, R.W.P. and WU, T.T. (1965): "Propagation of transient electromagnetic fields into cavity formed by two imperfectly conducting sheets", IEEE Trans., AP-13, 149-158.

HARRISON, C.S. Jnr and PAPAS, C.H. (1965): "Attenuation of transient fields by imperfectly conducting spherical shells", IEEE Trans., AP-13, 960-966.

- HARRISON, C.W.Jnr and WILLIAMS, C.S.Jnr (1965): "Transients in wide angle conical antennas", IEEE Trans., AP-13, 236-246.
- HARRISON, C.W.Jnr and KING, R.W.P. (1967): "On the transient response of an infinite cylindrical antenna", IEEE Trans., AP-15, 301-302.
- HU, K.C. (1963): "Improving pulse rise time with snap-off diodes", Electronics, 36, n7, February 15th, 68-70.
- HURD, R.A. (1969): The Antenna Admittance Problem. Report from Laboratory of Electromagnetic Theory, Technical University of Denmark, Lyngby, July.
- IEEE (1965): "Test procedure for antennas", IEEE Trans., AP-13, 437-466.
- IEEE (1967): IEEE Trans., AU-15, n2 (Special issue on fast-Fourier-transform and its application to digital filtering and spectral analysis).
- IEEE (1969): IEEE Trans., AU-17, n2 (Special issue on fast-Fourier-transform).
- JASIK, H. (Ed.) (1961): Antenna Engineering Handbook. McGraw-Hill, New York.
- JONES, D.S. (1964): The Theory of Electromagnetism. Pergamon, London.
- JORDAN, E.C. (1950): Electromagnetic Waves and Radiating Systems. Prentice-Hall, New Jersey.
- JORDAN, E.C., DESCHAMPS, G.A., DYSON, J.D. and MAYES, R.E. (1964): "Developments in broadband antennas", IEEE Spectrum, 1, n4, 58-71.
- JORDAN, E.C. and BALMAIN, K.G. (1968): Electromagnetic Waves and Radiating Systems. Prentice-Hall, New Jersey (2nd Ed.).

- KATAYAMA, K. and MUSHIAKE, Y. (1967): "Transient radiation characteristics of Yagi-Uda antenna", Electronics and Communication in Japan, 50, n6, 10-16.
- KING, R. (1955): "The end correction for a coaxial line when driving an antenna over a ground screen", IRE Trans., AP-3, 66-72.
- KING, R.W.P. (1956): The Theory of Linear Antennas. Harvard, Massachusetts.
- KING, R.W.P. and SCHMITT, H.J. (1962): "The transient response of linear antennas and loops", IRE Trans., AP-10, 222-228.
- KING, R.W.P. (1965): Transmission Line Theory. Dover, New York.
- KING, R.W.P. and HARRISON, C.W. Jnr (1968): "Transmission of electromagnetic waves and pulses into earth", J. Appl. Phys., 39, 4444-4452.
- KING, R.W.P. and HARRISON, C.W. Jnr (1969): Antennas and Waves: A Modern Approach. M.I.T. Press.
- KNOP, C.M. (1970): "On transient radiation from a log-periodic dipole array", IEEE Trans., AP-18, 807-808.
- KRAUS, J.D. (1950): Antennas. McGraw-Hill, New York.
- LATHAM, R.W. and LEE, K.S.H. (1970): "Transient properties of an infinite cylindrical antenna", Radio Science, 5, 715-723.
- LATHI, B.P. (1965): Signals, Systems and Communications. John Wiley, New York.
- MAGNUSON, W.G. (1963): "Variable width pulse generation using avalanche transistors", IEEE Trans., IM-12, 56-64.
- MANNEBACK, C. (1923): "Radiation from transmission lines", Journal AIEE, 42, 95-105.

- MASON, H.P. (1963): "Some factors influencing the design of broad-band HF monopole aeriads", Proc. IEE, 110, 1543-1553.
- MAYO, B.R. (1961): "Transient behaviour of aperture antennas", Proc. IRE, 49, 817-819.
- MAYO, B.R., HOWELLS, P.W. and ADAMS, W.B. (1961): "Generalised linear radar analysis", Microwave Journal, 4, n8, 79-84.
- MEIR, A.S. (1945): "Aircraft antenna design, part III", Proc. IRE, 33, 695-700.
- MEREWETHER, D.E. (1969): "Synthesis of an electromagnetic pulse generator", IEEE Trans., AP-17, 236-237.
- MERTZ, L. (1971): "Fourier spectroscopy, past, present, and future", Applied Optics, 10, 386-389.
- MEYER, P.L. (1965): Introductory Probability and Statistical Applications. Addison-Wesley, Massachusetts.
- MONTGOMERY, C.G. (Ed.) (1947): Technique of Microwave Measurements. McGraw-Hill, New York.
- MONTGOMERY, C.G., DICKE, R.H. and PURCELL, E.M. (Eds.) (1948): Principles of Microwave Circuits. McGraw-Hill, New York.
- MORENO, T. (1943): Microwave Transmission Design Data. McGraw-Hill, New York.
- MORGAN, S.P. (1962): "Transient response of the dipole antenna", J. Math. Phys., 3, 564-565.
- MOTOROLA (1963): Motorola High-Speed Switching Transistor Handbook. 2nd Edition, Motorola Inc.
- NICOLSON, A.M. (1968): "Broadband microwave transmission characteristics from a single measurement of the transient response", IEEE Trans., IM-17, 395-402.

- NICOLSON, A.M. (1969): "Wideband system function analyser employing time to frequency domain translation", presented at WESCON convention, session 22, San Francisco, August.
- NICOLSON, A.M. and ROSS, G.F. (1970): "The measurement of the intrinsic properties of materials by time domain techniques", IEEE Trans., IM-19, 377-382.
- N.P.L. (1961): Modern Computing Methods. National Physical Laboratory Notes on Applied Science n16. H.M.S.O., London.
- NYQUIST, D.P. and CHEN, K.M. (1968): "Travelling wave antenna with non-dissipative loading", IEEE Trans., AP-16, 21-31.
- O'DELL, T.H. (1969): "Series operation of avalanche transistors", Electron. Letts., 5, n5, 94-95.
- OTTO, D.V. (1967): "The admittance of cylindrical antennas driven from a coaxial line", Radio Science, 2, 1031-1042.
- OTTO, D.V. (1969): "The admittance of infinite cylindrical antennas", IEEE Trans., AP-17, 234-235.
- PALCIAUSKAS, R.J. and BEAM, R.E. (1970): "Transient fields of thin cylindrical antennas", IEEE Trans., AP-18, 276-278.
- PAPAS, C.H. (1949): "On the infinitely long cylindrical antenna", J. Appl. Phys., 20, 437-440.
- PAPAS, C.H. and KING, R. (1949): "Input impedance of wide-angle conical antennas fed by a coaxial line", Proc. IRE, 37, 1269-1271.
- PAPAS, C.H. and KING, R. (1951): "Radiation from wide angle conical antennas fed by a coaxial line", Proc. IRE, 49-51.
- PARKER, C.F. and ANDERSON, R.J. (1957): "Constant beam-width broadband antennas", IRE National Conventional Record, 5, pt.1, 87-98.

PIERCE, J.F. (1967): Semiconductor Junction Devices.

Merrill; Columbus, Ohio.

POCKLINGTON, H.C. (1897): "Electrical oscillations in wires", Cambridge Phil. Soc. Proc., 9, 324-332; corrections by the author in loc. cit., 12, 461.

POLK, C. (1960): "Transient behaviour of aperture antennas", Proc. IRE, 48, 1281-1288.

PULFER, J.K. (1961): "Dispersive properties of broad-band antennas", Proc. IRE, 49, 644.

REICH, H.J. (Ed.) (1947): Very High Frequency Techniques, volume 1. (compiled by the staff of the Radio Research Laboratory, Harvard University). McGraw-Hill, New York.

ROSS, G.F. (1965): "The synthetic generation of phase-coherent microwave signals for transient behaviour measurements", IEEE Trans., MTT-13, 704-706.

ROSS, G.F., BATES, R.H.T., HANLEY, G., ROBBINS, K. and SUSMAN, L. (1966a): "Transient behaviour of radiating elements", Interim Contract Report No. SRRC-CR-66-20, prepared for Air Force Systems Command by Sperry Rand Research Centre, Sudbury, Massachusetts, July.

ROSS, G.F., BATES, R.H.T., SUSMAN, L., HANLEY, G., SMITH, R. and ROBBINS, K. (1966b): "Transient behaviour of radiating elements", Contract Report No. SRRC-CR-66-40, prepared for Air Force Systems Command by Sperry Rand Research Centre, Sudbury, Massachusetts, November.

ROSS, G.F. (1966c): "A time domain determination of the driving point characteristics of the dipole", IEEE International Antennas and Propagation Symposium Digest, December, 205-212.

ROSS, G.F. (1967a): "A new wideband antenna receiving

- element", IEEE NEREM Digest, 78-79.
- ROSS, G.F. (1967b): "Series and parallel pulse forming networks for the generation of microwave energy", Microwave Journal, 10, September, 98-105.
- ROSS, G.F. (1968): "A time domain criterion for the design of wideband radiating elements", IEEE Trans., AP-16, 355-356.
- ROSS, G.F. (1969a): "The system function of a microwave dipole aerial derived from time domain considerations", IEE European Microwave Conference Proc., 393-396.
- ROSS, G.F. (1969b): "An improved pulse forming network for the generation of phase coherent microwave signals", IEEE Trans., MTT-17, 52-54.
- RUMSEY, V.H. (1957): "Frequency independent antennas", IRE National Convention Record, pt.1, 114-118.
- SCHULKUNOFF, S.A. (1943): Electromagnetic Waves. D. van Nostrand, New York.
- SCHULKUNOFF, S.A. (1952): Advanced Antenna Theory. John Wiley, New York.
- SCHULKUNOFF, S.A. and FRIIS, H.T. (1952): Antennas, Theory and Practice. John Wiley, New York.
- SCHMITT, H.J. (1960): "Transients in cylindrical antennas", Proc. IEE, Monograph 377E, pt.C, 292-298.
- SCHMITT, H.J. (1963): "Experimental observation of the transient response of linear antennas and loops", IEEE Trans., AP-11, 509-510.
- SCHMITT, H.J., HARRISON, C.W. Jnr and WILLIAMS, C.S. Jnr (1966): "Calculated and experimental response of thin cylindrical antennas to pulse excitation", IEEE Trans., AP-14, 120-127.

- SEEDS, R.B. (1960): "Triggering of avalanche transistor pulse circuits", Stanford Electronics Labs, Stanford University, California, Tech. Rept. No. 1653-1.
- SENGUPTA, D.L. and FERRIS, J.E. (1971): "Rudimentary horn antenna", IEEE Trans., AP-19, 124-126.
- SHARP, E.D. and TANNER, R.L. (1969): "Scale modelling of high frequency antennas", IEEE Trans., AP-17, 810-811.
- SILVER, S. (Ed.) (1949): Microwave Antenna Theory and Design. McGraw-Hill, New York.
- SMITH, R.S. (1969): "On error analysis in sampling theory", Research Report SRRC-RR-68-50, Sperry Rand Research Centre, Sudbury, Massachusetts.
- STRATTON, J.A. (1941): Electromagnetic Theory. McGraw-Hill, New York.
- STUCKERT, P.E. (1969): "Computer augmented oscilloscope system", IEEE Trans., IM-18, 299-306.
- TANG, C.H. (1964): "Input impedance of arc antennas and short helical radiators", IEEE Trans., AP-12, 2-9.
- TAYLOR, C.D. (1968): "Cylindrical transmitting antenna: tapered resistivity and multiple impedance loadings", IEEE Trans., AP-16, 176-179.
- TAYLOR, C.D. and SHUMPERT, T.H. (1970): "Electromagnetic pulse generation by an impedance loaded dipole antenna", IEEE Trans., AP-18, 110-112.
- THORNTON, R.D., DeWITT, D., CHENETTE, E.R. and GRAY, P.E. (1966): Characteristics and Limitations of Transistors. Semiconductor Electronics Education Committee series, 4, John Wiley, New York.



- WAIT, J.R. (1969): "Transient response of a dipole over a circular ground screen", IEEE Trans., AP-17, 806-809.
- WILLIAMS, C.S. (1963): "The reflected voltage of a line with an antenna load for pulse excitation", IEEE Trans., AP-11, 380-382.
- WU, T.T. (1961a): "Theory of the dipole antenna and two-wire transmission line", J. Math. Phys., 2, 550-574.
- WU, T.T. (1961b): "Transient response of a dipole antenna", J. Math. Phys., 2, 892-894.
- WU, T.T. (1962): "Input admittance of infinitely long dipole antennas driven from coaxial lines", J. Math. Phys., 3, 1298-1301.
- WU, T.T. and KING, R.W.P. (1963): "Transient response of linear antennas driven from a coaxial line", IEEE Trans., AP-11, 17-23.